TECHNIQUES FOR IDENTIFYING SEARCH AND RESCUE SATELLITE AIDED TRACKING (SARSAT) SIGNALS

BY

SAMIA MOHAMED ABOU EL-NAGA, B.Sc.

A Thesis

Submitted to the School of Graduate Studies

in Partial Fulfilment of the Requirements for

the Degree

Doctor of Philosophy

McMaster University

TECHNIQUES FOR IDENTIFYING SARSAT SIGNALS

IN THE NAME OF ALLAH, THE BENEFICENT, THE MERCIFUL.

32. They said: Be glorified! We have no knowledge saving that which Thou hast taught us. Lo! Thou, only Thou art the knower, the wise.

To

my mother, my husband

and

my daugher.

DOCTOR OF PHILOSOPHY (1986)
(Electrical and Computer Engineering)

McMASTER UNIVERSITY
Hamilton, Ontario, Canada

TITLE: TECHNIQUES FOR IDENTIFYING SEARCH AND RESCUE SATELLITE AIDED TRACKING (SARSAT) SIGNALS.

AUTHOR: SAMIA MOHAMED ABOU EL-NAGA
B.Sc. (Ain Shams University, Cairo, Egypt)

SUPERVISOR: PROFESSOR C. R. CARTER

NUMBER OF PAGES: xviii, 170

ABSTRACT

This dissertation studies the problem of identification of the emergency locator transmitter (ELT) signals as related to the Search and Rescue Satellite Aided Tracking (SARSAT) system. The ELT identification is particularly important in order to increase the probability of detection and eliminate sources of interference from the data set.

A set of parameters that uniquely characterizes the ELT signals is selected, namely; the width of the average spectrum sidebands, the ratio of the sideband plateaus of the average spectrum with respect to the carrier peak and the sweep period of the signals. Two methods for estimating the sweep period are developed theoretically. These are the sawtooth and the crosscorrelation methods.

The identification techniques are tested using computer generated signals and real testbed ELT signals recorded by the Communications Research Centre (CRC) in Ottawa.

A study of the different interference sources in the 121.5/243 MHz SARSAT frequency bands is provided. Three different sources of interference are generated and tested using the identification techniques.

The performance of the proposed techniques is further investigated using real data from two different passes of COSPAS statellite C1.

Using the identification techniques presented in this thesis, it is possible to consolidate the number of detections per day from multiple satellites and multiple satellite passes.

ACKNOWLEDGEMENTS

I would like to gratefully thank Dr. C.R. Carter for his encouragement, understanding, continued assistance and expert guidance and supervision during the course of this work.

I am thankful to the members of my supervisory committee, Dr. K.M. Wong and Dr. T.J. Kennett, for their guidance and encouragement. Special thanks to Mr. Richard Renner of Canadian Astronautics Limited of Ottawa for his useful suggestions.

I would like to thank the SARSAT Group of the Communications Research Centre (CRC), Ottawa, for many helpful discussions and contributions to this program. Also, I would like to extend my acknowledgement to NSERC for their continuing support for the project.

I would like to thank my colleagues, M.I. Dessouky, V. Dubey and T. Chung for their useful discussions. I greatly appreciate the effort of the staff of the Engineering Word Processing Centre at McMaster University for their excellent job in typing this thesis.

Last but not least, I would like to express my appreciation to my husband, Dr. Samy El-Hennawey, for his constant understanding and support, and for the many useful suggestions he made during this work. Special thanks also to my daughter, Marwa, for the sacrifices she unknowingly made. Also, I would like to express my appreciation to my mother, who always supports and encourages me, and to my brother, Moneer El-Naga, for his assistance and helpful discussions.

TABLE OF CONTENTS

TABLE OF CONTENTS (continued)

TABLE OF CONTENTS (continued)

LIST OF FIGURES

LIST OF FIGURES (continued)

LIST OF FIGURES (continued)

LIST OF FIGURES (continued)

LIST OF FIGURES (continued)

LIST OF FIGURES (continued)

LIST OF FIGURES (continued)

LIST OF FIGURES (continued)

LIST OF FIGURES (continued)

LIST OF FIGURES (continued)

LIST OF FIGURES (continued)

CHAPTER 1

INTRODUCTION

1.1 Overview

The number of private and commercial aircraft has greatly increased in the last 15 years. During this time, the problem of search and rescue of aircraft in distress has also become a significant problem. In Canada, it has become mandatory for every aircraft to carry an Emergency Locator Transmitter (ELT) unit since 1975. This equipment is activated either on impact with ground or by manually setting a switch. The ELT transmits a special signal, described later, which can be detected by either a search aircraft or a search and rescue satellite.

The main difficulty facing the victims of a crash is survival. It has been shown [1] that survival probability greatly decreases when the rescue extends beyond 6 hours after an aircraft crash. In Canada, the harsh environment in the north is particularly difficult in winter, and a blanket of snow can easily hide a crash scene. As well, an aircraft is nearly impossible to recognize by sight. Therefore, an international project has been established involving Canada, the United States, and France to employ satellite signalling to locate aircraft in distress. This project is called "Search And Rescue Satellite Aided Tracking" (SARSAT) and is a cooperative program with a separate project developed by the Soviet Union called COSPAS [2,3] and the overall venture is referred to as COSPAS-SARSAT. The SARSAT technique can also be applied to the Emergency Position Indicating Radio Beacon (EPIRB) signals of marine vessels in distress. Since the ELT and EPIRB signals have the same format, we refer to only ELT signals with the understanding that the results also apply to EPIRB signals.

Currently there are five satellites in orbit; three launched by the Soviet Union and two by the United States. Another SARSAT equipped satellite will be launched by the United States within the next few years.

In the SARSAT signal environment it is possible to receive within one satellite pass many (up to 20) simultaneous emergency beacon signals combined with voice signals and interference of various types, all signals simultaneously occupying essentially the same frequency-time space. It is important for the processor to be capable of distinguishing between the existing ELT signals for the following reasons:

(1) To be able to track the individual ELT signal in order to determine the position of the corresponding crash site.

(2) To complete the Doppler-curves for ELT signals, which are not received for the entire satellite pass.

(3) To separate ELT signal tracks overlapped by interference, which cause ambiguity in tracking each signal.

In addition, it is desirable to recognize interfering sources in order to consolidate the number of ELT detections from multiple satellite passes and multiple satellites. There are 5 satellites in orbit and each one passes over a location on the earth about 6 times/day. Consider the average number of signals per satellite pass to be 10, therefore the number of detections per day is given by:

$$\text{Number of Detections} = 10 \times 5 \times 6 = 300 \text{ detections/day}$$

This number of detections can be reduced considerably if the interfering signals which are mistakenly detected as ELT signals can be eliminated. These goals will be achieved through identification techniques developed and tested (with computer simulated and real data) in this dissertation.

1.2 SARSAT Theory of Operation

Basically, the system operates as shown in Fig. 1.1. After a crash, the Emergency Locator Transmitter (ELT) on board the distressed aircraft transmits the ELT signal. As the SARSAT satellite in the 850 km polar orbit approaches the crash site, the Doppler shift of the carrier becomes less until the minimum distance is reached, where the Doppler shift is zero. Beyond this point a negative Doppler shift occurs and a plot of frequency versus time produces the S-shaped curve in Fig. 1.2. This curve leads to a measure of ELT position with respect to known position of the satellite.

The measurment is achieved at an earth station, where signal processing is carried out. In the case of multiple signal environment, the location of the peaks of the signal power spectral density are estimated. Then, the dot-chart is obtained by plotting the spectrum peak frequencies versus time. From this chart, the S-shaped curves are extracted. Based on the slope at the inflection point of each S-shaped curve, the range to the corresponding crash site can be calculated directly. This can be simplified by considering the flat earth model of Fig. 1.3 [4]. The carrier frequency of the signal received by the satellite is given by:

$$f = f_o + f_d \frac{x}{(x^2 + h^2 + z_o^2)^{1/2}} \tag{1.1}$$

Where:

f = received frequency by the satellite

f_d = Doppler shift of the signal

f_o = transmitted carrier frequency of ELT

x = distance along the flight path

h = altitude of the satellite

z_o = displacement of unknown magnitude of direction

This signal is relayed from the satellite to a rescue coordinate centre. Calculating the first derivative with respect to time of eq. (1.1) yields:

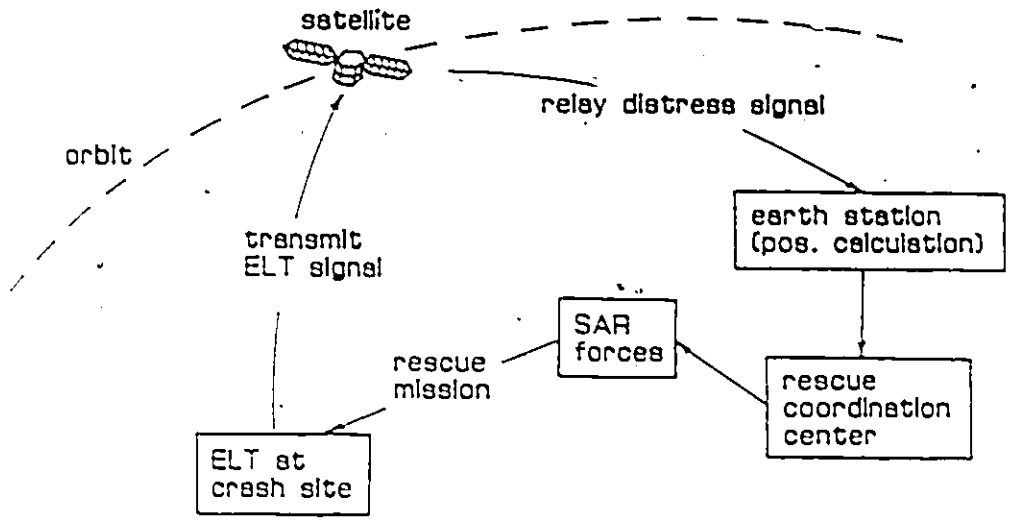

Fig. 1.1 Schematic diagram of SARSAT system.

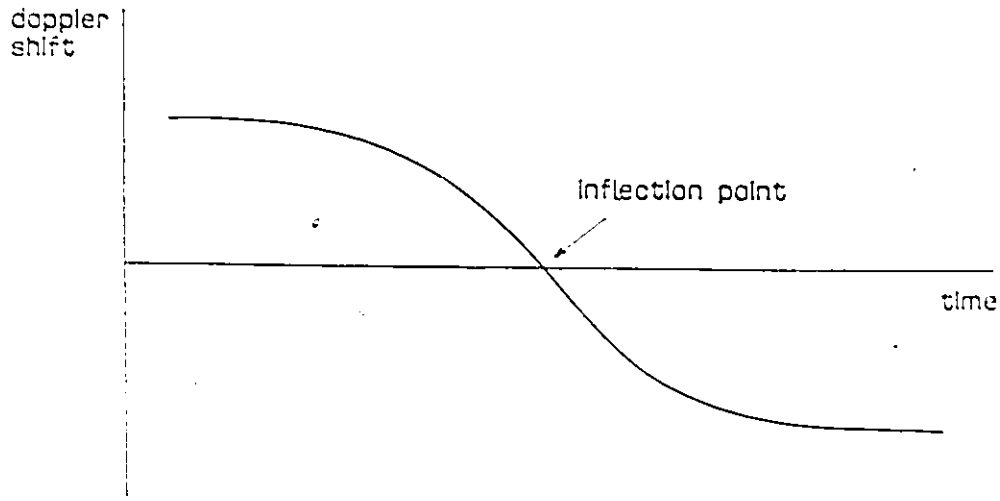

Fig. 1.2 The Doppler S-shaped curve.

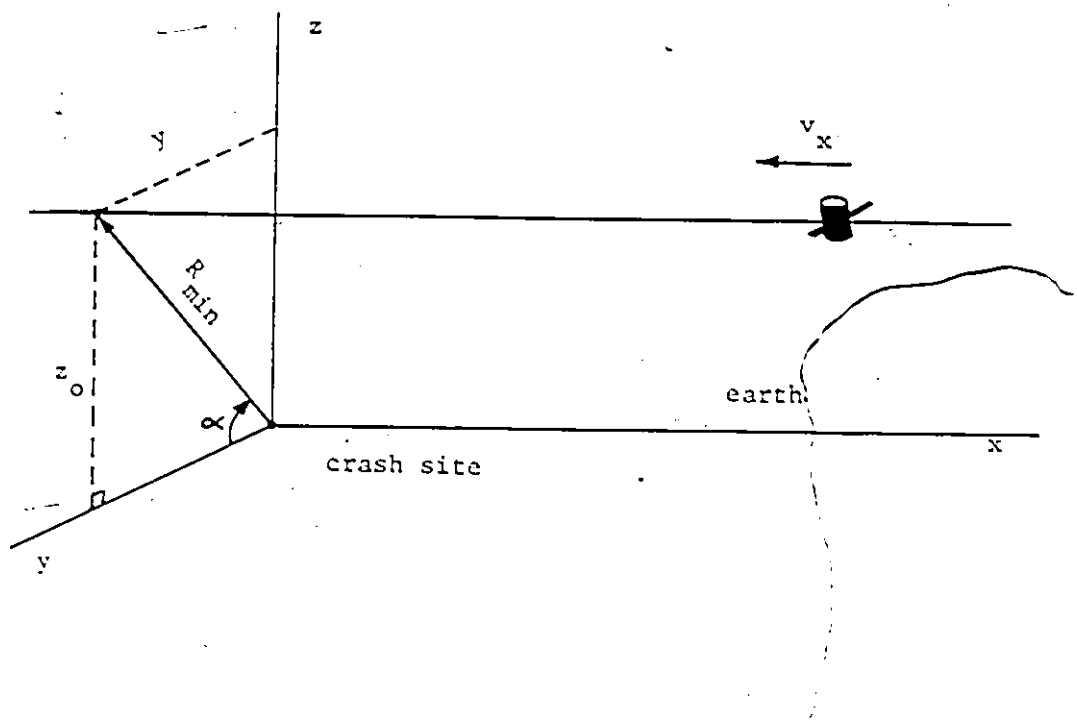

Fig. 1.3 Flat earth model of SARSAT geometry.

$$\frac{df}{dt} = \frac{f_d(-v_s)}{(x^2 + h^2 + z_o^2)^{1/2}}\left(1 - \frac{x^2}{x^2 + h^2 + z_o^2}\right) \tag{1.2}$$

where $v_s = -dx/dt$ = velocity of the satellite.

When $x=0$, the satellite is closest to the crash site, and consequently:

$$-\frac{df}{dt} = \frac{f_d v_s}{(h^2 + z_o^2)^{1/2}}\Bigg|_{x=0} \tag{1.3}$$

But, we have $(h^2 + z_o^2)^{1/2} = R_{min}$. Then,

$$R_{min} = \frac{f_d v_s}{-\left(\frac{df}{dt}\right)\Big|_{R_{min}}} \tag{1.4}$$

Now from Fig. 1.2, R_{min} occurs at the point of the inflection on the Doppler curve; hence this is measured. Both f_d and v_s are known for any satellite orbit, and consequently, R_{min} can be calculated. Knowing the coordinates of the satellite at the time of minimum distance occurence, the crash site can be determined.

1.3 ELT Signals

The ELT signals were originally intended for detection and recognition by a human operator. Thus a distinctive easily identifiable signal which may be represented by a modulated carrier waveform as shown in Fig. 1.4a was chosen.

The carrier frequency used is 121.5 MHz with an optional value of 243 MHz. The modulation can be represented in an exponential manner as shown in Fig. 1.4b, with the pulse-null duration varying approximately between 0.7 ms and 1.6 ms. The sweep period (T_s) of the signal may vary from 0.25 s to 0.5 s, depending on the particular unit. A summary of the pertinent specifications is given in Table 1.1 [5]. From this Table, the frequency tolerance is ± 50 ppm., thus for 121.5 MHz carrier frequency, the tolerance is given by:

$$f(121.\ \text{MHz}) = \pm 50 \times 10^{-6} \times 121.5 \times 10^{6}$$
$$= \pm 6\ \text{kHz}$$

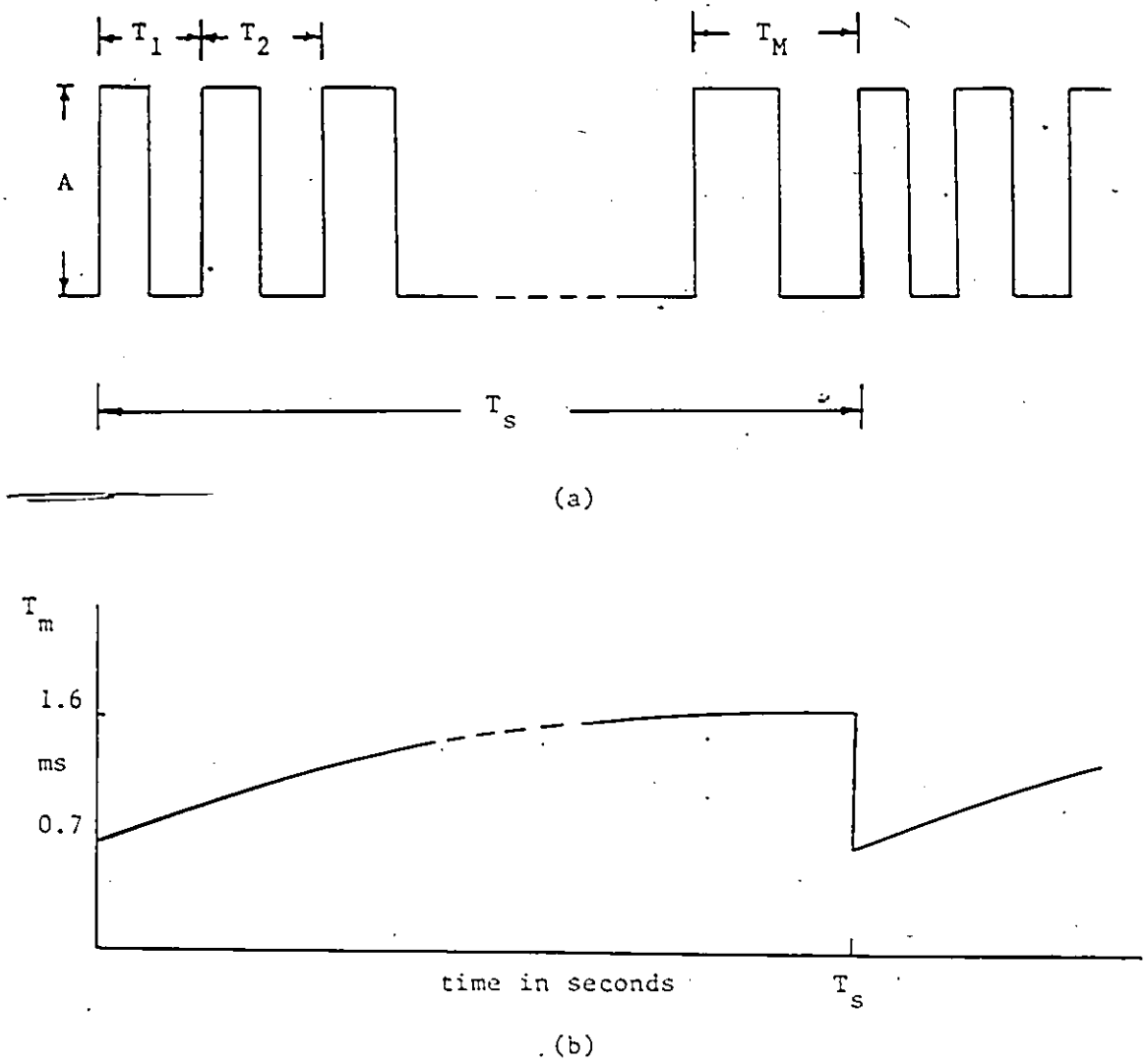

Fig. 1.4 (a) ELT signal comprising M pulse-null pairs of carrier.
(b) Variation in duration of the pulse-null pairs versus sweep time.

TABLE 1

ELT SPECIFICATIONS

carrier frequency	121.5 MHz (optional 243 MHz)
frequency tolerance	± 50 ppm
power output	approximately 100 mW
modulation type	pulse
pulse duration	33% to 55%
percentage modulation	> 85%
modulation frequency	downward swept
sweep rate	2 to 4 sweeps/second
modulation frequency change	700 Hz minimum
modulation frequency limits	300-1600 Hz

Thus, the carrier frequency range is 12 kHz. If the processing time is restricted to 20 ms, then the frequency resolution is ±50 Hz, therefore there are about 120 distinguishable carrier frequencies that can be obtained within the specifications. Similarly the pulse duration has a range from 0.33 to 0.55 which corresponds to approximately 2 dB in the amplitude variation of the spectrum sidebands. Therefore, for 1 dB accuracy it is possible to distinguish between 2 different signals. The percentage amplitude modulation also produces a 2 dB variation in the amplitude of the sidebands and for 1 dB accuracy, this corresponds to 2 distinguishable signals. From Table 1.1, it is seen that the sweep rate lies between 2 and 4 sweeps/second, i.e. corresponding to a sweep period between 0.25 s and 0.5 s. This allows for about 25 ELT signals with different sweep periods, that the spectral estimates are computed every 10 ms (1 K-FFT). Also, the frequency modulation limits (300-1600 Hz) can allow for an additional 13 distinguishable signals if the frequency resolution is ±50 Hz. Thus if the above modest range of variation of each term is considered, the number of different signal designs is approximately:

$$\text{The number of different designs} = 120 \times 2 \times 2 \times 25 \times 13 = 156{,}000$$

Therefore nearly a quarter of a million different implementations of ELT units can be obtained with just this variation in the range in the specifications.

1.3.1 Types of ELT Signals

There are many types of ELT signals. However, two classifications have been identified, those with coherent phase and those with non-coherent phase [6]. The former, shown in Fig.1.5a, can be generated by a carrier oscillator being gated through a switch to an antenna. Note that the phase characteristics from pulse to pulse is continuous as shown in Fig.1.5b.

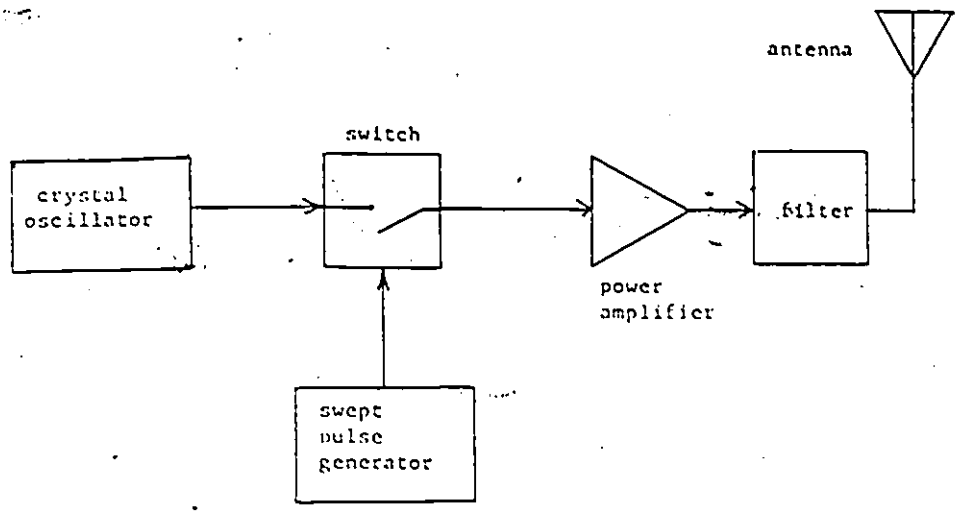

(a)

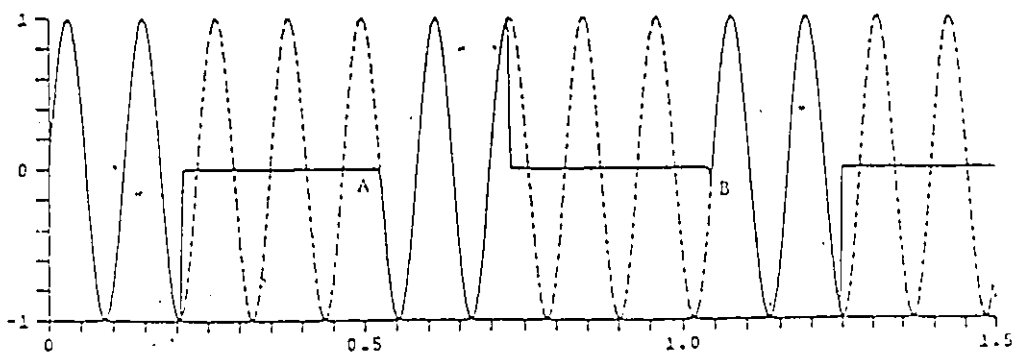

(b)

Fig. 1.5 (a) Block diagram for a coherent ELT signal.
(b) Portion of a coherent ELT signal with the ON time as a solid line and the OFF time dotted. Note the phase continuity at points A and B.

The non-coherent ELT units can be further subdivided into frequency-pulled non-coherent and random phase non-coherent. The first is simply a coherent ELT, in which the carrier frequency is affected by the modulation resulting in a small change in carrier frequency between OFF and ON. Since the ON duration due to the modulation increases with time along the signal, the frequency-pulling similarly increases producing an FM effect.

The random phase non-coherent ELT can be represented by an oscillator which is switched ON and OFF by the modulation as depicted in Fig. 1.6a. In this case there is essentially no relation between the phase of consecutive pulses of signal, as shown in Fig. 1.6b. This results in a wide band of energy in the spectrum, which makes it difficult to analyse.

A testbed consisting of 20 ELT units has been constructed at the Communication Research Centre (CRC) in Ottawa, Canada, which permits signals up to 10 ELT units to be combined and mixed to frequency range from 0 to 25 kHz. The testbed ELT signals are from different manufacturers and are numbered consecutively from 1 to 20, i.e. ELT01, ELT02, ..., and ELT20.

1.3.2 Data Available

In this thesis, three different classes of ELT signals are considered. The first, is a computer generated ELT signal, which permits the generation of wide variety of different types of ELT signals produced by different manufacturers.

The second type of data includes the testbed ELT signals which are provided by the CRC [7]. The following four testbed signals are chosen; ELT01 (Pointer), ELT12 (Garrett), ELT17 (Narco) and ELT19 (Narco). The names between brackets are the commercial producers. ELT01,ELT12 and ELT17 can be classified as frequency-pulled non-coherent signal. On the other hand, ELT19 can be considered as non-coherent signal.

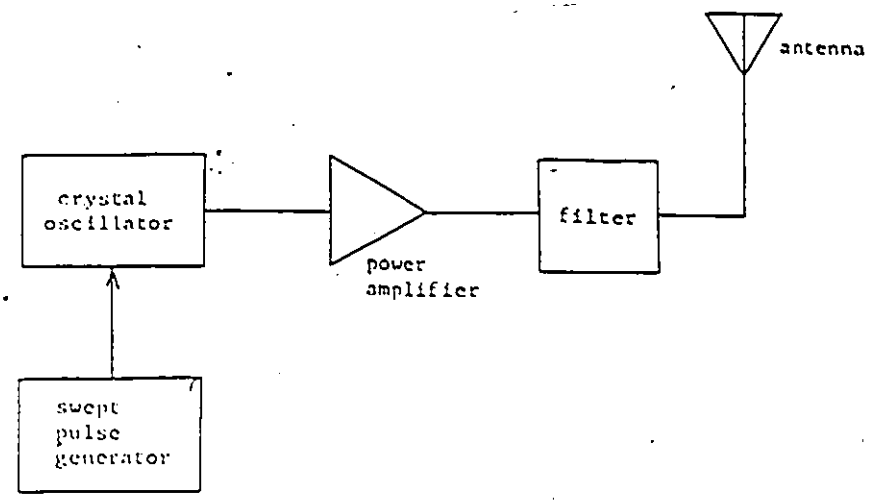

(a)

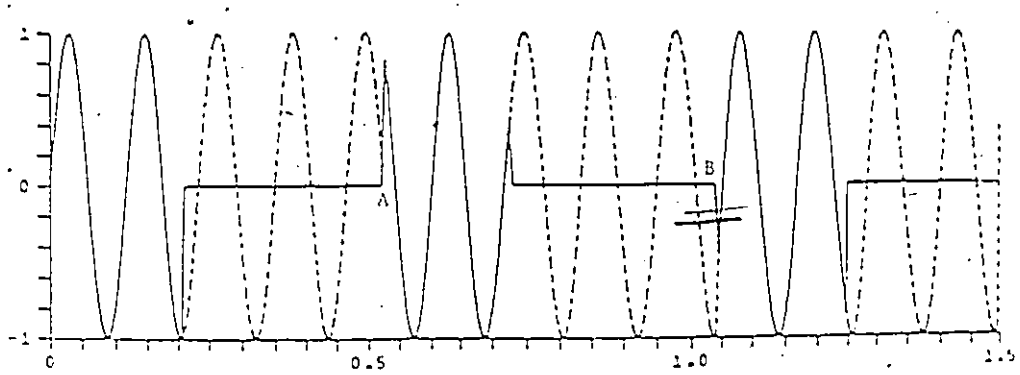

(b)

Fig. 1.6 (a) Block diagram for a non-coherent ELT signal.
(b) Portion of a non-coherent ELT signal with the ON time as a solid line and the OFF time dotted. Note the phase discontinuity at points A and B.

The third type of data available were taken form the first COSPAS satellite C1 and recorded on tape. The two available passes are recorded from orbits 860 and 861. Due to the satellite motion the maximum Doppler frequency shift in the signal is approximately ±3 kHz.

All signals available are occupying the frequency band 0-25 kHz and are digitized at a sampling rate of approximately 100 kHz. Sampling at rate higher than the Nyquist rate permits finer frequency resolution for the spectral estimates.

1.4 406 MHz ELT Signal

To overcome the problems associated with the non-coherent phase signals in the 121.5/243 MHz bands, a new type of ELT is being developed which transmits at 406 MHz. These signals are 440 ms in duration and have a repetition period of 50 s. In between these intervals the ELT transmits 121.5 or 243 MHz signals so that aircraft with detection equipment used at present can still aid the final stage of detection.

A description of the 406 MHz signal format is given in Fig. 1.7 [8]. An optional long message format provides 32 additional bits of data. From the short message format, we see that the signal can be divided into two parts; the continuous wave (CW) preamble and the modulated message following it. The CW preamble is at frequency of 406 MHz and has a duration of 160 ms. At the receiver, this preamble is processed to extract the Doppler curve. Information related to distress situation is digitally encoded to give the digital message which has a duration of 280 ms. It is intended that the 406 MHz signal be processed on board the satellite in order to allow larger coverage areas.

In fact, the 406 MHz units provide the ideal situation for signal processing by the SARSAT system. However, due to the tremendous number of the 121.5/243 MHz ELT units already existing in the market, it is believed that these types of ELT units will be used at

UNMODULATED CARRIER	BIT SYNC. (1)	FRAME SYNC. (2)	FORMAT FLAG (6)	USER CLASS	COUNTRY	IDENTIFICATION CODE	EMERGENCY CODE FLAG (3)	EMERGENCY SITUATION OR ELAPSED TIME	ERROR CORRECTION
160 milliseconds	15	9	1	4	8	48	1	15	21

280 milliseconds
MESSAGE

NOTES:
1) BIT SYNC - 15 "1" BITS
2) FRAME SYNC - 000101111
3) "1" BIT INCLUDES EMERGENCY CODE, "0" BIT INDICATES ELAPSED TIME
4) ELAPSED TIME IN ONE HOUR INCREMENTS; COUNT HELD AT 32 HOURS
5) TOTAL MESSAGE DURATION 440 MILLISECONDS
6) "1" BIT INDICATES LONG MESSAGE FORMAT
"0" BIT INDICATES SHORT MESSAGE FORMAT

Fig. 1.7 The 406 MHz ELT short message format.

least until the end of this century. Therefore, the processing of the existing ELT signals remains an important problem.

1.5 Scope of The Dissertation

In Chapter 2, a description of the identification parameters of the ELT signals is provided and the application of the averaged periodograms is investigated. Also, the methods are tested using real testbed ELT signals.

In Chapter 3, two techniques for estimating the sweep period are developed theoretically. The techniques are also tested using computer simulated and real testbed ELT signals.

The interference sources existing in the 121.5/243 MHz frequency bands are presented in Chapter 4. In this chapter, the proposed identification methods are tested in the case of overlapped (co-channel) interference and ELT signals. Also, the effect of automatic gain control (AGC) at the receiver is examined.

In Chapter 5, the identification techniques are applied to real satellite pass data. The data include two different satellite passes.

Finally, concluding remarks and suggestions for future research are included in Chapter 6.

2

For laura honda:JH ENGRG:MCMASTER

ELNAGA – Chap, 2

Created 22 – May – 86 11:58:24

Printed 22 – May – 86 11:59:44

7 Sheet(s), 1 Copy.

Xerox Print Service 8.0 on PS – 1

ELNAGA

CHAPTER 2

ELT PARAMETER IDENTIFICATION

2.1 Overview

In this chapter, the pertinent specifications given in Table 1.1 are examined in order to select the most effective parameters in identifying the ELT signals. The estimation of those parameters are carried out using the spectra of the ELT signals. Therefore we start the chapter by reviewing the spectral estimation techniques required, followed by the selected ELT signature parameters. The techniques for estimating some of those parameters are presented in this chapter and the rest are developed in Chapter 3.

2.2 Periodogram and Average Periodogram

In general, the ELT signal shown in Fig. 2 can be represented by the relation

$$x(t) = A\, m(t) \cos(2n\, f_c\, t + \theta) \tag{2.1}$$

where A = amplitude of the signal

$m(t)$ = pulse modulation

f_c = carrier frequency

θ = phase shift.

If f_c and θ are constant, the signal is classified as ideal coherent. In practice, this does not occur, however. When f_c and θ are nearly constant, which is true for a large number of ELT signals, the signal is classified as coherent. If f_c or θ change appreciably from pulse to pulse, the signal termed non-coherent and the resulting spectrum becomes broad and difficult to process [6].

To estimate the power spectral density using the periodogram, we use the following relation [9]:

$$I_{N_T}(f_j) = \frac{1}{N_T} \left| X(f_j) \right|^2 \tag{2.2}$$

where X(f) is the discrete Fourier transform of the real finite length sequence x(n), $0 \le n \le N_T-1$ defined by:

$$X(f_j) = \sum_{n=0}^{N_T-1} x(n)\, e^{-j2\pi f_j n} \tag{2.3}$$

Unfortunately, the periodogram provides a non-consistent estimate of the power spectral density, since the variance does not approach zero as the record length increases.

To overcome this problem we employ the average periodogram. In this approach, the data sequence x(n), $0 \le n \le N_T-1$ is divided into M segments of N samples each such that $N_T = MN$. Thus, the ith data segment is given by:

$$x_i(n) = x(n + iN - N) \qquad 0 \le n \le N-1, \quad 1 \le i \le M \tag{2.4}$$

Now, the ith periodogram is given by:

$$I_{N_i}(f_j) = \frac{1}{N} \left| \sum_{n=0}^{N-1} x_i(n)\, e^{-j2\pi f_j n} \right|^2 \tag{2.5}$$

Finally, the average spectrum (Welsh's method) is defined by:

$$S_A(f_j) = \frac{1}{M} \sum_{i=1}^{M} I_{N_i}(f_j) \tag{2.6}$$

It has been shown that the averaging procedure is equivalent to multiplying the autocorrelation by a triangular window and then applying directly the FFT to obtain the spectrum [9]. Other forms of windows have been suggested [10]. However, due to its computational efficiency the averaged periodogram is still considered the most attractive method and is used in most applications including SARSAT.

2.3 Selection of ELT Identification Parameters

As previously noted, the ELT transmits a periodic signal that comprises a set of pulses of carrier separated by nulls with pulse widths and null duration increasing with time. The ELT sweep period T_s varies between different ELT units (0.25 s to 0.5 s), and therefore it represents a suitable identification parameter. As well, we see that the modulation frequency limits for a given signal lie between 300 Hz and 1600 Hz, with a minimum difference of 700 Hz. This can be exploited by considering the periodogram of the ELT signals. In this case the difference between the carrier frequency and the sideband frequency would vary as the sweep progresses. This variation would have a minimum of 700 Hz and a maximum of 1300 Hz (it is referred to as the sideband width) and is very useful in identifying the ELT signals.

Due to the periodic nature of the modulation of the ELT signals, their spectra also exhibit time periodicity. This can be clearly seen upon examining successive spectra of different ELT units. The signal amplitudes of 5 ms duration of each of the four testbed signals introduced in Chapter 1 are given in Fig. 2.1 through Fig. 2.4. It is apparent that very little information can be extracted from the time domain. However, we can say that the pulse modulation is clear especially with Narco ELT17 and ELT19. Figure 2.5 through Fig. 2.8 show 26 successive spectra (from bottom, 1, to top, 26) representing 0.5 s of data for each of the above ELT units. Each spectrum is calculated using 2k-point FFT with 20 dB dynamic range. The bottom curve represents the average of the corresponding spectra (which are examined later in more detail in Fig. 2.9 through Fig. 2.12).

The following points are observed:

1. The carrier peak (indicated by the arrow) is well defined for the Pointer, Garrett and Narco ELT 17 signals. Furthermore, the sidebands slide in smoothly toward the carrier peak as the sweep progresses.

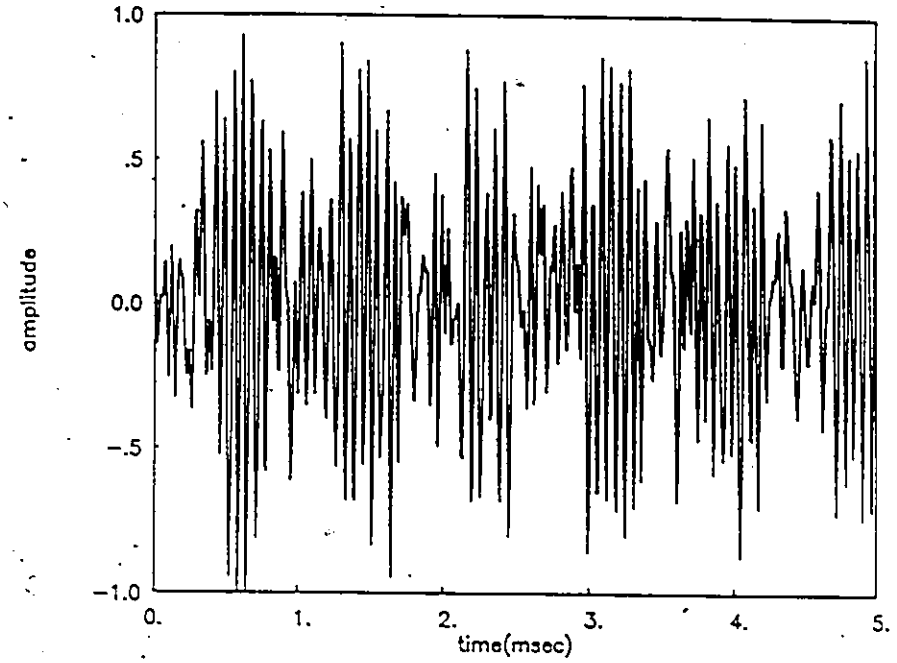

Fig. 2.1 Signal waveform for Pointer ELT01 testbed signal.

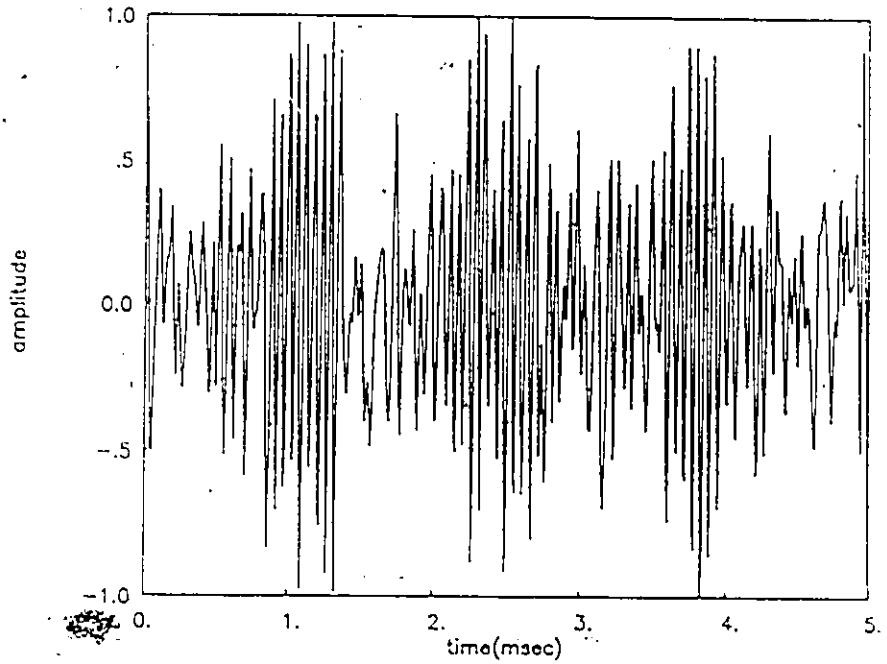

Fig. 2.2 Signal waveform for Garrett ELT12 testbed signal.

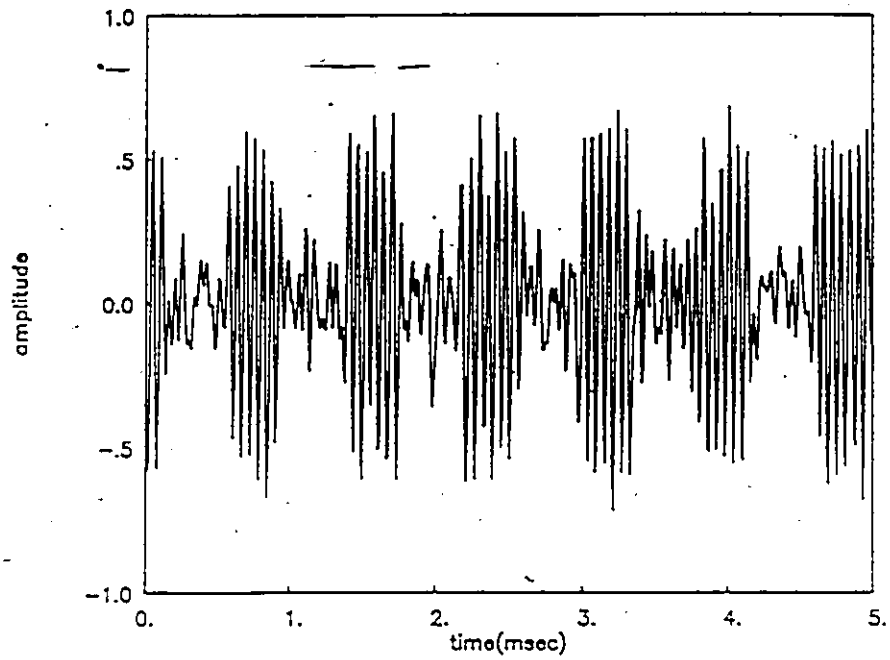

Fig. 2.3 Signal waveform for Narco ELT17 testbed signal.

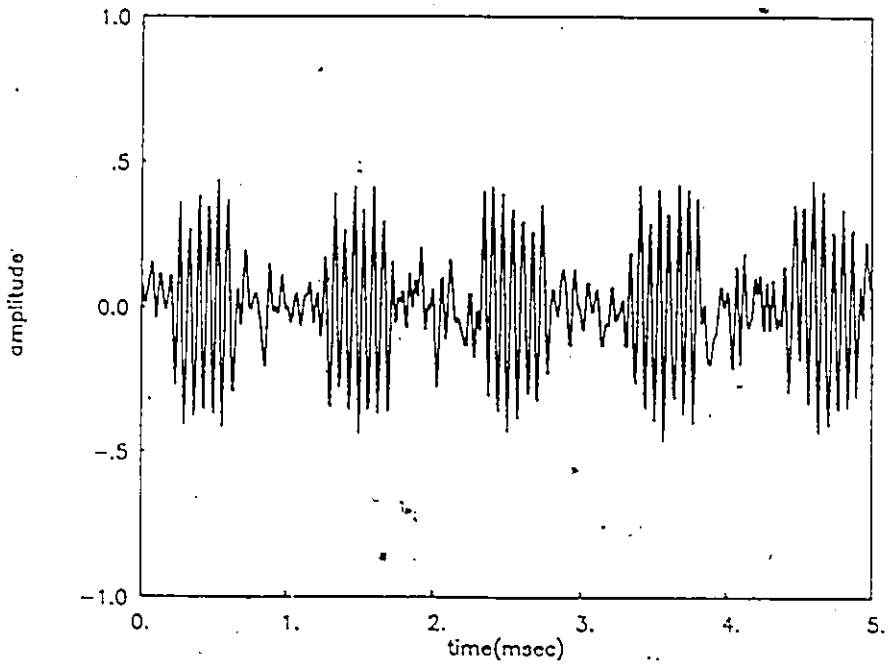

Fig. 2.4 Signal waveform for Narco ELT19 testbed signal.

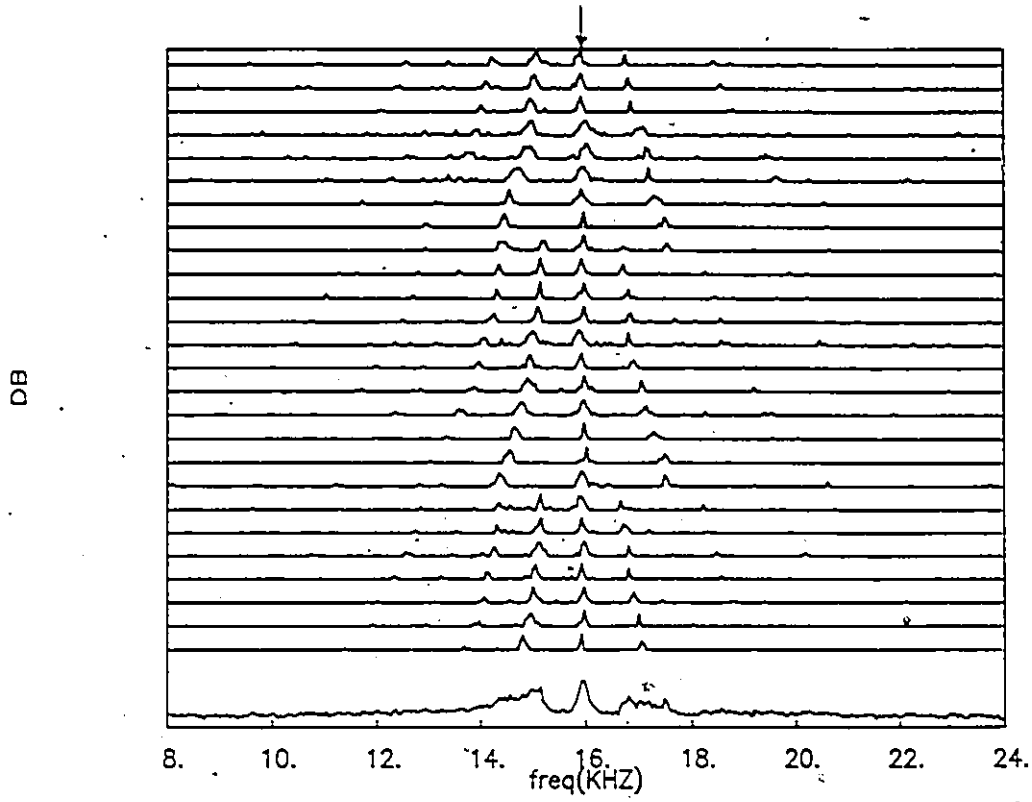

Fig. 2.5 Spectral plots of 26 contiguous blocks of data for Pointer ELT01 signal.

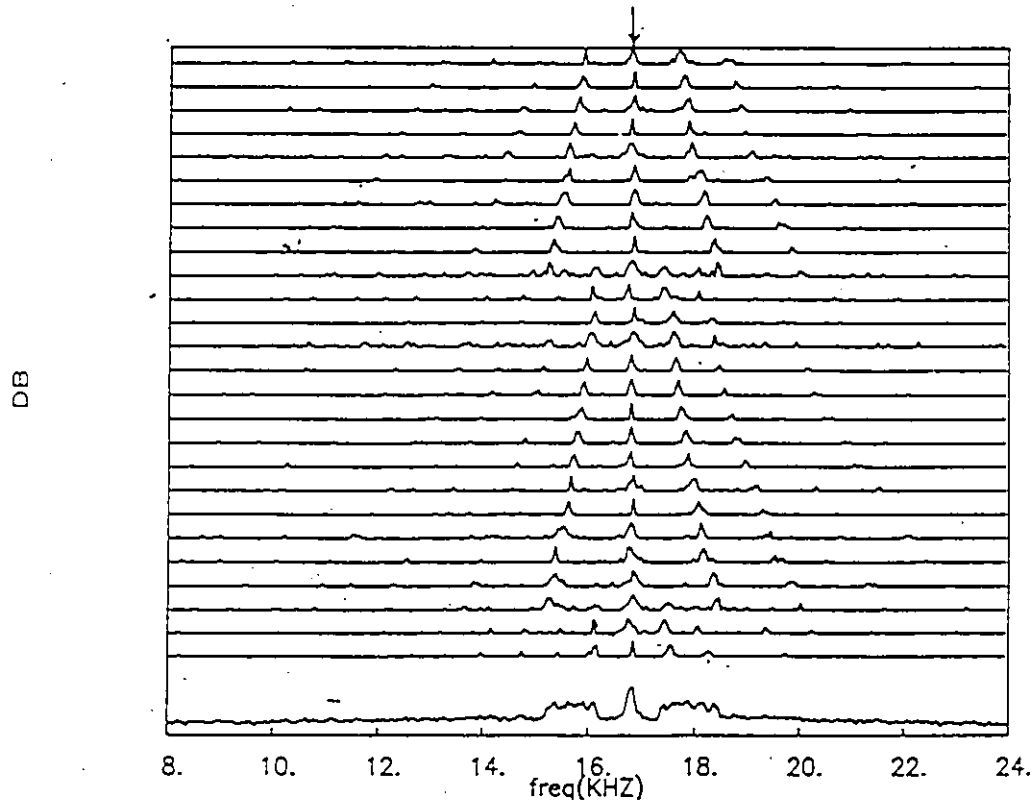

Fig. 2.6 Spectral plots of 26 contiguous blocks of data for Garrett ELT12 signal.

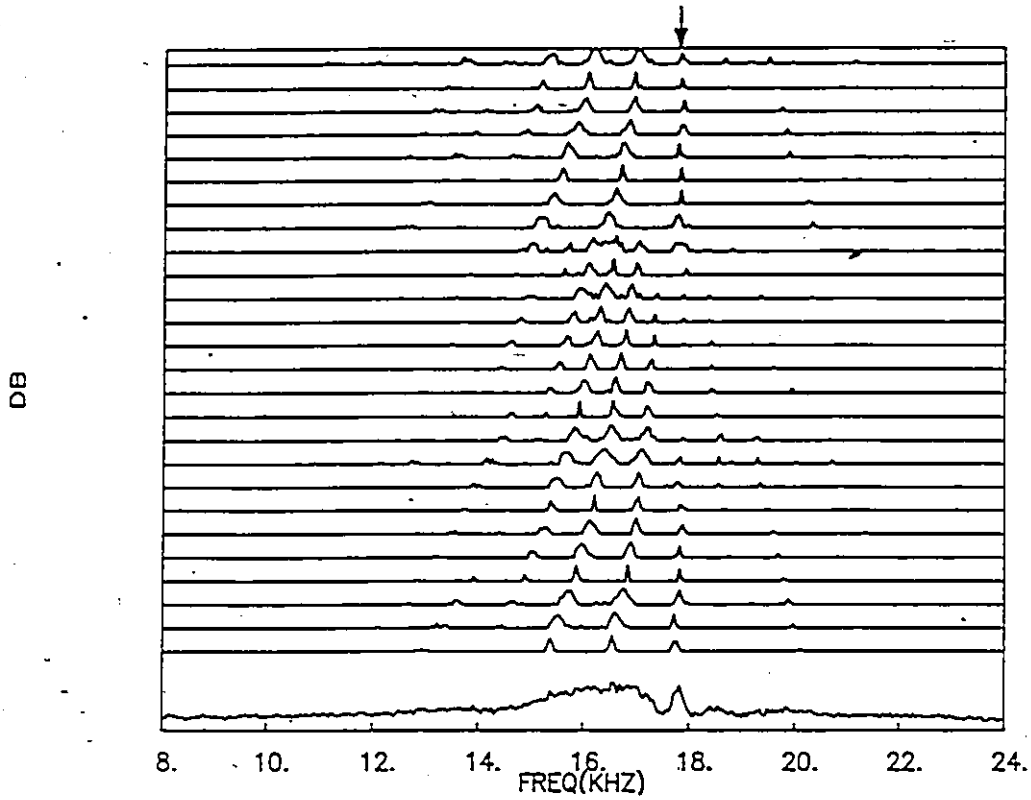

Fig. 2.7 Spectral plots of 26 contiguous blocks of data for Narco ELT17 signal.

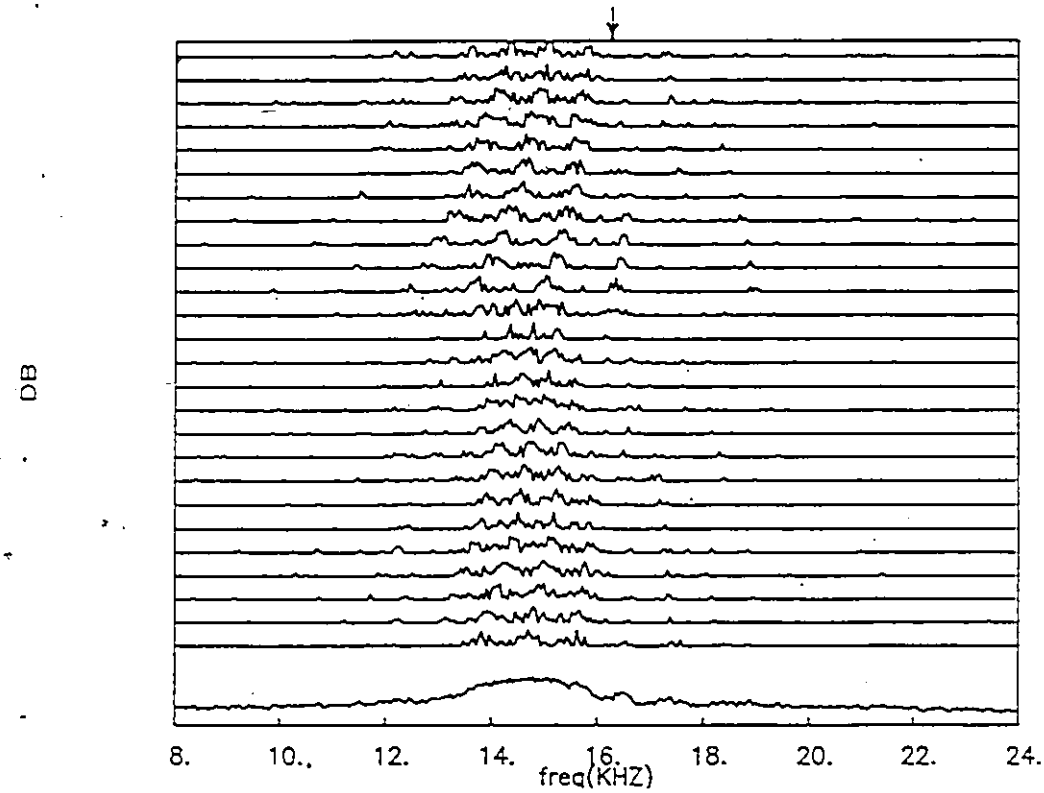

Fig. 2.8 Spectral plots of 26 contiguous blocks of data for Narco ELT19 signal.

2. The periodicity of the spectrum indicating the sweep period can be easily observed for the Pointer and Garrett ELT units.

3. Throughout the sweep period, the upper side band of the Narco ELT17 (Fig. 2.7) is seen to be decreasing. It almost vanishes and reappears at the following sweep. On the other hand the lower sideband is seen always to be present and of a larger magnitude.

4. From Fig. 2.8, we conclude that the Narco ELT19 produces a noncoherent signal, where little of the normal ELT pattern can be observed by the visual inspection. (However, it will be shown that the sweep period can be accurately determined using the proposed methods which will be discussed in Chapter 3).

As will be seen shortly, upon examining the averaged spectrum, the ratios of the lower sideband and the upper sideband with respect to the carrier vary from one signal to another. Therefore, these ratios can be used as identification parameters.

So far, we have introduced the following set of signature parameters: a) the sweep period T_s; b) sideband widths W1 and W2; and c) the ratio of the sideband plateaus B1 and B2 with respect to the carrier level A. In the following sections, we shall introduce and discuss methods for estimating these parameters from the received signals.

2.4 Evaluation of Sweep Widths and Sideband Plateaus

2.4.1 Average Method

The average spectrum is calculated for a long duration of time in order to include a significant number of sweeps. Figure 2.9 shows the average spectra of the ELT units for 150 4 k-point periodograms comprising 6s of data. Similar plots for Garrett, Narco ELT 17 and Narco ELT 19 are depicted in Fig. 2.10, 2.11 and 2.12 respectively. A close examination of these spectra indicates that each unit has its own signature. The sweep width (W1 and W2)

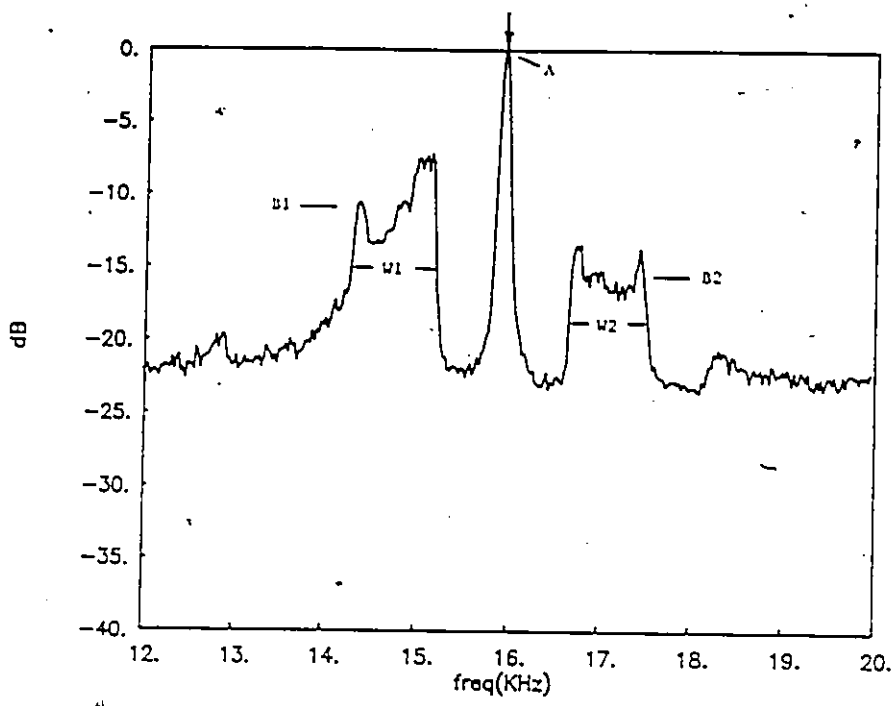

Fig. 2.9 Average of 150 4k-periodogram for Pointer ELT01 signal.

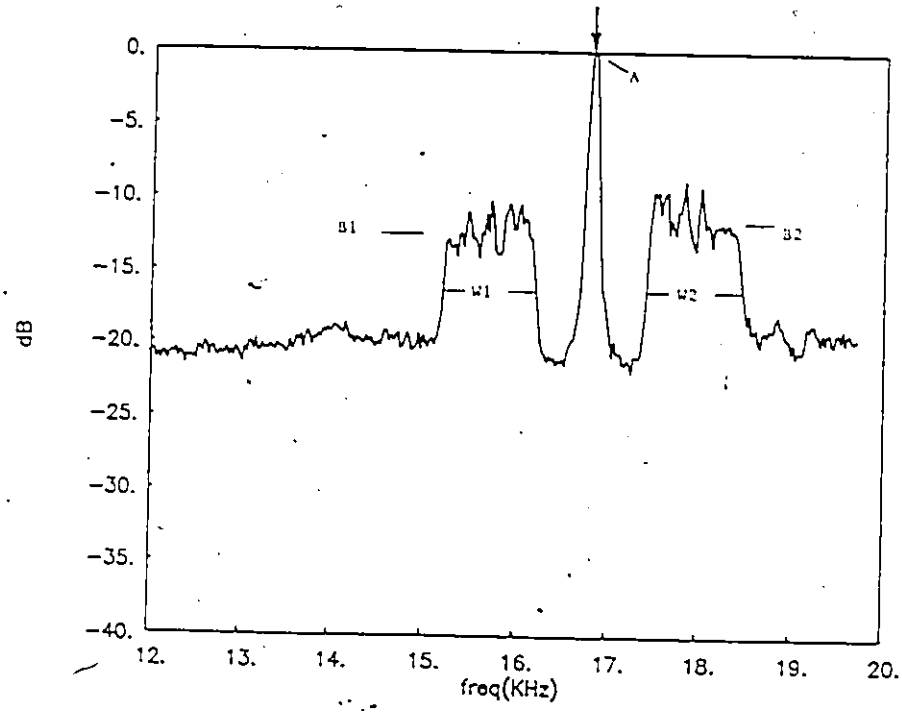

Fig. 2.10 Average of 150 4k-periodogram for Garrett ELT12 signal.

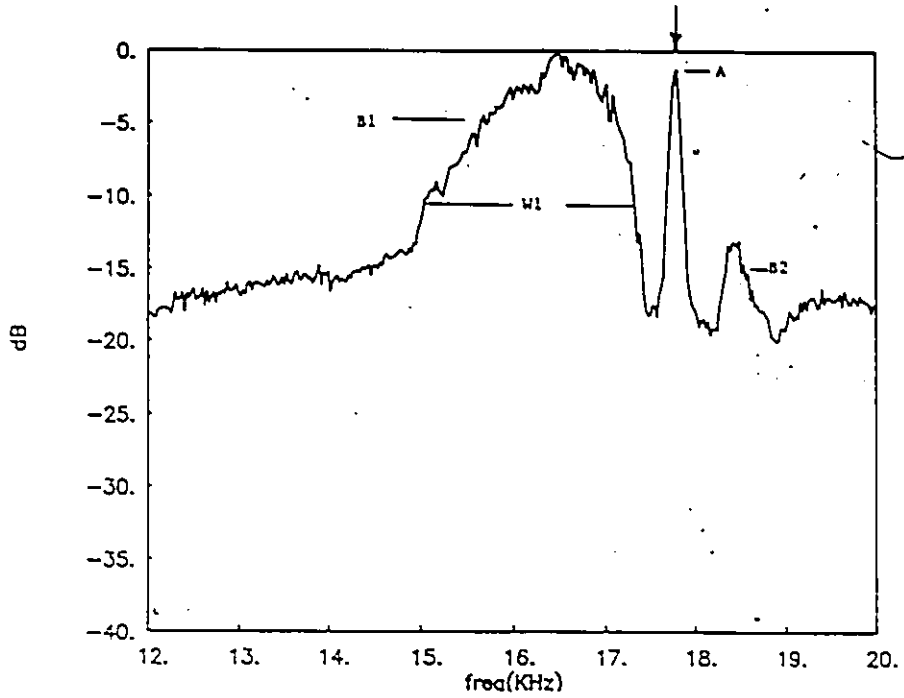

Fig. 2.11 Average of 150 4k-periodogram for Narco ELT17 signal.

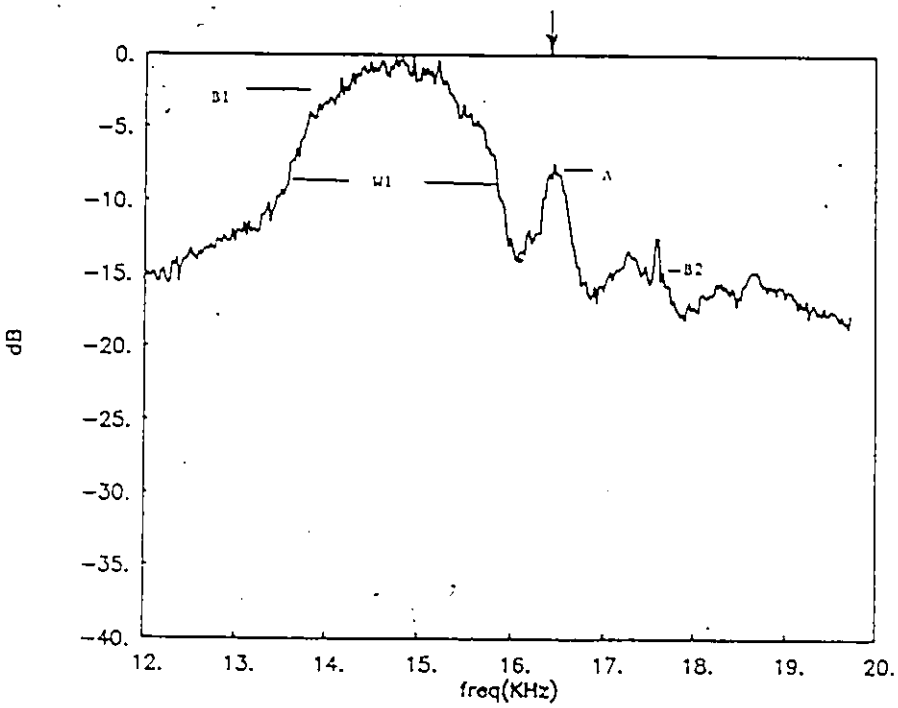

Fig. 2.12 Average of 150 4k-periodogram for Narco ELT19 signal.

and the relative amplitudes between the sideband plateaus (B1 and B2) and the carrier peak can be measured by selecting the proper threshold. However, due to the difference in the sideband levels from signal-to-signal and upper sideband to lower sideband in the same signal, selection of the appropriate threshold may not be simple. Thus, we suggest a second method which is particularly applicable to good-quality coherent ELT signals.

2.4.2 Integrated Average Method

In order to obtain a more reliable estimate of these parameters, we introduce the following function:

$$L(f) = \int S_{AV}(f)\,df \tag{2.7}$$

where $S_{AV}(f)$ is the average spectrum. The closed expression of eq. (2.7) is rather difficult to obtain and therefore we shall employ numerical integration method.

If L(f) is plotted versus f for the testbed signals used earlier, it produces very smooth curves as shown in Fig. 2.13 through Fig. 2.16. Comparing Fig. 2.9 with Fig. 2.13, we conclude the following points:

1. The background interference level of the average spectrum in Fig. 2.9 corresponds to a line with slope a_1 for $f < f_1$ and slope a_7 for $f > f_6$, as shown in Fig. 2.13.
2. As the level of $S_A(f)$ increases, the slope of L(f) also increases. Hence, the lower sideband starts at frequency f_1 which indicates the point of change of the slope (corner frequency). In the frequency band f_1 to f_2 the slope is almost constant and equal a_2. This region corresponds to W_1, i.e.,

$$W_1 = f_2 - f_1 \tag{2.8}$$

Similarly the region from f_5 to f_6 with slope a_6 represents the upper sideband and the width W_2 can be obtained by:

$$W_2 = f_6 - f_5 \tag{2.9}$$

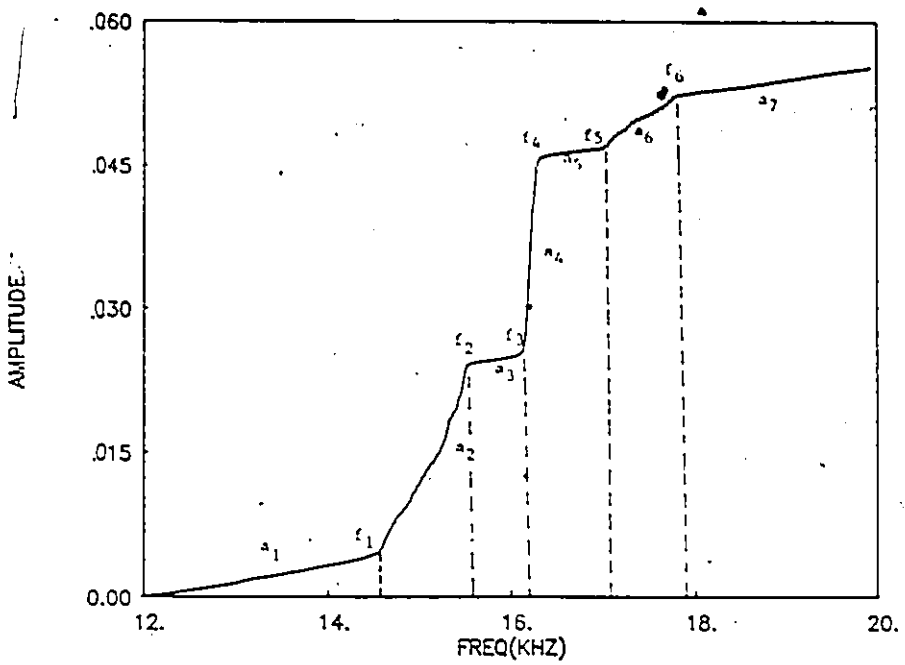

Fig. 2.13 Plot of the integral function L(f) for Pointer signal.

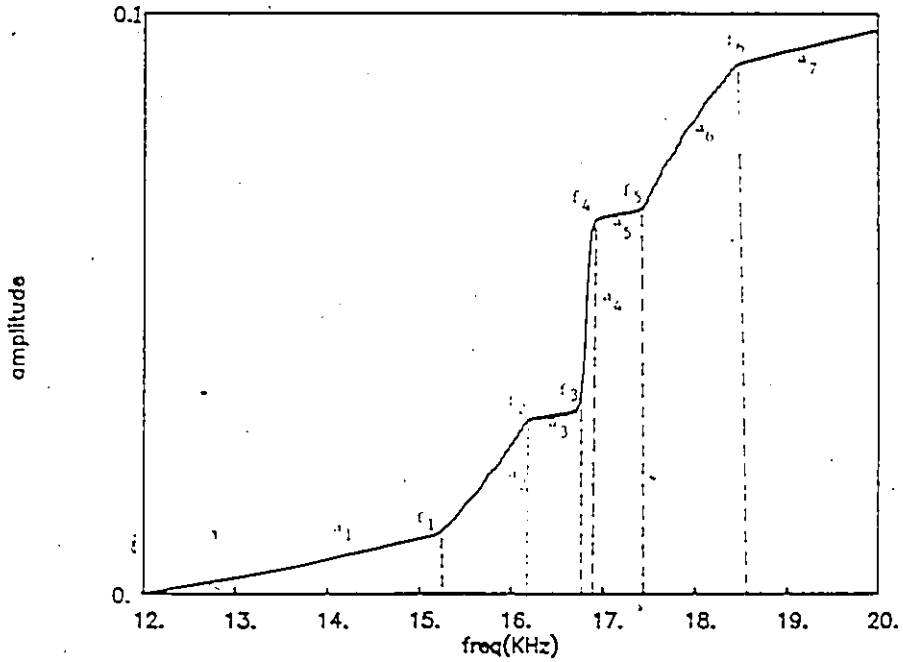

Fig. 2.14 Plot of the integral function L(f) for Garrett signal.

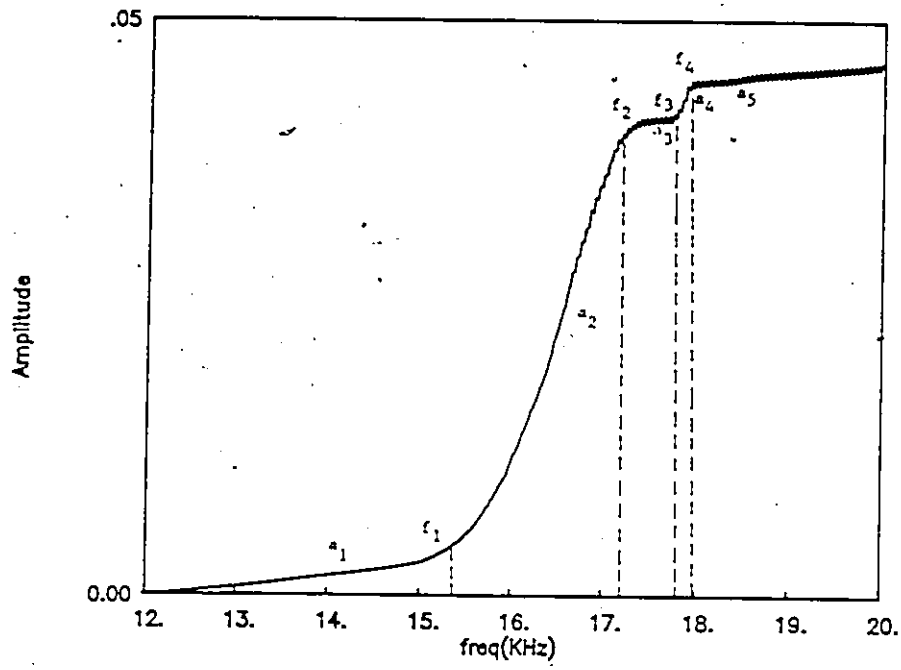

Fig. 2.15 Plot of the integral function L(f) for Narco ELT17 signal.

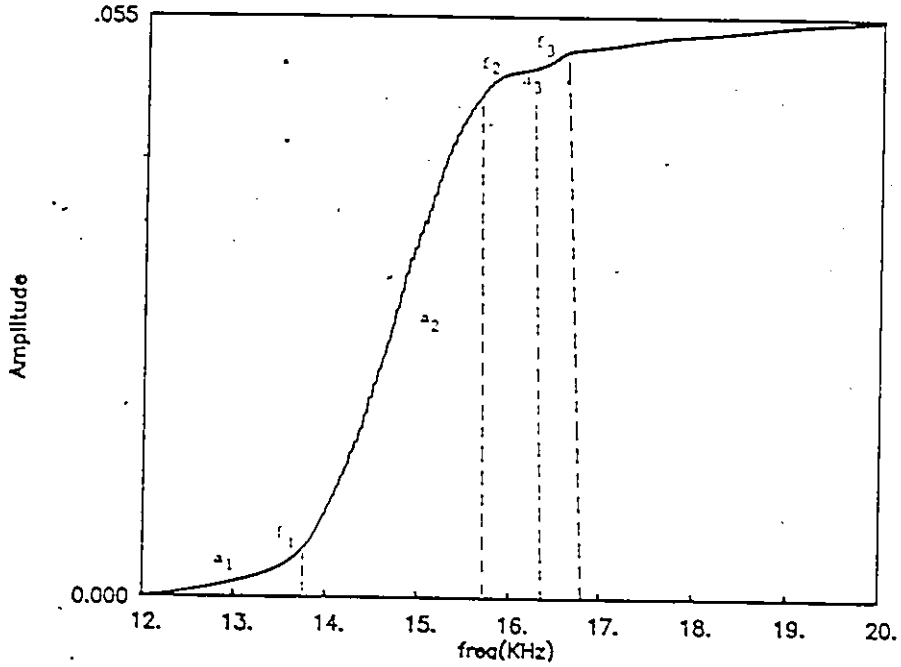

Fig.2.16 Plot of the integral function L(f) for Narco ELT19 signal.

Note that the slope a_2 in Fig. 2.13 is greater than the slope a_6. This indicates that the level of the lower sideband is higher than that of the upper sideband for the Pointer ELT signal. The sideband plateaus B_1 and B_2 can be estimated by averaging the spectrum of Fig. 2.9 over the frequency bands f_1 to f_2 and f_5 to f_6, respectively.

3. The regions from f_2 to f_3 and f_4 to f_5 in Fig. 2.13 have slopes a_3 and a_5 respectively and represent the deep valleys on both sides of the carrier.

4. The largest slope a_4 (between f_3 and f_4) represents the peak of the spectrum due to the carrier.

5. It is noticeable that L(f) has a distinctive characteristic in the region f_2 to f_5 which can be considered as a special signature of ELT signals.

The L(f) for the Garrett signal depicted in Fig. 2.14 is similar to that of the Pointer except now the slopes a_2 and a_6 are comparable indicating that both lower and upper sidebands have approximately the same level. On the other hand, both Narco ELT17 and ELT19 signals, which have poorer quality, give quite different results as shown in Figs. 2.15 and 2.16. In these figures, the lower sideband is dominant and the upper sideband almost vanishes and it is difficult to detect the change of the slope beyond f_5. The width of the lower sideband can still be measured using eq. (2.8).

The measurement of the corner frequencies f_i and the different slopes a_i of L(f) can be carried out by forming the following function:

$$L_c(f) = \begin{cases} a_1 f & , \quad 0 < f < f_1 \\ a_1 f_1 + a_2(f - f_1) & , \quad f_1 < f < f_2 \\ a_1 f_1 + a_2(f_2 - f_1) + \ldots + a_i(f - f_{i-1}) , & \quad f_{i-1} < f < f_i \end{cases} \tag{2.10}$$

with the corresponding error function given by:

$$e = L_c(f) - L(f) \tag{2.11}$$

where L(f) is the observed function as obtained from equation (2.7) and $L_e(f)$ is the explicit function of eq. (2.10). Note that an optimization package could be employed to deduce the best-fit of a_i and f_i values which would then be included as signature parameters. Thus, the evaluation of these parameters is carried out in an automatic manner.

2.5 Summary

(1) The spectral estimation techniques are reviewed. Those are the periodogram and the averaged periodogram.

(2) Some identification parameters of ELT signals are introduced; namely, the sweep period, the sweep width and the ratios of the sideband levels to the carrier level.

(3) The average spectrum and the integration of the average spectrum are introduced as identification techniques to estimate the sweep width and the ratios of side band levels to the carrier level.

CHAPTER 3

EVALUATION OF THE SWEEP PERIOD

3.1 Overview

In this chapter, two methods for estimating the sweep period are developed along with their theoretical analysis. The first, is the sawtooth method which is effective for high values of signal-to-noise (SNR) ratio and the second is the crosscorrelation method which is suitable for the noisy environment. An upper bound for the error in estimating T_s is provided. Also, the methods are tested using both computer and real testbed signals.

3.2 Theoretical Analysis

3.2.1 Sawtooth Method

The modulation frequency sweep as a function of time has a sawtooth waveform. To plot this waveform, the carrier frequency f_c is estimated first. The signal x(t) is divided into M segments. The periodogram of each segment is calculated. Knowing that each segment corresponding to a certain period of time (i.e. 1024 point FFT ≈ 10 ms.), the difference between the estimated carrier frequency f_c and the lower sideband peak (or upper sideband peak) frequency f_L (or f_H) is determined for each segment and plotted versus time, yielding a sawtooth waveform, shown in Fig. 3.1.

The average sawtooth period (sweep period) is then given by

$$T_s = \frac{1}{k} [T_{s1} + T_{s2} + T_{s3} - - - T_{sk}] \tag{3.1}$$

where k is the number of sawtooth periods within the processed data. Moreover, the height of the sawtooth is a measure of the sweep width, W_1 (or W_2).

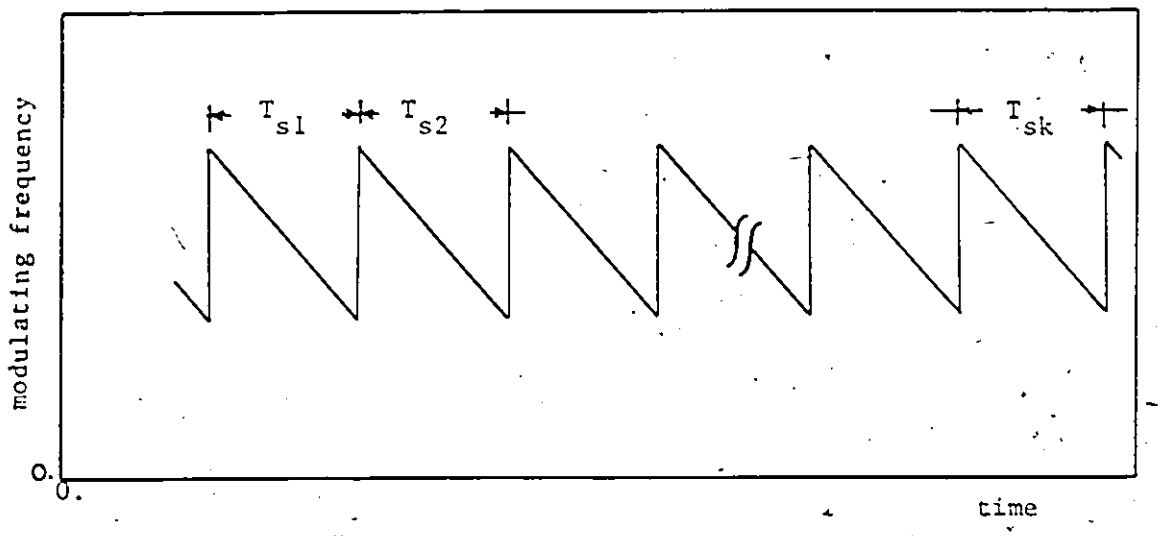

Fig. 3.1 Plot of the sweep frequency versus time for hypothetical ELT signal.

This method is very simple but unfortunately in the presence of noise, spurious peaks occur that may lead to false estimation of the sideband position. Thus, the use of this method is limited to the noiseless or very high values of signal to noise (SNR) ratio cases. A second method is introduced in the following section, which is considered robust in the noisy case.

3.2.2 Crosscorrelation Method

This method is based on the fact that the spectrum of any segment is repeated after approximately the sweep period T_s. It is seen that there is a strong correlation between the spectrum at time t_1 and the spectrum at time $t_1 + T_s$. In the following we will derive an expression for the crosscorrelation function.

In this approach the signal x(t) is divided into M segments each of duration T_{seg} and the pulse-null periods are considered constant within each segment, but differing from one segment to the next as shown in Fig. 3.2. Therefore x(t) can be expressed in the form:

$$x(t) = \sum_{m=1}^{M} x_m(t) \tag{3.2}$$

Two cases can be considered. The first assumes the number of pulse-null pairs within each segment is infinite. Although this is a hypothetical case, it is discussed because it will clarify the main concepts in a simple way. The second case, which is the actual case, assumes the number of pulse-null pairs within one segment to be limited to N pairs. The spectrum of each segment will be derived for both cases.

a) <u>Infinite Number of Pulse-Null Pairs</u>

Each segment can be represented by:

$$x_m(t) = \sum_{i=-\infty}^{\infty} x_{mi}(t) \tag{3.3}$$

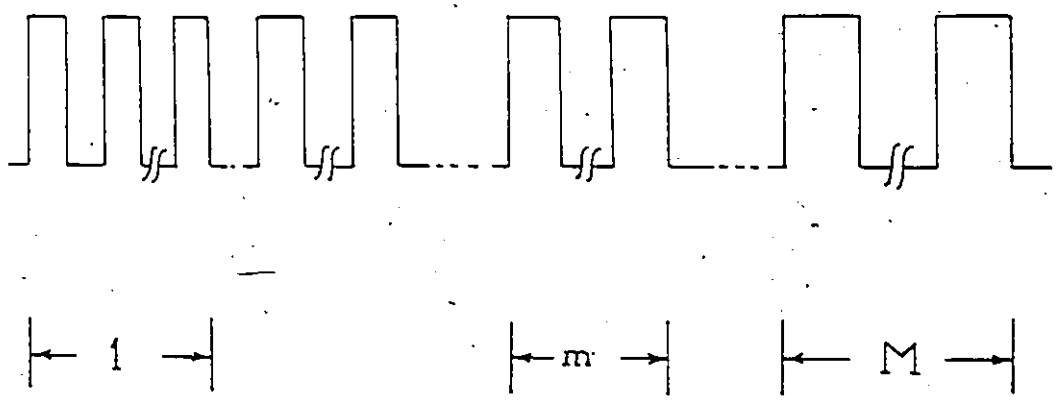

Fig. 3.2 The signal is divided into M segments. No variation in pulse-null periods within each segment.

where $x_{mi}(t)$ is the signal for the ith pulse-null pair of the mth segment. Therefore $x_{mi}(t)$ is given by:

$$x_{mi}(t) = \begin{cases} A\cos(2\pi f_c t + \theta_{mi}) \; ; & t_{mi} - \dfrac{dT_{mi}}{2} \le t \le t_{mi} + \dfrac{dT_{mi}}{2} \\ 0 \; ; & \text{elsewhere} \end{cases} \tag{3.4}$$

where A = amplitude of the signal

f_c = carrier frequency

T_{mi} = the duration of the ith pulse-null pair of the mth segment

d = duty ratio

θ_{mi} = phase shift of the ith pulse of the mth segment.

The Fourier transform of the ith pulse is given by

$$X_{mi}(f) = \frac{AdT_{mi}}{2} \operatorname{sinc}\left\{(f-f_c)\,dT_{mi}\right\} \tag{3.5}$$

Hence, the Fourier transform of the mth segment of infinite pulse-null pairs is

$$X_m(f) = \sum_{i=-\infty}^{\infty} X_{mi}(f)$$

$$= \sum_{i=-\infty}^{\infty} \frac{AdT_{mi}}{2} \operatorname{sinc}\left[(f-f_c)\,d\,T_{mi}\right] \exp\left(2\pi f t_{mi} - \theta_{mi}\right) \tag{3.6}$$

At $f = f_c$ the exponential must be maximum (i.e. equal unity), this implies that

$$\theta_{mi} = 2\pi f_c t_{mi} \tag{3.7}$$

According to the assumption of constant pulse-null duration within the mth segment ($T_{mi} = T_m$), t_{mi} is given by

$$t_{mi} = i\,T_m \tag{3.8}$$

substituting in eq. (3.6) we find that:

$$X_m(f) = \frac{AdT_m}{2} \operatorname{sinc}\left\{(f-f_c)\,d\,T_m\right\} \sum_{i=-\infty}^{\infty} \exp\left\{-j\,2\pi(f-f_c)\,i\,T_m\right\} \tag{3.9}$$

The spectrum of the mth segment is defined by

$$S_m(f) = \left| X_m(f) \right|^2 \tag{3.10}$$

Using the identity

$$\sum_{i=-\infty}^{\infty} \exp\left(-j\,2\pi\,(f-f_c)\,i\,T_m\right) = \frac{1}{T_m} \sum_{k=-\infty}^{\infty} \delta\left(f-f_c-\frac{k}{T_m}\right)\Bigg\} \tag{3.11}$$

And since

$$\left| \sum_{k=\infty}^{\infty} \delta\,(f-f_c-\frac{k}{T_m}) \right|^2 = \sum_{k=\infty}^{\infty} \delta\left(f-f_c-\frac{k}{m}\right)\Bigg\}$$

we find that

$$S_m(f) = \left(\frac{Ad}{2}\right)^2 \mathrm{sinc}^2\left\{(f-f_c)d\,T_m\right\} \sum_{k=-\infty}^{\infty} \delta\left(f-f_c-\frac{k}{T_m}\right) \tag{3.12}$$

Thus, the spectrum is just a product of two quantities, the first being a sinc function which has a peak at f_c, and the second is a series of delta functions spaced by $(1/T_m)$. The two quantities are shown in Fig. 3.3a and 3.3b for f_c = 16 kHz and T_m = 1 ms. The spectrum of the mth segment $S_m(f)$ is shown in Fig. 3.3c.

Figure 3.4 shows the spectra of three different segments along the sweep, from which we see that the carrier peak always occurs at the same frequency. Note that the locations of the sidebands differ from one segment to another. Therefore if the crosscorrelation of the first and second spectra is performed, the sidebands will be cancelled and only a delta function at the carrier frequency is obtained. On the other hand, if the autocorrelation of the first spectrum is obtained, it is much larger than the crosscorrelation between the first and second. This idea is exploited by defining the following crosscorrelation function $R_m(\ell)$

$$R_m(\ell) = \sum_{j=j_1}^{j_2} S_m(f_j)\; S_{m+\ell}(f_j) \tag{3.13}$$

where

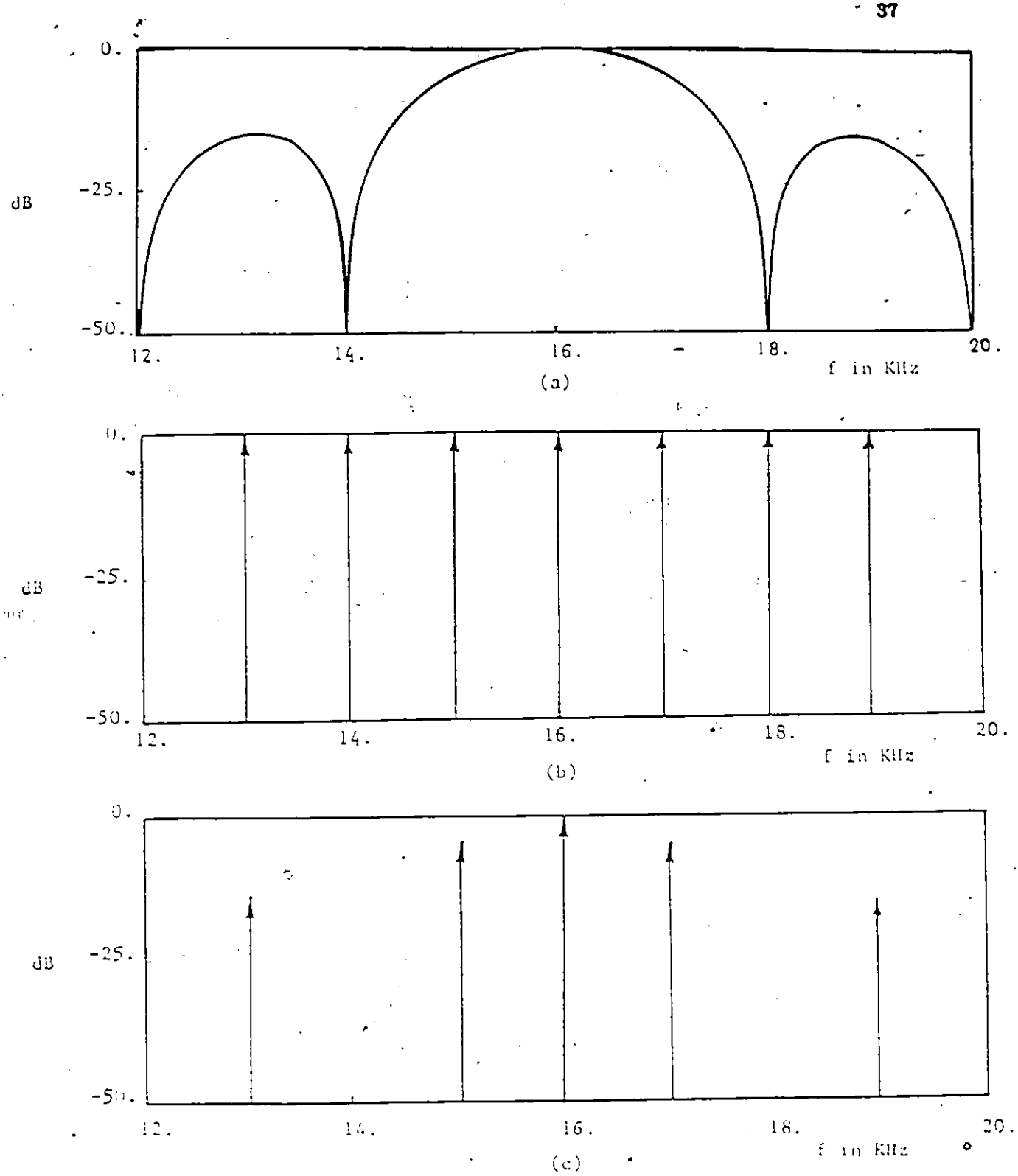

Fig. 3.3 (a) Plot of $\text{sinc}^2[(f-f_c)\,d\,T_m]$ for $f_c = 16$ kHz, $d = 0.5$, and $T_m = 1$ ms.
(b) Plot of a set of delta functions spaced in frequency by $1/T_m$.
(c) Plot of $S_m(f)$.

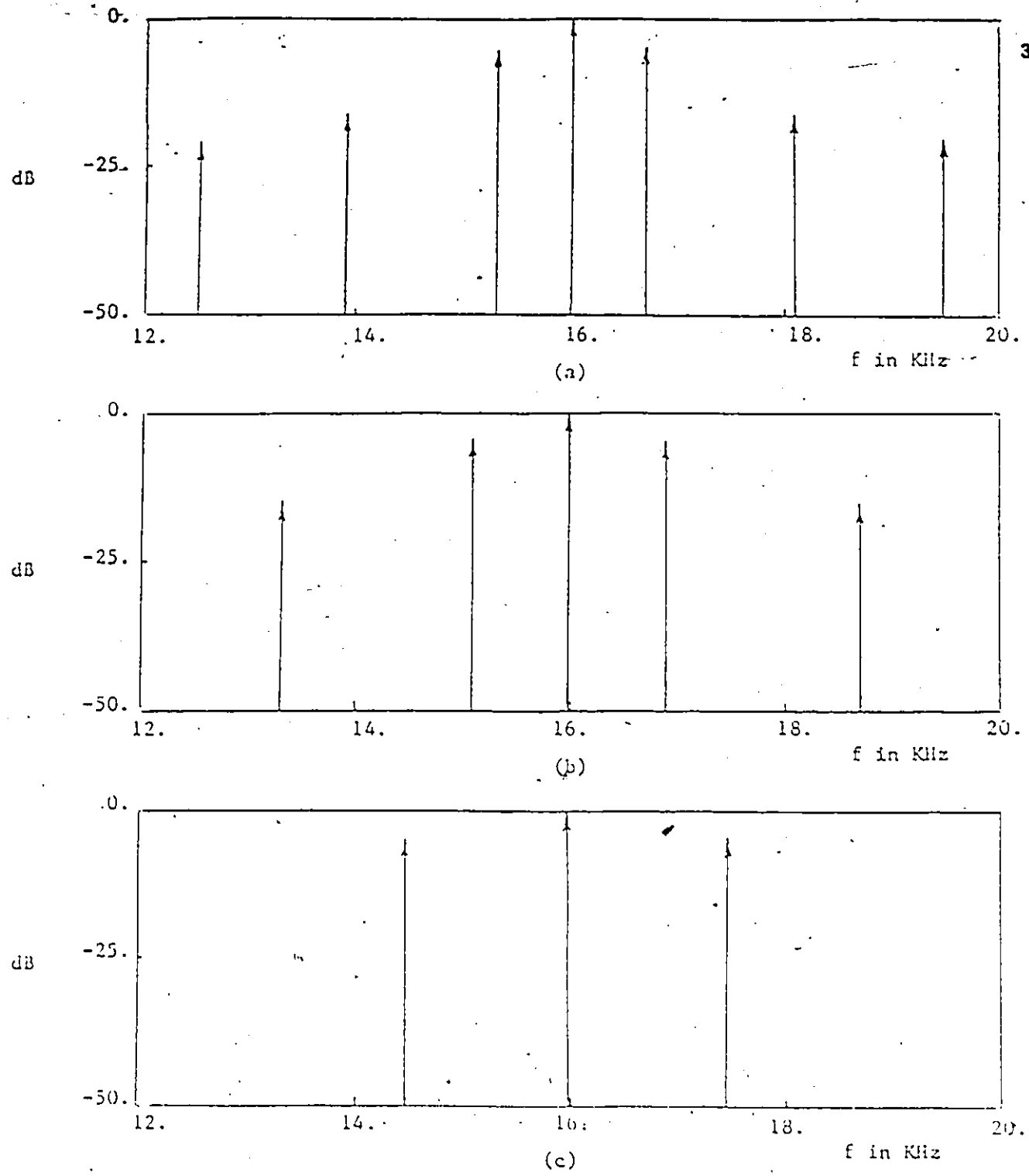

Fig. 3.4 Spectra of three different segments with f_c = 16 kHz and d = 0.5 for three different values of T_m.
(a) T_m = 1.42 ms.
(b) T_m = 1.11 ms.
(c) T_m = 0.67 ms.

f_{j_1}, f_{j_2} = the chosen frequency band edges within the bandwidth of the signal x(t). The choice of this band depends on the expected location of the received signal.

ℓ = the crosscorrelation lag $0 < \ell < M - 1$

Substituting eq. (3.12) into eq. (3.13) we get

$$R_m(\ell) = \sum_{j=j_1}^{j_2} \left[\left(\frac{Ad}{2} \right)^4 \mathrm{sinc}^2\left\{ (f_j - f_c)\, d\, T_m \right\} \mathrm{sinc}^2\left\{ (f_j - f_c)\, d\, T_{m+\ell} \right\} \right.$$

$$\left. \cdot \sum_{k=-\infty}^{\infty} \sum_{i=-\infty}^{\infty} \delta\left(f_j - f_c - \frac{k}{T_m} \right) \delta\left(f_j - f_c - \frac{i}{T_{m+\ell}} \right) \right] \tag{3.14}$$

Note that

$$\delta\left(f_j - f_c - \frac{k}{T_m} \right) \delta\left(f_j - f_c - \frac{i}{T_{m+\ell}} \right) = \begin{cases} 0 & \frac{k}{T_m} \neq \frac{i}{T_{m+\ell}} \\ \delta\left(f_j - f_c - \frac{k}{T_m} \right); & \frac{k}{T_m} = \frac{i}{T_{m+\ell}} \end{cases} \tag{3.15}$$

Note that each segment corresponds to a period of time equal T_{seg}. Then, the time lag τ of the crosscorrelation is

$$\tau = \ell\, T_{seg} \tag{3.16}$$

Let L_s denote the number of spectra corresponding to one sweep period T_s, thus

$$T_s = L_s\, T_{seg} \tag{3.17}$$

Therefore when $\tau = nT_s$ (i.e. $\ell = nL_s$), the spectrum of the mth segment is very close in shape to the spectrum of $(m + nL_s)$th segment i.e.

$$S_m(f) \approx S_{m+nL_s}(f)$$

$$\text{and} \qquad T_m \approx T_{m+nL_s} \tag{3.18}$$

Taking into account that $S_m(f)$ is a series of delta functions as shown in Figure 3.3c, the crosscorrelation $R(\ell)$ will be maximum at $\ell = nL_s$, $(n = 0,1,2,\ldots)$. Therefore the plot of $R(\ell)$ versus ℓ produces a periodic pattern with period L_s (i.e. time period of T_s), as shown in

Fig. 3.5. Note the delta functions with reduced strength that are randomly located between the main peaks. These can be explained using eq. (3.15), from which we find that $R(\ell)$ has values other than zero only when $(T_m/T_{m+\ell})$ forms a ratio of integer values. Consider Fig. 3.6 where two spectra with 16 kHz carrier frequency are plotted. The first has pulse-null period of 2 ms and the second has pulse-null period of 1.5 ms and both have a duty ratio d = 0.4. A portion of the sidebands of the two spectra are aligned with each other (at f = 14 kHz and 18 kHz), resulting in the existence of a relatively low peak in the crosscorrelation function. This alignment occurs only if the ratio $T_m/T_{m+\ell}$ is an integer.

b) Finite Number of Pulse-Null Pairs

Consider the number of pulse-null pairs to be limited to N. This modifies eq. (3.9) yielding:

$$X_m(f) = \frac{AdT_m}{2} \operatorname{sinc}\left\{(f-f_c)\,dT_m\right\} \sum_{i=0}^{N-1} \exp\left\{-j2\pi(f-f_c)\,iT_m\right\} \tag{3.19}$$

The last term is just a geometric progression which can be summed by a conventional method to give

$$\sum_{i=0}^{N-1} \exp\left\{-j2\pi(f-f_c)\,iT_m\right\} = \frac{1-\exp[-j2\pi(f-f_c)NT_m]}{1-\exp[-j2\pi(f-f_c)T_m]} \tag{3.20}$$

Therefore, the spectrum is given by:

$$S_m(f) = \left(\frac{AdT_m}{2}\right)^2 \operatorname{sinc}^2\left\{(f-f_c)\,dT_m\right\} \left\{\frac{\sin(\pi(f-f_c)NT_m)}{\sin(\pi(f-f_c)T_m)}\right\}^2 \tag{3.21}$$

Now, the term:

$$\left\{\frac{\sin(\pi(f-f_c)NT_m)}{\sin(\pi(f-f_c)T_m)}\right\}^2$$

is plotted versus frequency as shown in Fig. 3.7, which is a multi-peak pattern, with peaks being located at $f = f_c \pm k/T_m$, $k = 1, 2, 3, \ldots\ldots$ instead of series of impulses given in Fig. 3.3b.

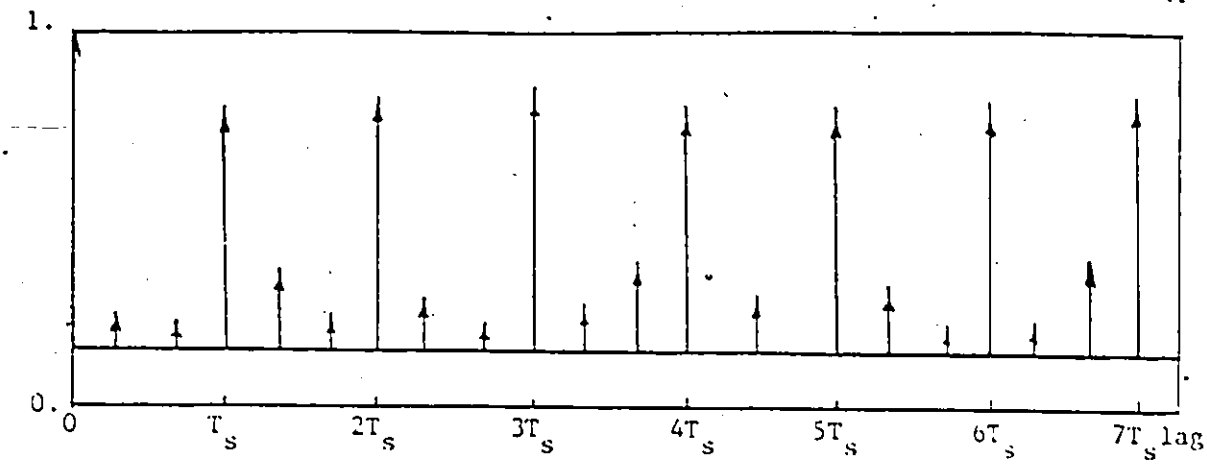

Fig. 3.5 Crosscorrelation function versus time-lag, where T_s is the sweep period.

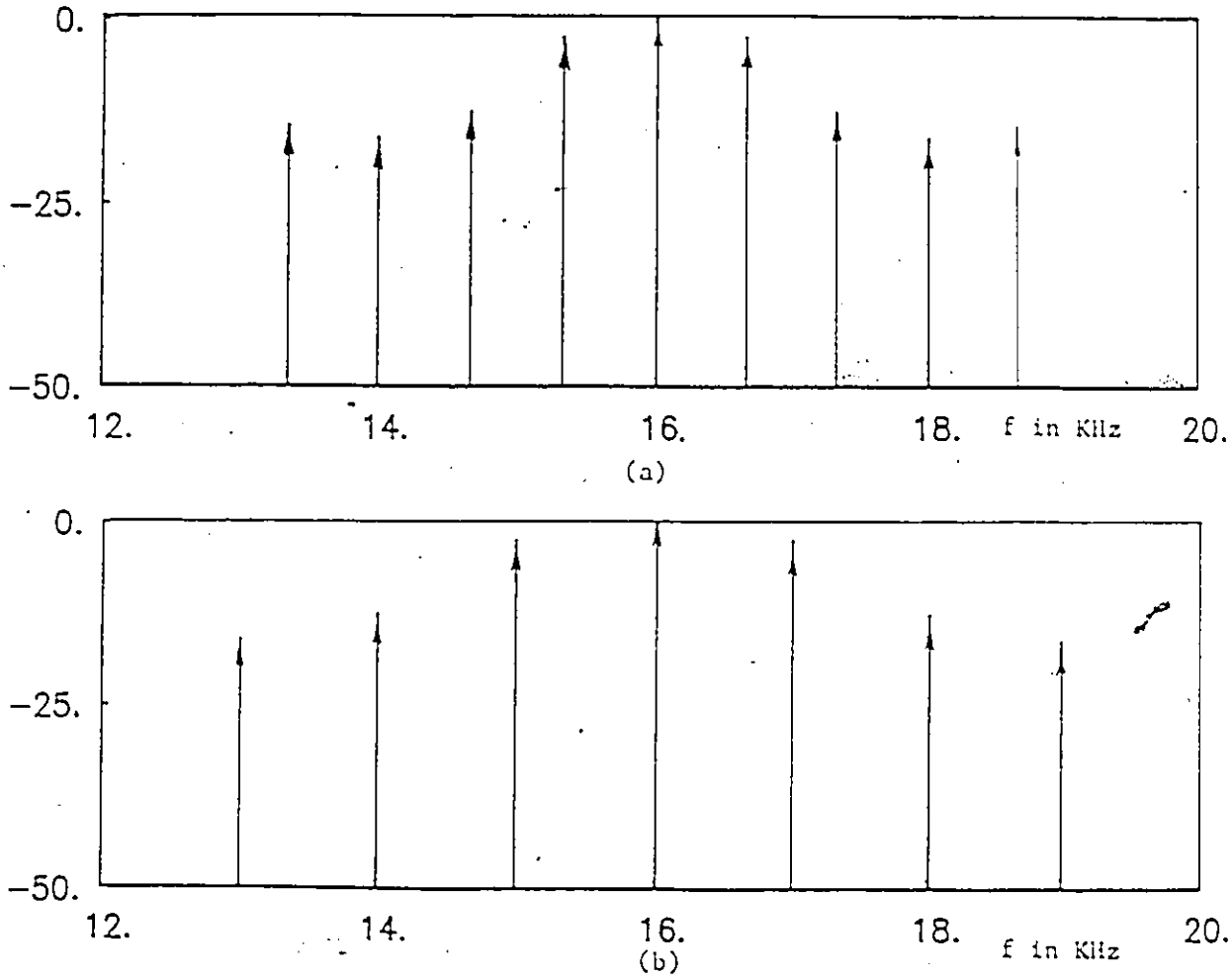

Fig. 3.6 Plot of $S_m(f)$ for $f_c = 16$ kHz, d = 0.4 and two values of T_m.
(a) $T_m = 2$ ms.
(b) $T_m = 1.5$ ms.

The crosscorrelation with finite pulse-null pairs can be obtained by substituting eq. (3.21) in eq. (3.13), yielding

$$R_m(\ell) = \sum_{j=j_1}^{j_2} \left[\left(\frac{AdT_m}{2} \right)^4 \mathrm{sinc}^2 \left\{ (f_j - f_c) dT_m \right\} \cdot \mathrm{sinc}^2 \left\{ (f_j - f_c) dT_{m+\ell} \right\} \right.$$

$$\left. \cdot \left\{ \frac{\sin [\pi (f_j - f_c) NT_m)}{\sin [\pi (f_j - f_c) T_m)} \right\}^2 \cdot \left\{ \frac{\sin (\pi (f_j - f_c) NT_{m+\ell})}{\sin (\pi (f_j - f_c) T_{m+\ell})} \right\}^2 \right] ; \; 0 \le \ell \le m - k \tag{3.22}$$

A plot of the crosscorrelation versus lag is shown in Fig. 3.8 by a dashed line, which is the envelope of the crosscorrelation pattern under the assumption of infinite pulse-null pairs.

On applying the above method directly to real data, we find that the pattern obtained using the crosscorrelation of just two spectra may yield a large number of spurious peaks and the sweep period is not well defined. In order to obtain smooth plots, we choose a small number of contiguous spectra and perform the correlation with this set. The correlator selects the first K records (reference spectra) of individual spectra and performs a time correlation with the entire record. Whenever the K-record set matches the main set, a peak is produced at the output of the correlator. Otherwise, destructive interference occurs in the correlation and the output of the correlator is reduced. In this case the modified crosscorrelation is given by:

$$R_T(\ell) = \sum_{m=1}^{K} R_m(\ell) \quad 0 \le \ell \le M - K \tag{3.23}$$

3.3 Application to ELT Signals

In this section both the sawtooth and the crosscorrelation methods are tested using simulated and testbed signals. Both methods are applied to simulated ELT signals at different carrier-to-noise density ratio (CNDR) values in order to evaluate their performance in the noisy environment. Also the proposed techniques are applied to real testbed signals to

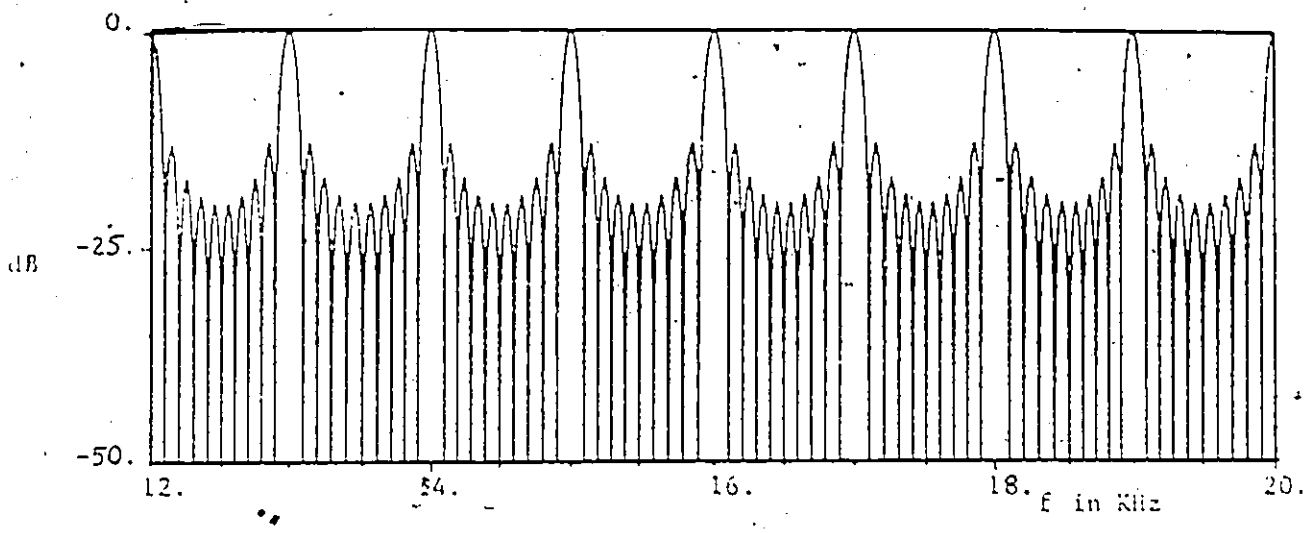

Fig. 3.7 Plot of the square of the ratio of two sine functions for f_c = 16 kHz, N = 10 and T_m = 1 ms.

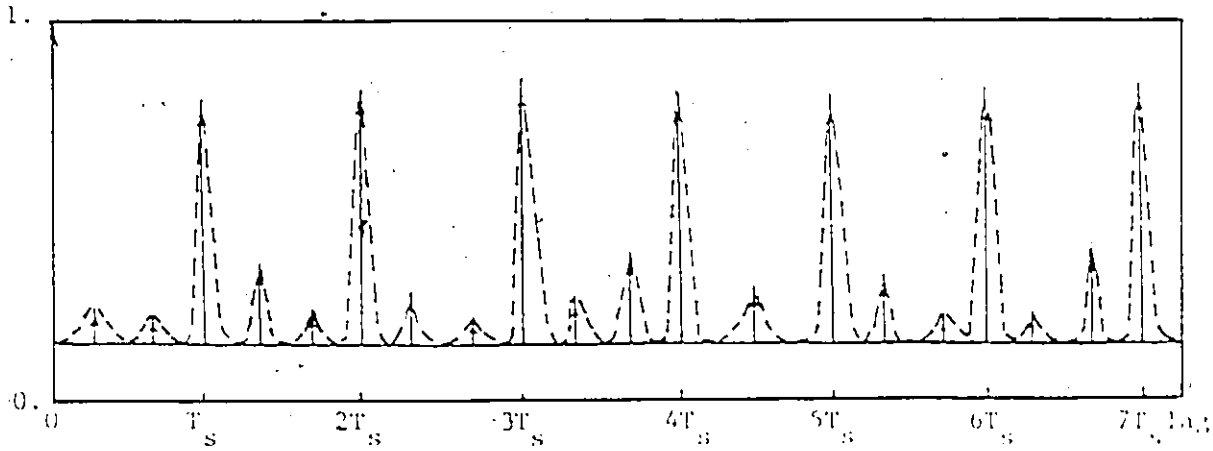

Fig. 3.8 The crosscorrelation function versus time lag for infinite number of pulse-null pairs (solid line) and finite number of pulse-null pairs (dashed line).

show the change in the sweep period from one ELT unit to another even within the same manufacturer.

For both simulated and testbed signals, a 2 s of data sampled at 100 kHz are used. The data points are divided into 200 segments (1024 points each) and their corresponding periodograms are obtained in order to get the sawtooth and crosscorrelation curves. For automatic estimation of the sweep period, a 1024-point FFT of this curve is obtained by padding the available 200 points with zeroes.

3.3.1 Carrier-to-Noise Density Ratio (CNDR)

For SARSAT signals, the carrier-to-noise density ratio (CNDR) is used as a measure of signal in a noisy background. This can be defined by the relation

$$\mathrm{CNDR} = \frac{A^2}{2\,N_o} \tag{3.24}$$

where A is the amplitude of the ELT signal and N_o is the noise spectral density. It has been shown that the CNDR can be related to standard signal-to-noise ratio (SNR) by [11]

$$\mathrm{CNDR} = \frac{\mathrm{SNR}}{2\,d\,T_D} \tag{3.25}$$

where d is the duty cycle of the ELT signal and T_D is the window length of data.

Normally, detection takes place when the SNR exceeds approximately 10 dB. Using d = 0.5 and T_D = 10 ms (1 K periodogram with sampling rate 100,000 samples per second), we find that the CNDR level required for detection is 30 dB-Hz [9].

3.3.2 Error in Sweep Period Estimate Due to FFT

There are two sources that incorporate error in estimating the sweep period T_s. The first (ΔT_{s1}) is due to the use of a finite duration spectrum calculated by the periodogram. The spectrum is considered periodic with a period of T_s, while it is calculated in discrete steps.

In each step, we use a certain number of data points which is equivalent to a period, say T_1. In general, T_s/T_1 is not an integer value and therefore error may occur.

The second source of error (ΔT_{s2}) is due to the use of the FFT applied to the cross-correlation sequence to find T_s. Also, the FFT is calculated at discrete values, thus an error could take place.

Here, we shall find an upper bound of the error in T_s (ΔT_{smax}) estimate due to the above factors.

- <u>Calculation of ΔT_{s1}</u>

Assume that the periodogram is calculated for data segments, each with length T_{seg} second. Then, the error in T_s can be simply calculated by noting

$$\Delta T_{s_1} \leq T_{seg}/2 \qquad \text{or equivalently,}$$

$$\Delta T_{s_1} \leq \frac{N_{seg}}{2 F_{samp}} \tag{3.26}$$

where N_{seg} is the number of points within each segment and F_{samp} is the sampling frequency of the received ELT signal.

- <u>Calculation of ΔT_{s2}</u>

Assume that we obtain the crosscorrelation sequence for N_L lags. When the FFT is applied to the crosscorrelation data, we get a frequency resolution of

$$\Delta f = \frac{1}{N_L T_{seg}} \tag{3.27}$$

where T_{seg} corresponds to the period between successive crosscorrelation points.

$$\Delta f = \frac{F_{samp}}{N_L T_{seg}} \tag{3.28}$$

The FFT error is then calculated as:

$$\Delta F_s \leq \frac{\Delta f}{2} = \frac{F_{samp}}{2N_L N_{seg}} \tag{3.29}$$

Since we estimate the sweep period T_s by its reciprocal F_s, we can find the error ΔT_{s2} as follows:

$$T_s = \frac{1}{F_s}$$

$$\therefore |\Delta T_{s_2}| \leq \left| \frac{\partial T_s}{\partial F_s} \right| \cdot |\Delta F_s|_{max}$$

$$\leq \frac{1}{F_s^2} |\Delta F_s|_{max}$$

$$= T_s^2 \cdot \frac{F_{samp}}{2N_L N_{seg}} \tag{3.30}$$

Combining equations 3.26 and 3.30, the total error can be bounded by:

$$\Delta T_s \leq \frac{N_{seg}}{2F_{samp}} + \frac{F_{samp}}{2N_L N_{seg}} \cdot T_s^2 \tag{3.31}$$

$$\frac{\Delta T_s}{T_s} \leq \frac{N_{seg}}{2F_{samp} \cdot T_s} + \frac{F_{samp}}{2N_L N_{seg}} \cdot T_s \tag{3.32}$$

The number of points N_{seg} is chosen to minimize the total error ΔT_s and can be calculated as follows

$$\frac{\partial\left(\frac{\Delta T_s}{T_s}\right)}{\partial N_{seg}} = \frac{1}{2F_{samp} \cdot T_s} - \frac{F_{samp} \cdot T_s}{2N_L N_{seg}^2}$$

$$= 0 \tag{3.33}$$

$$\therefore (N_{seg})_{optimum} = F_{samp} \cdot T_s \cdot \sqrt{\frac{1}{N_L}} \tag{3.34}$$

In our application to ELT signals, we choose the number of lags equal to 200 and pad with by zeroes to form 1024 points. Therefore, $N_L = 1024$ to improve the resolution of the

FFT. For $F_{samp} = 100$ kHz and $T_s = 0.3$ s, the value of N_{seg} used is 1024 point. For the above values, the error is given by:

$$\frac{\Delta T_s}{T_s} \leq 0.017 + 0.0143$$

$$\leq 0.0314$$

$$\leq 3.14\,\% \tag{3.35}$$

3.3.3 Simulated ELT Signals

The ELT signals are simulated using the frequency-pulled noncoherent model [6], which reflects the operation of most of the actual ELT units. In this case, it is assumed that the crystal controlled oscillator (Fig. 1.5) operates at frequency f_c when the switch is closed and $f_c + f_p$ when the switch is open due to the problems previously discussed. Therefore the signal for the ith pulse-null pair can be expressed as:

$$x_i(t) = \begin{cases} A\cos(2\pi f_c t + \theta_i) & t_i - \dfrac{dT_i}{2} \leq t < t_i + \dfrac{dT_i}{2} \\ 0 & \text{elsewhere} \end{cases} \tag{3.36}$$

where T_i is the duration of the ith pulse-null pair and t_i is the time shift from the centre of the first pulse to the centre of the ith pulse.

The phase shift θ_i for the ith pulse is given by

$$\theta_i = 2\pi f_c t_i + \sum_{j=1}^{i-1} 2\pi f_p (1-d) T_i \tag{3.37}$$

and $f_p(1-d) = f_s$ defined to be the frequency shift.

By changing the duty ratio d as well as the frequency shift f_s, it is possible to obtain different types of ELT signals corresponding to different manufacturers. For example, for $f_p = 1$ kHz and $d = 0.5$, it is found that the carrier occurs at a constant frequency and the first upper and lower sidebands slide reasonably smoothly toward the carrier with time. The

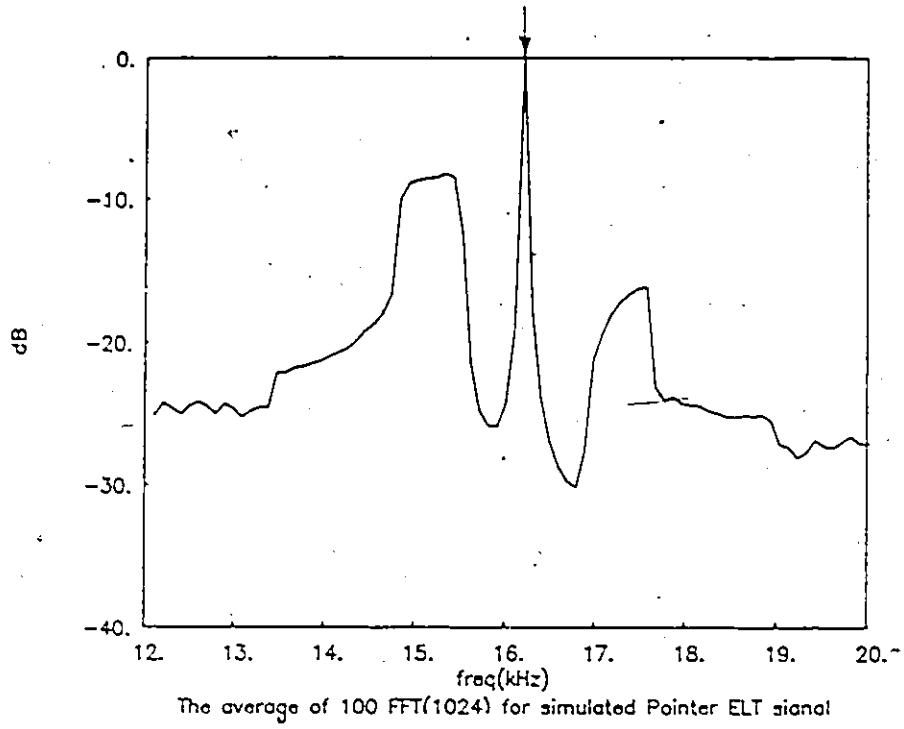

Fig. 3.9 Average of 100 1 k-periodogram for simulated Pointer ELT signal.

average of 100 1 K-point periodograms (1 s) of this signal is shown in Fig. 3.9. Comparing this figure with the average spectrum of the real Pointer ELT signal Fig. 2.9, we find that:

(1) The carrier peaks are both well defined.

(2) The lower sidebands are approximately 10 dB below the carrier peak.

(3) The upper sidebands are approximately 15 dB below the carrier peak.

Consequently, the modelled signal accurately represents the actual ELT signal.

The sawtooth method is applied for the simulated Pointer signal with sweep period $T_s = 0.3$ s and CNDR 47 dB-Hz, and the corresponding curve is depicted in Fig. 3.10a. The periodicity of the pattern is clear and the sweep period can be estimated easily. The FFT is applied to the sawtooth curve and the resulting spectrum is shown in Fig. 3.10b where the arrow indicates the sweep frequency F_s ($F_s = 1/T_s$). The estimated sweep period T_s from this figure is 0.292 s with an error of 2.6% which lies within the error bound. On the other hand, Fig. 3.11 gives the sawtooth curve and its periodogram for the same signal but at CNDR = 32 dB-Hz. In this case, the sawtooth method fails to give an estimate of the sweep period as expected from low values carrier-to-noise density ratios. The lowest CNDR for the application of the sawtooth method is seen to be 40 dB-Hz.

Similar curves for the crosscorrelation method as applied to the simulated pointer are shown in Figs. 3.12 and 3.13 for CNDR = 47 and 32 dB-Hz respectively. It is clearly seen that the crosscorrelation method estimates the sweep period to be 0.292 s in both cases and it is effective down to approximately 30 dB-Hz. Of course, this achievement is at the expense of higher computation complexity.

Now if f_p and d are changed, we can simulate the Garrett ELT signal. Figure 3.14 demonstrates the sawtooth and crosscorrelation for $T_s = 0.28$ s, $f_p = -0.5$ kHz and d = 0.36. The estimated sweep period is 0.271 s.

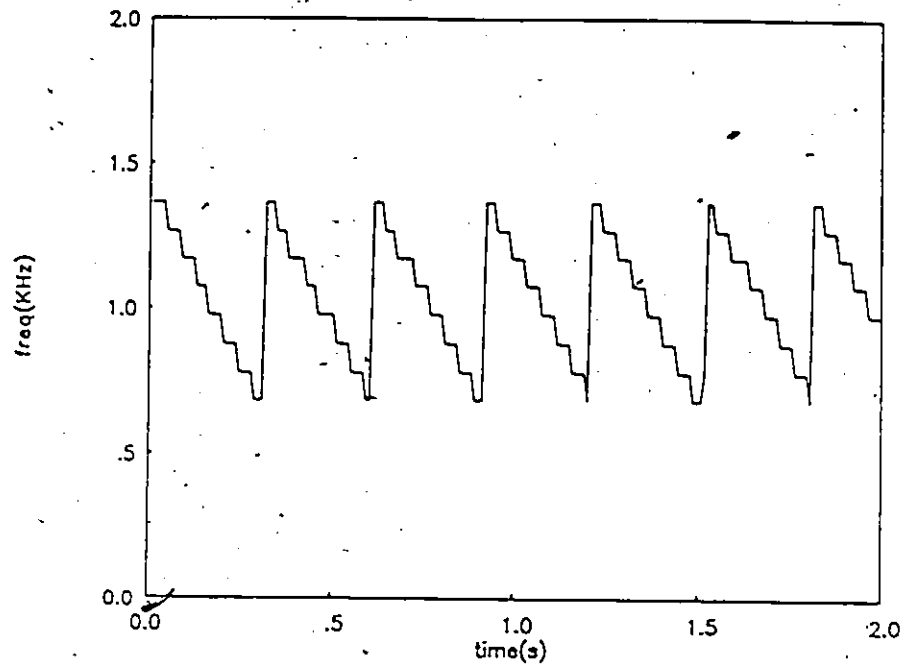

Sawtooth curve for simulated Pointer ELT (Ts=.3s & CNDR=47 dB-Hz)

(a)

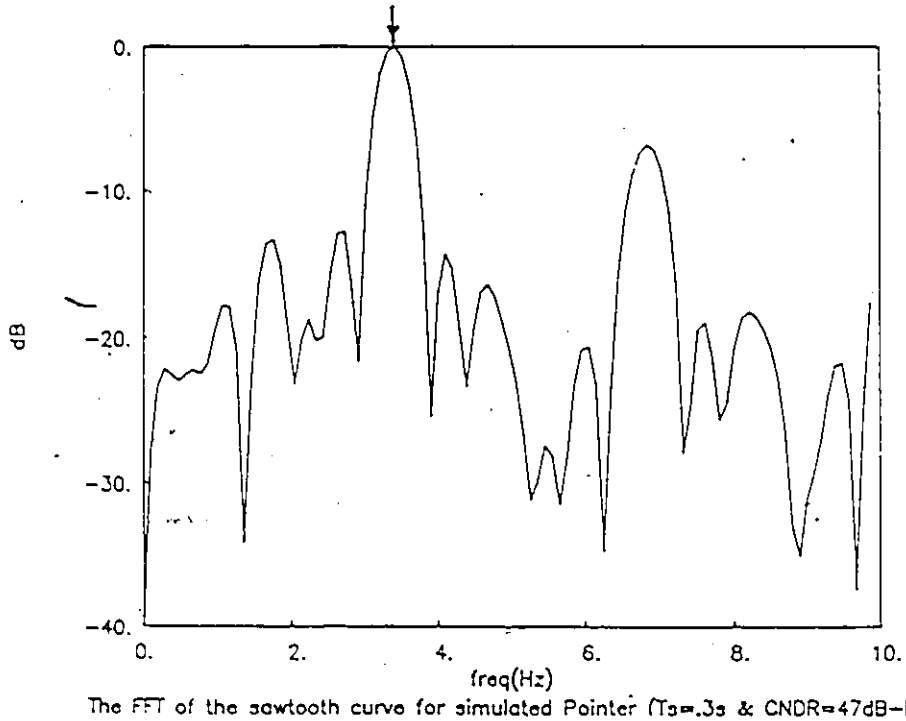

The FFT of the sawtooth curve for simulated Pointer (Ts=.3s & CNDR=47dB-Hz)

(b)

Fig. 3.10 Simulated Pointer ELT signal (T_s = .3 s and CNDR = 47 dB-Hz)
(a) The sawtooth curve.
(b) The FFT of the sawtooth curve.

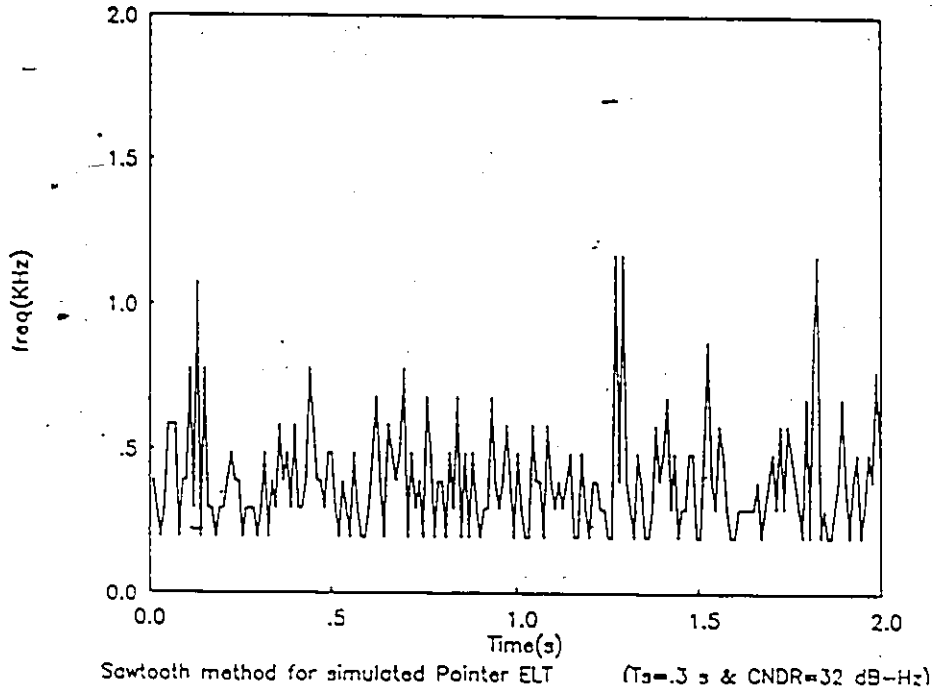

(a)

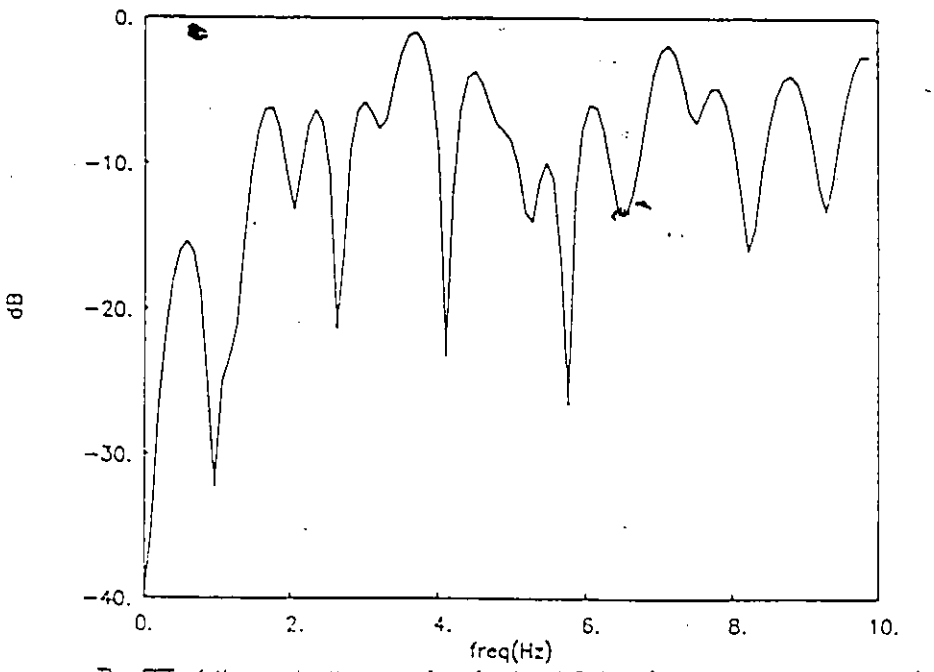

(b)

Fig. 3.11 Simulated Pointer ELT signal (T_s = .3 s and CNDR = 32 dB-Hz).
(a) The sawtooth curve.
(b) The FFT of the sawtooth curve.

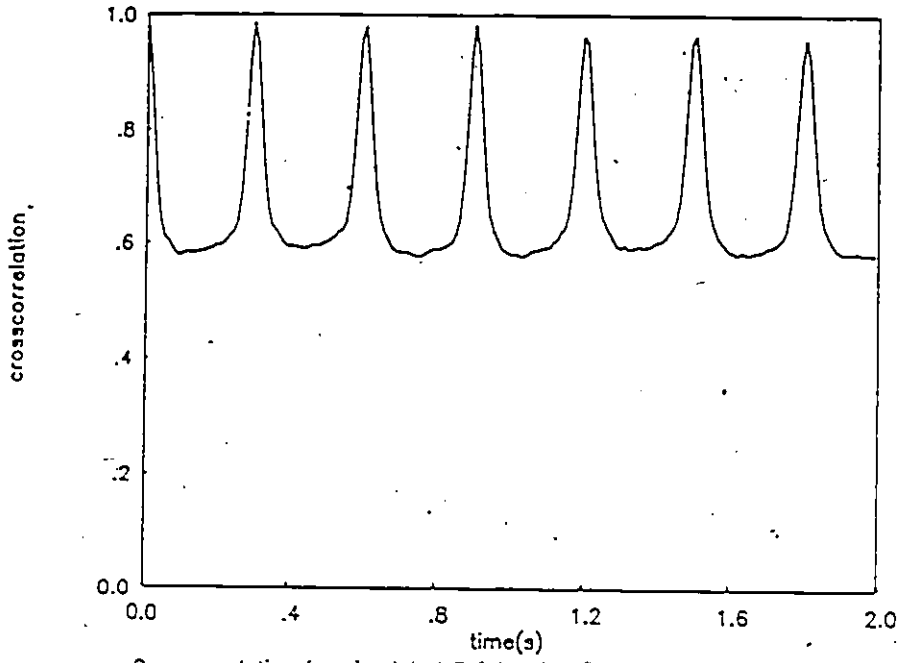

Crosscorrelation for simulated Pointer ELT (Ts=.3s & CNDR=47 dB-Hz)

(a)

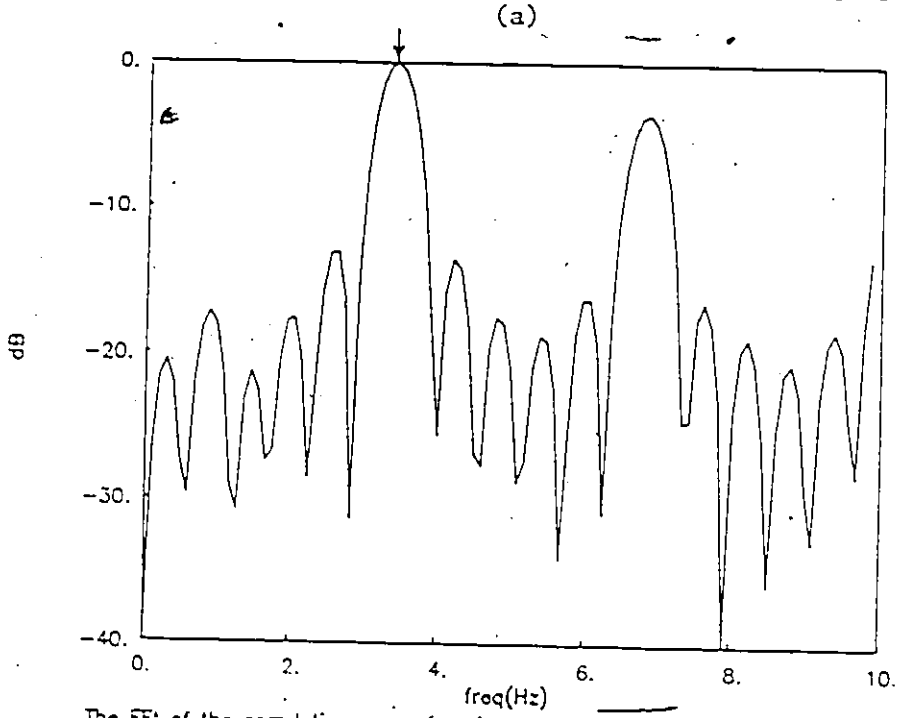

The FFt of the correlation curve for simulated Pointer(Ts=.3s &CNDR=47dB-Hz)

(b)

Fig. 3.12 Simulated Pointer ELT signal (T_s = . 3 s and CNDR = 47 dB-Hz)
(a) The crosscorrelation curve.
(b) The FFT of the crosscorrelation curve.

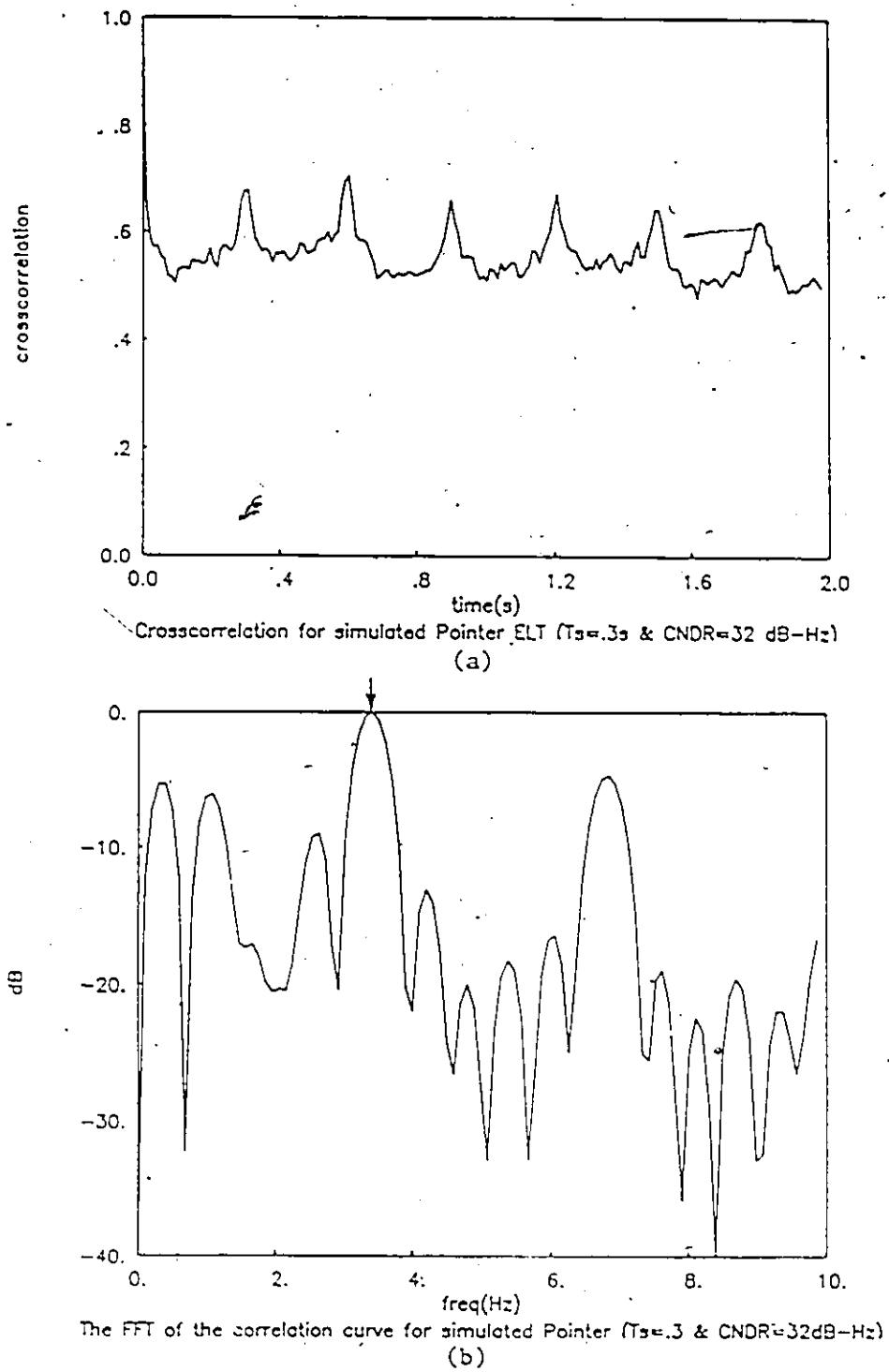

Fig. 3.13 Simulated Pointer ELT signal (T_s = .3s and CNDR = 32 dB-Hz)
(a) The crosscorrelation curve.
(b) The FFT of the crosscorrelation curve.

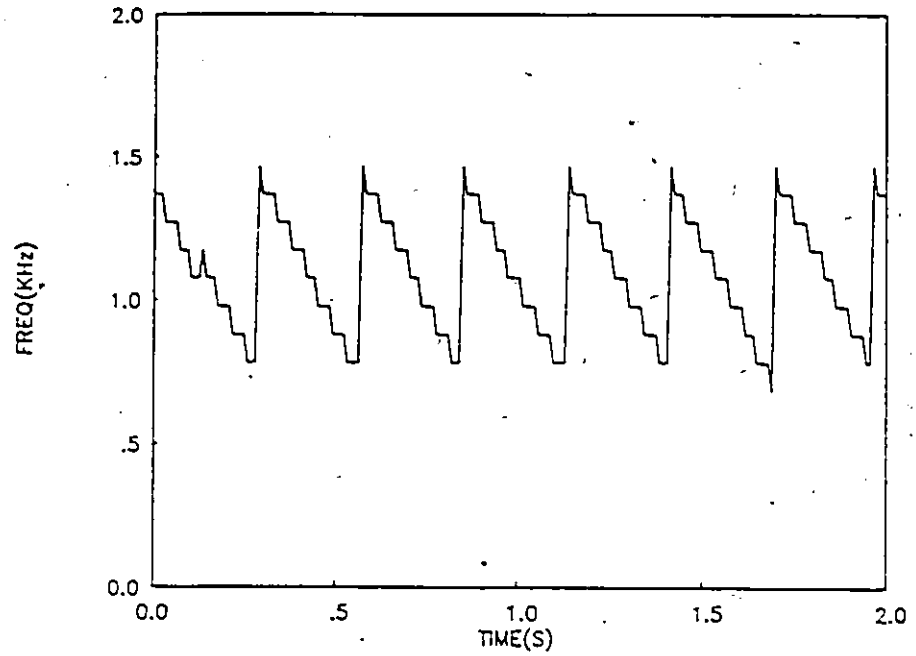

Sawtooth method for Simulated Garrett ELT signal (Ts=.28 s)

(a)

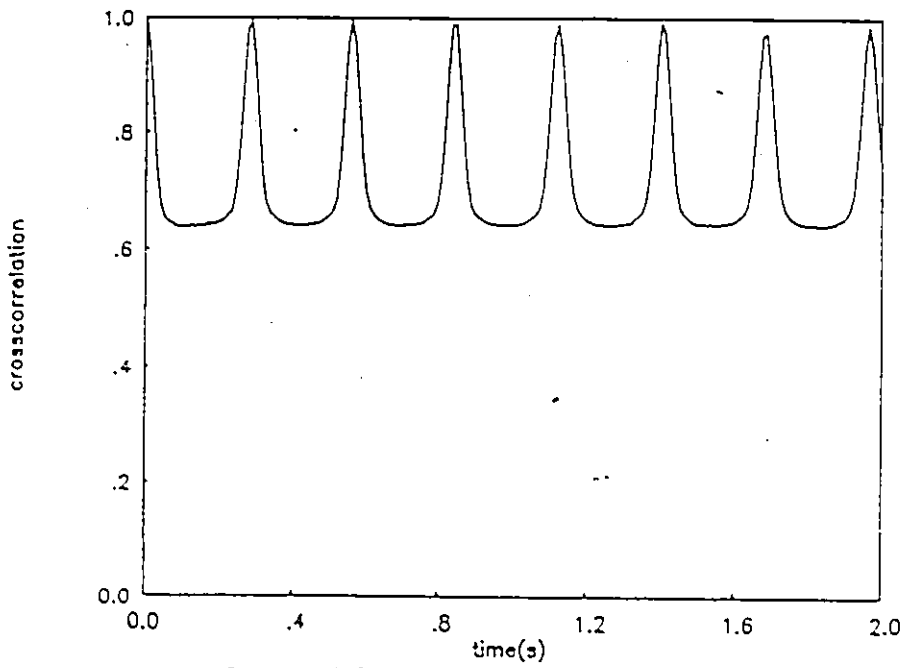

Crosscorrelation curve for simulated Garrett ELT signal

(b)

Fig. 3.14 Simulated Garrett ELT signal
(a) The sawtooth curve.
(b) The crosscorrelation curve.

When f_p is increased to 4 kHz, the carrier component of the spectrum is nulled in some positions and a large amount of the power is presented in the lower sideband while the carrier component is weakened. This characterizes the ELT units manufactured by Narco. The sawtooth and the crosscorrelation curves is such a case as presented in Fig. 3.15a. The actual sweep period is chosen to be 0.38 s and it is estimated as $T_s = 0.37$ s using both the methods.

From the above study we can see that, both the sawtooth and crosscorrelation methods agree for simulated data at high CNDR. Only, the crosscorrelation method is seen to be effective at low CNDR.

3.3.4 Testbed ELT Signals

In order to test the sawtooth method and the crosscorrelation technique using real data, four ELT units from three different manufacturers are chosen. The first and the second are manufactured by Pointer and Garrett, respectively. These signals represent good ELT units in the sense that the carrier frequency is stable and the sidebands move smoothly towards the carrier frequency, as illustrated earlier by the consecutive periodograms in Fig. 2.5 and Fig. 2.6 respectively. On the other hand, the third and fourth are manufactured by Narco which has a very poor spectral properties since the carrier frequency disappears for some portions within the sweep period. Also most of the energy is concentrated in the lower sideband as seen in Figs. 2.7 and 2.8.

Figure 3.16 shows the sawtooth curve for Pointer ELT signals which agrees with the simulated results of Fig. 3.10. From its periodogram of Fig. 3.16, the sweep period is estimated approximately as 0.21 s. The crosscorrelation method is applied to the same set of data and the resulting curve is depicted in Fig. 3.17 along with its periodogram the same value of the sweep period is estimated.

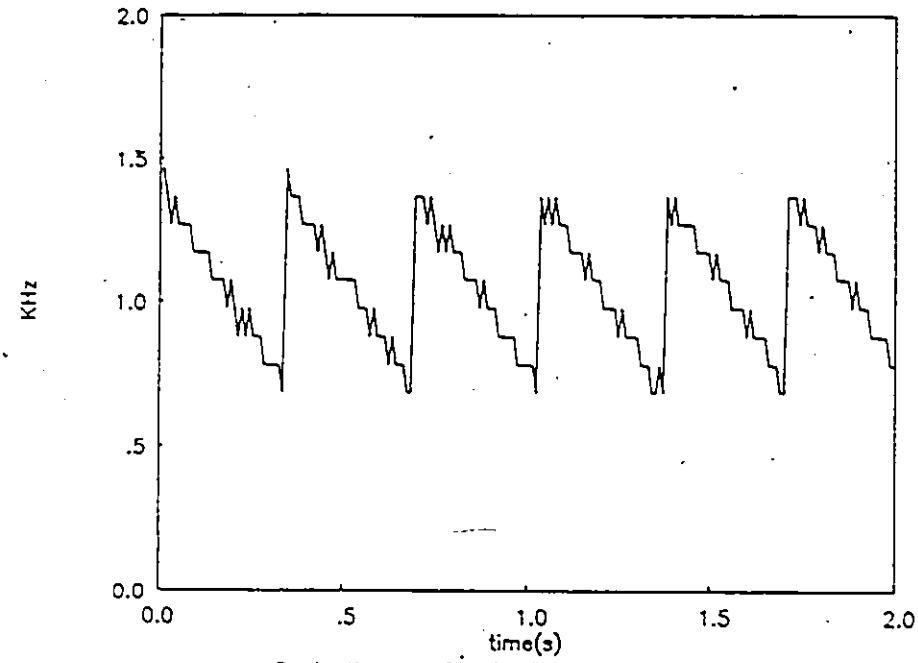

Sawtooth curve for simulated Narco ELT signals

(a)

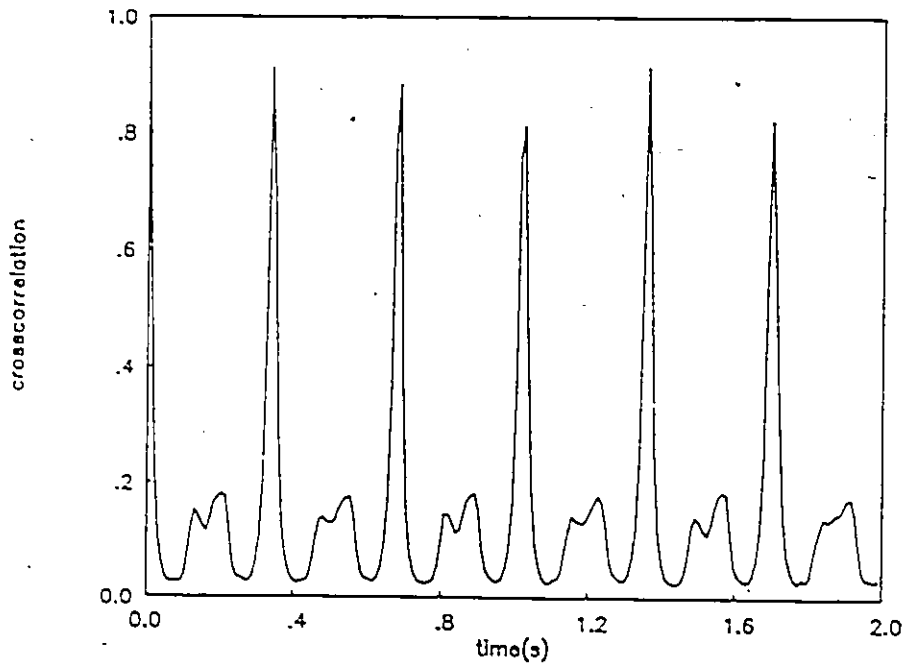

Crosscorrelation for simulated Narco ELT signal

(b)

Fig. 3.15 Simulated Narco ELT signal.
(a) The sawtooth curve.
(b) The crosscorrelation curve.

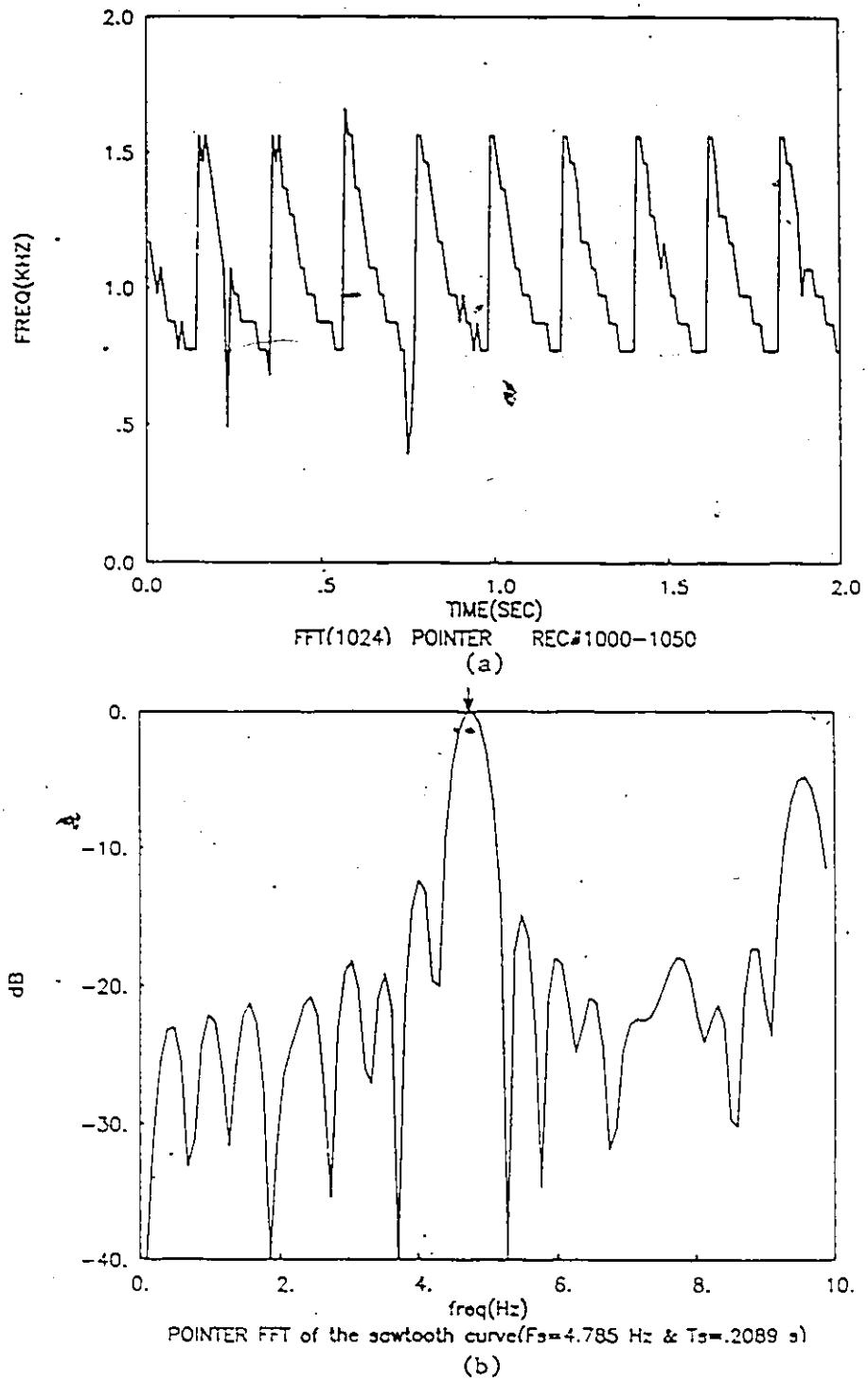

Fig. 3.16 Testbed Pointer ELT signal.
(a) The sawtooth curve.
(b) The FFT of the sawtooth curve.

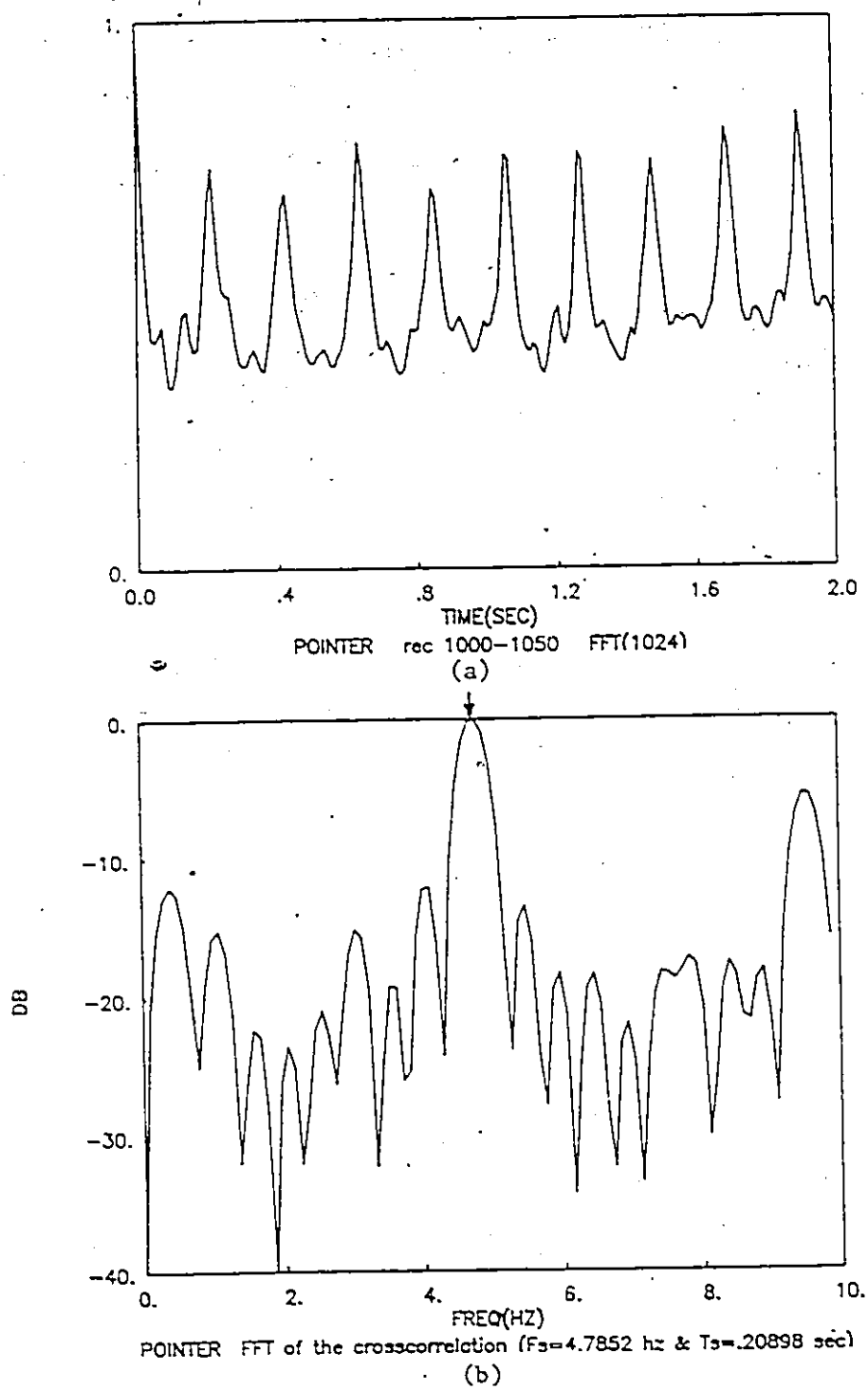

Fig. 3.17 Testbed Pointer ELT signal.
(a) The crosscorrelation curve.
(b) The FFT of the crosscorrelation curve.

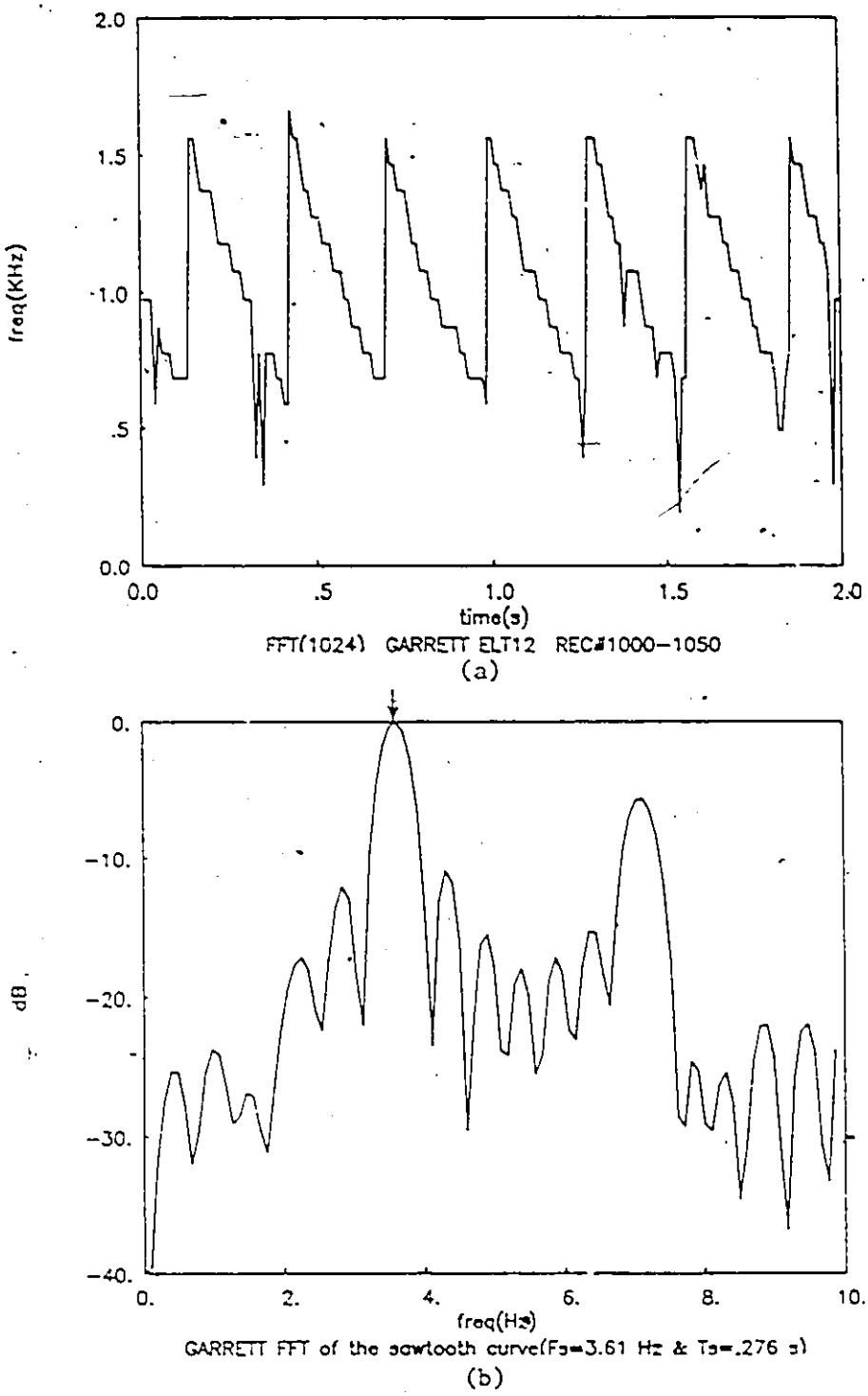

Fig. 3.18 Testbed Garrett ELT signal.
(a) The sawtooth curve.
(b) The FFT of the sawtooth curve.

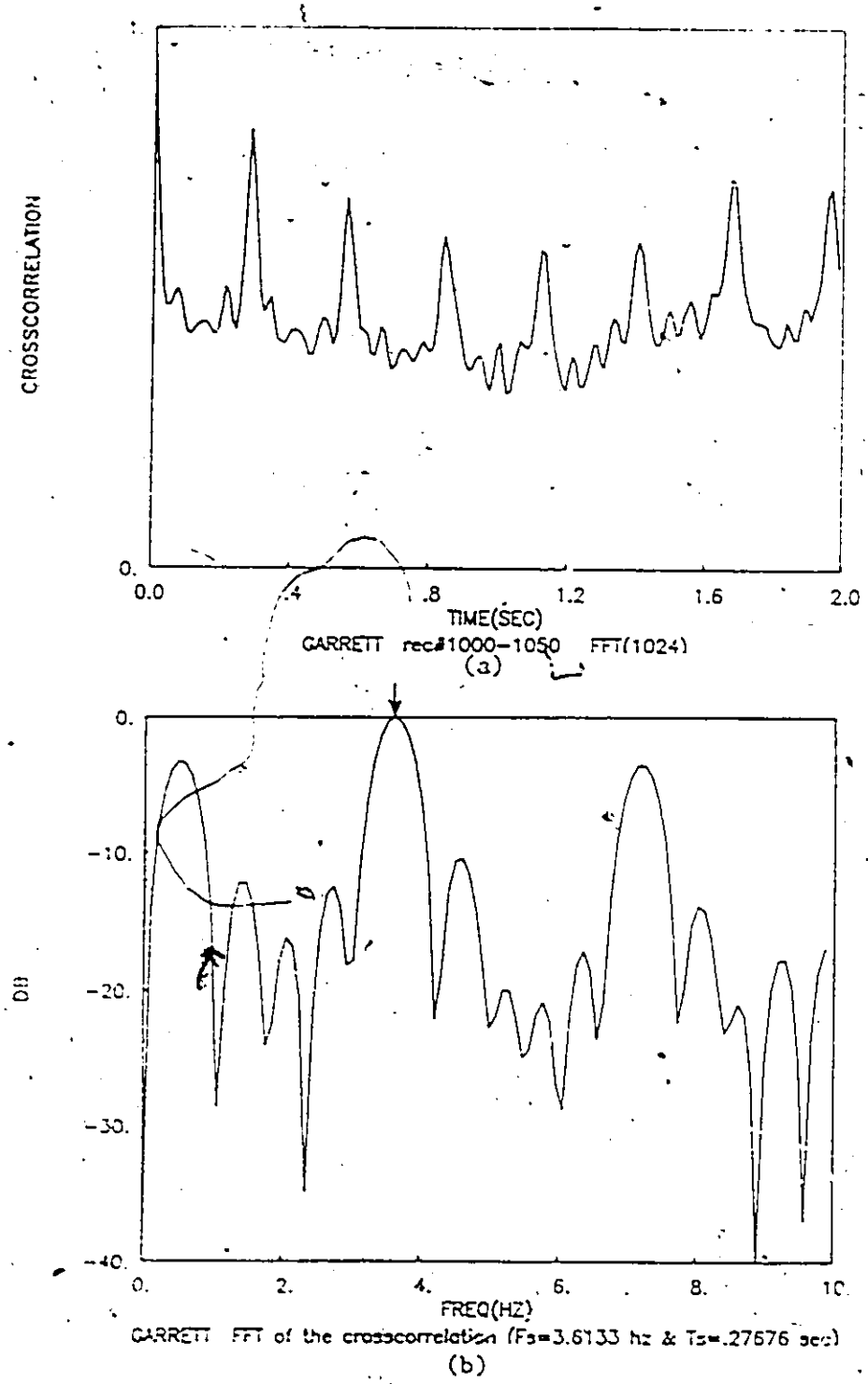

Fig. 3.19 Testbed Garrett ELT signal.
(a) The crosscorrelation curve.
(b) The FFT of the crosscorrelation curve.

Similar plots for Garrett ELT signals are shown in Figs. 3.18 and 3.19, respectively. The two methods agree in estimating the same value of the sweep period as 0.28 s.

Referring to Fig. 2.7 for Narco ELT 17, we find that the sweep period is hardly recognized using successive periodograms. The corresponding sawtooth and crosscorrelation curves for this signal are shown in Figs. 3.20 and 3.21 respectively. It is clear that the sweep period is now well-defined and it is estimated directly from the periodogram. Note that, the FFT shown in Fig. 3.21 has many peaks but we are interested only in the peak that lies within the specifications (i.e. from 2 Hz to 4 Hz). Therefore, the estimated sweep period for Narco ELT 17 is $T_s = 0.37$ s.

For Narco 19, which has very poor spectral properties, the methods are still effective as seen in Figs. 3.22 and 3.23 and the sweep period is estimated as 0.423 s.

Comparing the crosscorrelation curves for the four testbed ELT signals, we find that each one has its own characteristics. Therefore, if a signal is present, it is possible to be tracked using the identification techniques. The remaining problem is to separate the ELT signals from interference sources to reduce the false alarms. This problem will be discussed in the next chapter.

3.4 Summary

1. Two methods for estimating the sweep period are described, the first is the sawtooth method which is applicable for high signal-to-noise ratio, and the second is the crosscorrelation procedure which can be used in any environment.
2. A theoretical analysis for the crosscorrelation method is developed.

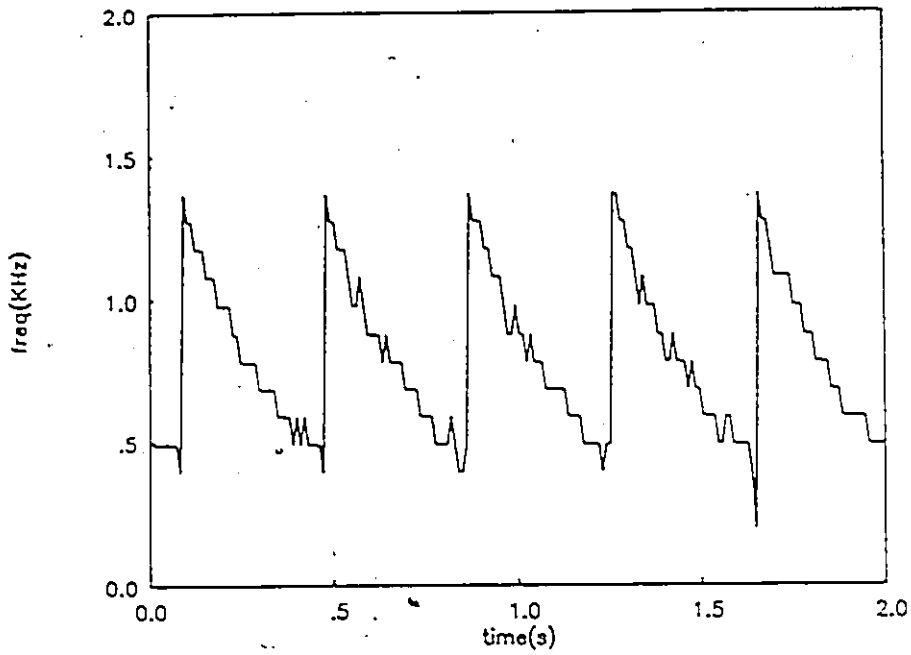

FFT(1024) NARCO ELT17 REC#1000-1050

(a)

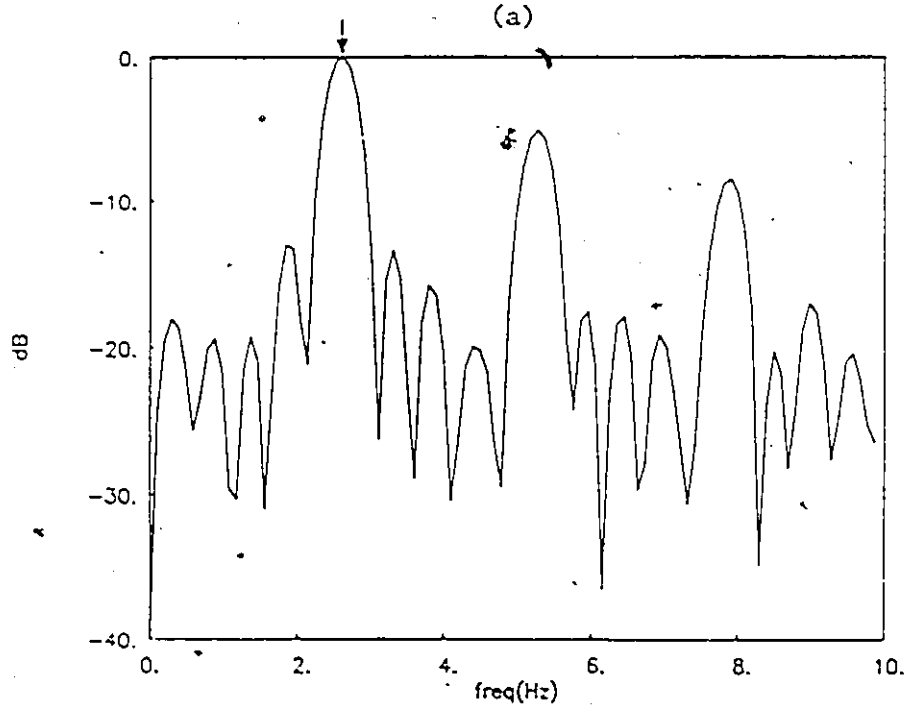

NARCO ELT17 FFT of the sawtooth curve(Fs=2.63Hz & Ts=.379s)

(b)

Fig. 3.20 Testbed Narco ELT17 signal.
(a) The sawtooth curve.
(b) The FFT of the sawtooth curve.

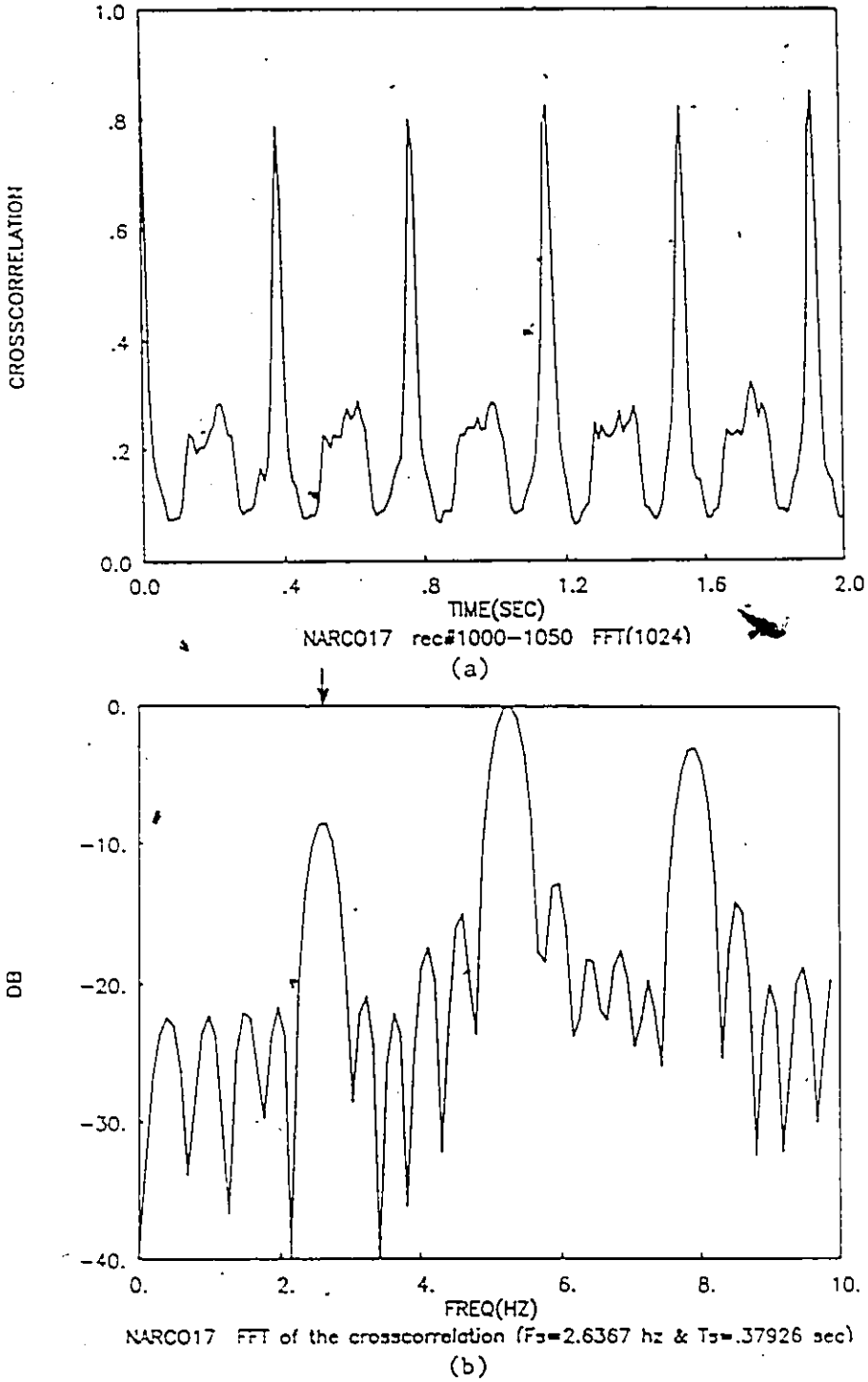

Fig 3.21 Testbed Narco ELT17 signal.
(a) The crosscorrelation curve.
(b) The FFT of the crosscorrelation curve.

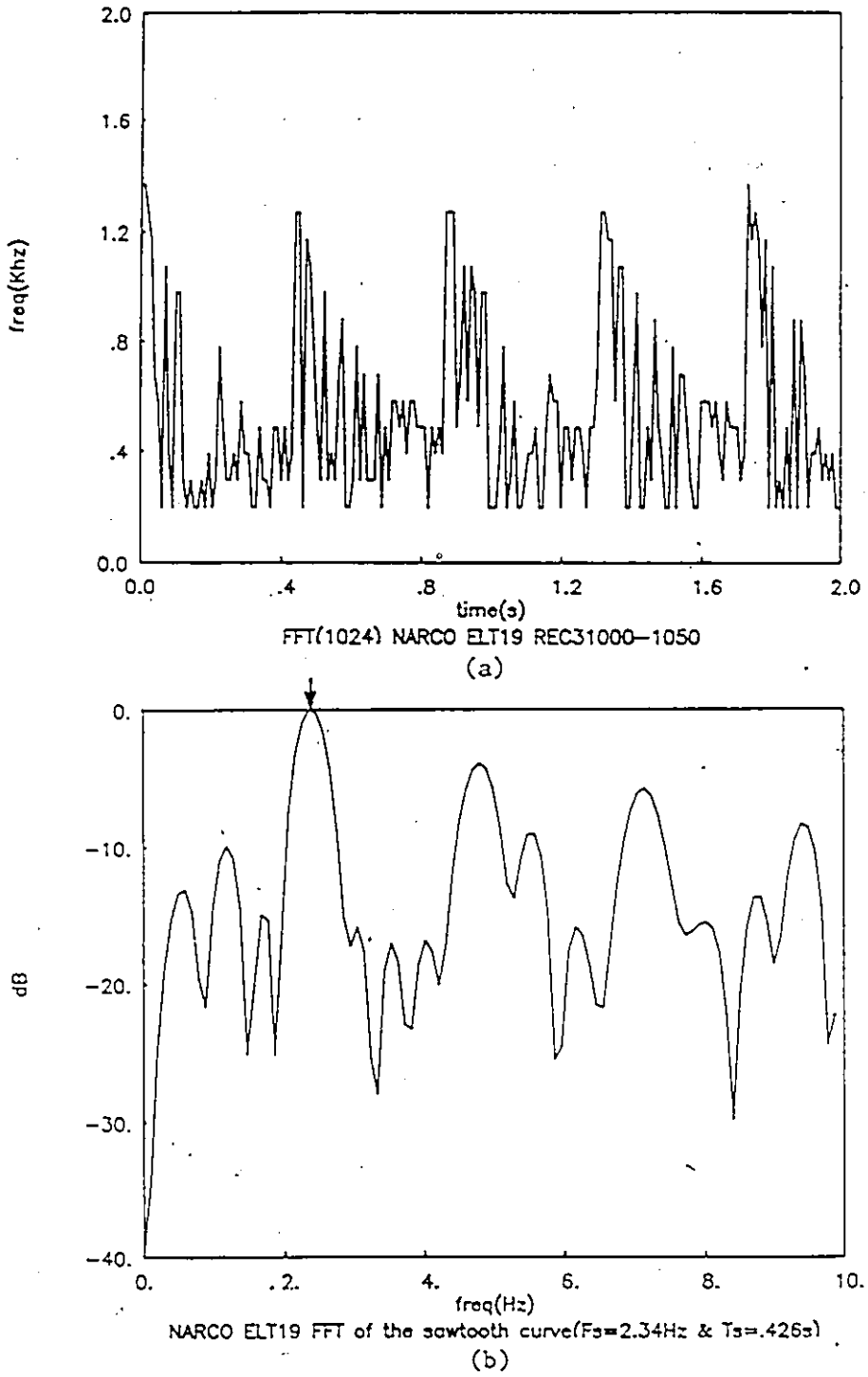

Fig. 3.22 Testbed Narco ELT19 signal.
(a) The sawtooth curve.
(b) The FFT of the sawtooth curve.

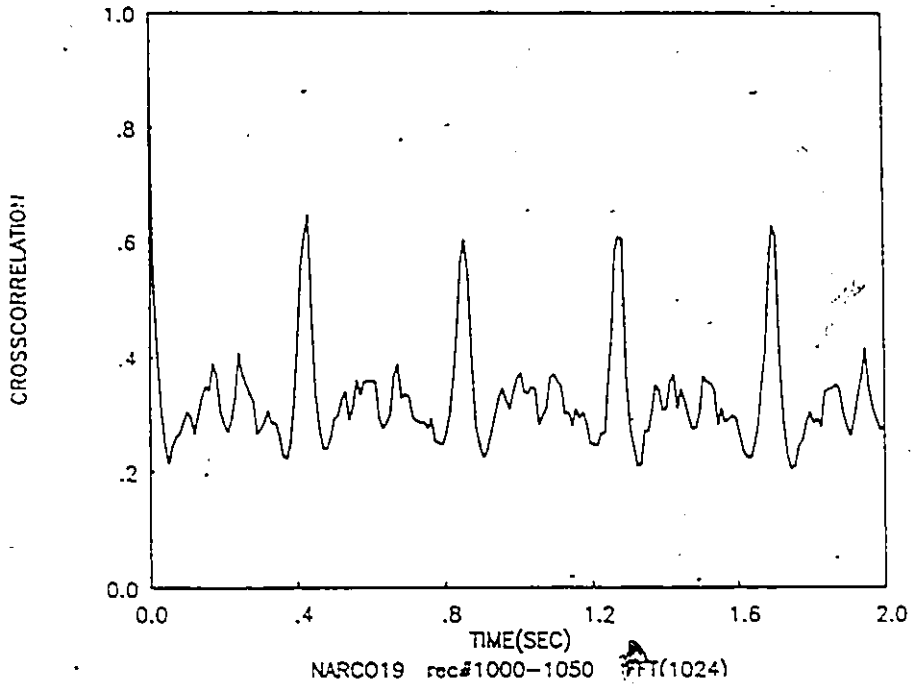

(a)

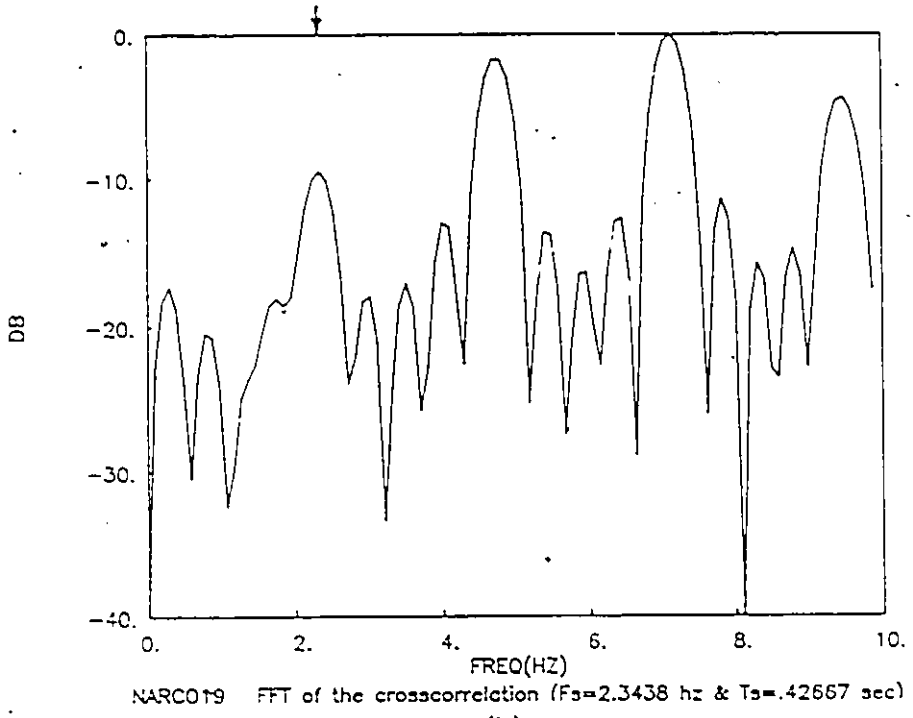

(b)

Fig. 3.23 Testbed Narco ELT19 signal.
(a) The crosscorrelation curve.
(b) The FFT of the crosscorrelation curve.

3. A theoretical calculation of the upper bound of the error in calculating the sweep period is provided.

4. The crosscorrelation and the sawtooth methods are applied to both simulated signals and real data recorded from Communication Research Centre (CRC) in Ottawa. Both methods give the same sweep period for all cases.

5. It is seen that using the identification of ELT signals, we are able to solve some of the existing problems, namely:

   (a) to separate the S-shaped curves that cross

   (b) to connect the scattered portions of the S-shaped curves.

CHAPTER 4

ELT SIGNAL IDENTIFICATION IN THE PRESENCE OF INTERFERENCE

4.1 Overview

In this chapter, we examine the problem of interference which is related specifically to the 121.5 MHz and 243 MHz SARSAT frequency bands. A computer literature search of interfering sources in the frequency band from 100 to 500 MHz reveals the possible sources of background noise and interference [12]. These can be divided into: natural sources such as atmospheric noise, galactic noise, solar flare interference and the like; and man-made interference such as automobile ignition noise, power generating facility interference, scientific interference and industrial equipment noise, CB radio and amateur radio interference and so on [13-15]. We focus our study on man-made interference, since it is always dominant. Some possible sources of this type of interference are due to harmonics of radio [16-18] that produce unmodulated or modulated carriers which fall in the SARSAT bands.

First, the interference types are examined. Some of these interference sources are selected, and modelled by computer simulation. Then the crosscorrelation technique is applied in the presence of each interference when the ELT signal occupies the same band (called co-channel interference). Finally, some practical considerations concerning the effect of automatic gain control (AGC) and limiting are discussed.

4.2 Types of Interference Sources

All sources of interference in the COSPAS-SARSAT system are classified as narrow band since the system bandwidth B is very small compared to the carrier frequency fc,

i.e. $B << f_c$. However, within the band we denote different bandwidths of various interference sources. For instance, unmodulated carrier produces a near line spectrum. Voice produces up to 10 kHz bandwidth interference and other sources essentially fill the entire 25 kHz bandwidth. Thus we shall use the following classifications:

CW – Interference produced by an unmodulated carrier

NB – Narrowband interference such as that produced by voice (up to 10 kHz).

WB – Wideband interference which fills most of the 25 kHz bandwidth.

The CW and NB interferences create three problems for the SARSAT system. First, they produce clutter that appears on the frequency plot which increases the complexity of the signal processing strategy. Second, is the problem of reduced dynamic range and thresholding when automatic gain control or a limiter is employed. Third, is the problem of FFT dynamic range when strong CW signals appear with weaker ELT signals and background noise.

Normally, the effect of increased clutter on the frequency plot is not severe since the signal occupies a very narrow band of frequencies. However, the other two problems are far more serious and are examined in this chapter.

Before attempting to discuss the ELT detection in the presence of noise, a necessary step is to specify the models of interference sources as shown next.

4.2.1 CW Interference

The unmodulated carrier can be generated using a cosine function:

$$c(t) = C_o \cos(2\pi f_i t) \qquad ; \; 0 < f_i < 25 \text{ kHz} \tag{4.1}$$

where C_o is amplitude of the CW interference and f_i is the carrier frequency.

This function is plotted versus time as shown in Fig. 4.1a. The spectrum of c(t) is calculated using the FFT and the corresponding envelope is depicted in Fig. 4.1b.

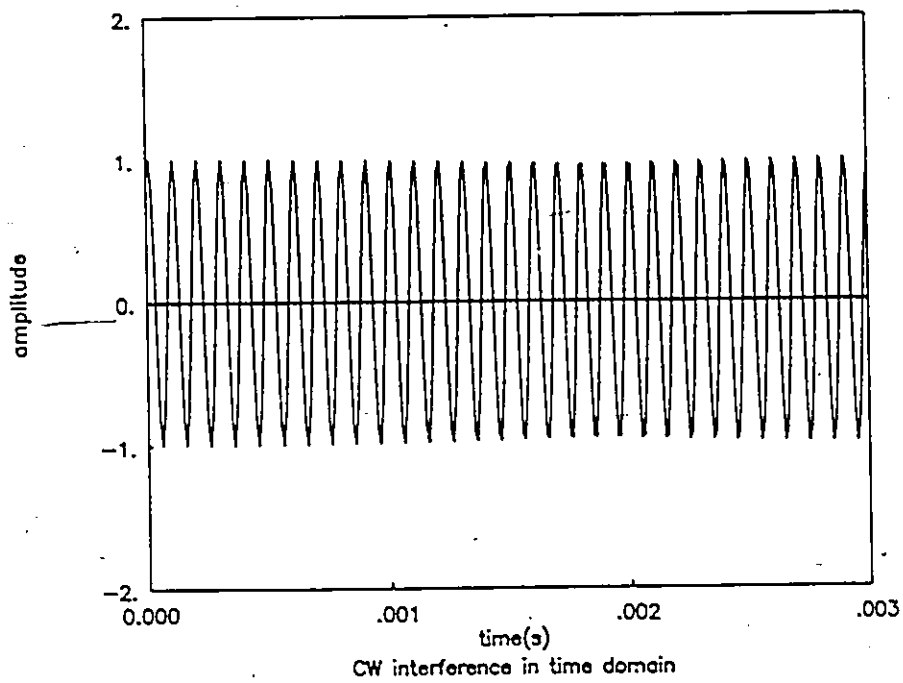

(a)

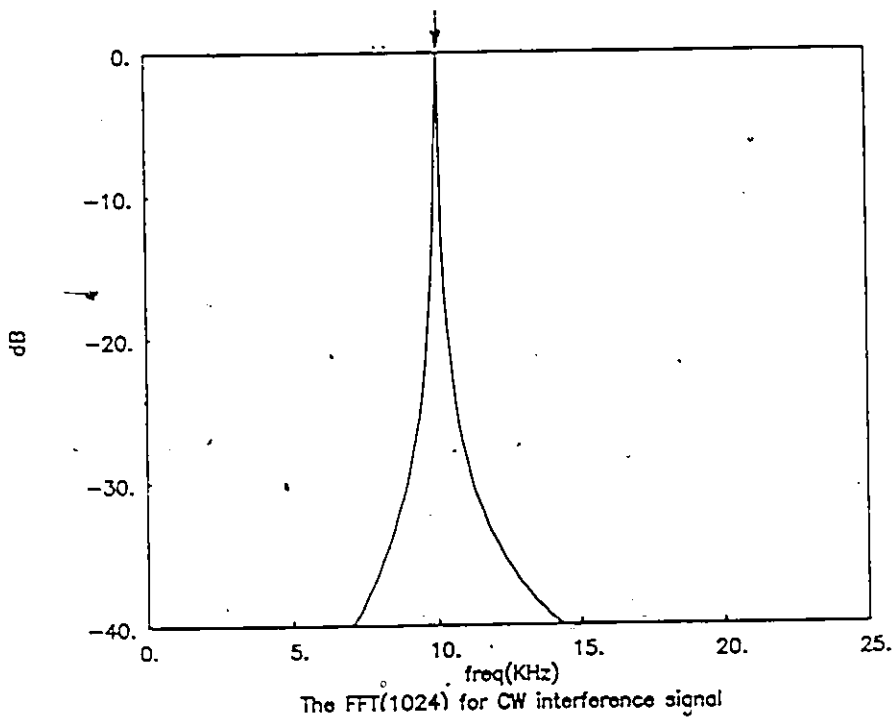

(b)

Fig. 4.1 The CW interference
(a) Signal amplitude.
(b) Signal spectrum envelope.

4.2.2 Narrowband Interference

The narrowband interference refers to interference having a bandwidth which is considerably less than the 25 kHz bandwidth being processed for 121.5 MHz signal band. Here, we consider two types of narrowband interference, namely amplitude modulated (AM) signal (voice interference) and phase shift keying interference (PSK).

The AM interference is generated using the following equation:

$$a(t) = A_o (1 + m \cos 2\pi f_m t) \cos 2\pi f_i t \tag{4.2}$$

where A_o is the amplitude of the AM signal, m is the modulation index, $0 < m < 1$; and f_m is the modulating frequency which is chosen to lie between 500 Hz and 1000 Hz (typical for speech). The carrier frequency f_i may vary from 0 to 25 kHz. An example of the AM modulated signal in time domain and its envelope are given in Fig. 4.2a and Fig. 4.2b respectively.

The PSK, is generated using the following function:

$$s(t) = S_o \cos(2\pi f_i t + \theta_1)$$

or

$$= S_o \cos(2\pi f_i t + \theta_2) \qquad -T/2 < t < T/2 \tag{4.3}$$

where S_o is the amplitude of the PSK signal, f_i is the carrier frequency and θ_1 and θ_2 are the phase shifts. The pulse width T represents the binary bit duration and a binary sequence can be generated using this function, by making a '1' corresponds to phase θ_1, and a '0' corresponds to θ_2. For simplicity, we choose $\theta_1 = 0$. and $\theta_2 = \pi$. In this case the phase shift keyed signal is given by:

$$s(t) = \pm S_o \cos(2\pi f_i t) \qquad -T/2 < t < T/2 \tag{4.4}$$

As an example the pulse width T is chosen to be 0.64 ms since one case of real PSK interference has 0.6 ms pulse duration [12]. For worst case the binary sequence consists of one's and zero's alternatively changed as shown in Fig. 4.3a, along with the corresponding frequency response given in Fig. 4.3b.

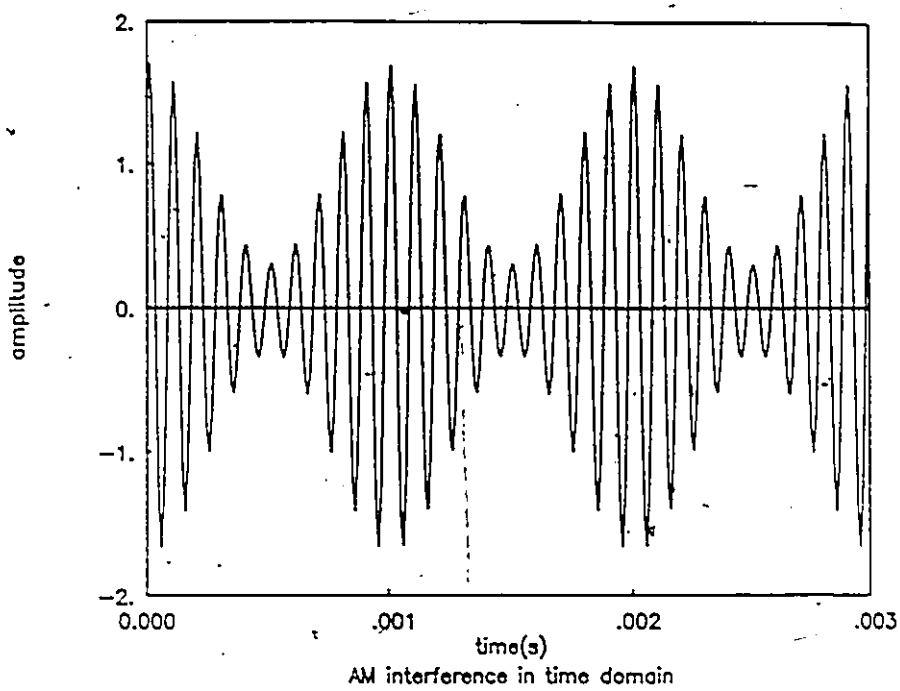

(a)

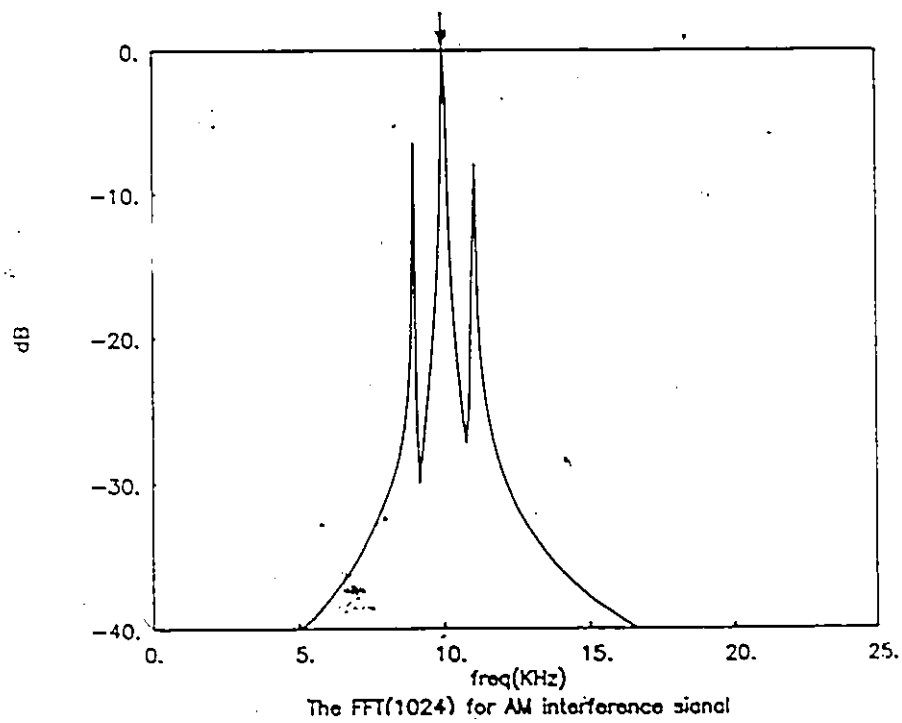

(b)

Fig. 4.2 The AM interference
(a) Signal amplitude.
(b) Signal spectrum envelope.

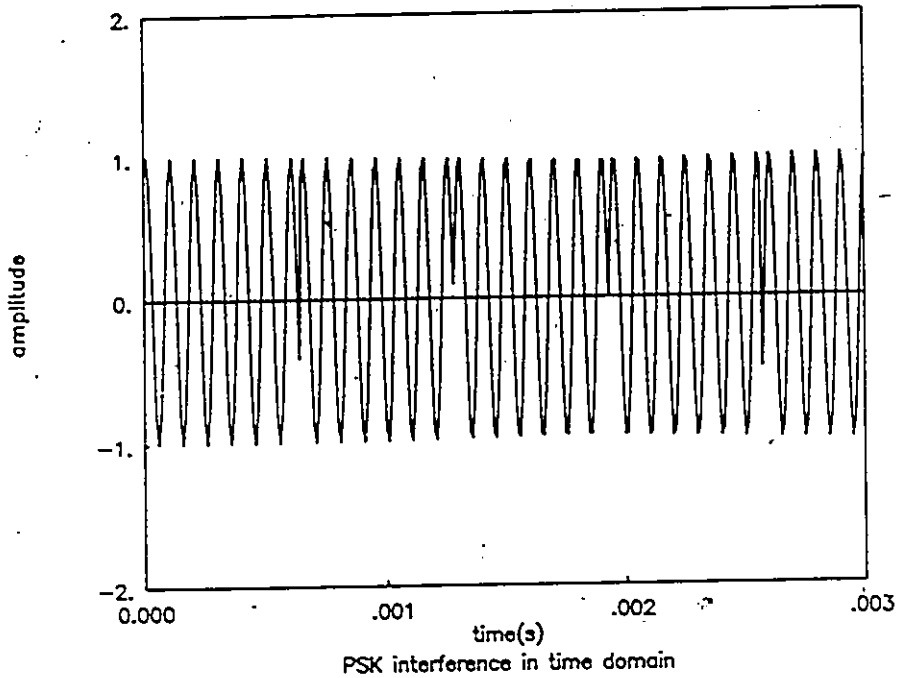

(a)

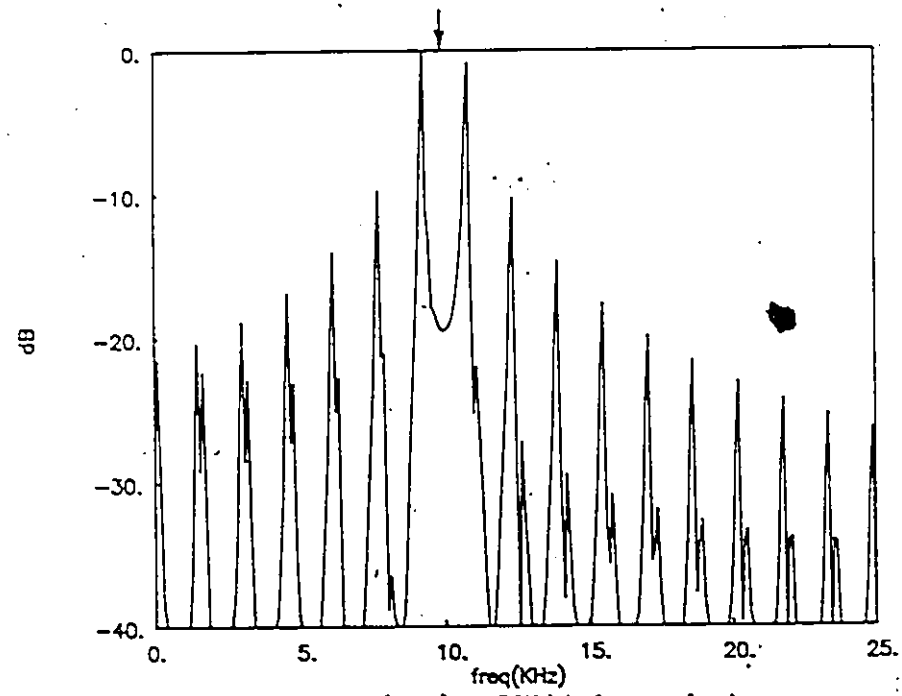

(b)

Fig. 4.3 The PSK interference
(a) Signal amplitude.
(b) Signal spectrum envelope.

4.2.3 Wideband Interference

Wideband interference is considered to be that which covers most of the 25 kHz bandwidth of the ELT signals. Thus most of the band may be increased by approximately the same level. Wideband interference can be produced by several means, including the effects of a large number of low power impulsive sources, the shock excitation produced by a small number of high power impulses or by the wideband modulation of a carrier. This type of interference has a spectrum similar to that of the noise. Therefore it will not be discussed here since the noise effects have been discussed in the previous chapter.

4.2.4 The Crosscorrelation of the Interference Signals

It has been shown that the ELT signals have special characteristics, amongst which, the sidebands of the spectrum are not fixed but move toward the carrier as the sweep progresses. This is not the case with the interference sources, since the spectrum is almost the same at any instant of time. Therefore if the crosscorrelation method discussed earlier is applied to interference sources, the pattern obtained is expected to be smooth. This is evident as shown in Fig. 4.4, which represents the crosscorrelation curve for simulated CW interference. As seen from this figure, the crosscorrelation curve is flat.

The noticeable difference between the crosscorrelation of ELT signals and that for the interference sources makes it possible to use the crosscorrelation method to separate the ELT signals from the interfering signals. This can be achieved by dividing the ELT bandwidth (0-25 kHz) into sub-bands or equivalently the signal is filtered using bank of filters that covers the whole band. Since the spectrum of the received signal is obtained using the linear FFT processor, the corresponding sub-band is obtained assuming zero spectrum outside it. Therefore no actual filtering operation is performed and processing time is saved. The above

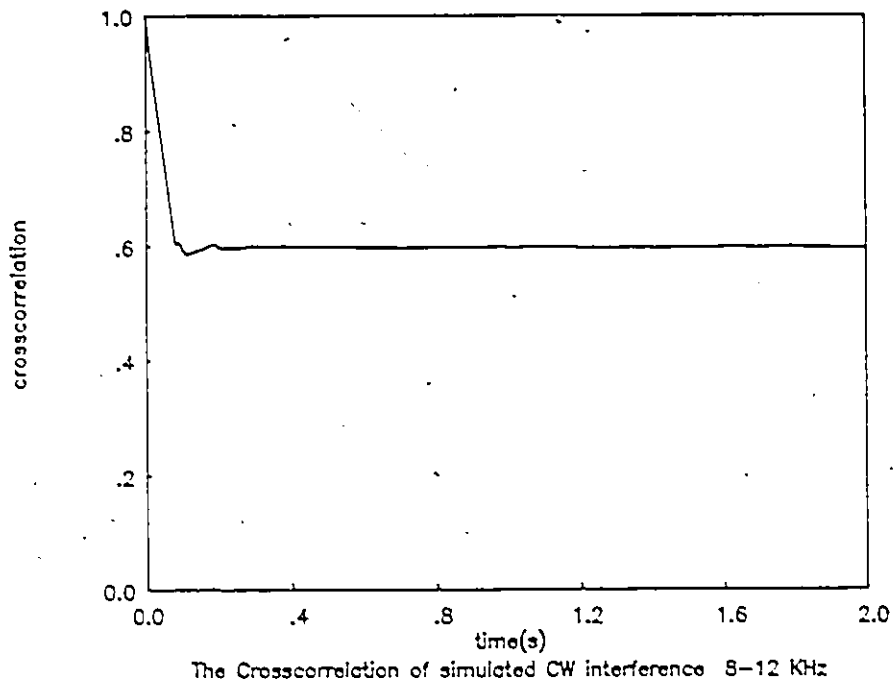

Fig. 4.4 The crosscorrelation curve for simulated CW interference.

process is repeated for many other sub-bands, then the crosscorrelation curve corresponding to each sub-band is obtained. The decision of having an ELT signal or interference can then be based on the shape of the crosscorrelation curve, whether being a multipeak pattern or a flat response. This can be achieved automatically by applying the FFT to each cross-correlation curve as done previously. In the case of interference the peak of the FFT will always be at the zero frequency i.e. outside the frequency limit (2-4 Hz) and, thus, it will be easy to distinguish between ELT signals and non-overlapping interference.

On the other hand, the ELT signal may be masked if it is overlapped with strong interference. When the interference occupies the same band of the ELT signal, it is referred to as co-channel interference. In the following section, the effect of co-channel interference is studied using simulated signals.

4.3 Co-channel Interference and ELT Signals

To study the problem of detecting the ELT signal in the presence of co-channel interference, both signals are simulated such that the carrier frequency of the ELT signal is fixed, while the frequency of the interference signal is chosen to take values in steps of 1 kHz. For each step, the crosscorrelation curve is obtained for different types of interference sources.

Before proceeding, we introduce here the term signal-to-interference ratio (SIR), which is defined as:

$$\mathrm{SIR}\,(S/I) = 10 \log (P_s/P_i) \quad \mathrm{dB} \tag{4.5}$$

where P_s and P_i are the power levels of the ELT and interference signals, respectively.

P_s can be obtained from the following relation [19]:

$$P_s = 1/2 \times A_c^2 \times d \tag{4.6}$$

where A_c is the amplitude of the ELT signal and d is the duty ratio.

P_i is obtained for the different types of interference sources as follows[20]:

For CW interference:

$$P_{cw} = 1/2 \times C_o^2 \tag{4.7}$$

For AM interference :

$$P_{am} = 1/2 \times A_o^2 \times (1 + m^2/2) \tag{4.8}$$

For PSK binary sequence interference:

$$P_{psk} = 1/2 \times S_o^2 \tag{4.9}$$

In the following, we start by examining the case of CW interference overlapped with the desired ELT signal for different values of SIR. The ELT and the CW signals are simulated such that both carrier frequencies lie at 10 kHz, with the SIR set to zero dB. The sweep period of the ELT signals is chosen to be 0.3 s to meet the specifications. A 1 K-point FFT of such signal is generated and the spectrum is shown in Fig. 4.5. The arrows indicate the carrier frequencies for both ELT signal (letter S) and interference (letter I). As the cross-correlation method is applied, the resultant curve is shown in Fig. 4.6a, and the 1 k-periodogram of the crosscorrelation curve is depicted in Fig. 4.6b. It is clear that the crosscorrelation curve has a repetition frequency higher than that of the sweep, therefore, the maximum amplitude of the spectrum occurs at the third hamonics of the sweep frequency. But according to the specifications in Table 1.1, we find that the sweep frequency lies in the range of 2 to 4 Hz. Hence the search is restricted to this region, and from Fig. 4.6b, it is apparent that the FFT is able to detect the correct sweep frequency which is indicated by the arrow. The estimated sweep period ($\hat{T}_s = 1/\hat{F}s$) is equal to 0.292 s with an error of 2.7% from the actual period of $T_s = 0.3$ s. This error is due to the limited resolution of the FFT and lies within the error bound derived in section 3.3.2.

Now the carrier frequency of the ELT signal is kept constant, while that of the CW interference is incremented by 1 kHz as shown in Fig. 4.7. From the crosscorrelation curve and its periodogram depicted in Fig. 4.8a and Fig. 4.8b respectively, we find that the sweep period can be measured with the above accuracy of 2.7%. The same results are obtained when

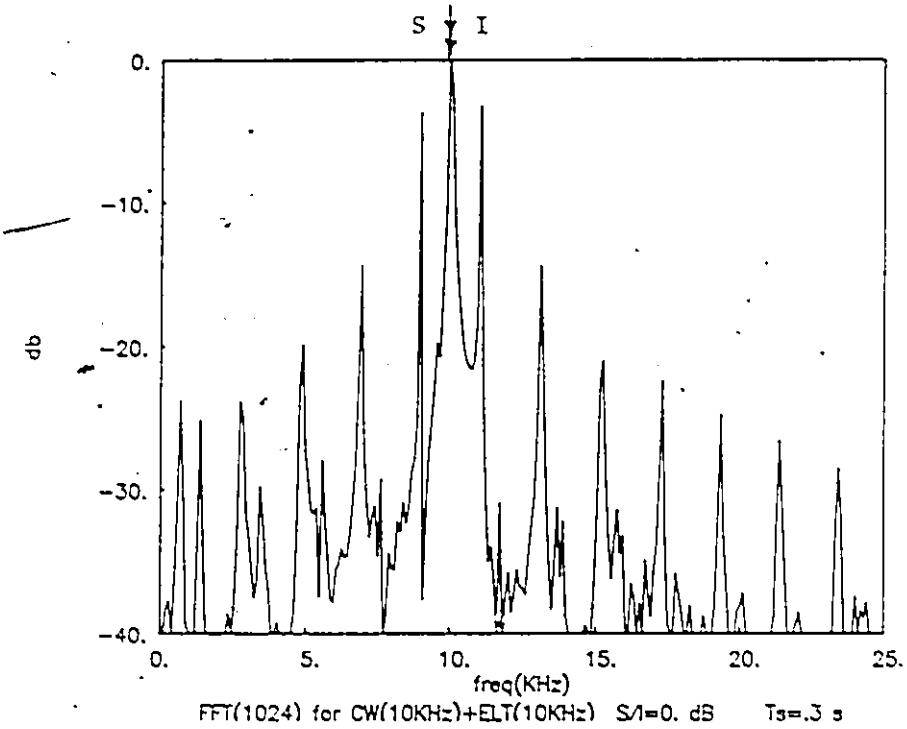

Fig. 4.5 Plot of 1 k-FFT of ELT signal (f_c = 10 kHz) + co-channel CW interference (f_i = 10 kHz). SIR = 0 dB.

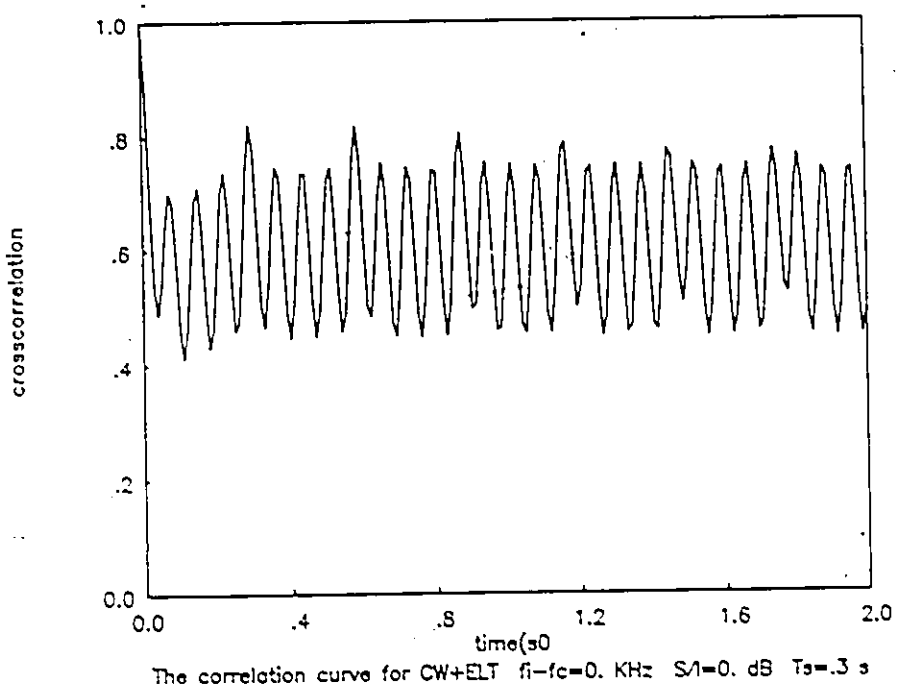

(a)

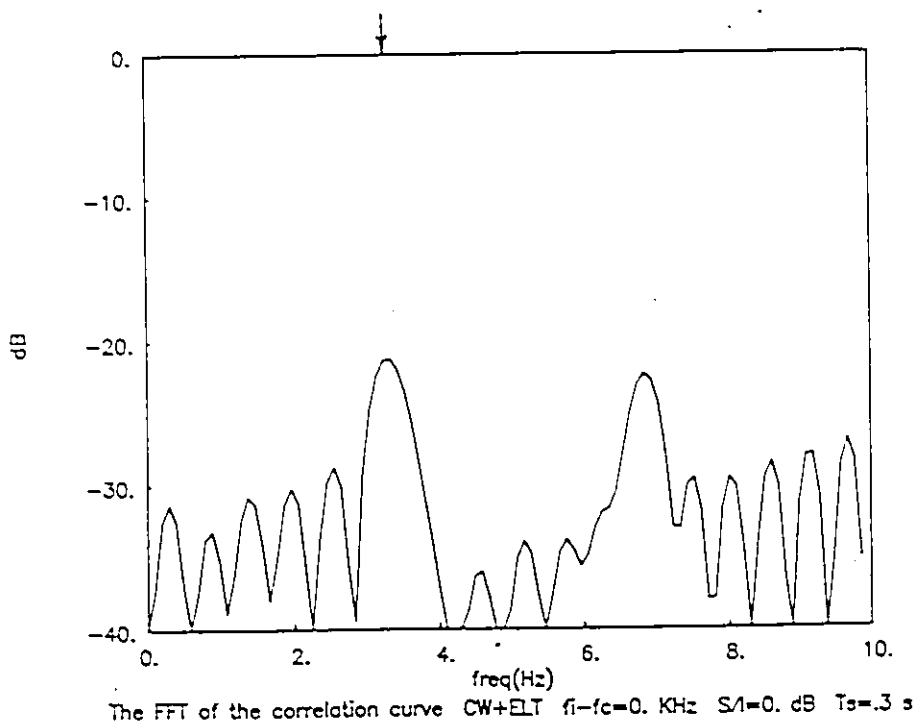

(b)

Fig. 4.6 ELT signal (f_c = 10 kHz) + co-channel CW interference (f_i = 10 kHz). SIR = 0 dB.
(a) The crosscorrelation curve.
(b) The periodogram of the crosscorrelation curve.

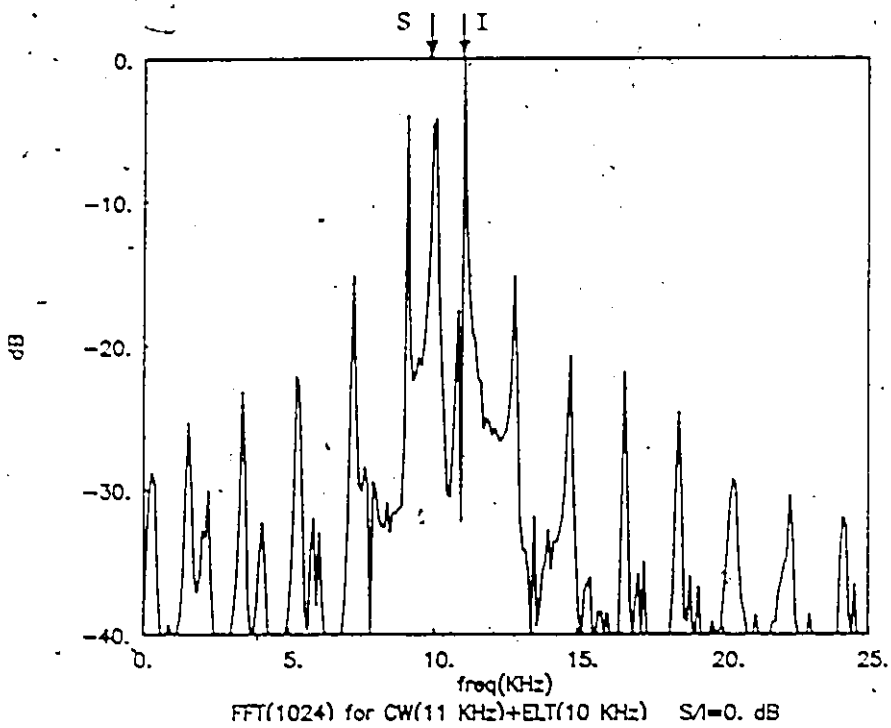

Fig. 4.7 Plot of 1k-FFT of ELT signal (f_c = 10 kHz) + co-channel CW interference (f_i = 11 kHz). SIR = 0 dB.

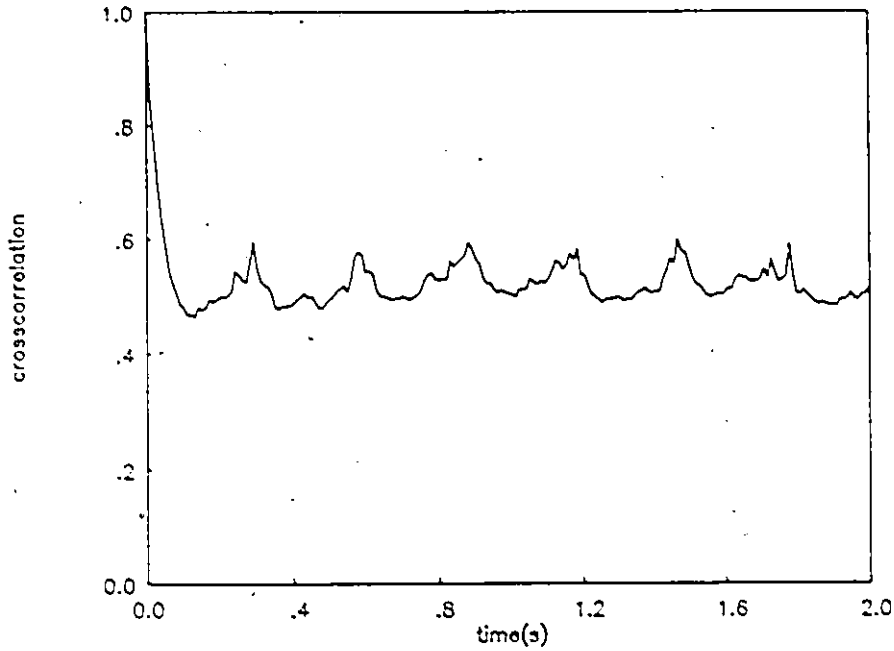

(a)

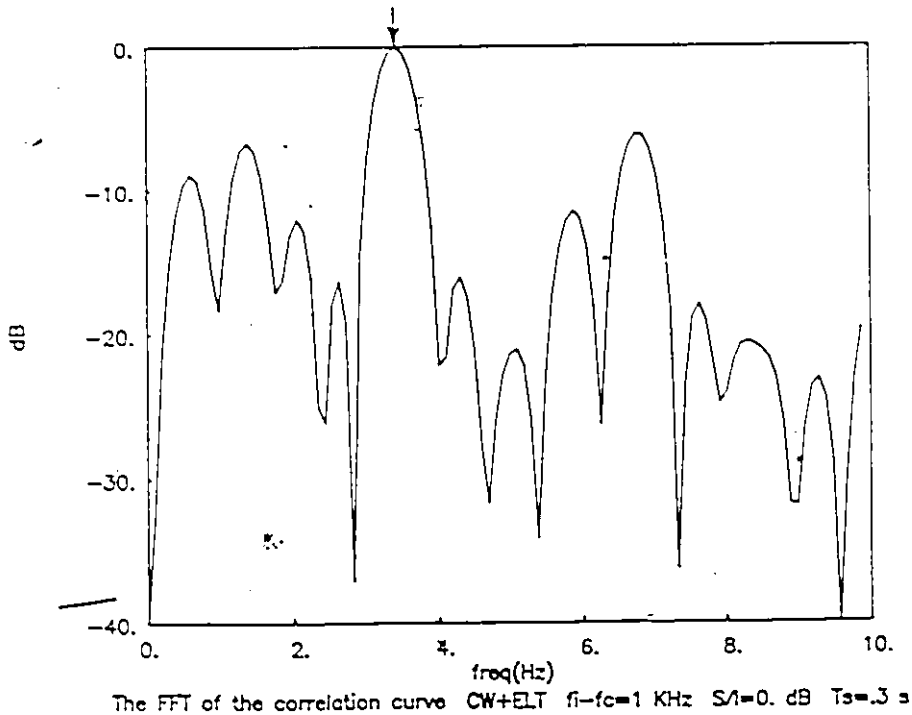

(b)

Fig. 4.8 ELT signal (f_c = 10 kHz) + co-channel CW interference (f_i = 11 kHz). SIR = 0 dB.

(a) The crosscorrelation curve.

(b) The periodogram of the crosscorrelation curve.

the interference carrier frequency is moved to 12 kHz as seen from Fig. 4.9 and Fig. 4.10. We conclude that in the case of CW co-channel interference at SIR = 0 dB, the ELT signal can be well detected.

The method is also tested for PSK co-channel interference. The modulating frequency is chosen as 0.78 kHz (corresponds to pulse width duration of .64 ms). Figure 4.11 shows the 1 K-FFT when the PSK interference and the ELT signal lie at 10 kHz with SNR = 0 dB. The crosscorrelation curve for this case and the corresponding FFT are given in Fig. 4.12a and Fig. 4.12b respectively. As seen the sweep period is well defined and it is estimated with an accuracy of 2.7% using the FFT. Fig. 4.13 through Fig. 4.16 show the case of PSK interference for f_i = 11 kHz and 12 kHz and the method is seen effective in estimating the sweep period

Also, the proposed technique is tested in the case of AM interference as depicted in Fig. 4.17 through Fig. 4.22 for f_i = 10, 11 and 12 kHz. The sweep period can still be estimated with 2.7% accuracy.

Therefore for these types of interference sources, the proposed crosscorrelation method is seen to be capable of detecting the presence of an ELT signal at SIR = 0 dB.

The above procedure is repeated for different values of SIR and the crosscorrelation technique is seen to be effective in detecting the presence of an ELT signal down to SIR = −5 dB. This can be shown through the following two cases. The first, demonstrates the case of CW interference with f_i = 10 kHz as seen in Fig. 4.23 and Fig. 4.24. The cross-correlation curve in Fig. 4.24a is multipeak pattern and the sweep period is estimated as 0.292 s. The second, is the case of PSK with f_i = 11 kHz. The results are depicted in Fig. 4.25 and Fig. 4.26 indicating the detection of the ELT signal.

In the following section, the problem of automatic gain control (AGC) and the limiting at the receiver is studied.

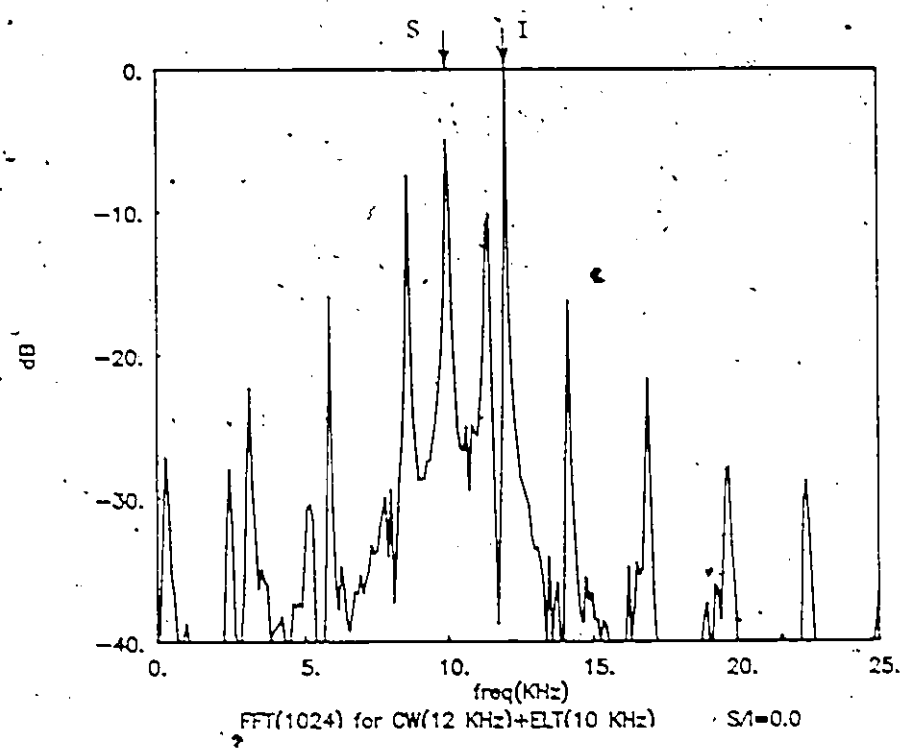

Fig. 4.9 Plot of 1 k-FFT of ELT signal (f_c = 10 kHz) + co-channel CW interference (f_i = 12 kHz). SIR = 0 dB.

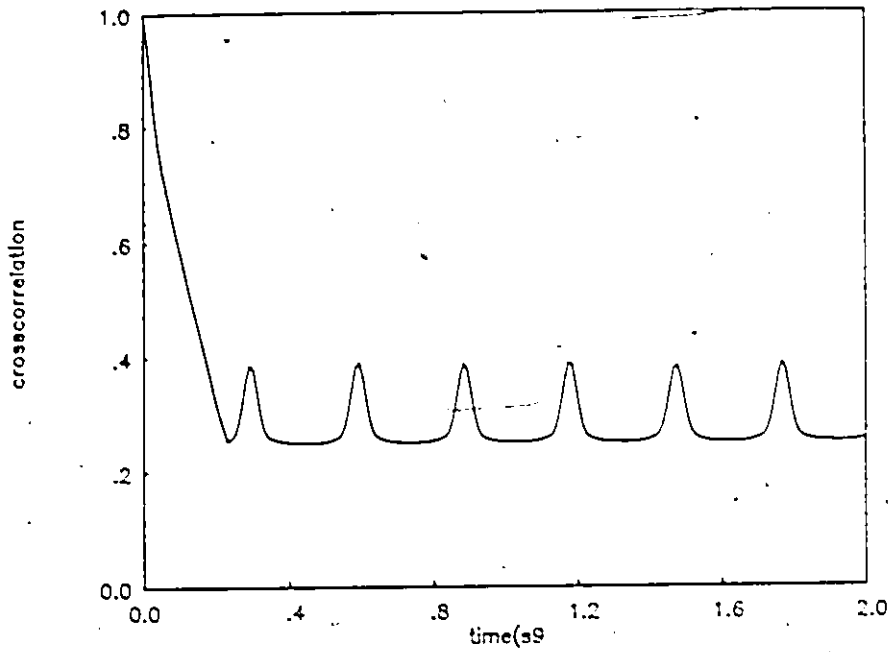

(a)

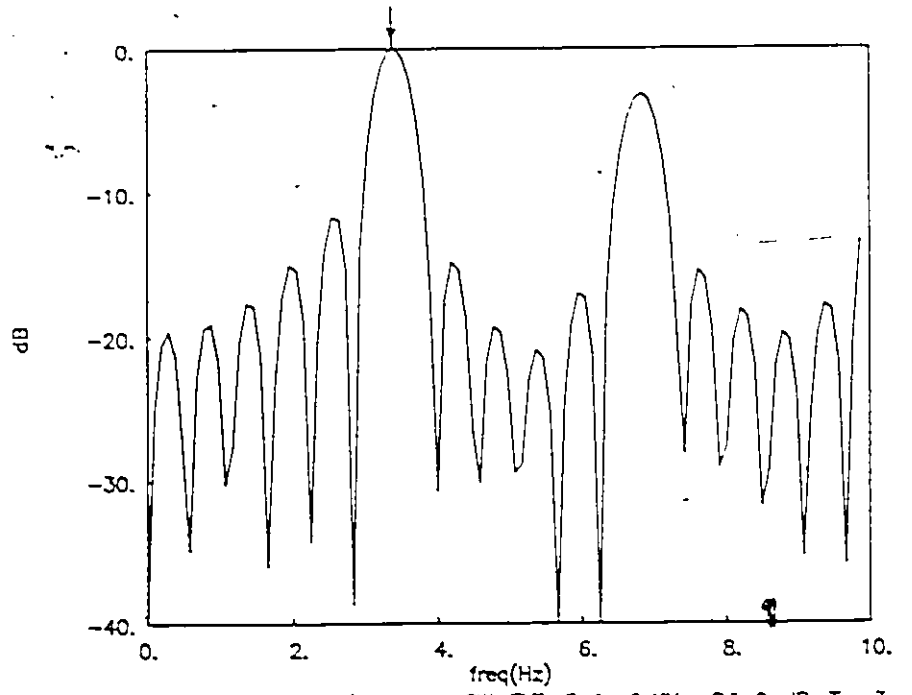

(b)

Fig. 4.10 ELT signal (f_c = 1 kHz) + co-channel CW interference (f_i = 12 kHz). SIR = 0 dB.
(a) The crosscorrelation curve.
(b) The periodogram of the crosscorrelation curve.

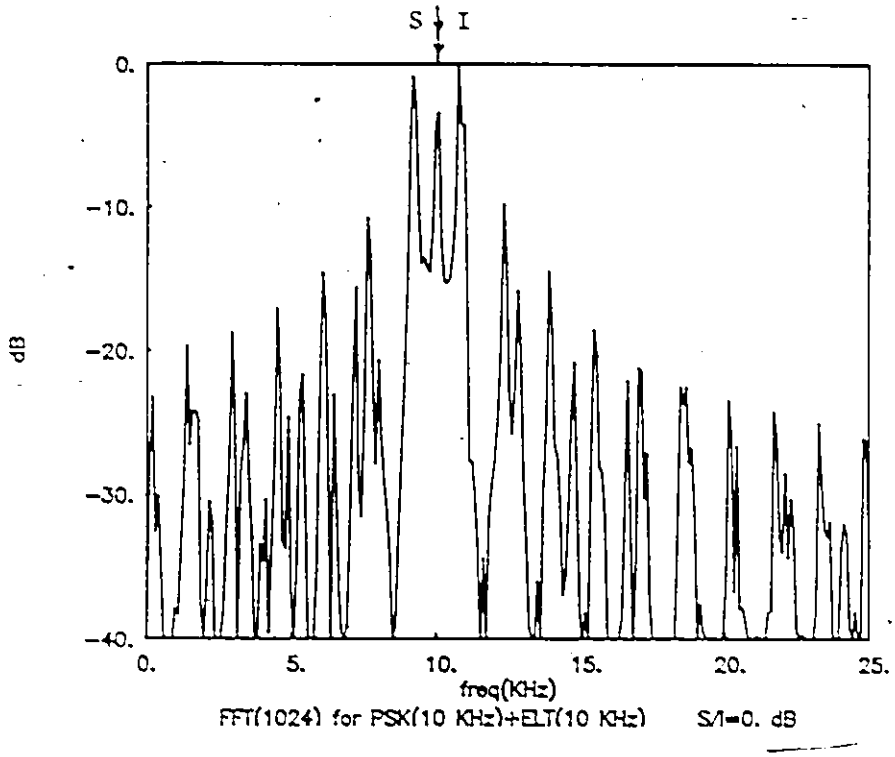

Fig. 4.11 Plot of 1 k-FFT of ELT signal (f_c = 10 kHz) + co-channel PSK interference (f_i = 10 kHz). SIR = 0 dB.

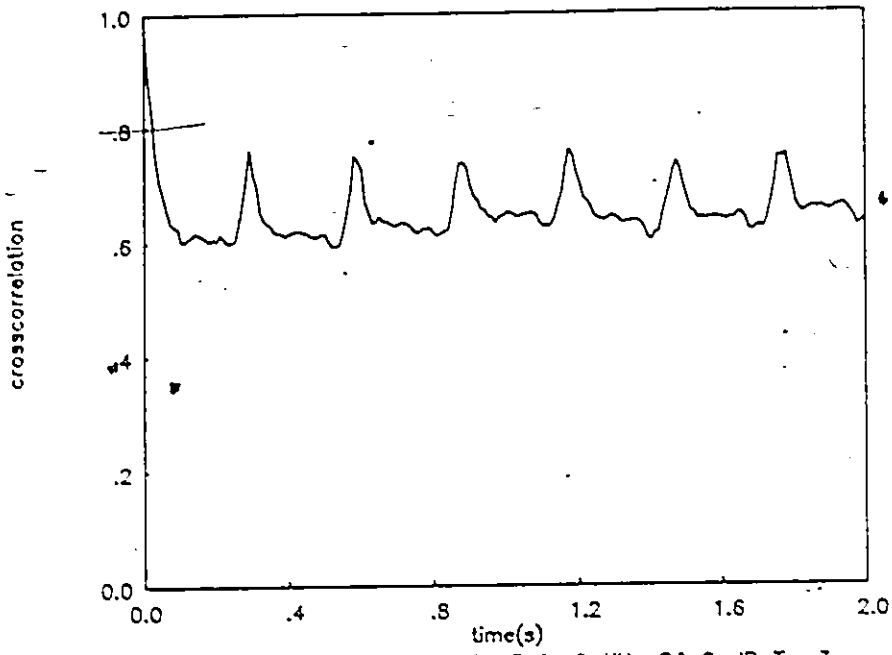

(a)

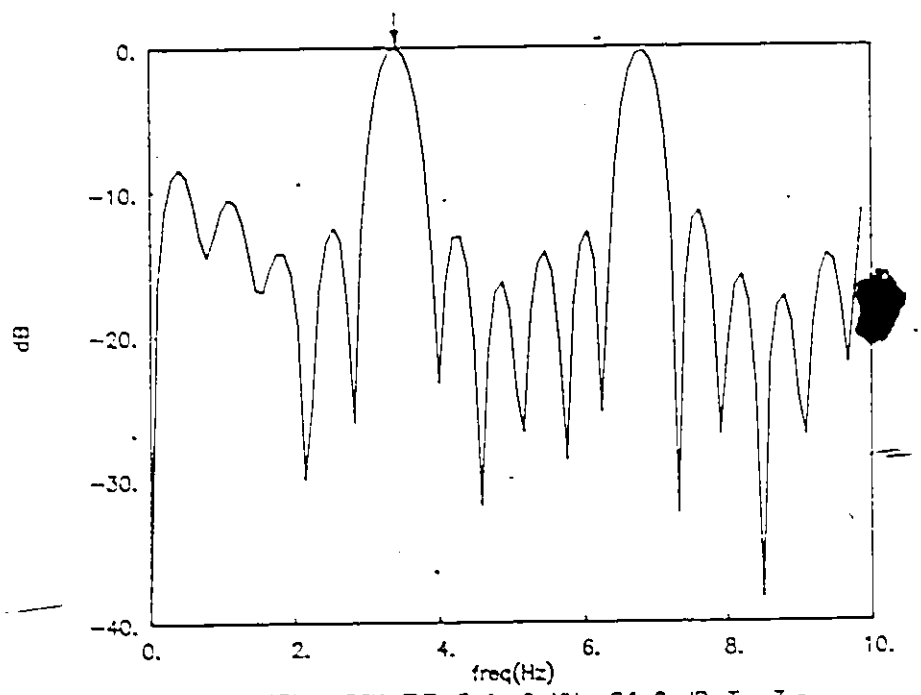

(b)

Fig. 4.12 ELT signal (f_c = 10 kHz) + co-channel PSK interference (f_i = 10 kHz). SIR = 0 dB.

(a) The crosscorrelation curve.

(b) The periodogram of the crosscorrelation curve.

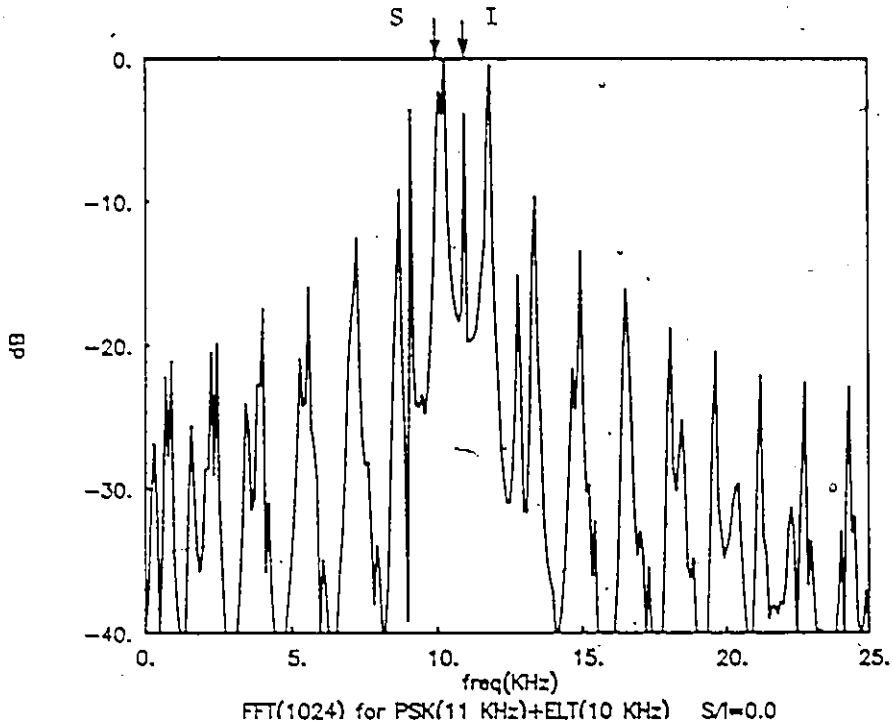

Fig. 4.13 Plot of 1 k-FFT of ELT signal (f_c = 10 kHz) + co-channel PSK interference (f_i = 11 kHz). SIR = 0 dB.

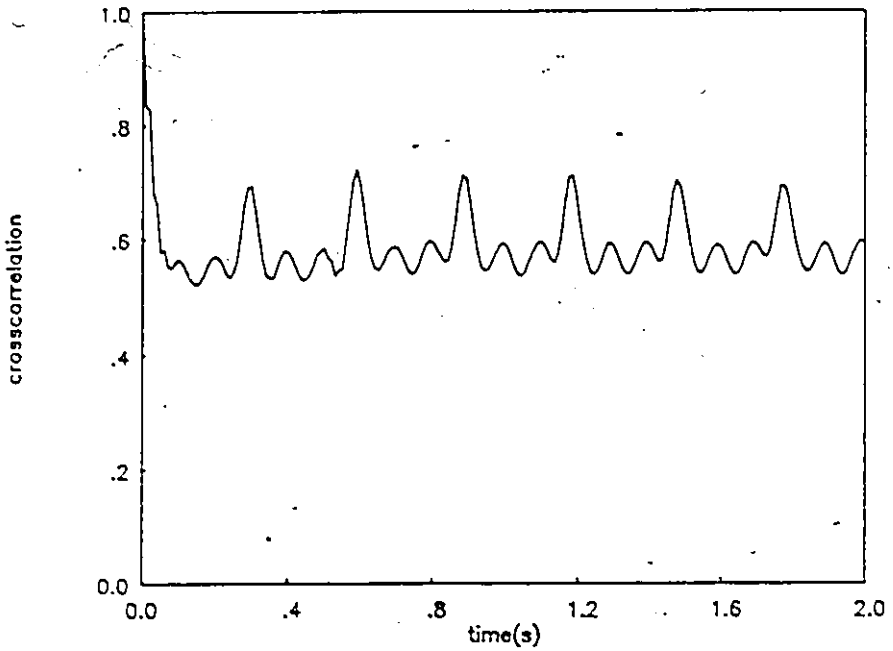

(a)

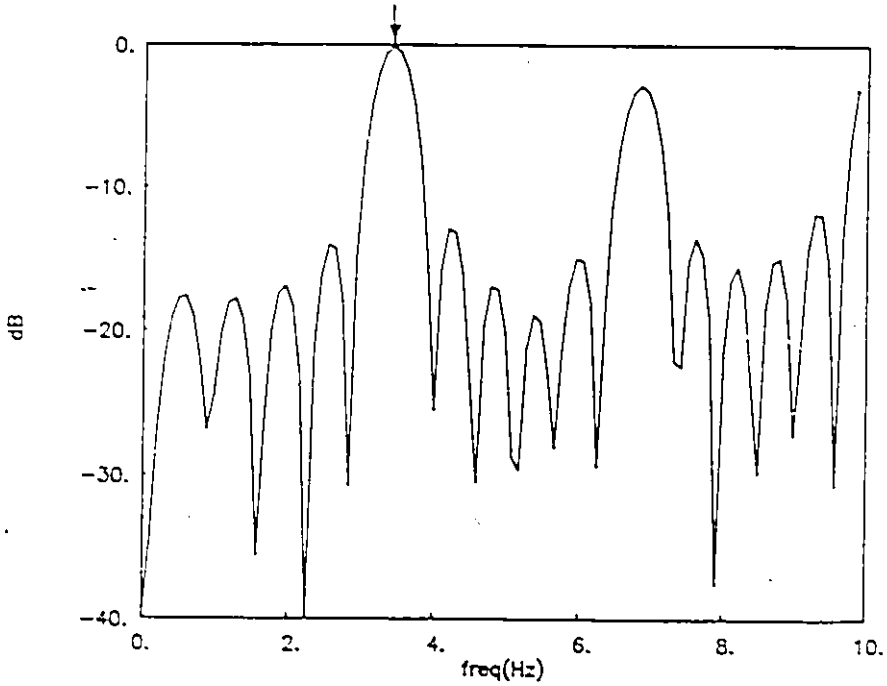

(b)

Fig. 4.14 ELT signal (f_c = 10 kHz) + co-channel PSK interference (f_i = 11 kHz). SIR = 0 dB.

(a) The crosscorrelation curve.

(b) The periodogram of the crosscorrelation curve.

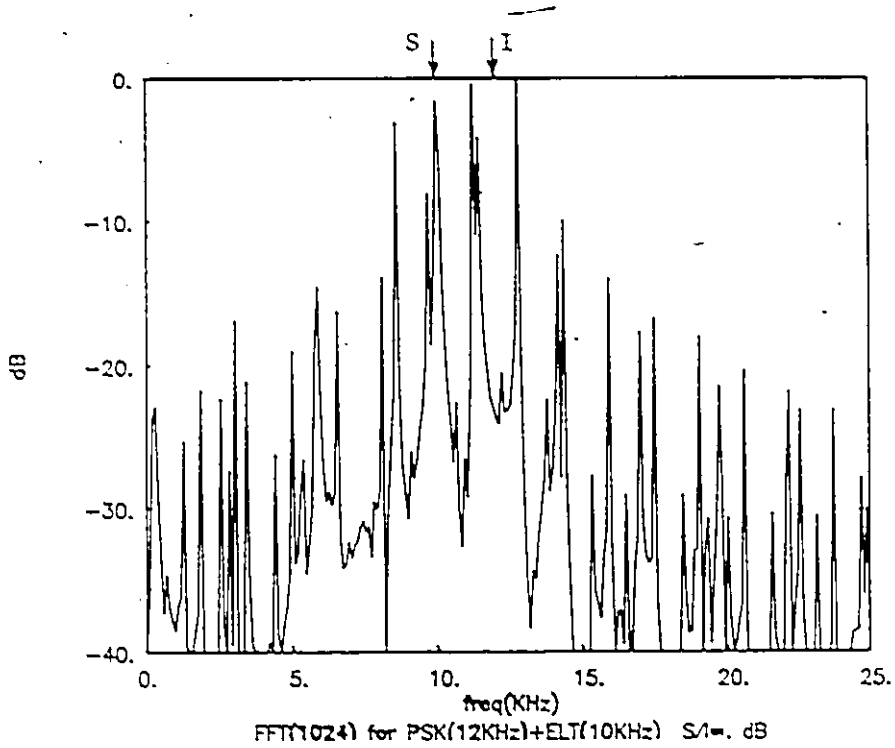

Fig. 4.15 Plot of 1 k-FFT of ELT signal ($f_c = 10$ kHz) + co-channel PSK interference ($f_i = 12$ kHz). SIR = 0 dB.

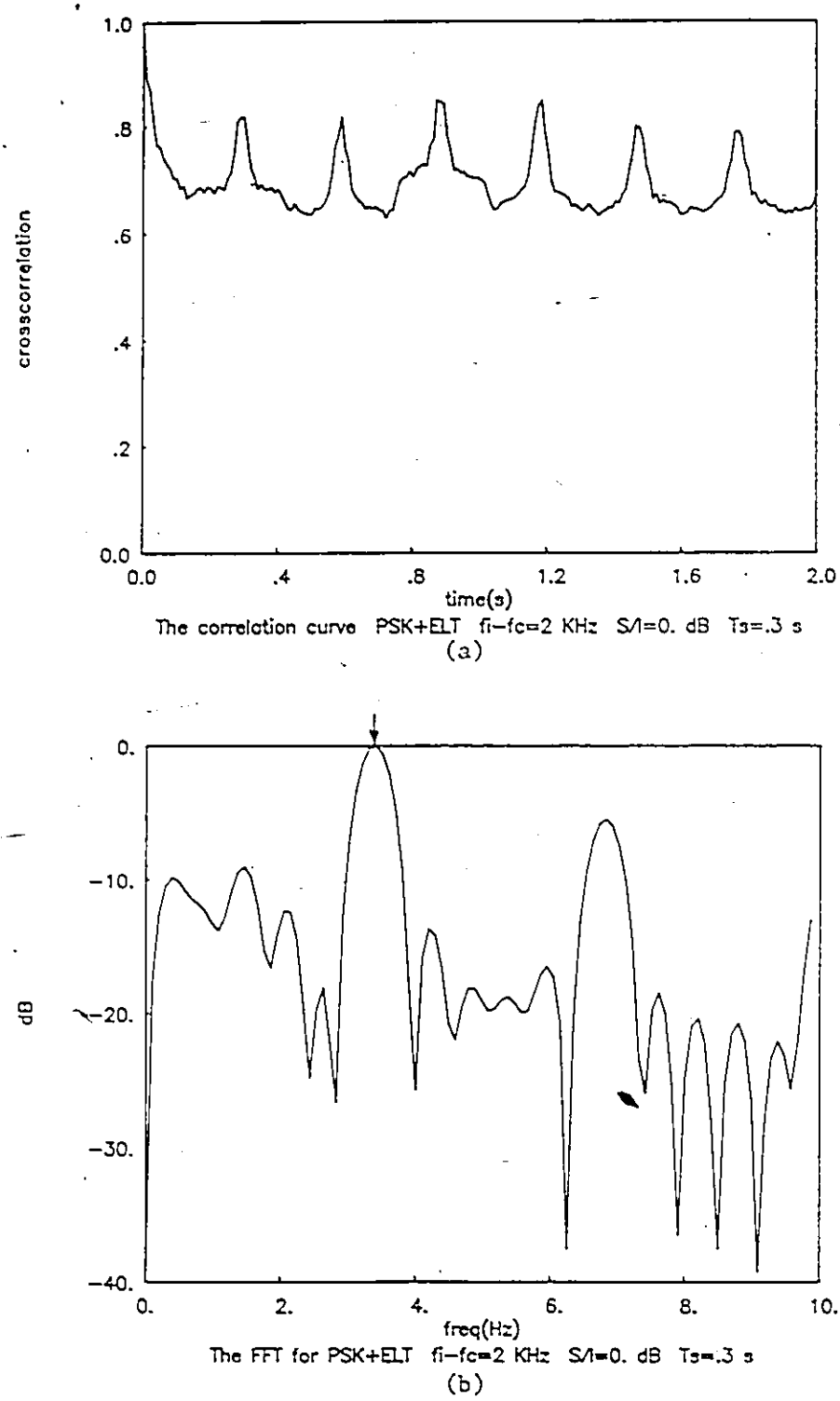

Fig. 4.16 ELT signal ($f_c = 10$ kHz) + co-channel PSK interference ($f_i = 12$ kHz). SIR = 0 dB.

(a) The crosscorrelation curve.

(b) The periodogram of the crosscorrelation curve.

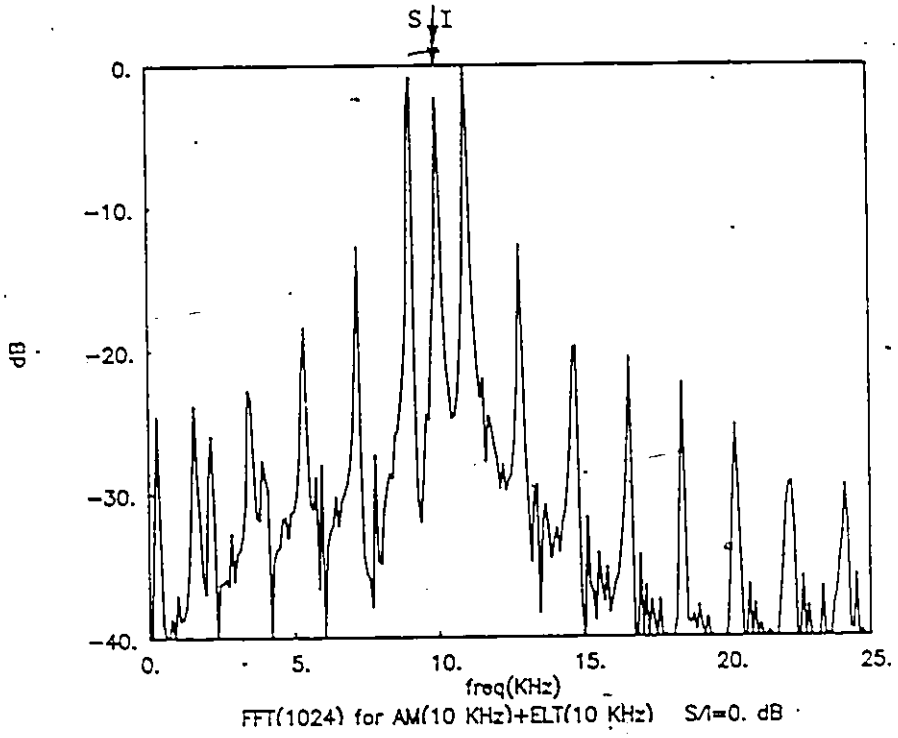

Fig. 4.17 Plot of 1 k-FFT of ELT signal (f_c = 10 kHz) + co-channel AM interference (f_i = 10 kHz). SIR = 0 dB.

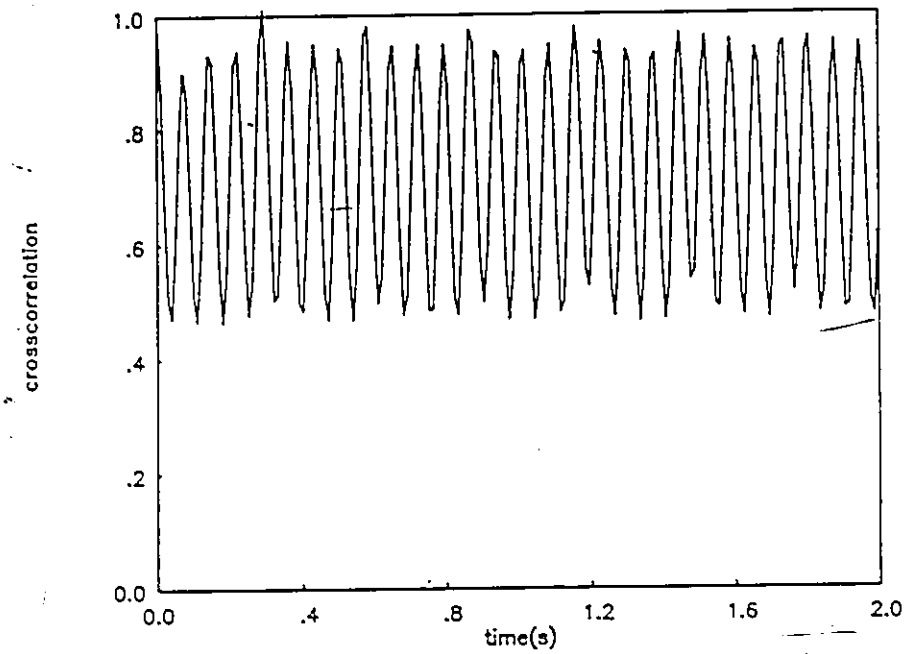

(a)

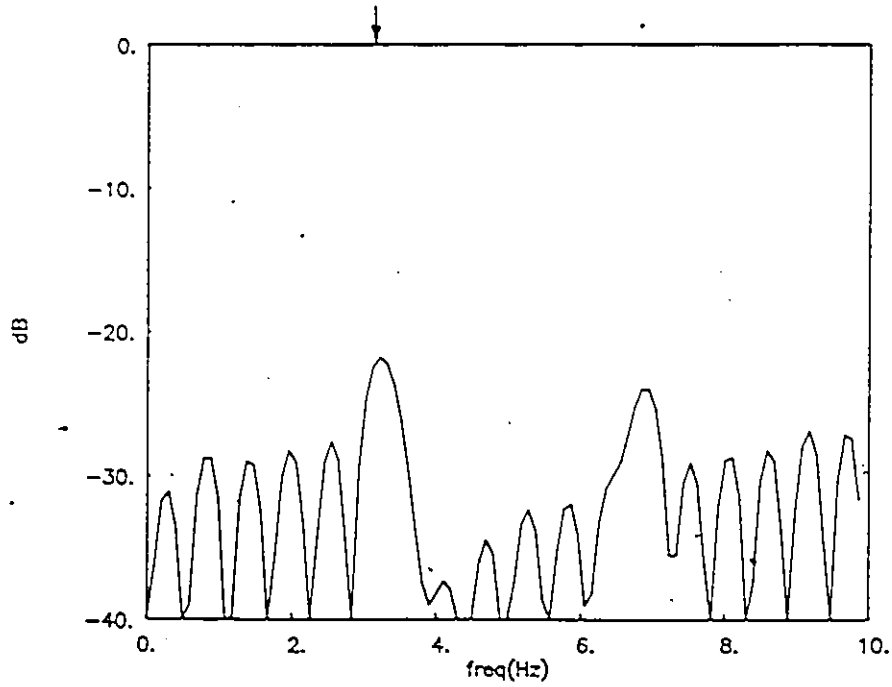

(b)

Fig. 4.18 ELT signal (f_c = 10 kHz) + co-channel AM interference (f_i = 10 kHz). SIR = 0 dB.

(a) The crosscorrelation curve.

(b) The periodogram of the crosscorrelation curve.

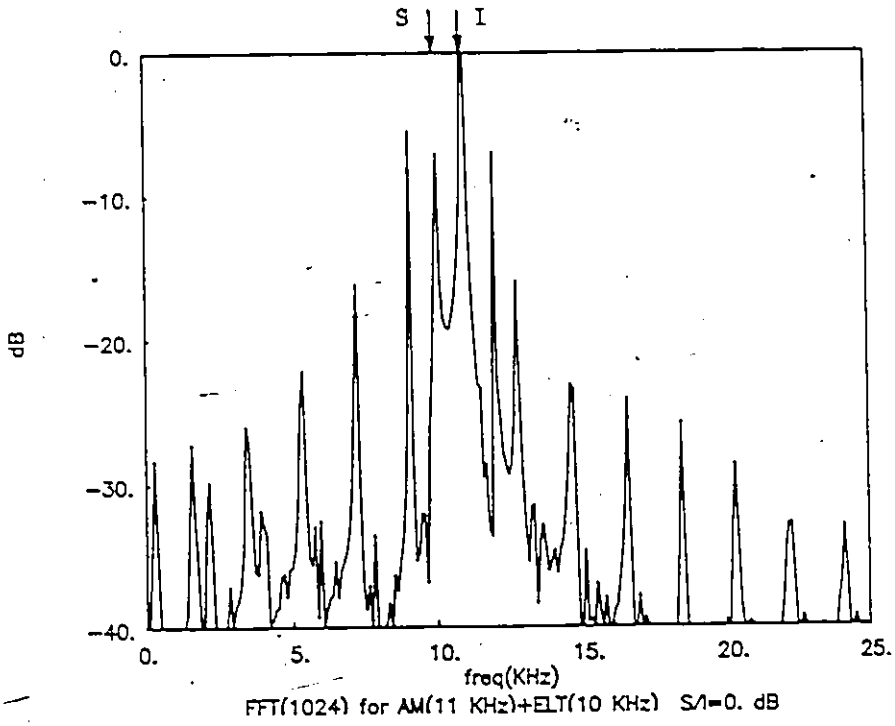

Fig. 4.19 Plot of 1 k-FFT of ELT signal (f_c = 10 kHz) + co-channel AM interference (f_i = 11 kHz). SIR = 0 dB.

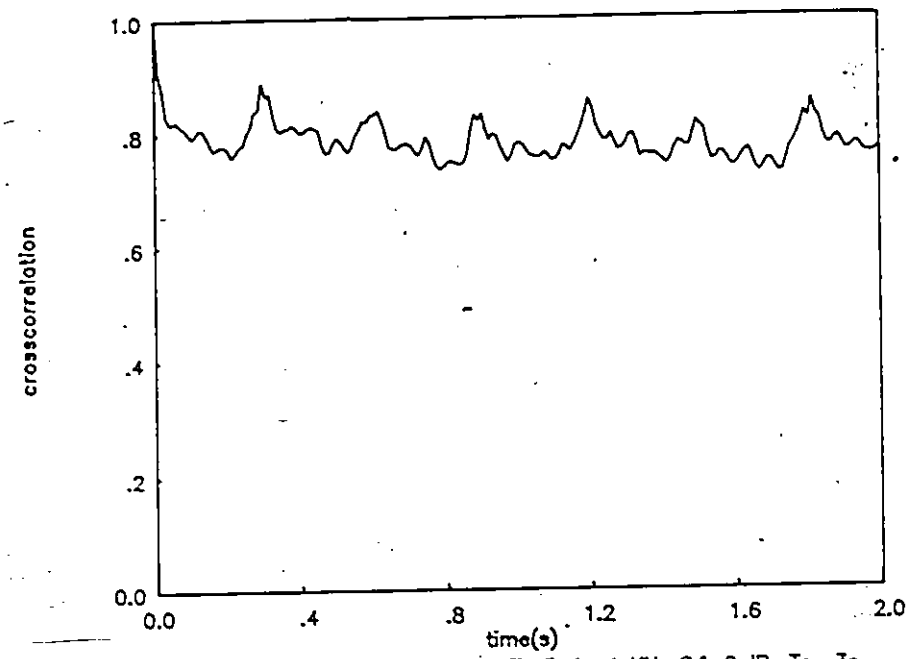

The correlation curve of AM+ELT fi−fc=1 KHz S/I=0.dB Ts=.3s

(a)

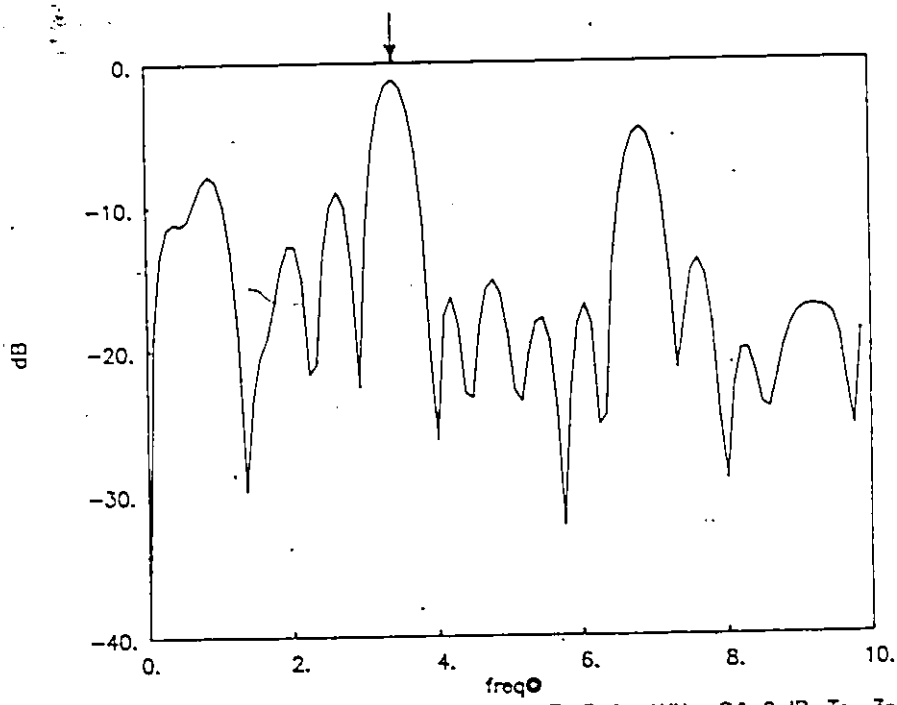

The FFT of the correlation curve AM+ELT fi−fc=1KHz S/I=0.dB Ts=.3s

(b)

Fig. 4.20 ELT signal ($f_c = 10$ kHz) + co-channel AM interference ($f_i = 11$ kHz). SIR = 0 dB.

(a) The crosscorrelation curve.

(b) The periodogram of the crosscorrelation curve.

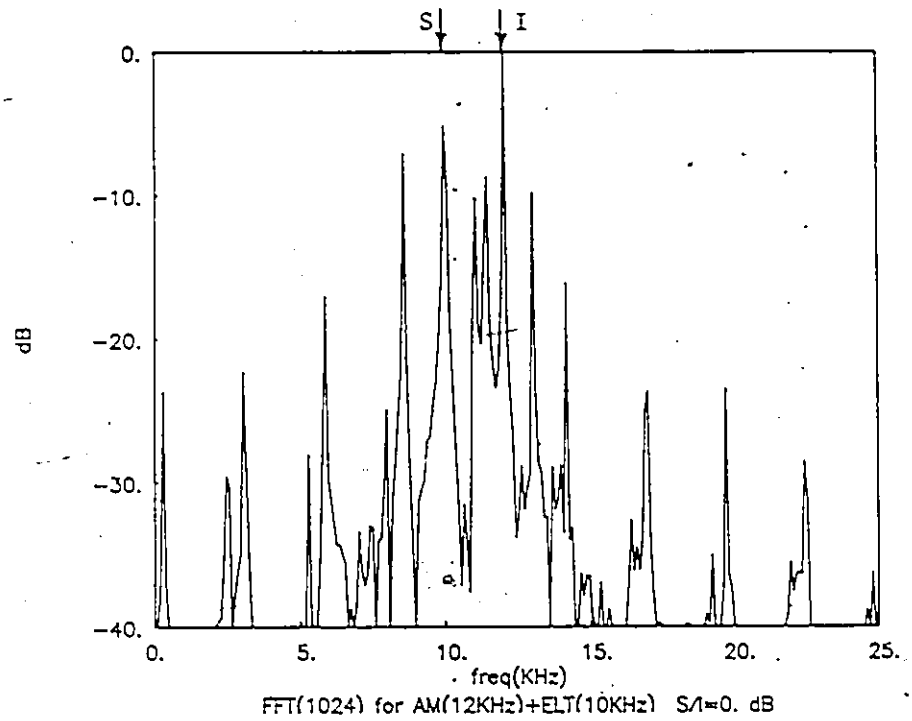

Fig. 4.21 Plot of 1 k-FFT of ELT signal (f_c = 10 kHz) + co-channel AM interference (f_i = 12 kHz). SIR = 0 dB.

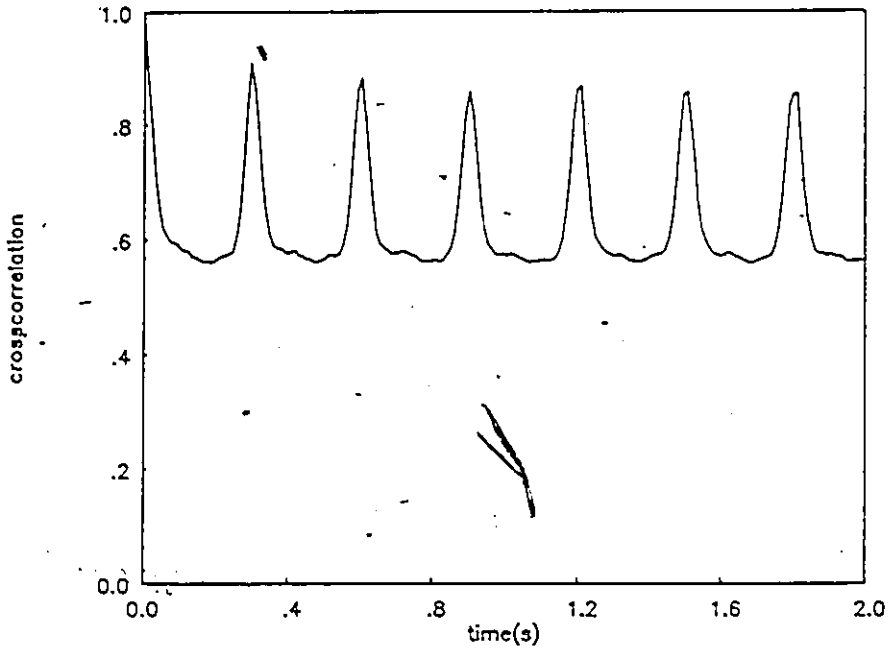

(a)

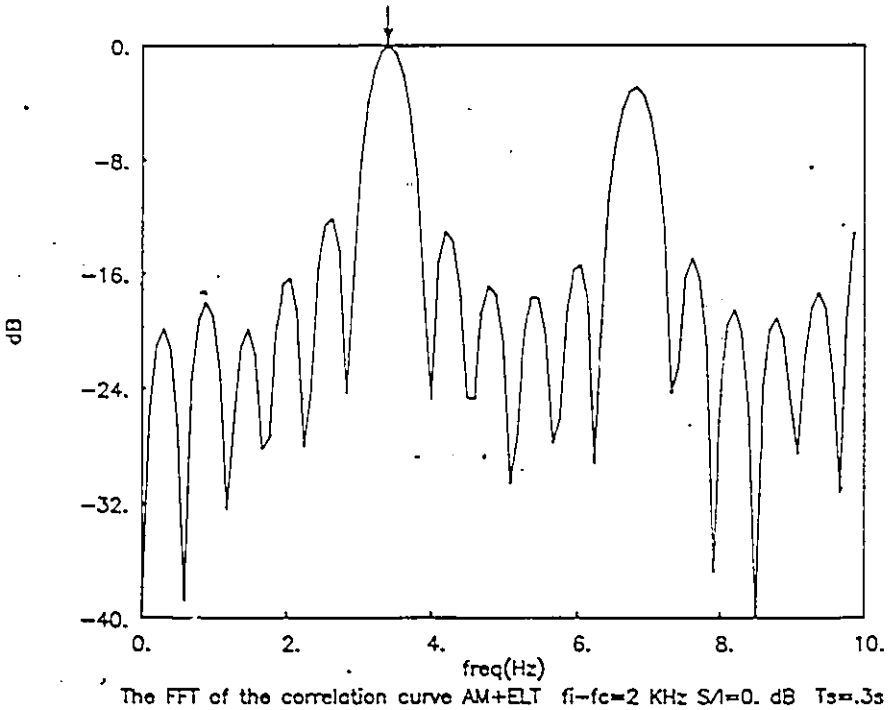

(b)

Fig. 4.22 ELT signal ($f_c = 10$ kHz) + co-channel AM interference ($f_i = 12$ kHz). SIR = 0 dB.

(a) The crosscorrelation curve.

(b) The periodogram of the crosscorrelation curve.

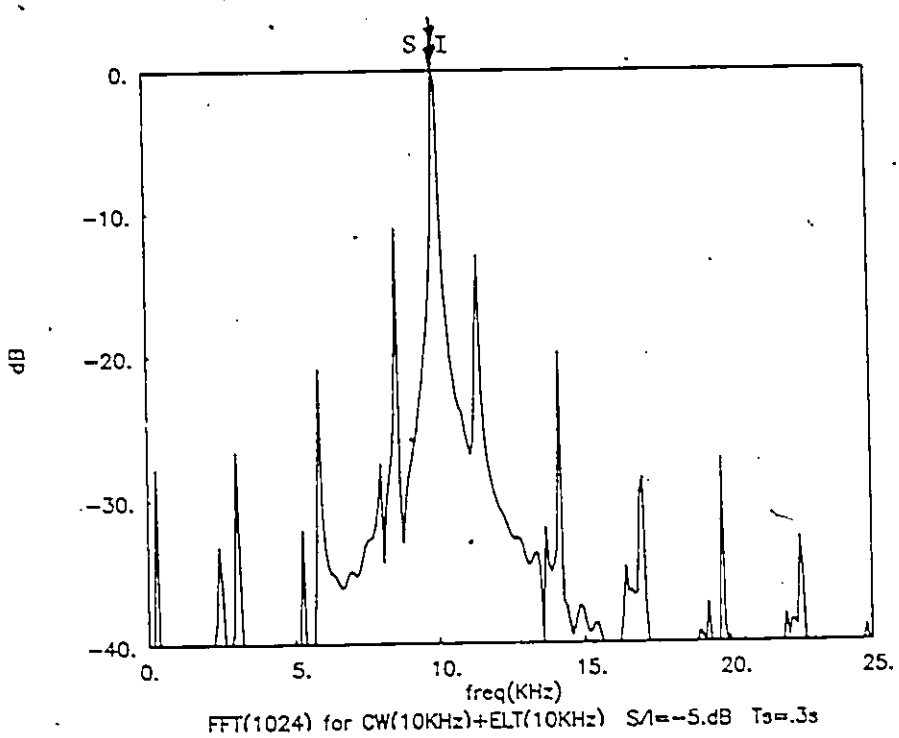

Fig. 4.23 Plot of 1 k-FFT of ELT signal (f_c = 10 kHz) + co-channel CW interference (f_i = 10 kHz). SIR = −5 dB.

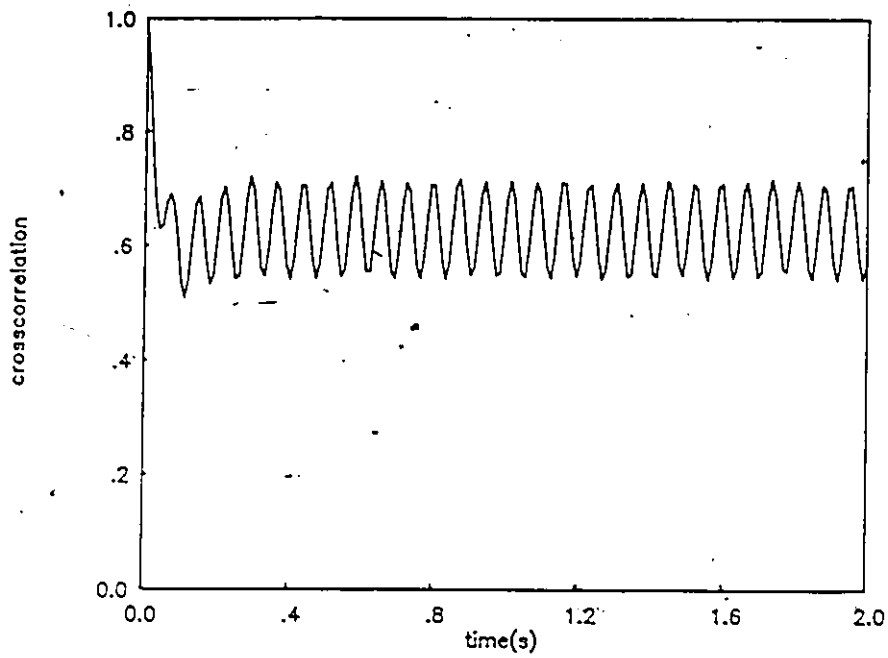

The correlation curve CW+ELT fi−fc=0. KHz S/I=−5 dB Ts=.3 s

(a)

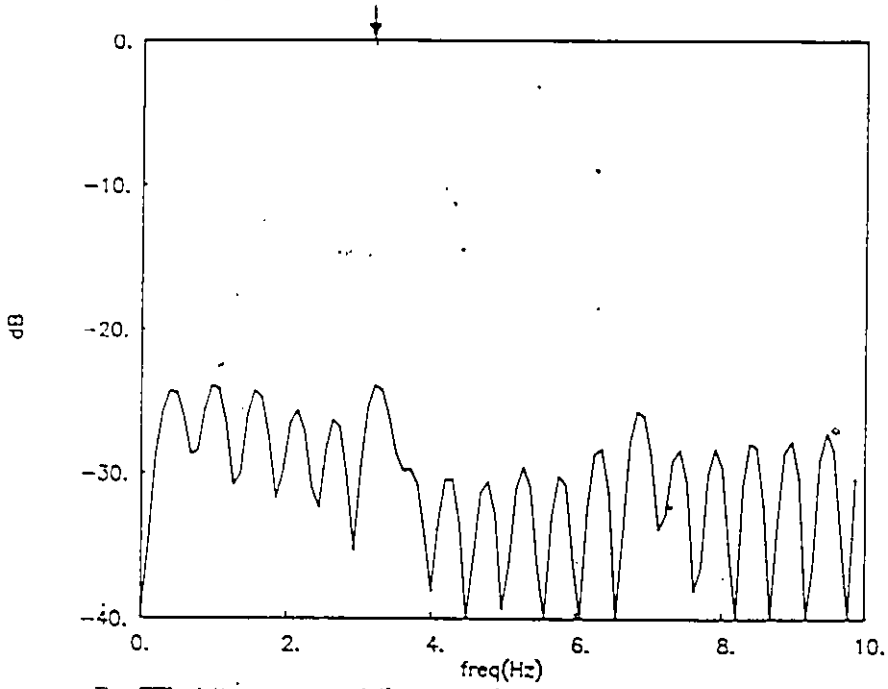

The FFT of the crosscorrelation curve CW+ELT fi−fc=0. kHz S/I=−5 dB Ts=.3s

(b)

Fig. 4.24 ELT signal ($f_c = 10$ kHz) + co-channel CW interference ($f_i = 10$ kHz). SIR = −5 dB.

(a) The crosscorrelation curve.

(b) The periodogram of the crosscorrelation curve.

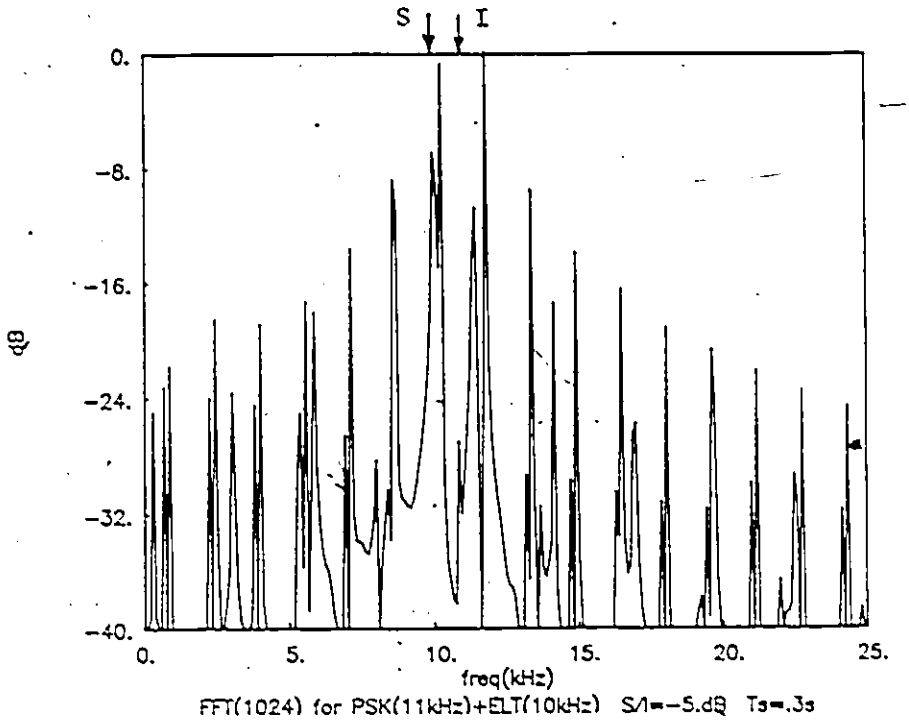

Fig. 4.25 Plot of 1 k-FFT of ELT signal (f_c = 10 kHz) + co-channel PSK interference (f_i = 11 kHz). SIR = −5 dB.

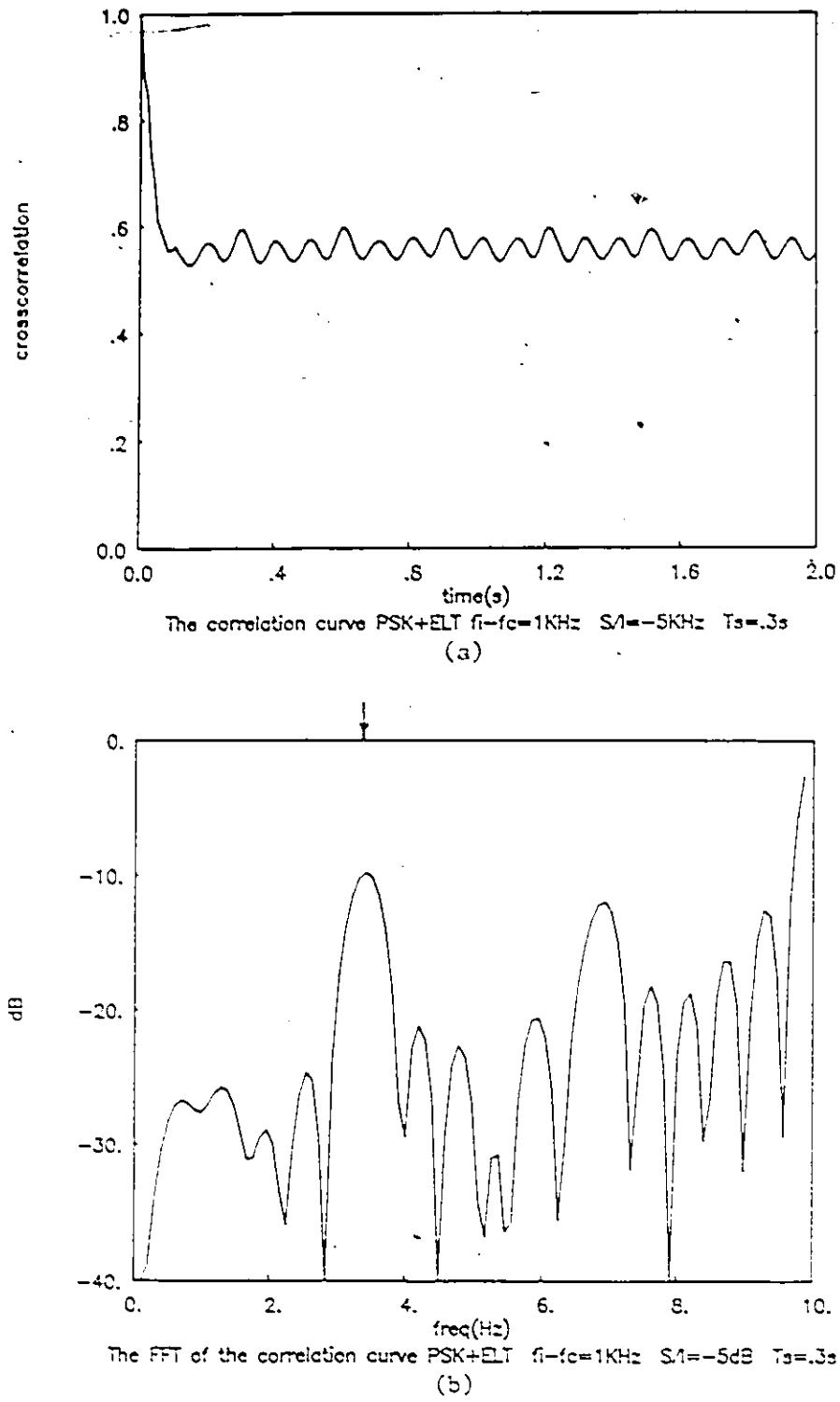

Fig. 4.26 ELT signal (f_c = 10 kHz) + co-channel PSK interference (f_i = 11 kHz). SIR = −5 dB.

(a) The crosscorrelation curve.

(b) The periodogram of the crosscorrelation curve.

4.4 Automatic Gain Control and Limiter

Automatic gain control and limiting have essentially the same effect on the signal, however the implementations are slightly different. Let us now consider the case of AGC.

Usually the AGC is applied to the analog amplifier stage of the receiver in the form of amplitude control of the time signal. The gain of any AGC amplifier can be written as:

$$G = P_o/P_i \tag{4.10}$$

where

P_o = the total output power

P_i = the total input power from M sources

$$= \sum_{m=1}^{M} P_{im}$$

Now, if we assume that the output power is constant, which is typical of most AGC systems, then the gain of the amplifier varies inversely as the input power.

Let us assume that one source, namely the jth source of interference, is far stronger than the other sources of signal and background noise, then the gain of the AGC amplifier is given approximately by:

$$G = P_o/P_{ij} \tag{4.11}$$

where P_{ij} = input power from the jth source.

Then, for the kth signal, which may be an ELT, the output signal for the AGC amplifier is simply given by:

$$\begin{aligned} P_{ok} &= G \times P_{ik} \\ &= P_o \times P_{ik}/P_{ij} \end{aligned} \tag{4.12}$$

Both P_o and P_{ik} are constant. Therefore, as the power of the jth interfering source increases, the output power of the kth source decreases. Thus, the unwanted high amplitude

interfering signal is easily received, while the weaker signal disappears which is highly undesirable.

The effect of AGC or limiter can be further investigated by computer simulation. Consider the limiter transfer characteristics as shown in Fig. 4.27 where the output voltage is limited to v_{lim} when the input exceeds v'. The following function represents the limiter characteristics:

$$v_o = \begin{cases} -v_{lim} & v_{in} < v' \\ G\,v_{in} & -v' < v_{in} < v' \\ v_{lim} & v' < v_{in} \end{cases}$$

where G is the limiter gain. The case of no limiting corresponds to unity gain. As the gain increases, the limiting effect increases.

The following values of the gain will be considered in our study G = 1, 10 and 100. To test the limiter effect, the interference signal is simulated to have a carrier frequency at 10 kHz, while the ELT signal carrier frequency is approximately 16 kHz. Figures 4.28a, 4.28b and 4.29a show the 1 K-periodogram of CW + ELT signals with SIR = 0 dB for limiter gain of 1, 10 and 100 respectively. The arrows indicate the carrier frequencies where letter S indicates the ELT signal and letter I indicates the interference. As seen, when the gain increases, the average background level increases but the ELT signal is still detectable. Performing the crosscorrelation for the case of SIR = 0 dB and gain = 100, the curve at Fig. 4.29b is obtained. This curve has multipeak pattern indicating the existence of an ELT signal.

Figures 4.30 and 4.31 provide the crosscorrelation results for the case of SIR = −10 dB. From these figures, it is noticed that as the gain increases, the level of the ELT signal decreases by approximately 5 dB. The crosscorrelation curve calculated for gain = 100 is depicted in Fig. 4.31b where the sweep period can be easily measured,

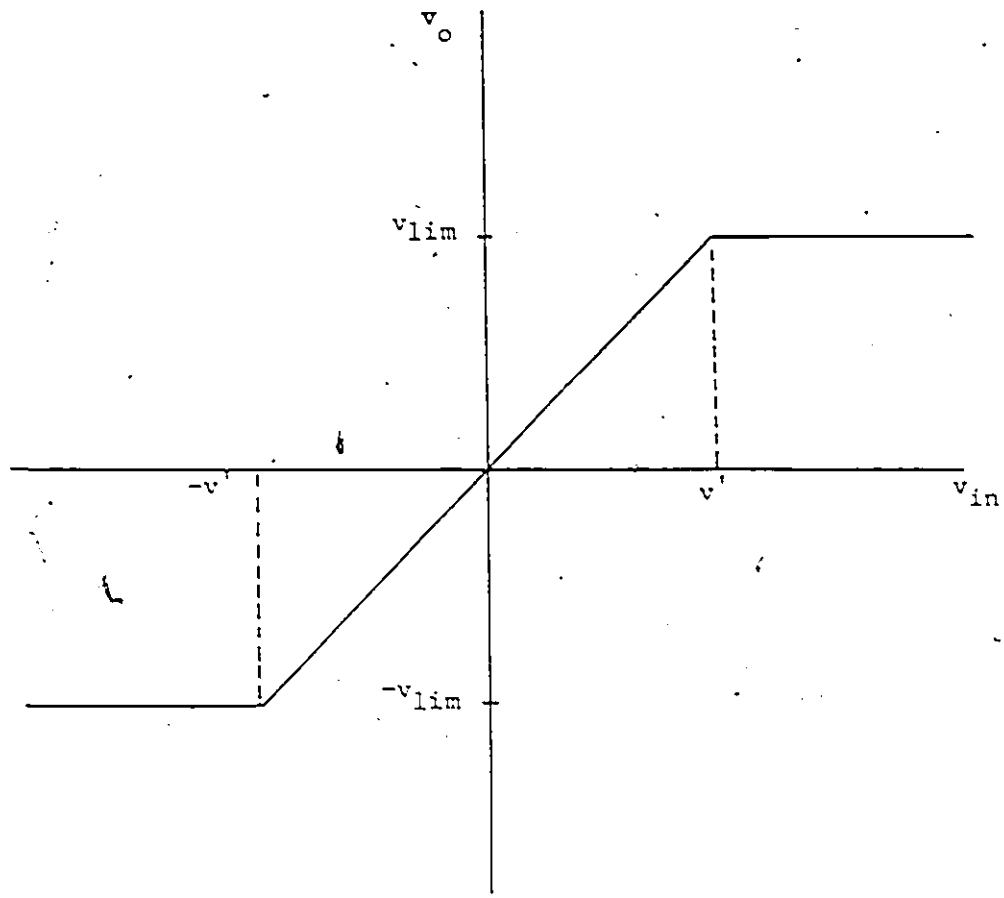

Fig. 4.27 The limiter transfer characteristics.

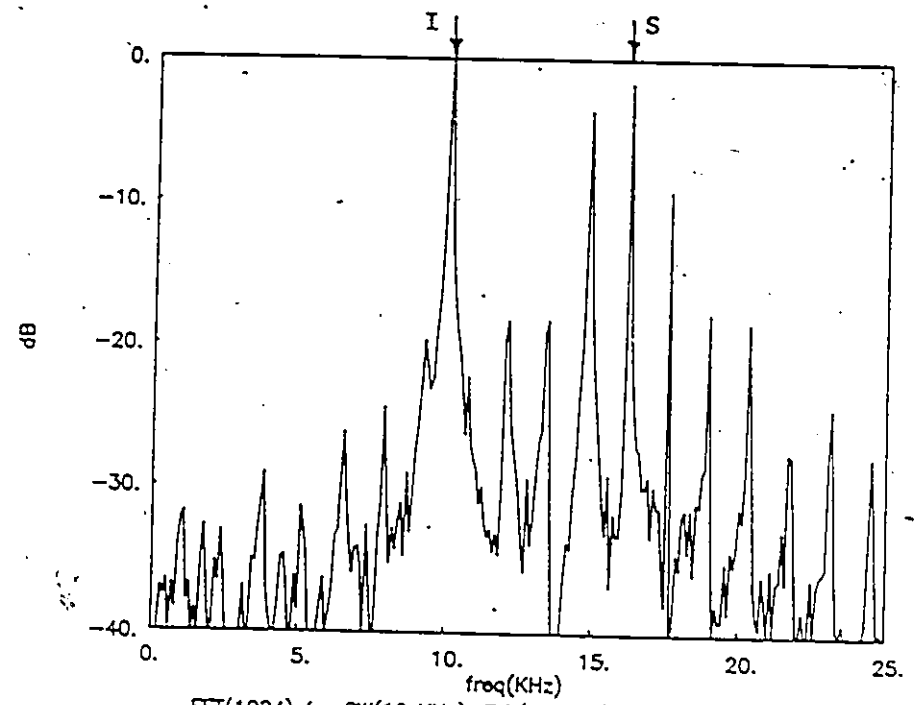

(a)

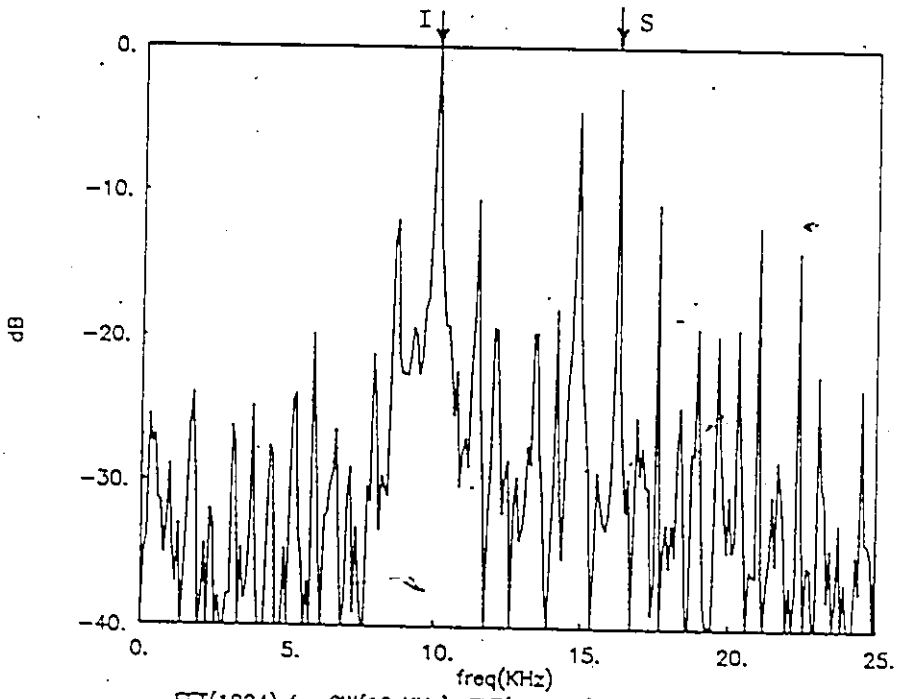

(b)

Fig. 4.28 Plot of 1 k-FFT for ELT signal (16 kHz) + CW interference (10 kHz) for SIR = 0. dB.
(a) Gain = 1
(b) Gain = 10

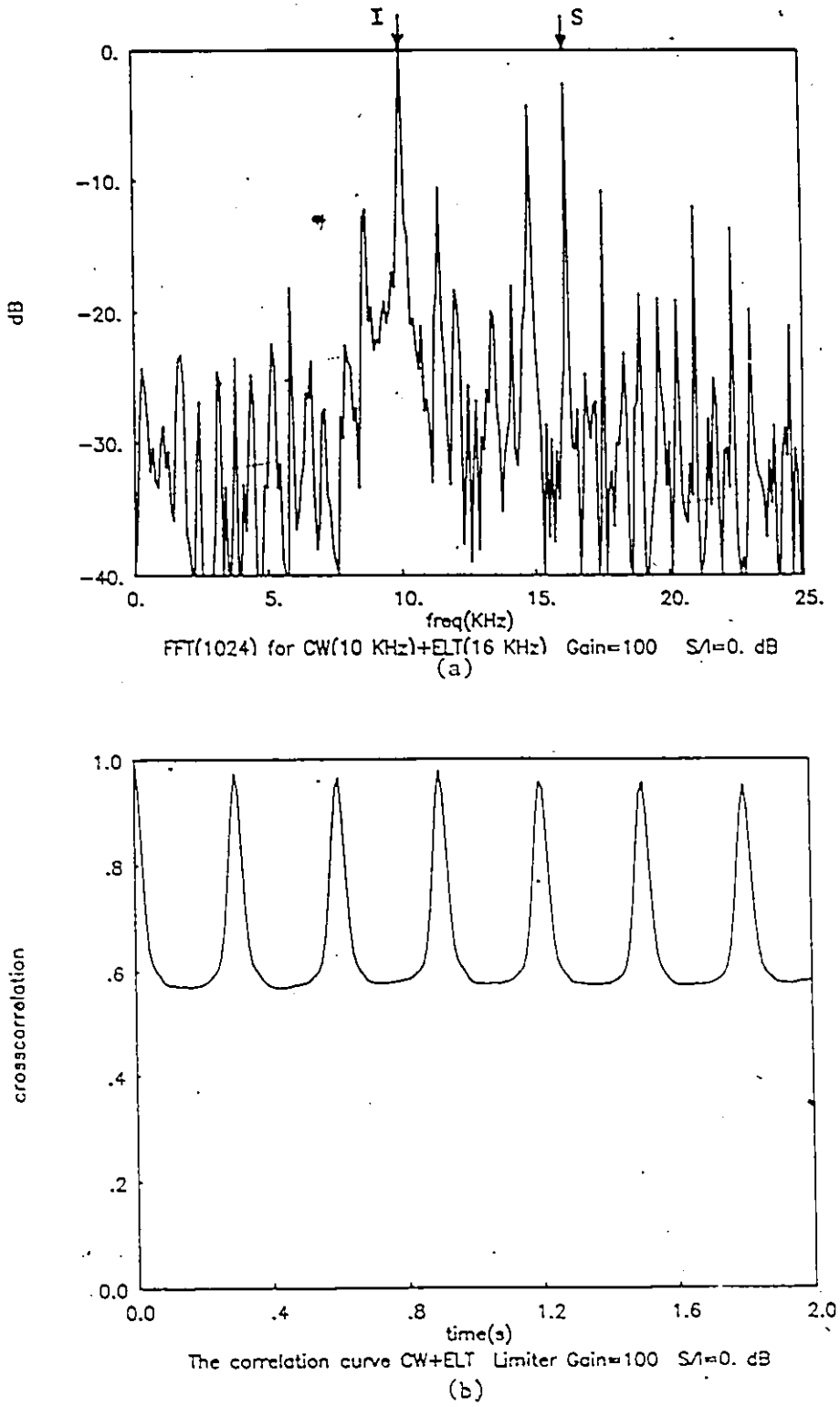

Fig. 4.29 ELT signal (16 kHz) + CW interference (10 kHz) for Gain = 100 and SIR = 0. dB.
(a) 1 k-FFT
(b) The crosscorrelation curve.

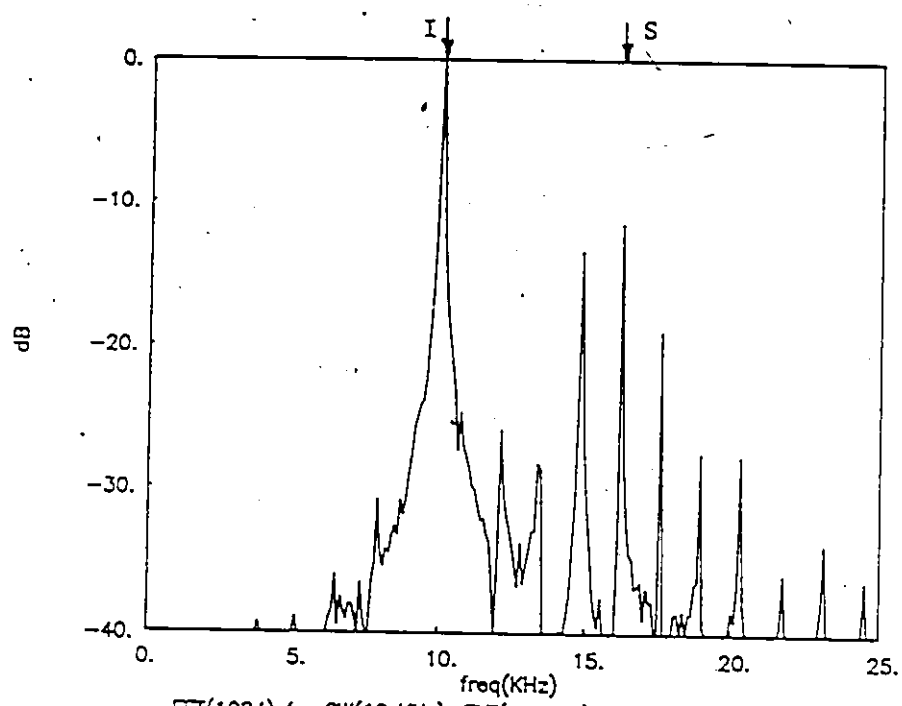

(a)

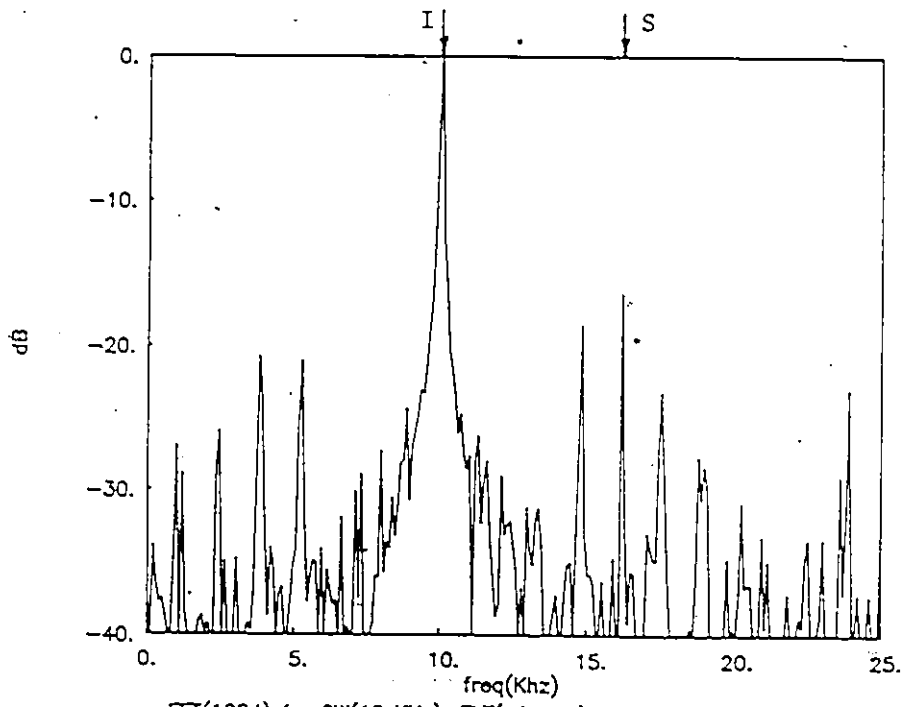

(b)

Fig. 4.30 Plot of 1 k-FFT for ELT signal (16 kHz) + CW interference (10 kHz) for SIR = −10. dB.
(a) Gain = 1
(b) Gain = 10

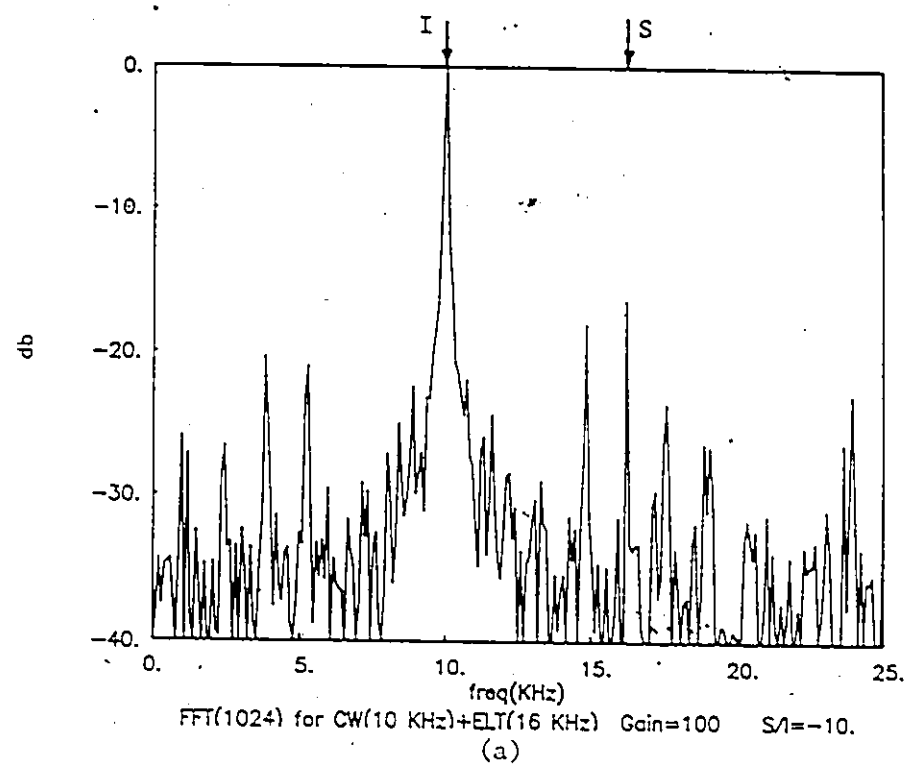

(a)

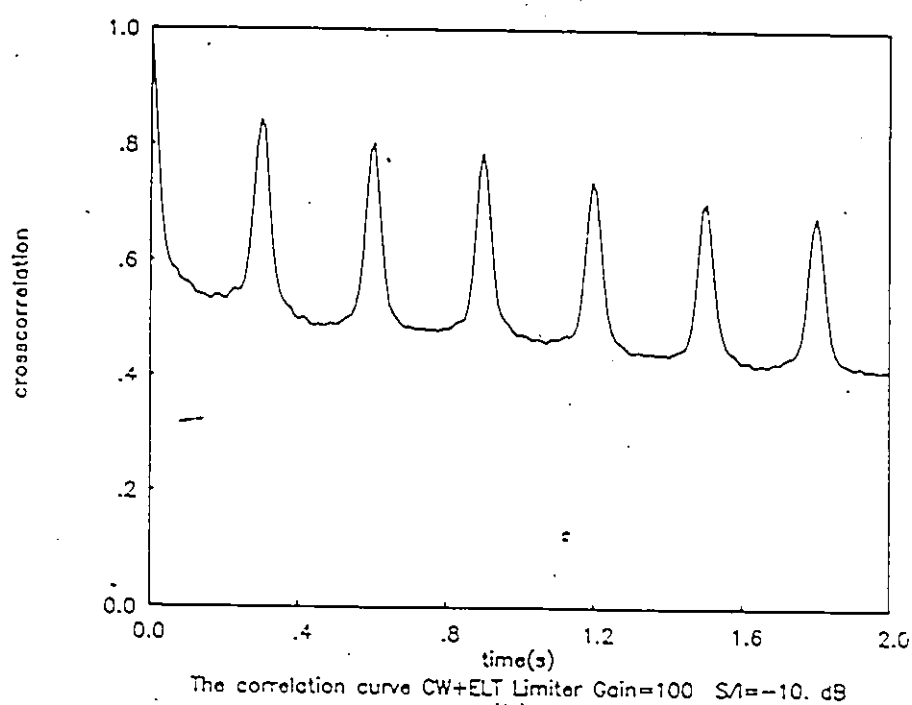

(b)

Fig. 4.31 ELT signal (16 kHz) + CW interference (10 kHz) for Gain = 100 and SIR = −10. dB.

(a) 1 k-FFT

(b) The crosscorrelation curve.

indicating again the detection of an ELT signal. Similar plots for SIR = −15 dB are given in Fig. 4.32 and Fig. 4.33.

From the above study, we find that by using the crosscorrelation technique, it is possible to overcome some of the problems associated with the use of limiter or AGC. This technique is seen to be effective down to SIR = −15 dB. Beyond this point the cross-correlation method becomes ineffective as seen in Fig. 4.34 and Fig. 4.35 for SIR = −20 dB, where the ELT signal is dominated by interference. As seen the crosscorrelation curve in Fig. 4.35b is flat and no detection of the ELT signal is achieved.

The same study is applied for the other two types of interference, namely PSK and AM signals. Figure 4.36a and Fig. 4.36b show the periodograms in the case of PSK for gain = 1 and 10 respectively with SIR = 0. dB. Note that the back ground noise increases as the gain increases. In addition hand Fig. 4.37 depicts the case of gain = 100 along with the corresponding FFT where sharp peaks are obtained indicating the sweep period. Similar procedure is provided for the case of SIR = −10 and −15 dB as seen in Fig. 4.38 through Fig. 4.41. Note that the level of the peaks of the crosscorrelation curve decreases as the limiter SIR decreases making the detection of the ELT signal more difficult when the SIR is less than −15 dB. Figure 4.42 through Fig. 4.47 show the case of AM interference for different values of limiter gain and SIR ratio and same results are obtained indicating the effectiveness of the proposed method to combat the limiter effect.

4.5 Summary

1. In this chapter, a thorough study of the interference sources in 121.5 and 243 MHz bands have been performed.

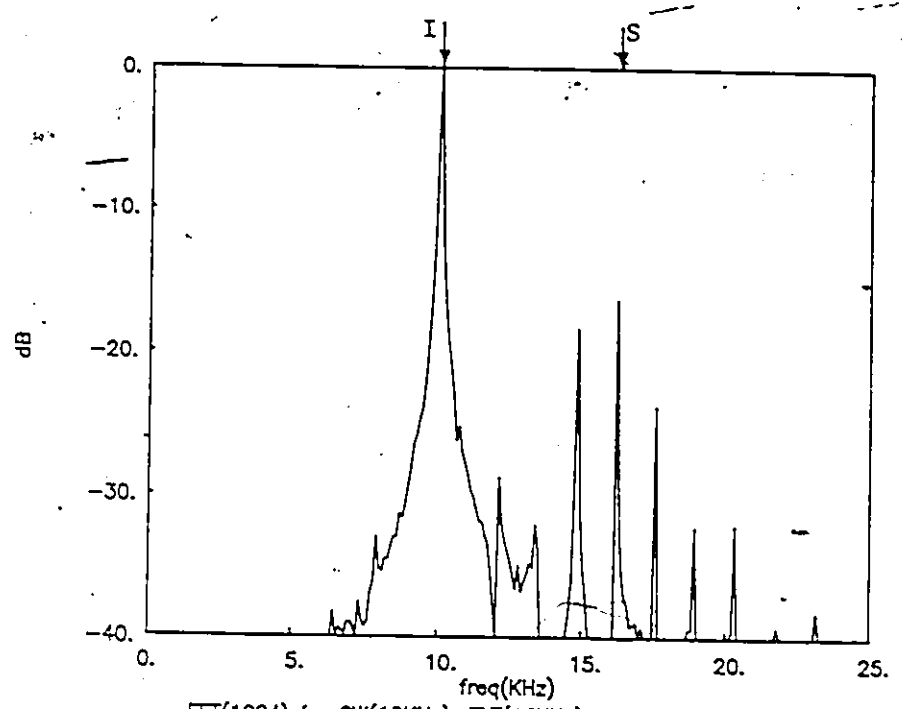

(a)

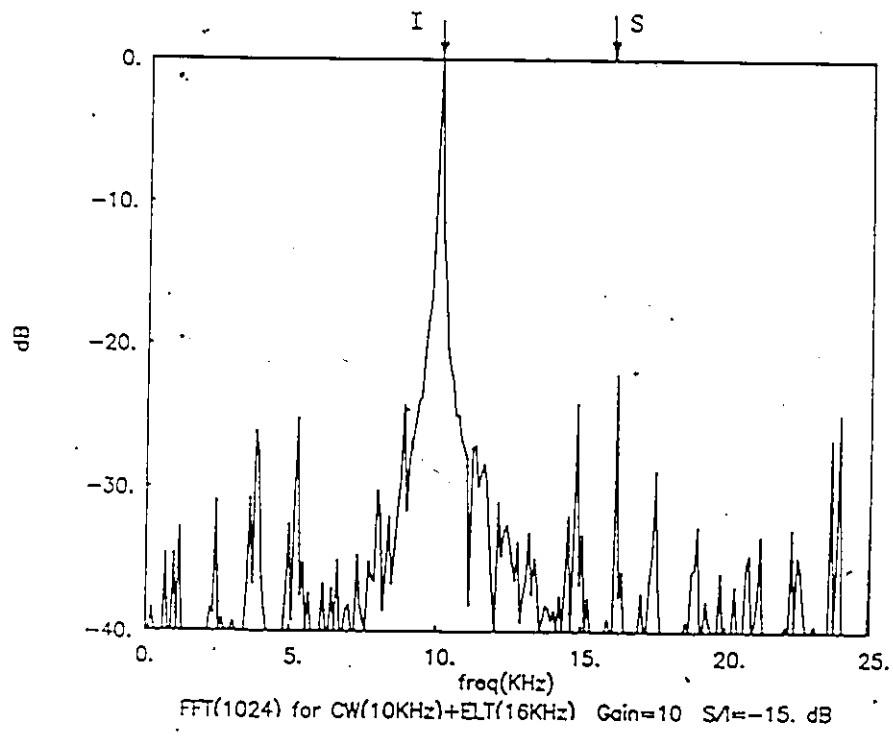

(b)

Fig. 4.32 Plot of 1 k-FFT for ELT signal (16 kHz) + CW interference (10 kHz) for SIR = −15. dB.
(a) Gain = 1
(b) Gain = 10

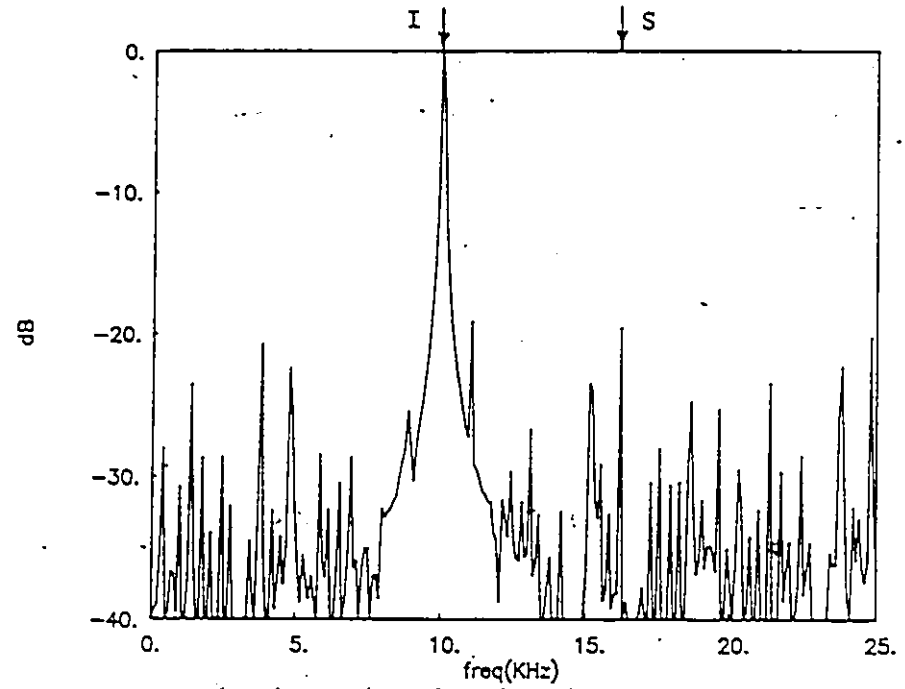

(a)

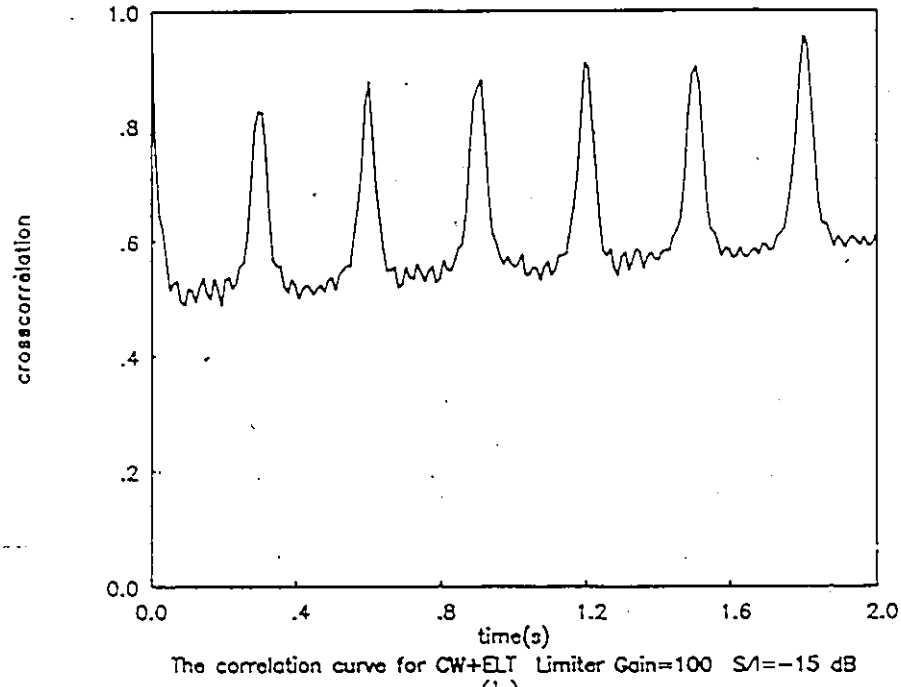

(b)

Fig. 4.33 ELT signal (16 kHz) + CW interference (10 kHz) for Gain = 100 and SIR = −15. dB.
(a) 1 k-FFT
(b) The crosscorrelation curve.

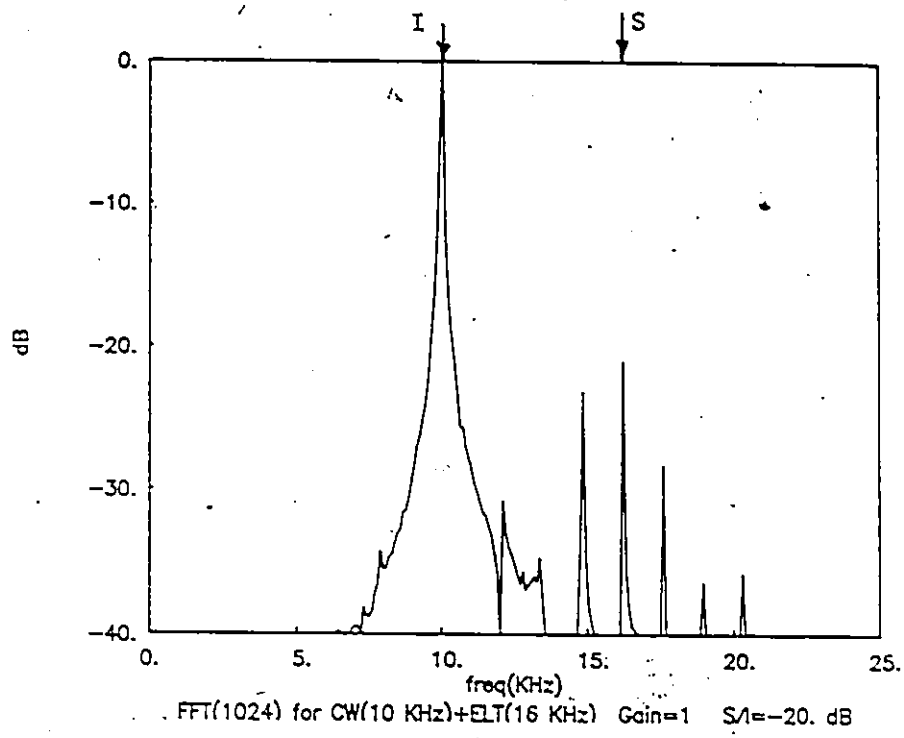

(a)

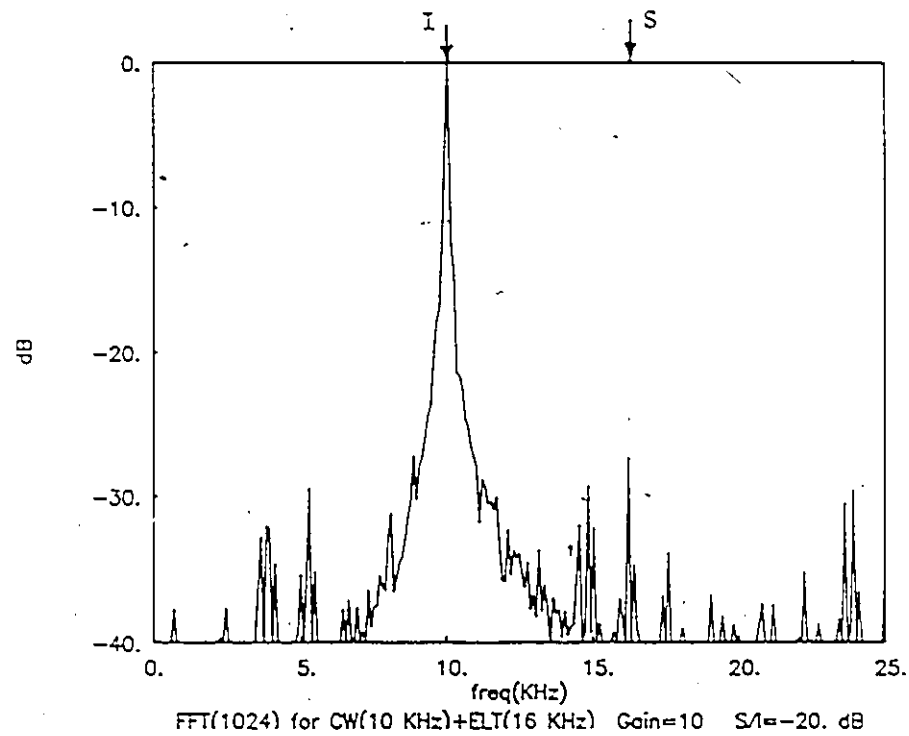

(b)

Fig. 4.34 Plot of 1 k-FFT for ELT signal (16 kHz) + CW interference (10 kHz) for SIR = −20. dB.
(a) Gain = 1
(b) Gain = 10

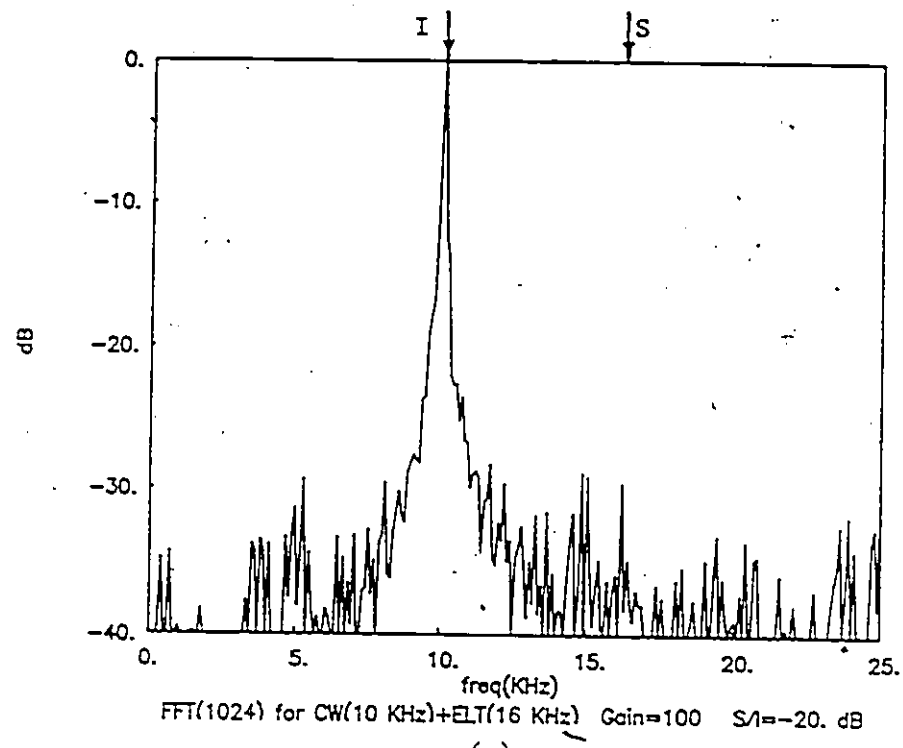

(a)

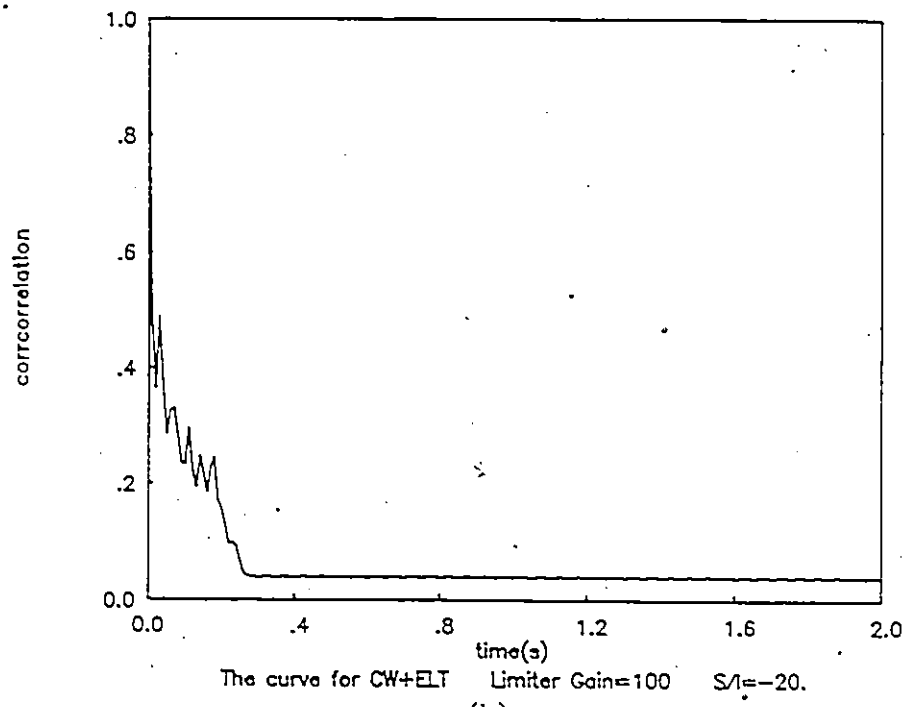

(b)

Fig. 4.35 ELT signal (16 kHz) + CW interference (10 kHz) for Gain = 100 and SIR = −20. dB.
(a) 1 k-FFT
(b) The crosscorrelation curve.

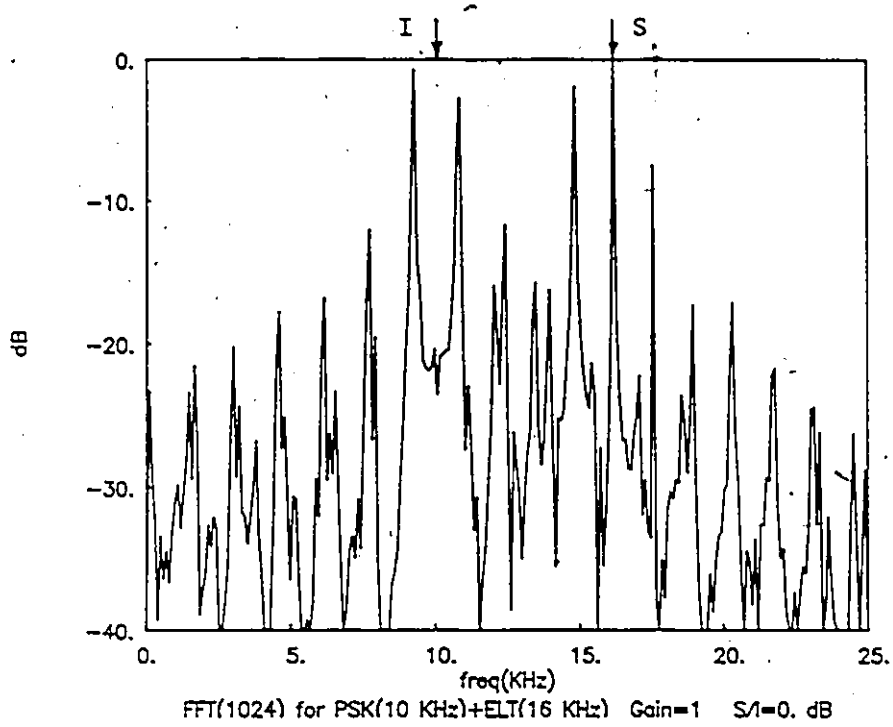

(a)

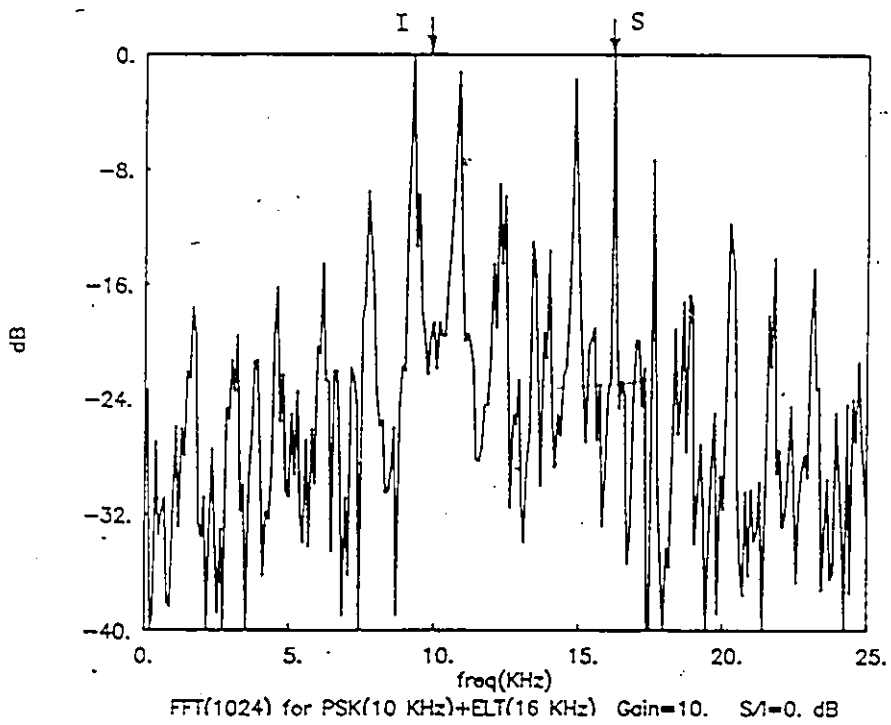

(b)

Fig. 4.36 Plot of 1 k-FFT for ELT signal (16 kHz) + PSK interference (10 kHz) for SIR = 0. dB.

(a) Gain = 1

(b) Gain = 10

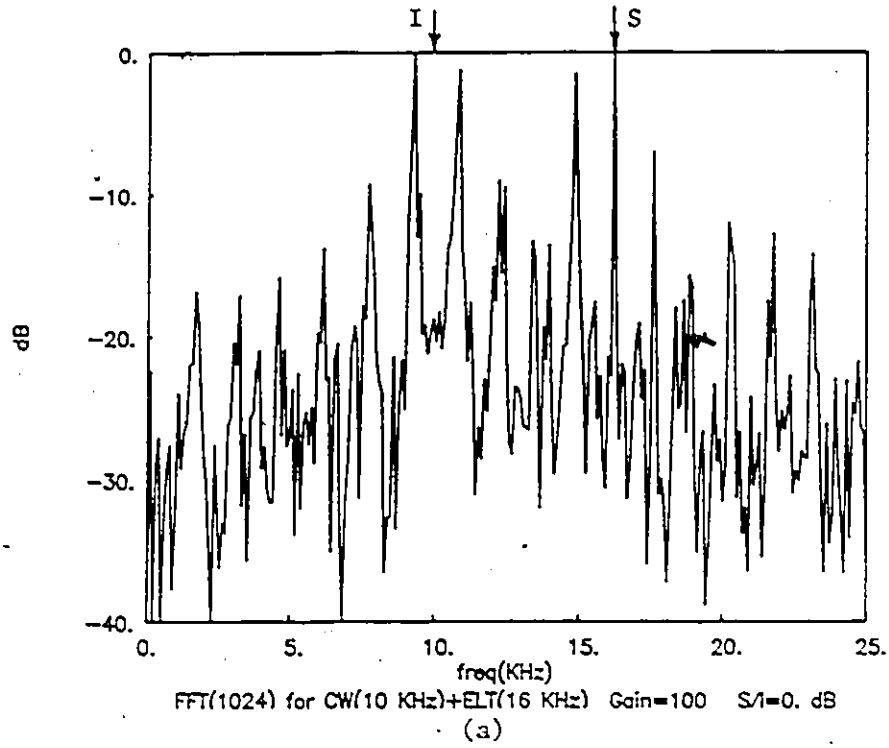

(a)

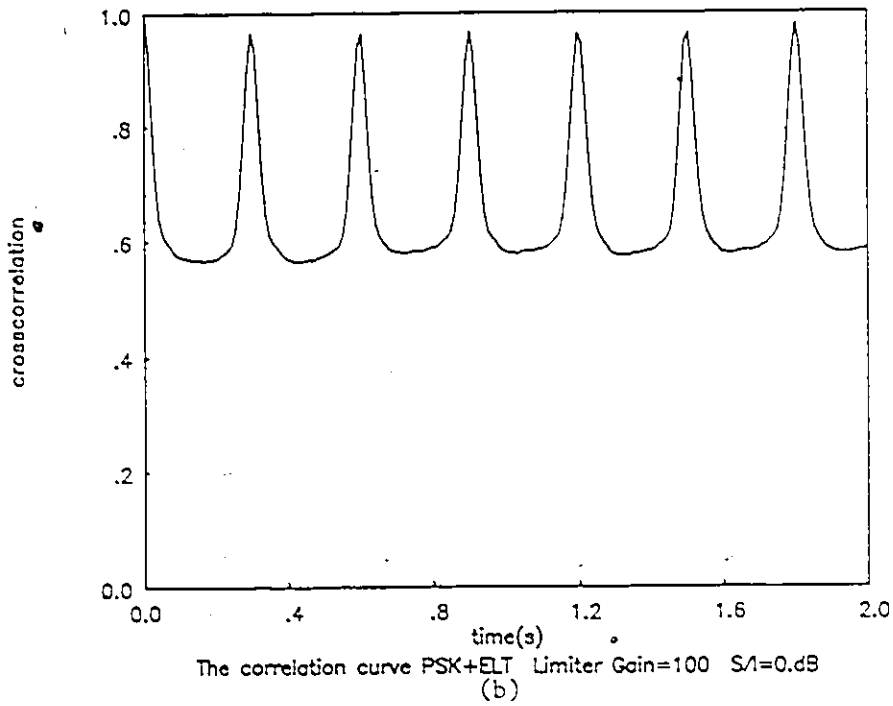

(b)

Fig. 4.37 ELT signal (16 kHz) + PSK interference (10 kHz) for Gain = 100 and SIR = 0. dB.
(a) 1 k-FFT
(b) The crosscorrelation curve.

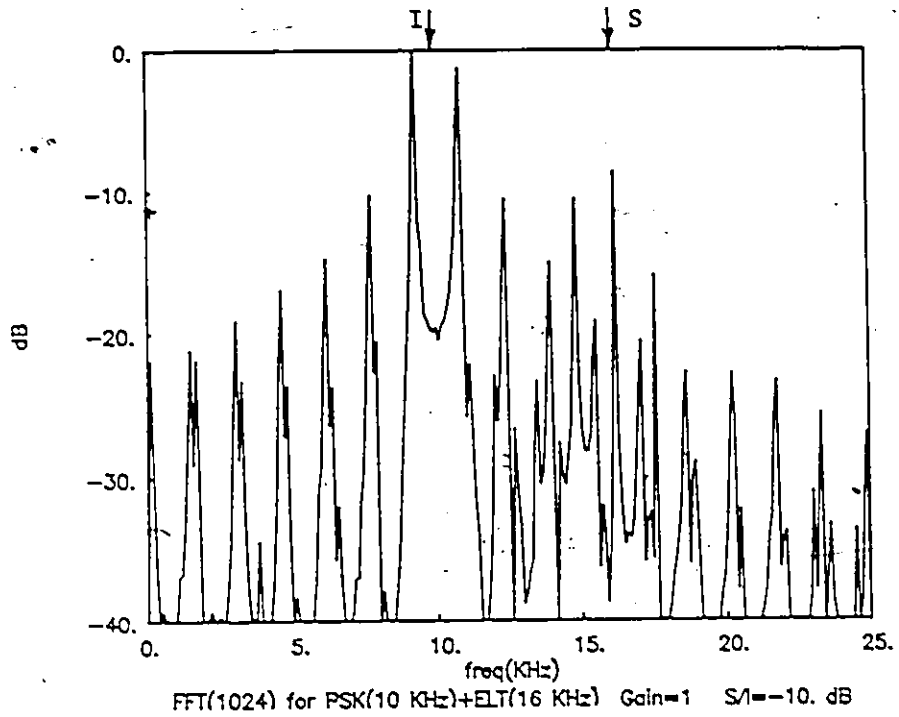

(a)

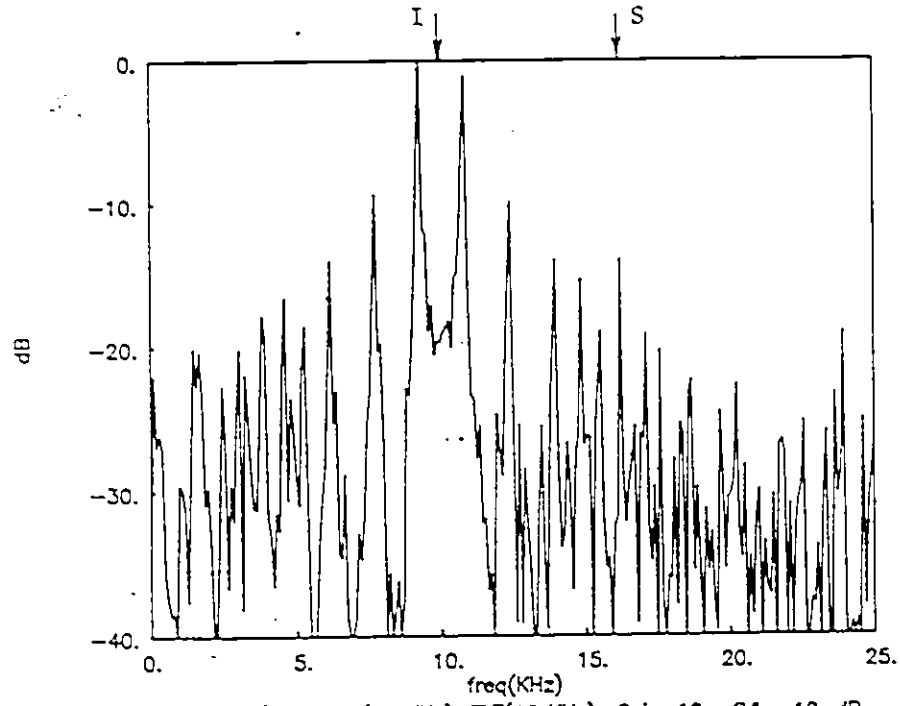

(b)

Fig. 4.38 Plot of 1 k-FFT for ELT signal (16 kHz) + PSK interference (10 kHz) for SIR = −10. dB.
(a) Gain = 1
(b) Gain = 10

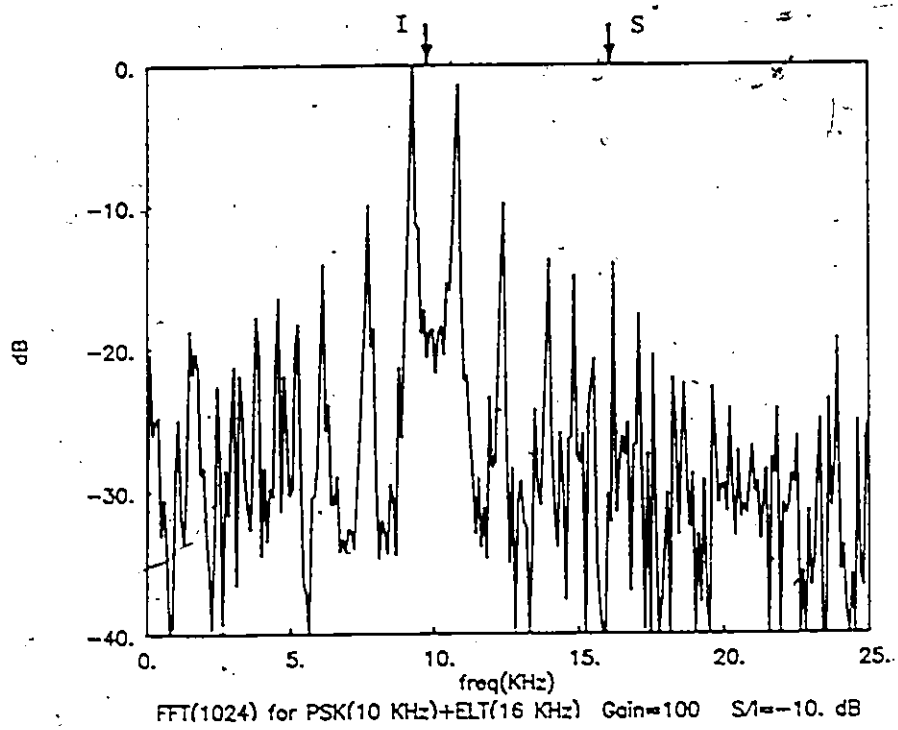

(a)

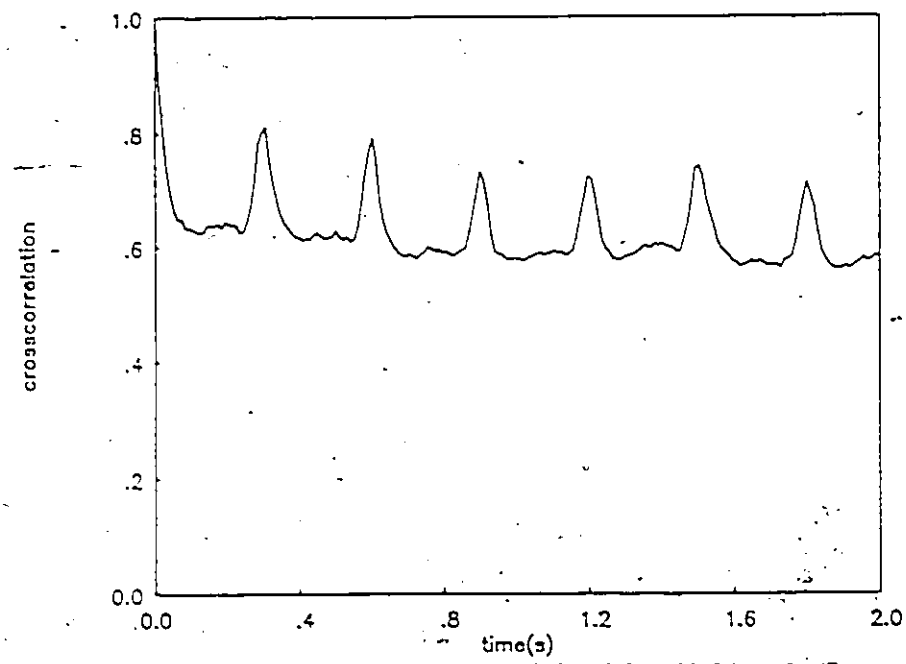

(b)

Fig. 4.39 ELT signal (16 kHz) + PSK interference (10 kHz) for Gain = 100 and SIR = −10. dB.
(a) 1 k-FFT
(b) The crosscorrelation curve.

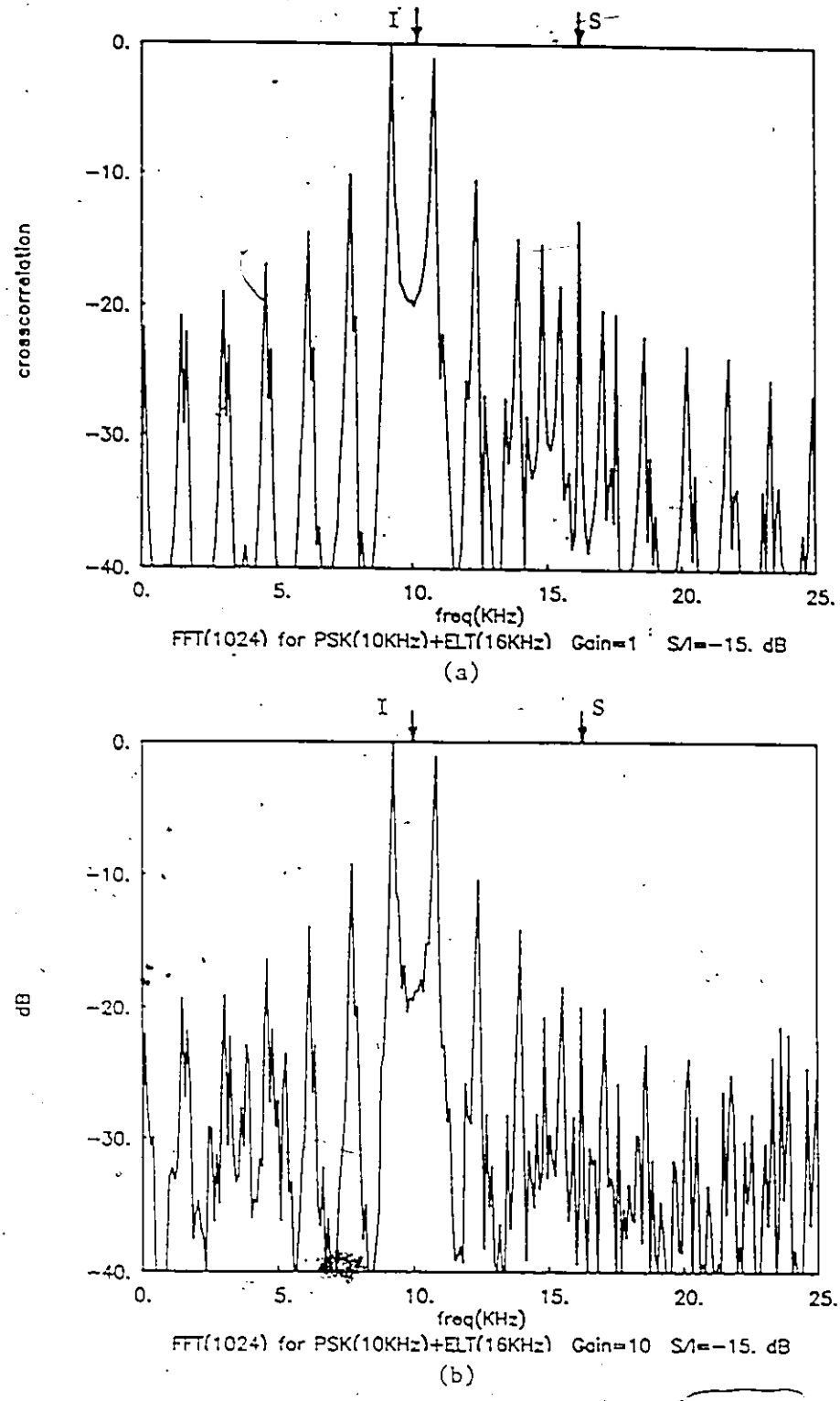

Fig. 4.40 Plot of 1 k-FFT for ELT signal (16 kHz) + PSK interference (10 kHz) for SIR = −15. dB.

(a) Gain = 1

(b) Gain = 10

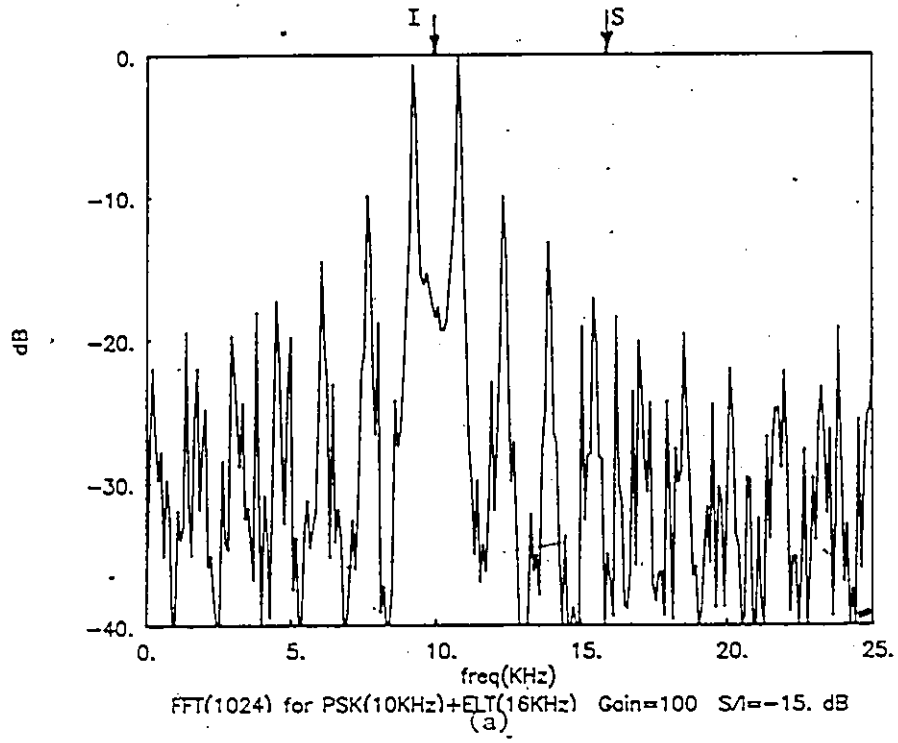

(a)

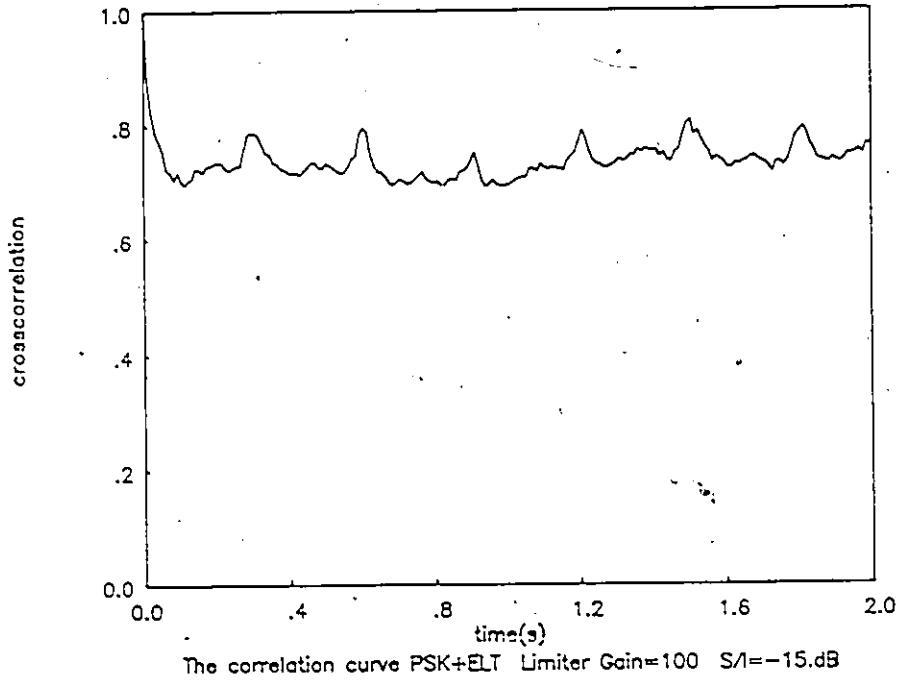

(b)

Fig. 4.41 ELT signal (16 kHz) + PSK interference (10 kHz) for Gain = 100 and SIR = −15. dB.
(a) 1 k-FFT
(b) The crosscorrelation curve.

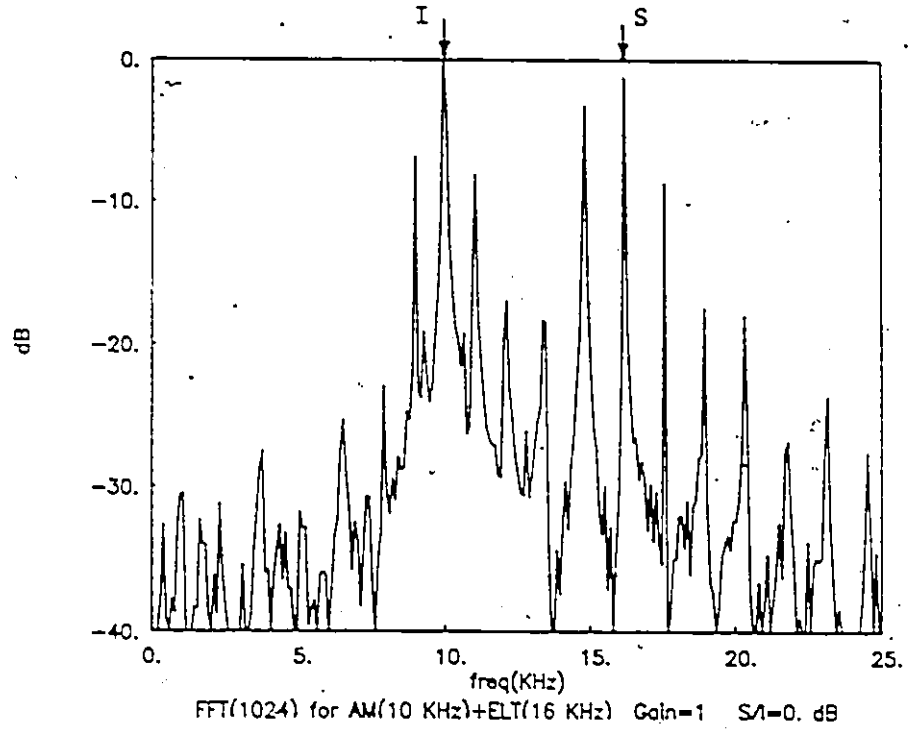

(a)

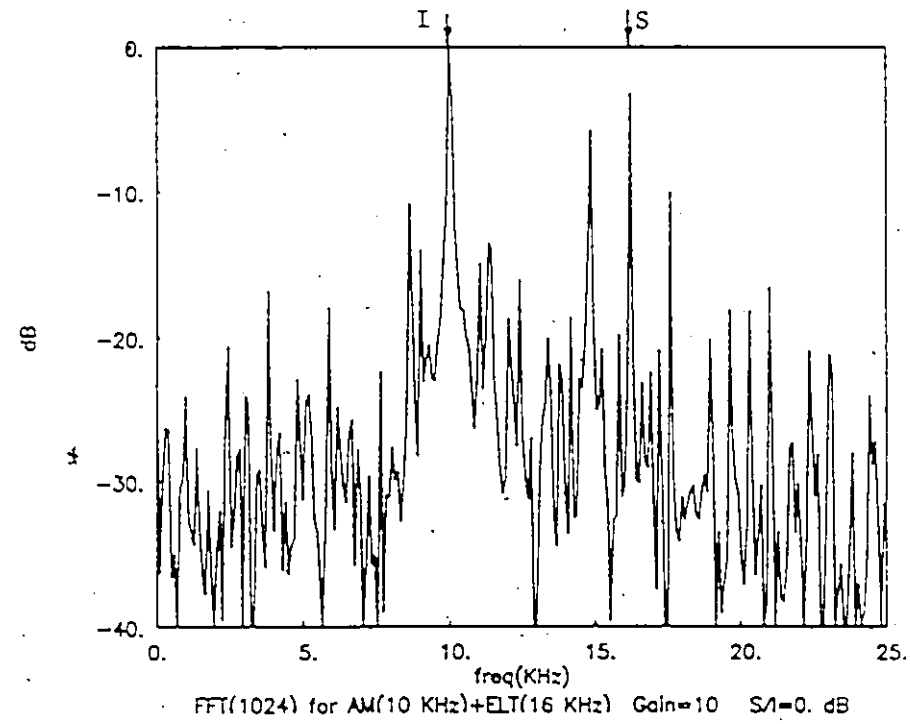

(b)

Fig. 4.4 2 Plot of 1 k-FFT for ELT signal (16 kHz) + AM interference (10 kHz) for SIR = 0. dB.

(a) Gain = 1

(b) Gain = 10

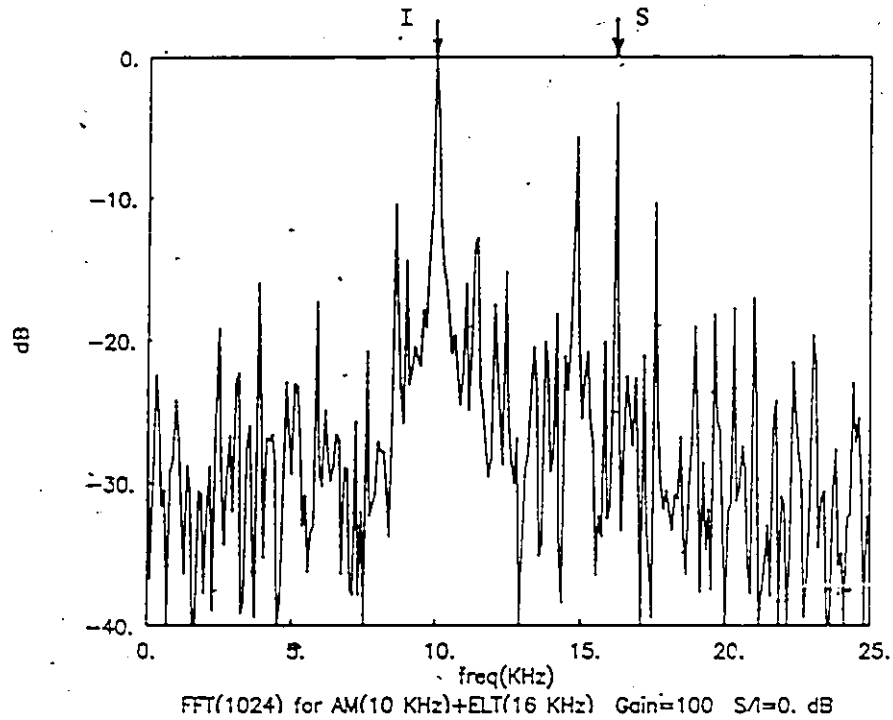

(a)

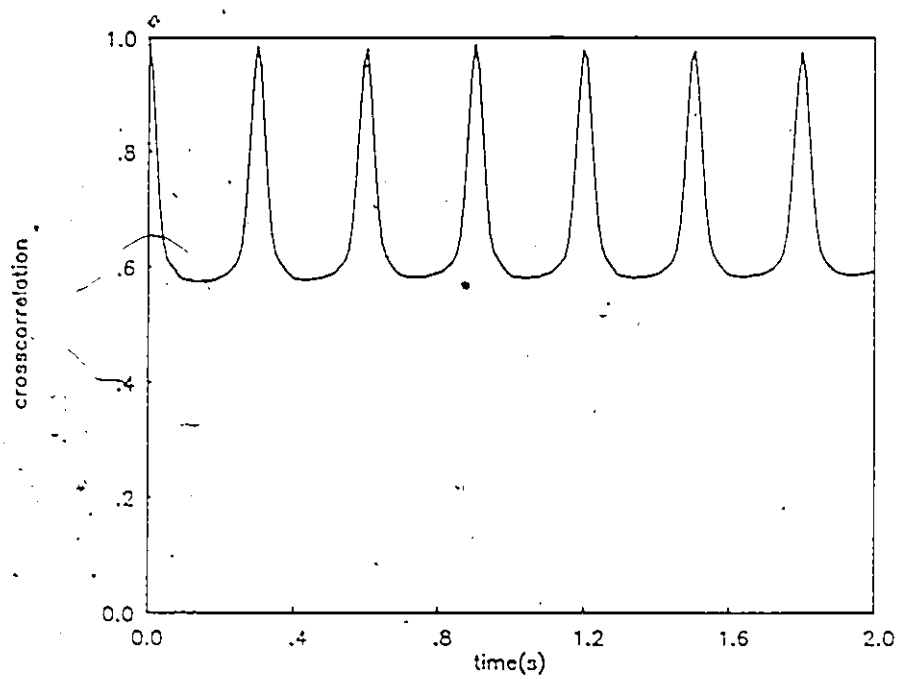

(b)

Fig. 4.43 ELT signal (16 kHz) + AM interference (10 kHz) for Gain = 100 and SIR = 0. dB.
(a) 1 k-FFT
(b) The crosscorrelation curve.

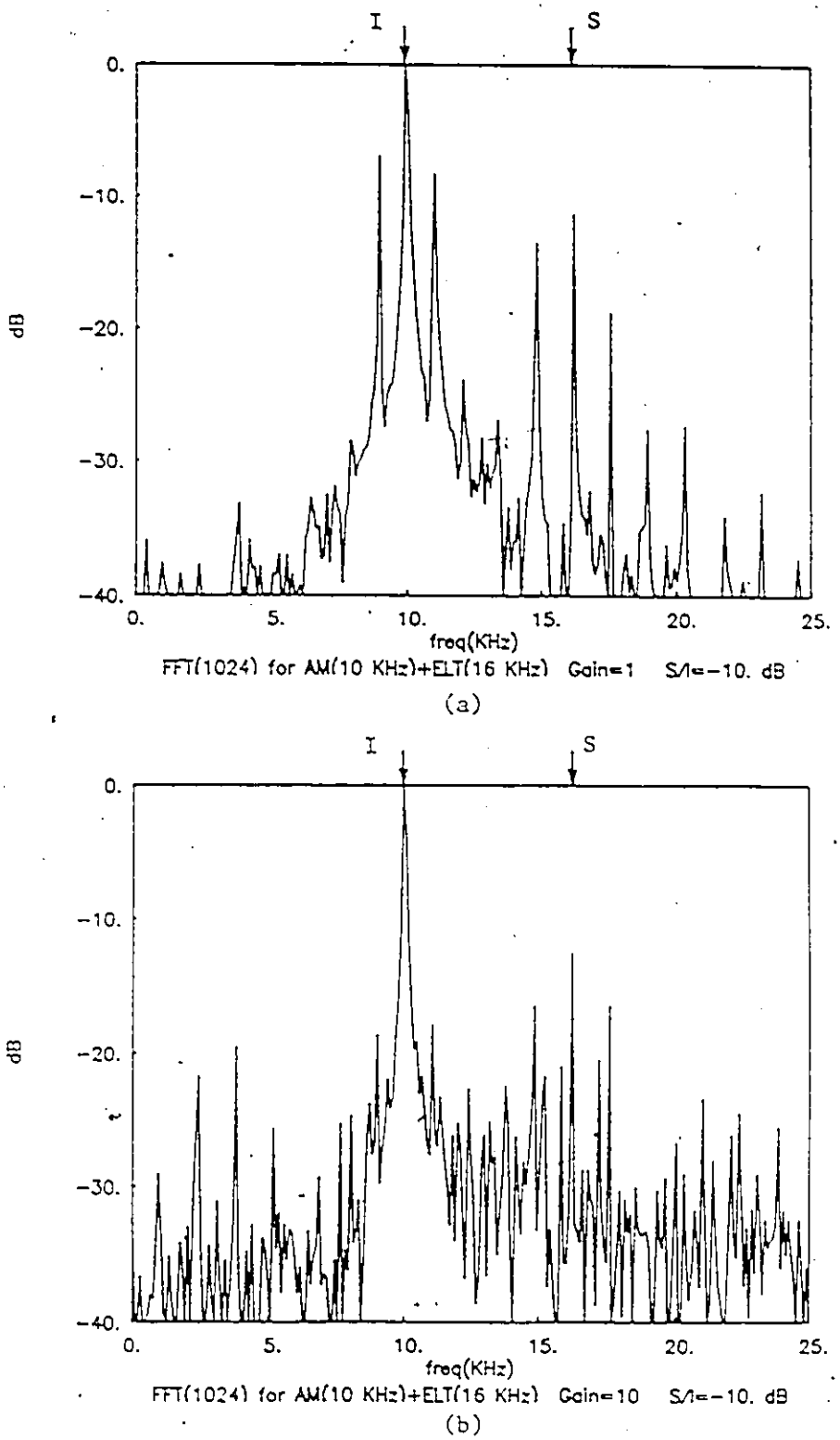

Fig. 4.44 Plot of 1 k-FFT for ELT signal (16 kHz) + AM interference (10 kHz) for SIR = −10. dB.
(a) Gain = 1
(b) Gain = 10

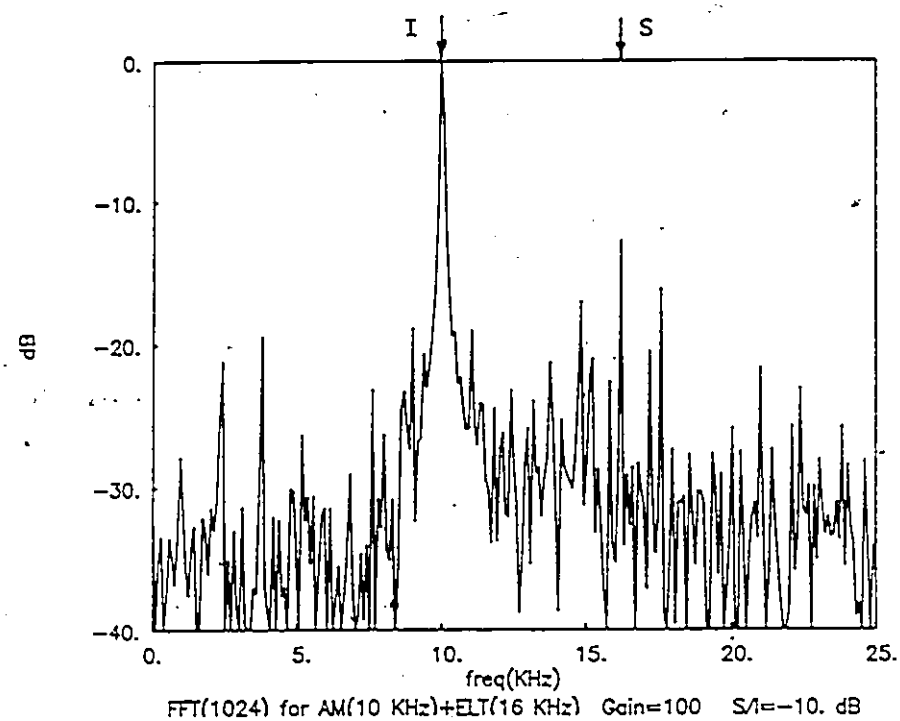

(a)

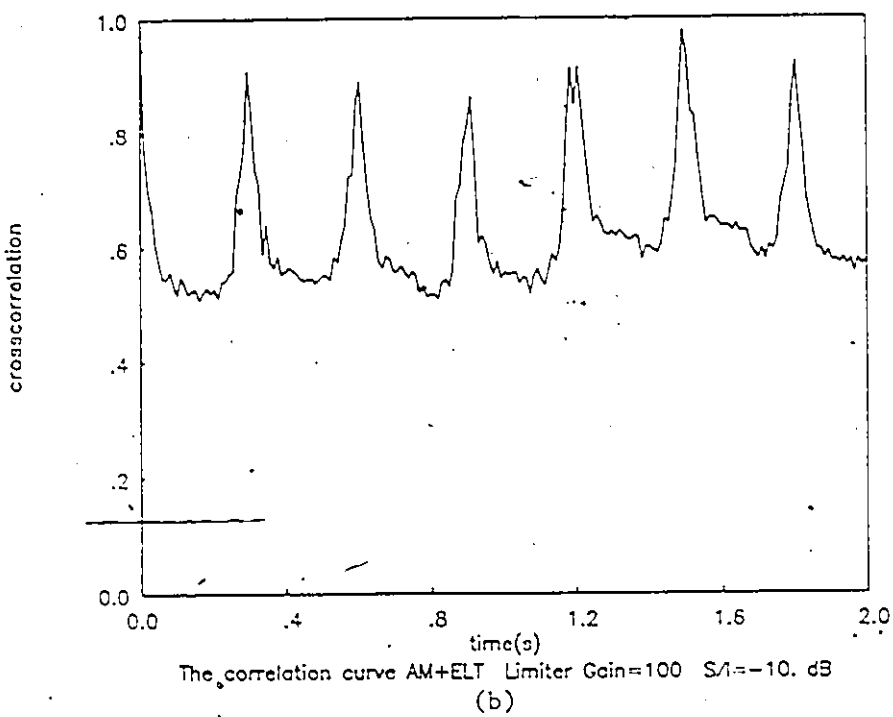

(b)

Fig. 4.45 ELT signal (16 kHz) + AM interference (10 kHz) for Gain = 100 and SIR = −10. dB.
(a) 1 k-FFT
(b) The crosscorrelation curve.

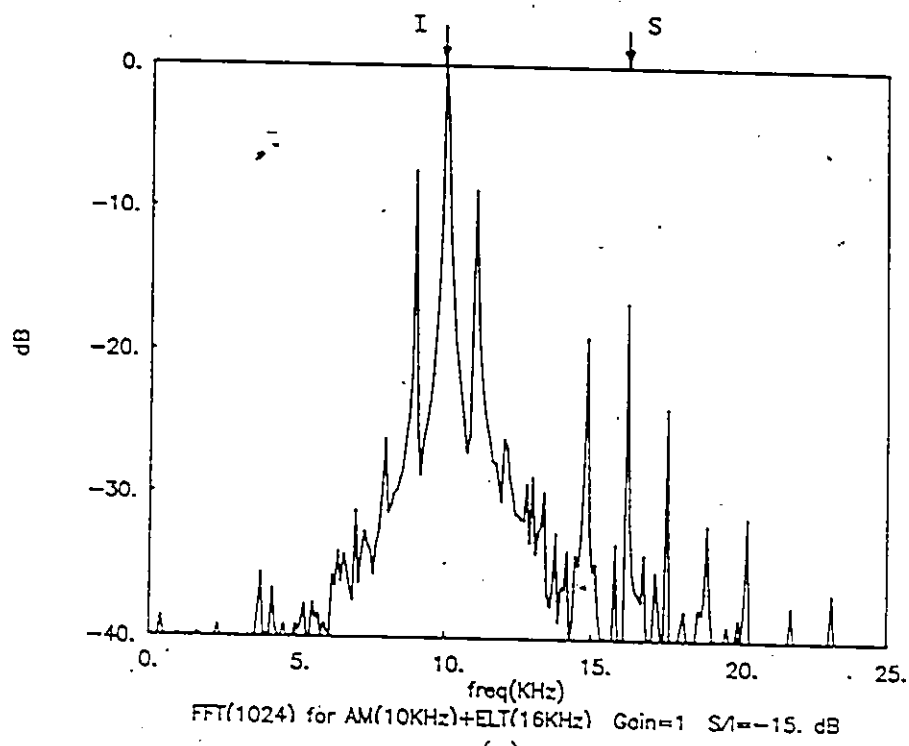

(a)

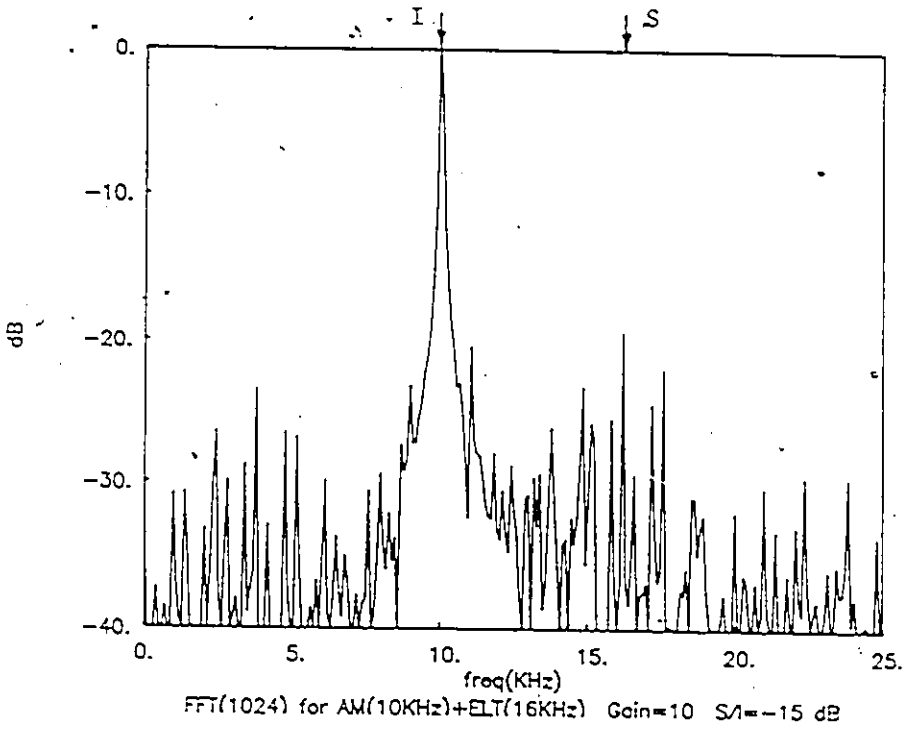

(b)

Fig. 4.46 Plot of 1 k-FFT for ELT signal (16 kHz) + AM interference (10 kHz) for SIR = −15. dB.
(a) Gain = 1
(b) Gain = 10

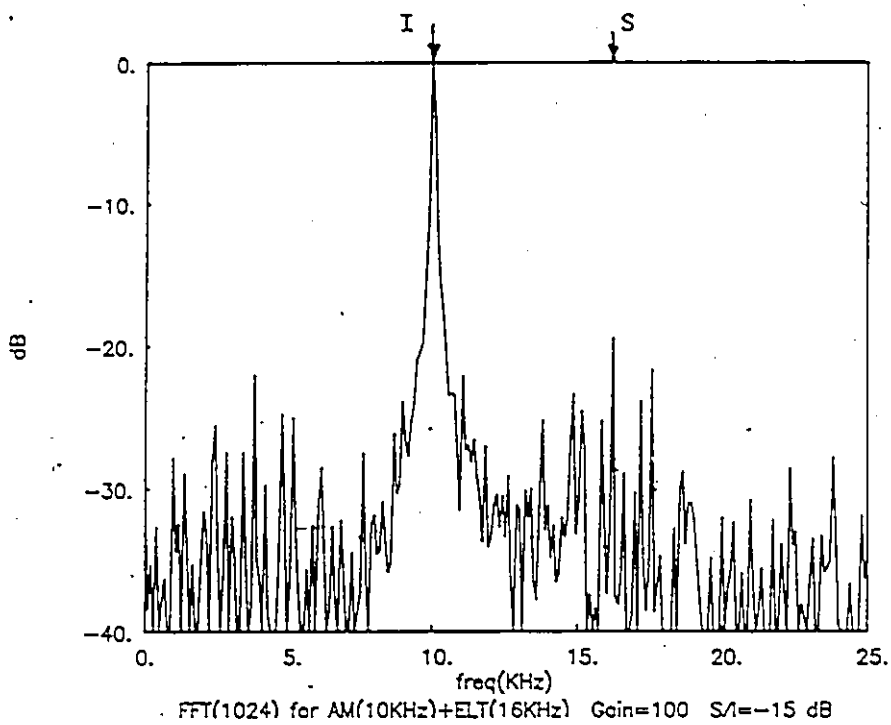

(a)

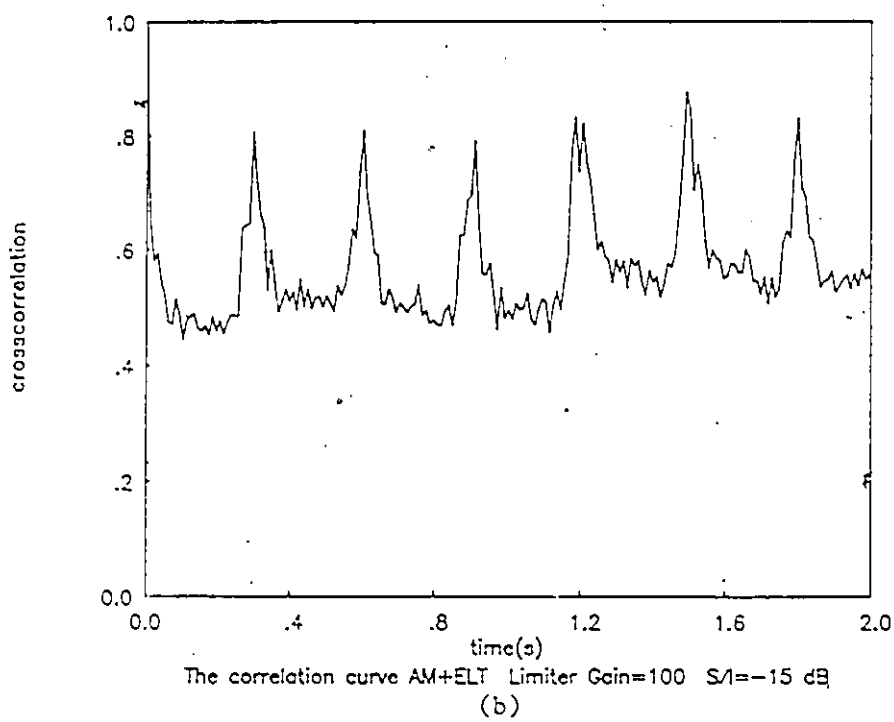

(b)

Fig. 4.47 ELT signal (16 kHz) + AM interference (10 kHz) for Gain = 100 and SIR = −15. dB.

(a) 1 k-FFT

(b) The crosscorrelation curve.

2. Three different models of interferences are presented, those are CW, PSK and AM interferences. The crosscorrelation method is applied to those sources and the resultant curves are seen to be flat.
3. The proposed crosscorrelation method is seen to be capable to distinguishing between ELT signals and interference if they are not overlapped.
4. The crosscorrelation technique is also effective in detecting an ELT signal overlapped by interference in the case of co-channel interference down to SIR = -5 dB.
5. Finally some practical considerations concerning the problems associated with AGC or limiter at the receiver are studied. The results show that the method is effective to combat the limiter effects down to SIR = -15 dB.

CHAPTER 5

IDENTIFICATION TECHNIQUES AS APPLIED TO SATELLITE PASS DATA

5.1 Overview

As seen in the last two chapters, using the proposed crosscorrelation technique, we are able to solve some of the problems facing the SARSAT system. First, it is possible to track an ELT signal using the crosscorrelation curve signature. Second, it is possible to separate any overlapped Doppler shift curves. Third, it is possible to distinguish between the ELT signals and the interference sources.

In this chapter we focus on applying the crosscorrelation technique to real ELT signals obtained from satellite passes. The signals are received from orbits 860 and 861 of COSPAS satellite C1. Due to satellite motion, a Doppler shift of up to approximately ± 3 kHz may be added to the signal carrier frequency depending on the time of the pass. The analog tapes supplied by CRC were digitized at sampling rate of approximately 100 kHz. As mentioned earlier, each pass may contain many simultaneous ELT signals as well as voice signals and interference of various types. Our main concern here is to estimate the possible number of existing ELT signals within each pass. Moreover, it is required to identify the interference signals in order to avoid false alarms.

Our procedure for processing the SARSAT signals consists of three steps. First, the spectral estimation technique, based on the periodogram, is employed to locate the positions of the peaks which may characterize the signal carrier frequencies. Second, certain peaks are selected according to fixed or adaptive thresholding techniques, to obtain a frequency versus time dot plot, where each dot represents one of the chosen peaks. Third, the dot-chart is

analysed using the identification techniques in order to estimate the number of ELT signals within the pass.

5.2 Thresholding and Dot-chart

As previously noted, the location of the crash site depends on the slope at the inflection point of the S-shaped curve. In order to obtain the the S-shaped curves, the data received and relayed by SARSAT satellite is divided into small segments such that the Doppler shift in the carrier frequency within each segment is negligible. Each segment is processed individually to get the corresponding power spectrum. Thresholding techniques are performed on the spectra and the frequency locations of the peaks are determined. Each peak is plotted as a dot on the time slot. From this dot-chart, the S-shaped curves can be extracted. The thresholding techniques are now investigated, followed by practical examples of the dot-charts.

5.2.1 Thresholding Techniques

Thresholding is a major problem, since the probability of detection depends on the technique used to set the threshold level. In the following, we discuss two methods of thresholding; namely, fixed and adaptive.

Consider the periodogram of three coherent ELT signals shown in Fig.5.1. Signal A is stronger than both signals B and C. Thus, if a fixed threshold level is set sufficiently high, the strong signal A will be detected, whereas the weak signals may be lost. The fixed threshold level must be low if weak signals to be detected, but it cannot be so low that numerous noise peaks cross the threshold level and give false indications of the presence of ELT signals. Therefore, the selection of the proper fixed level is a compromise that depends on the importance of either (1) failing to recognize a signal that is present (probability of

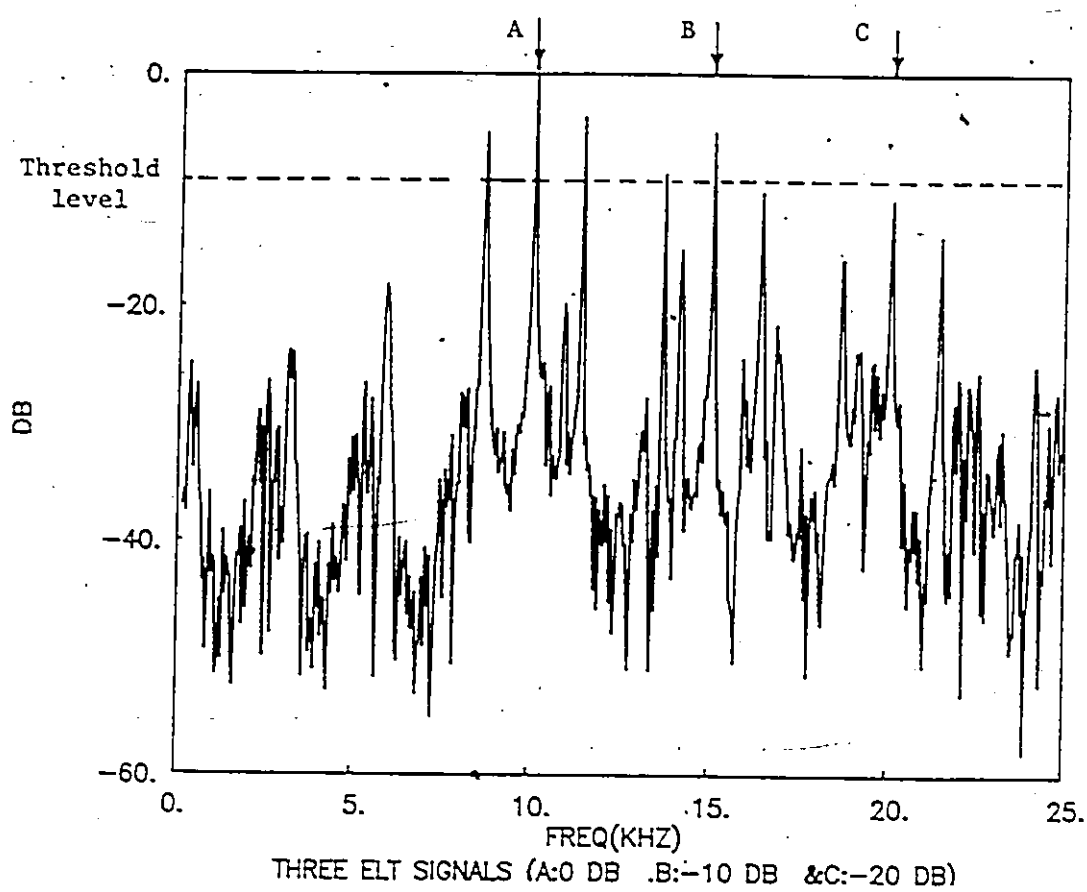

Fig. 5.1 Periodogram of three ELT signals with different levels showing the threshold.

miss) or (2) falsely indicating the presence of signals when none exists (probability of false alarm).

In our case, it is undesirable to exclude any signal that is present; thus, a low threshold level is preferable. However, this leads to a cluttered dot-chart such that it is difficult to recognize S-shaped curves [12]. To overcome this problem, we employ an adaptive threshold. In this technique, a certain number of peaks which have the highest magnitude are selected. This number is chosen to exceed the expected maximum number of ELT units. In practice, this number could range between, perhaps 10 and 100.

5.2.2 Dot-chart for Testbed ELT Signals

In this section, the dot-charts for Pointer, Garrett, Narco ELT17 and Narco ELT19 are obtained using both fixed and adaptive thresholds. These charts can be used in our study for the individual testbed signals to estimate their frequencies accurately. The dot-chart for the Pointer ELT signal using an arbitrary fixed threshold of -16 dB is shown in Fig. 5.2a. The plot represents 4 s of data. The data are divided into 40 ms segments and the corresponding periodograms are computed. The dot-chart of the same data is given in Fig. 5.2b using an adaptive threshold with the largest 6 peaks selected. The sawtooth pattern of the sidebands is clearly displayed as the sweep progresses. The arrow indicates the carrier frequency which is estimated as 15.9 kHz. The effectiveness of the adaptive threshold over fixed threshold is clear. Although using higher threshold level decreases the clutter, it also decreases the amount of information and ELT signal may be missed. This is examined in the next section. The dot-charts for Garrett, Narco ELT17 and Narco ELT19 are depicted in Fig. 5.3, Fig. 4.4 and Fig. 4.5, respectively. The sawtooth pattern is not well defined for Narco signals, since the lower sidebands are dominant. The estimated carrier frequencies for

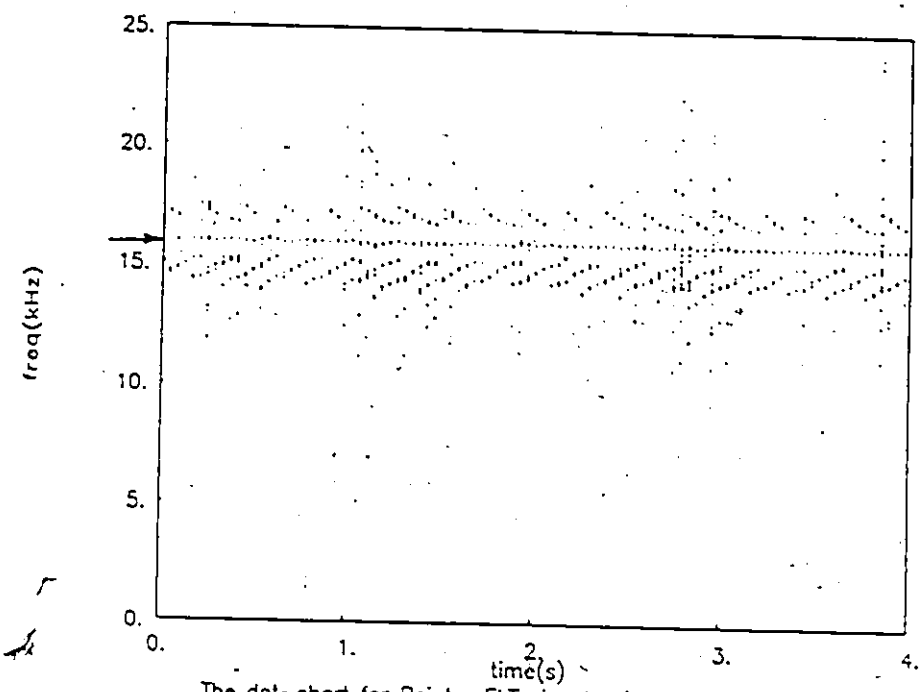

The dot-chart for Pointer ELT signal using fixed th= −16 dB
(a)

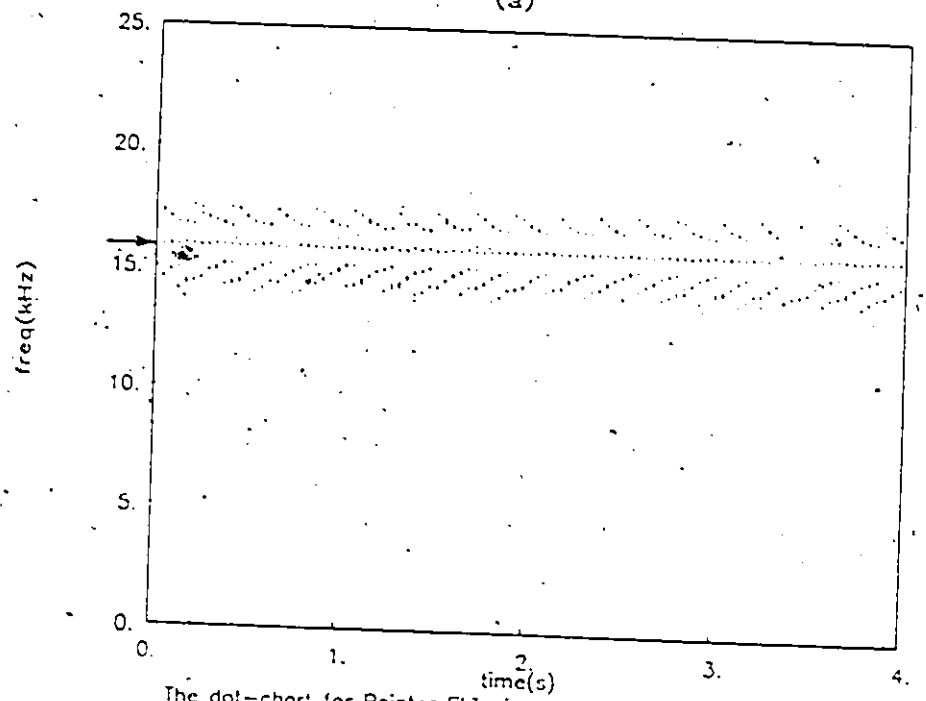

The dot-chart for Pointer ELT signal using adaptive th of 6 peaks
(b)

Fig. 5.2 Dot-chart of Pointer ELT signal
(a) Fixed threshold at − 16 dB.
(b) Adaptive threshold of 6 peaks maximum.

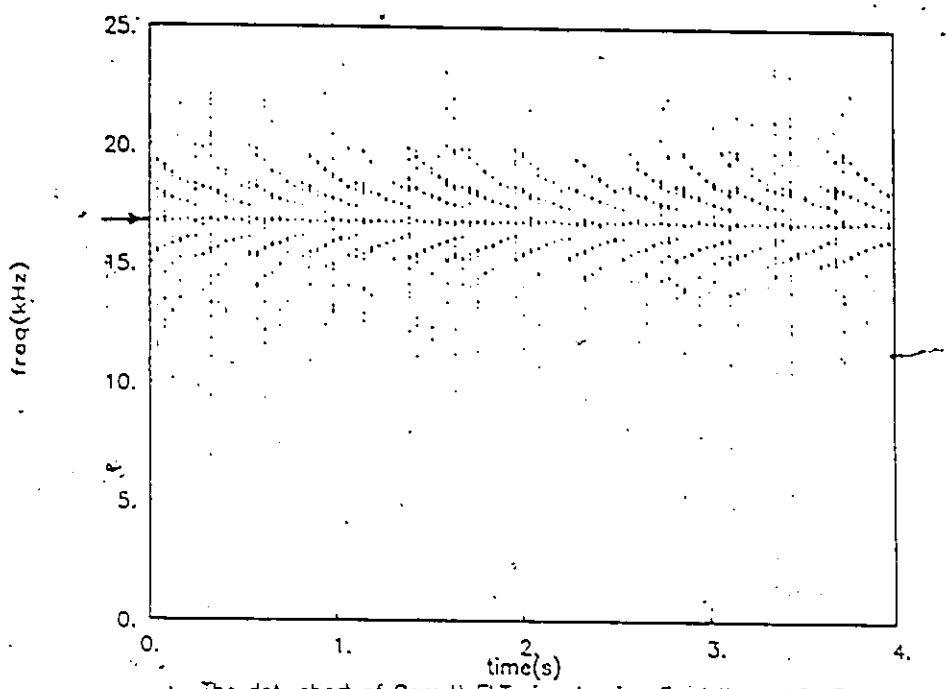

The dot-chart of Garrett ELT signal using fixed th= −16 dB

(a)

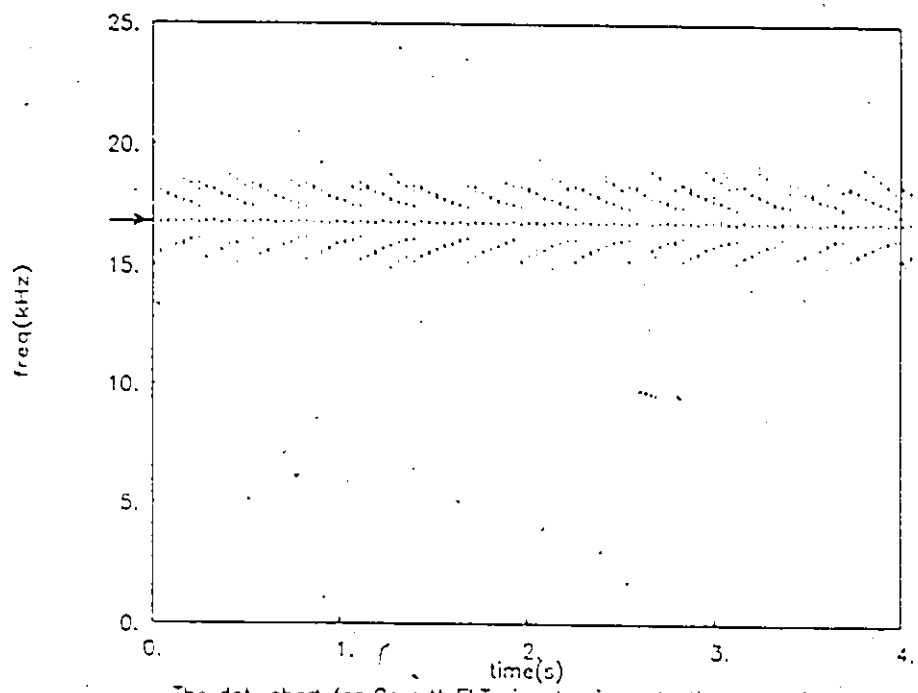

The dot-chart for Garrett ELT signal using adaptive th of 6 peaks

(b)

Fig. 5.3 Dot-chart of Garrett ELT signal
(a) Fixed threshold at − 16 dB.
(b) Adaptive threshold of 6 peaks maximum.

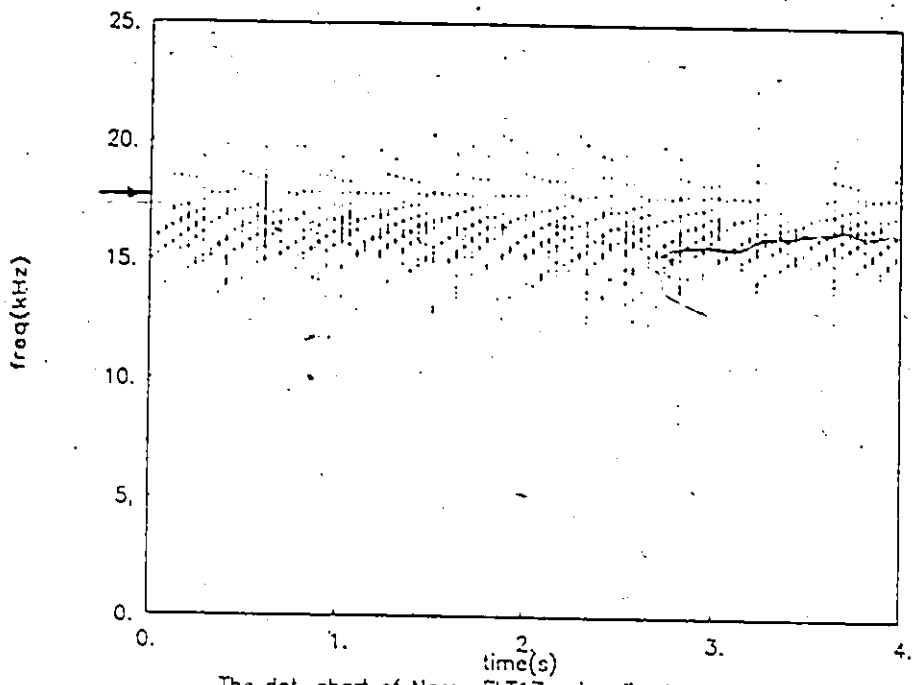

The dot-chart of Narco ELT17 using fixed th = −16 dB.

(a)

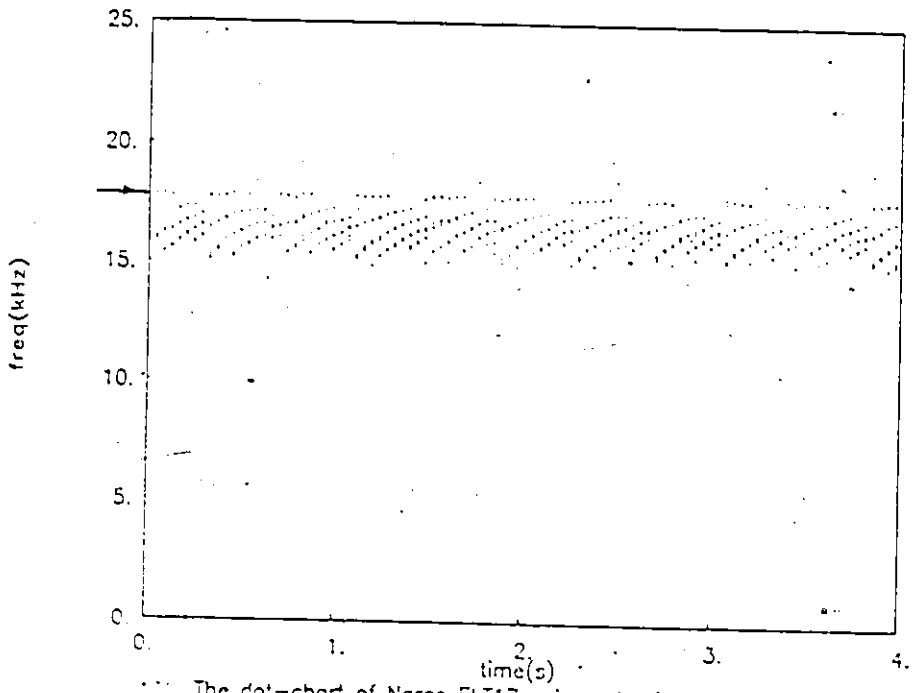

The dot-chart of Narco ELT17 using adaptive th of 6 peaks

(b)

Fig. 5.4 Dot-chart of Narco ELT17 signal
(a) Fixed threshold at −16 dB.
(b) Adaptive threshold of 6 peaks maximum.

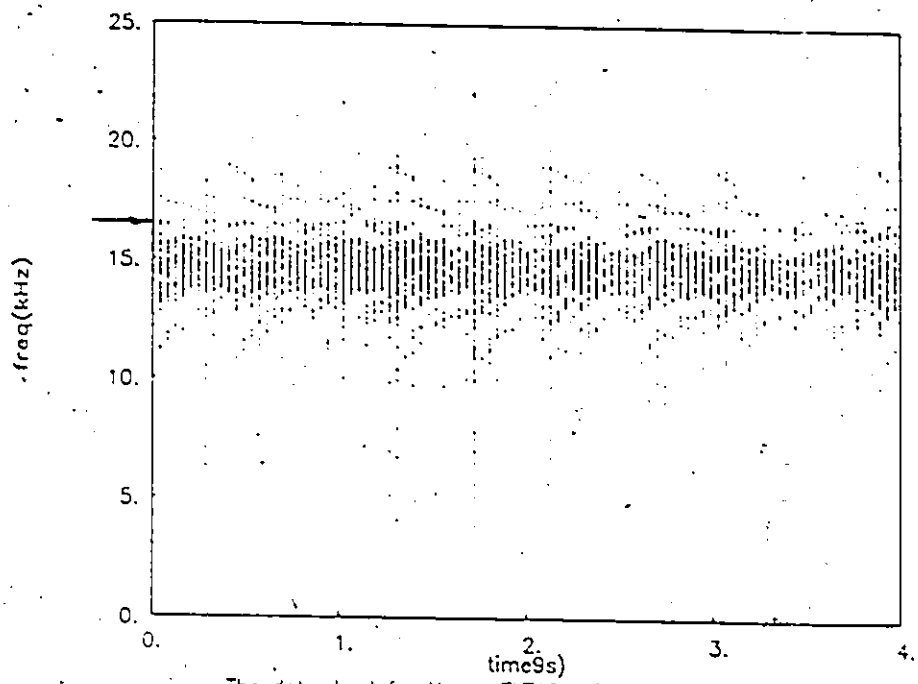

The dot-chart for Narco ELT19 using fixed th= −16 dB
(a)

(a)

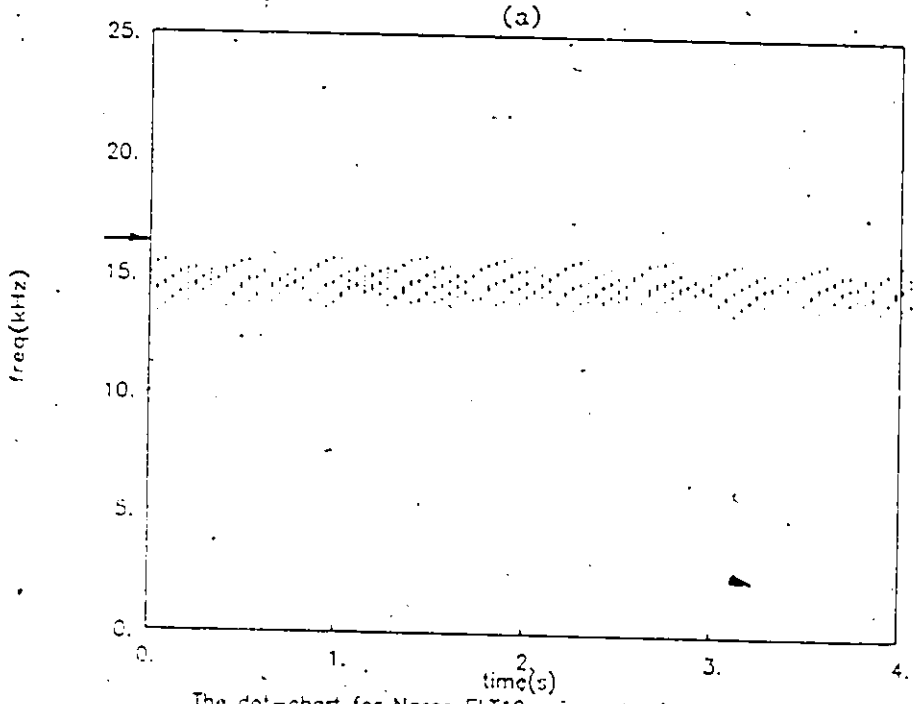

The dot-chart for Narco ELT19 using adaptive th of 6 peaks
(b)

Fig. 5.5 Dot-chart of Narco ELT19 signal.
(a) Fixed threshold at − 16 dB.
(b) Adaptive threshold of 6 peaks maximum.

Garrett, Narco ELT17 and Narco ELT19 are 16.8 kHz, 17.8 kHz and 16.5 kHz, respectively as indicated by the arrows.

5.2.3 Dot-chart For Real Satellite Passes

In the following, we give examples of dot-charts using both fixed and adaptive thresholding. The satellite pass data of 15 minutes length obtained from COSPAS satellite orbit 861 are divided into 900 segments, each segment being 1 s in length. To reduce the clutter of the plot, only 1 s of data is presented every 5 s. This reduces the number of segments to 180. A 4 k-point periodogram is applied to each 40 ms duration of data and 25 of these periodograms are averaged to give a 1 s segment spectral estimate. The highest point is normalized to 0 dB.

An arbitrary fixed threshold of -12 dB is set for each spectrum. The locations of the peaks that exceed the threshold are plotted on a time-frequency chart (dot-chart) as shown in Fig. 5.6 from this figure we note the large block of interfering dots at the 16th and 17th minute intervals, which is due to wideband interference such that almost all the peaks exceed the threshold level. This causes a serious problem if this block happens to include the inflection point of an S-shaped curve. In this case it would be difficult to measure the slope at this point and consequently the range to the crash site.

On the other hand, if an adaptive threshold of 20 peaks is applied on the same set of spectra, the corresponding dot-chart of Fig. 5.7 is obtained. As seen, the interfering block of dots is not present and the signals can be tracked. Also it is clear that some other information is present in Fig. 5.7 and missed in Fig. 5.6. This can be observed in areas E, F and G of Fig. 5.7. We conclude that adaptive threshold is more useful in our case than fixed threshold.

In studying Fig. 5.7, two important problems are noted. First, is the problem of deciding whether any of the S-shaped curves in this figure are due to real ELT signals. The

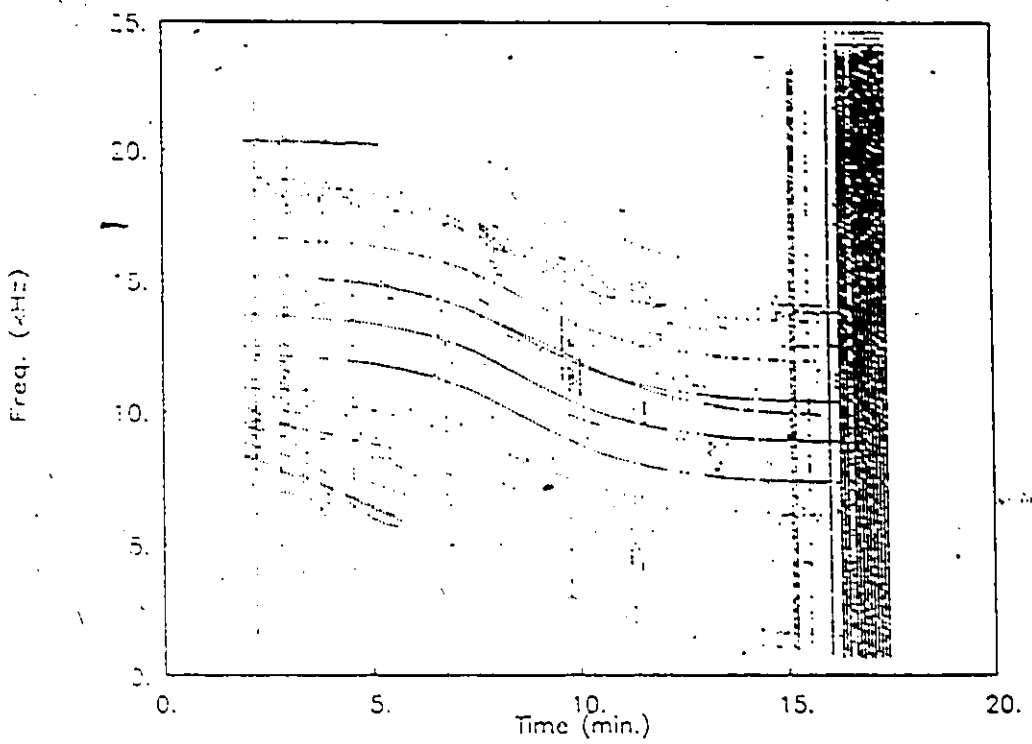

Fig. 5.6 Dot-chart of satellite pass orbit 861 using fixed threshold at −12 dB.

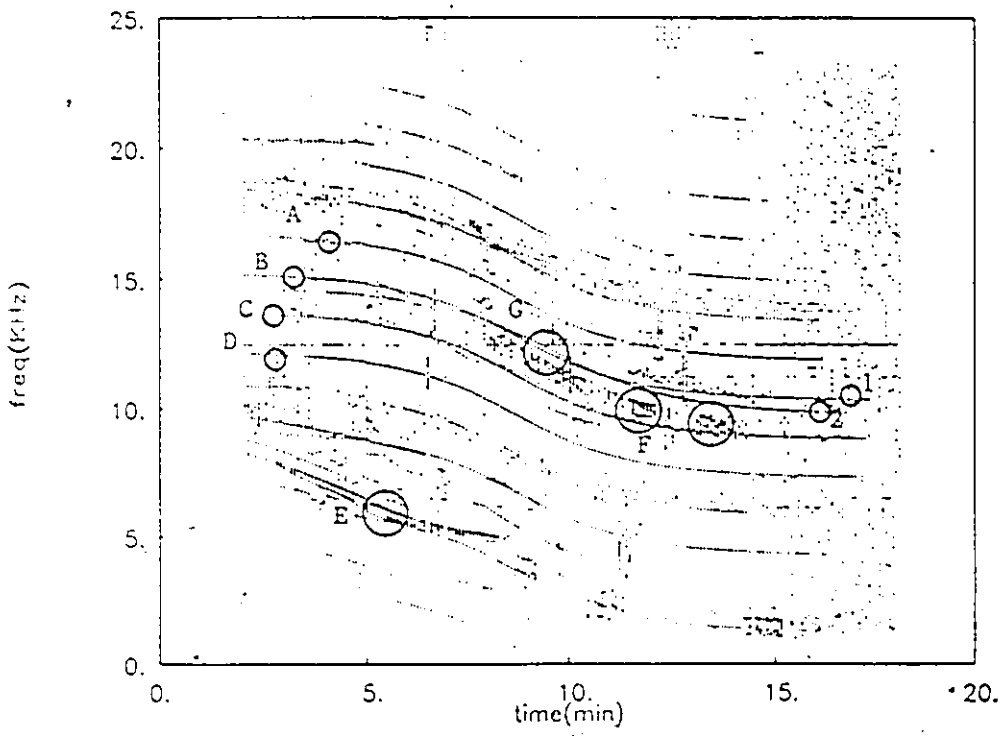

Fig. 5.7 Dot-chart of satellite pass orbit 861 using adaptive threshold with 20 peaks.

second problem is how to separate the intersecting curves as seen in area G. These problems are examined next.

5.3 Analysis of Satellite Pass Orbit 861

The first step in the analysis is to plot the dot-chart of the available data to give a complete picture of the pass. The dot-chart of orbit 861 is presented in Fig. 5.7. As seen there are some complete S-shaped curves (A, B, C and D), two intersecting curves (1 and 2) and also areas of concentrated dots (E and F). The total number of signals within the pass is approximately 16.

Until now we cannot judge whether the existing S-shaped curves are due to ELT signals or to interference sources. Also we can not tell if the areas of concentrated dots are due to signals or due to noise.

The second step is to divide the frequency band into 2 kHz passband sections. Each section is processed to obtain the corresponding crosscorrelation curve. Depending on the shape of this curve (i.e. flat or multiple peak pattern), the decision of detecting an ELT signal can be made. The above procedure is repeated at the start of each minute to obtain a macroscopic scan of the pass.

In our analysis we start at the 3rd minute and plot until the 12th minute. The corresponding plots are given in Fig. 5.8 through Fig. 5.17. The arrows indicate the curves that might be due to ELT signals, with the remaining curves most probably being due to interferences. Once this preliminary scan is obtained, the regions where ELT signals are expected can be analysed in more detail. From Fig. 5.9 and Fig. 5.10, we observe the beginning of the reception of an ELT signal occupying, the passband 4-8 kHz during the 4th minute. The reception of this signal continues until the 7th minute where it then disappears as seen from Figs. 5.13 and 5.14.

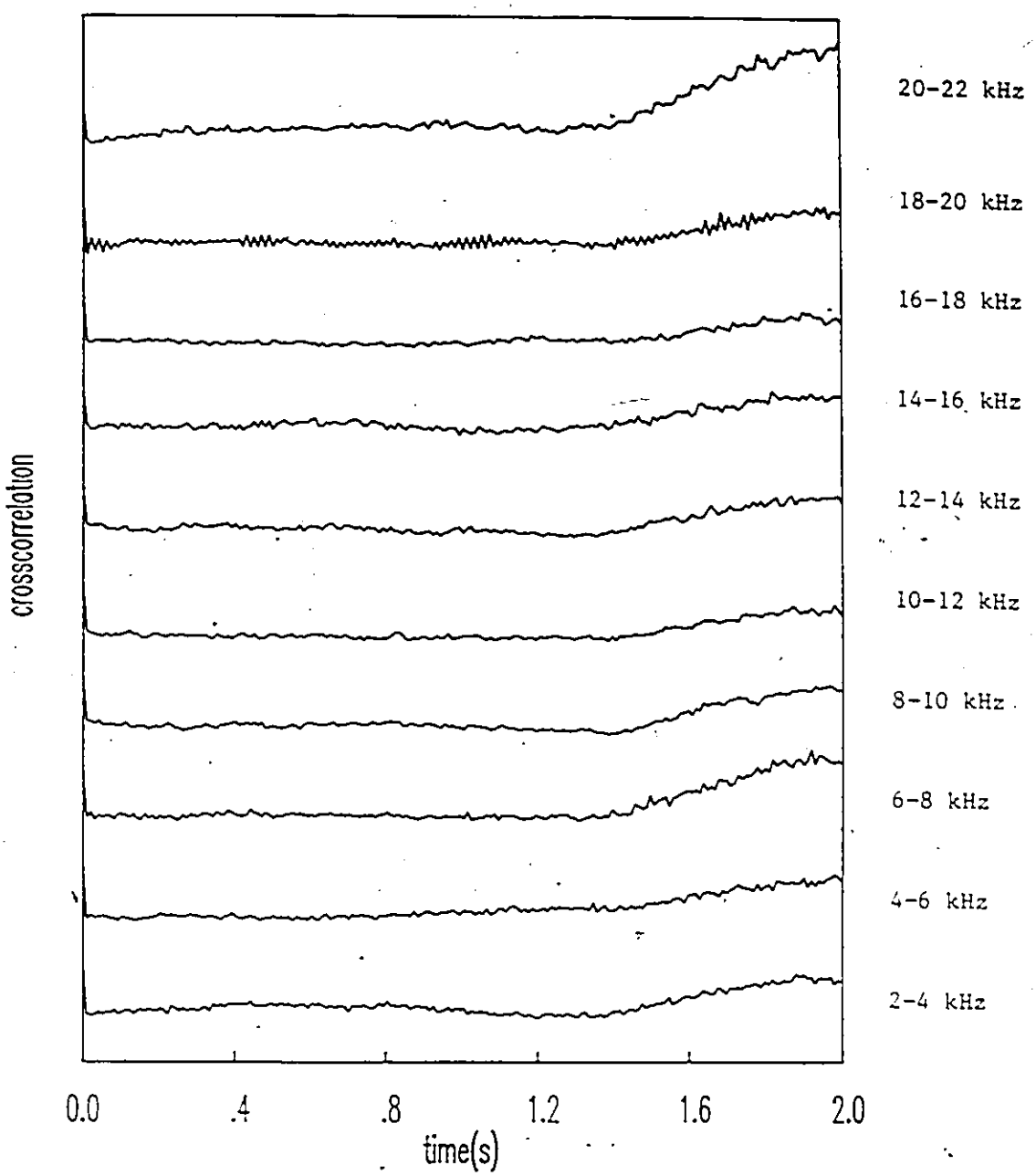

Fig. 5.8 The crosscorrelation curves for 10 different portions of orbit 861 at the 3rd minute.

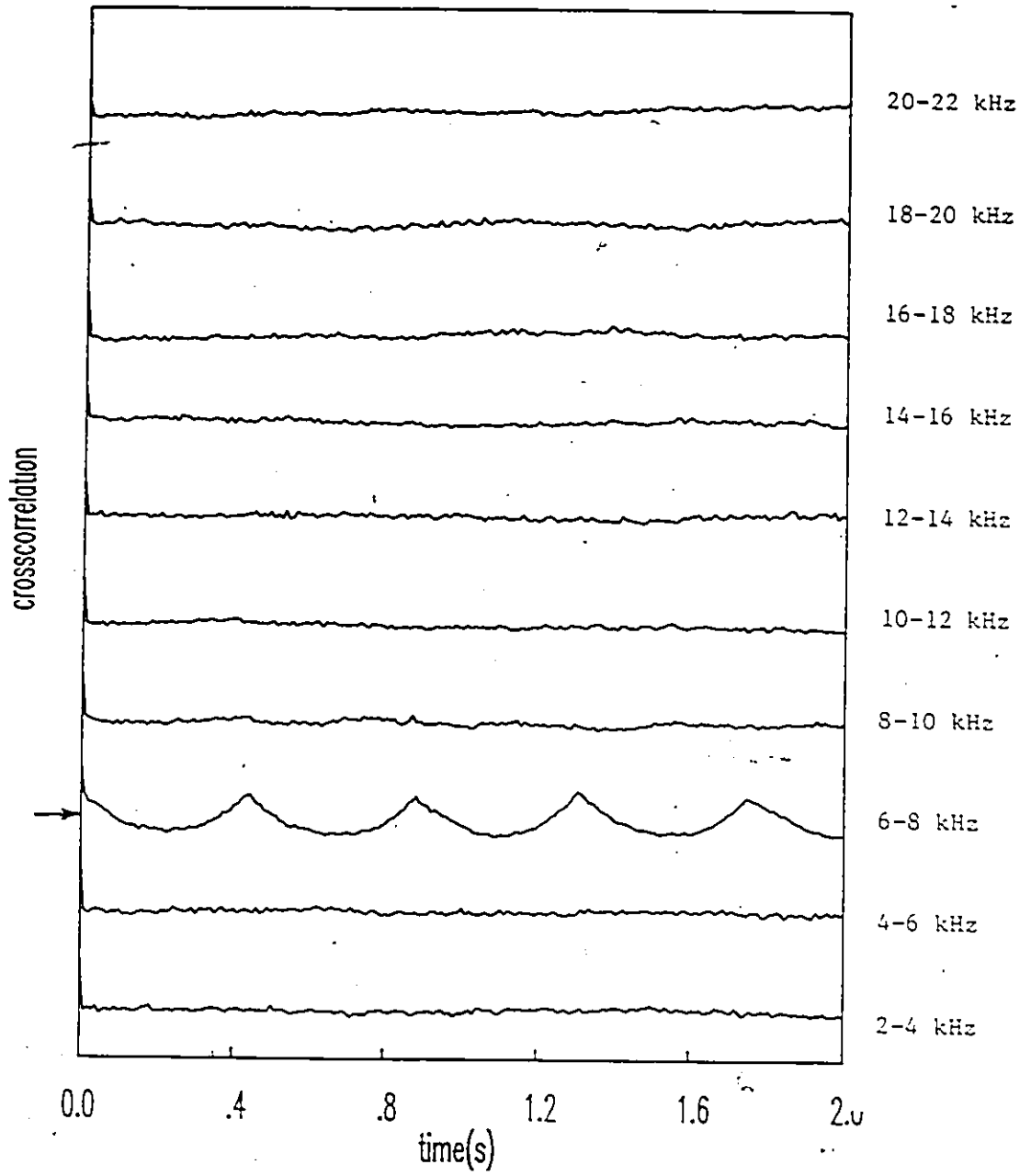

Fig. 5.9 The crosscorrelation curves for 10 different portions of orbit 861 at the 4th minute.

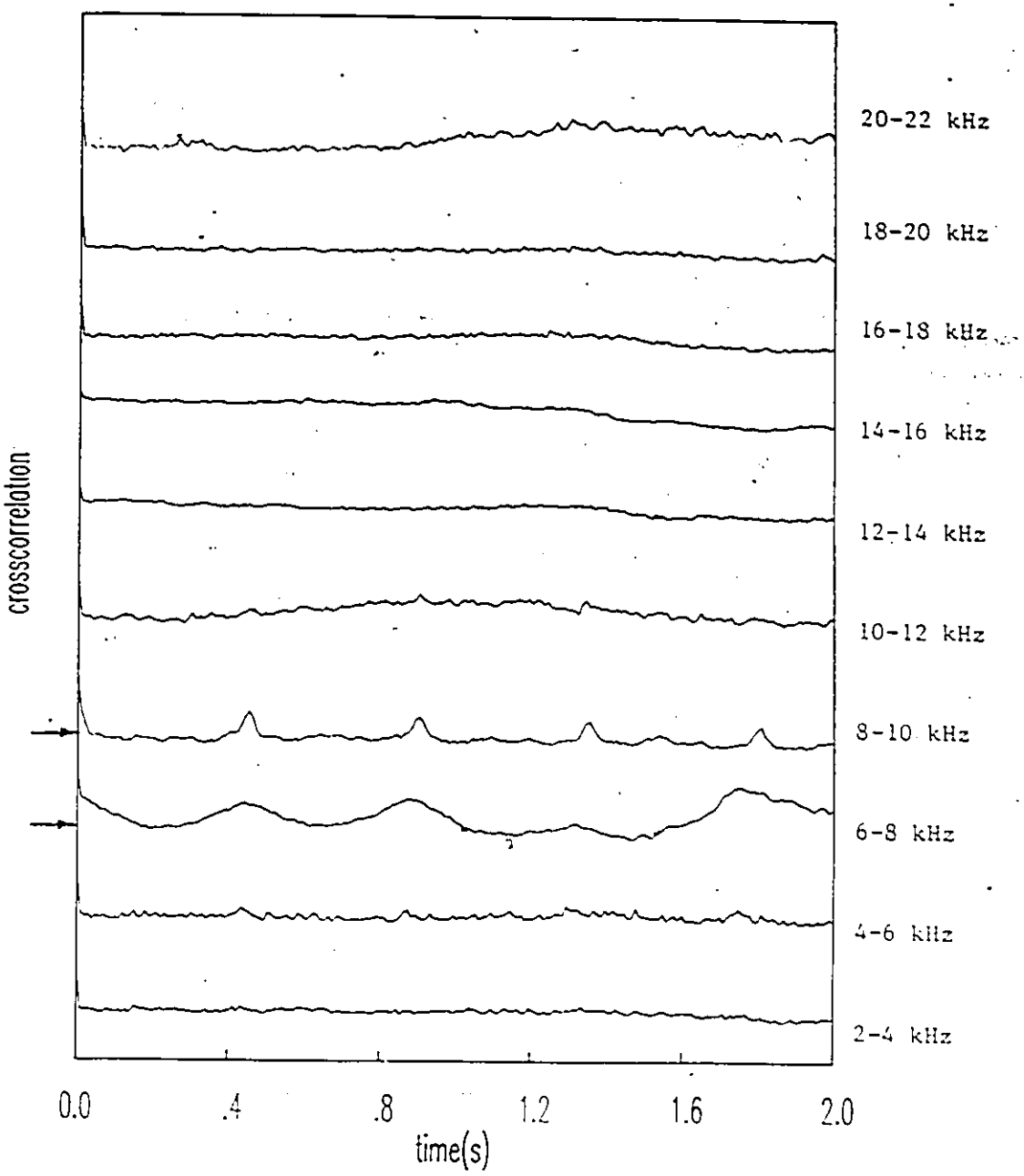

Fig. 5.10 The crosscorrelation curves for 10 different portions of orbit 861 at the 5th minute.

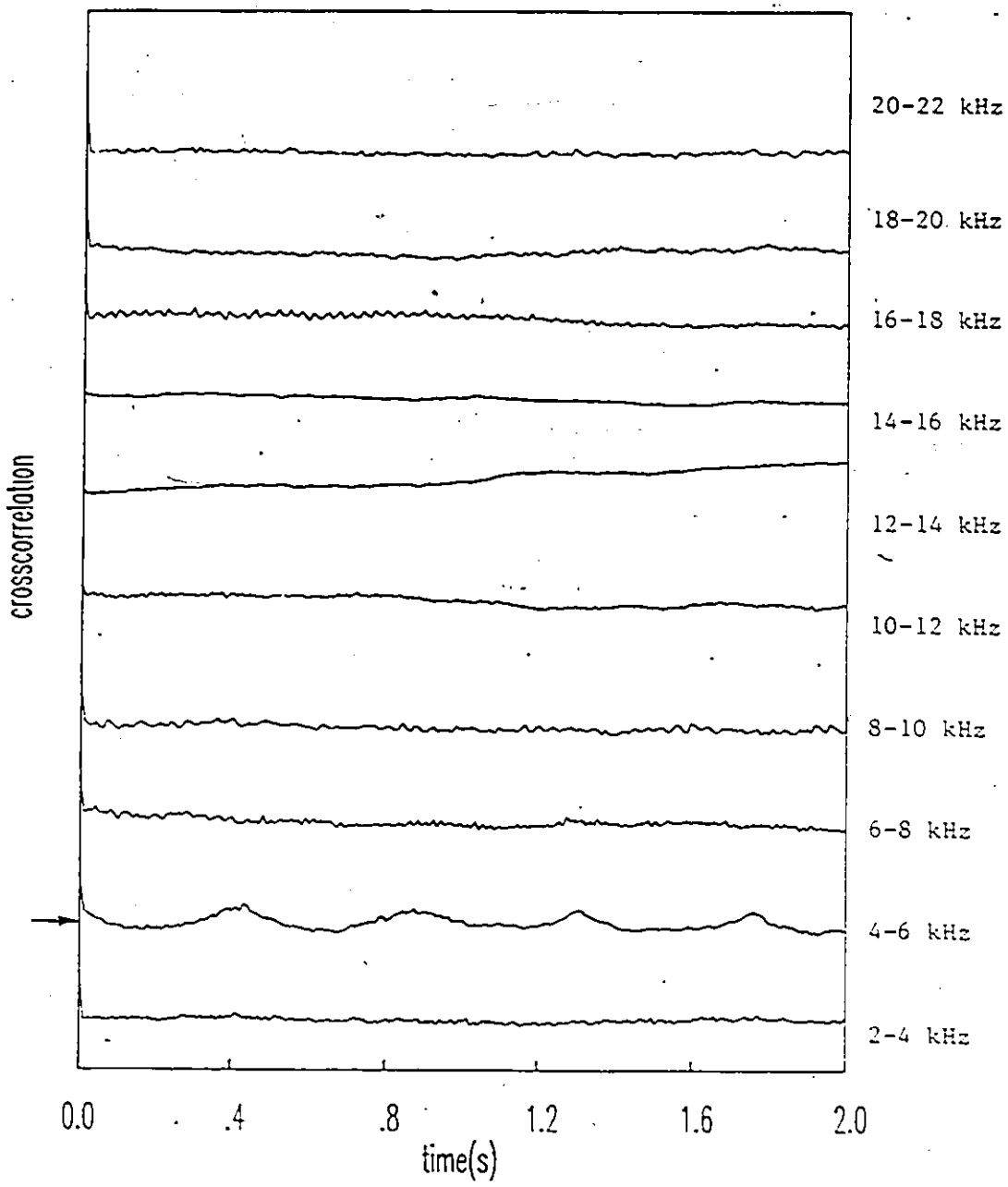

Fig. 5.11 The crosscorrelation curves for 10 different portions of orbit 861 at the 6th minute.

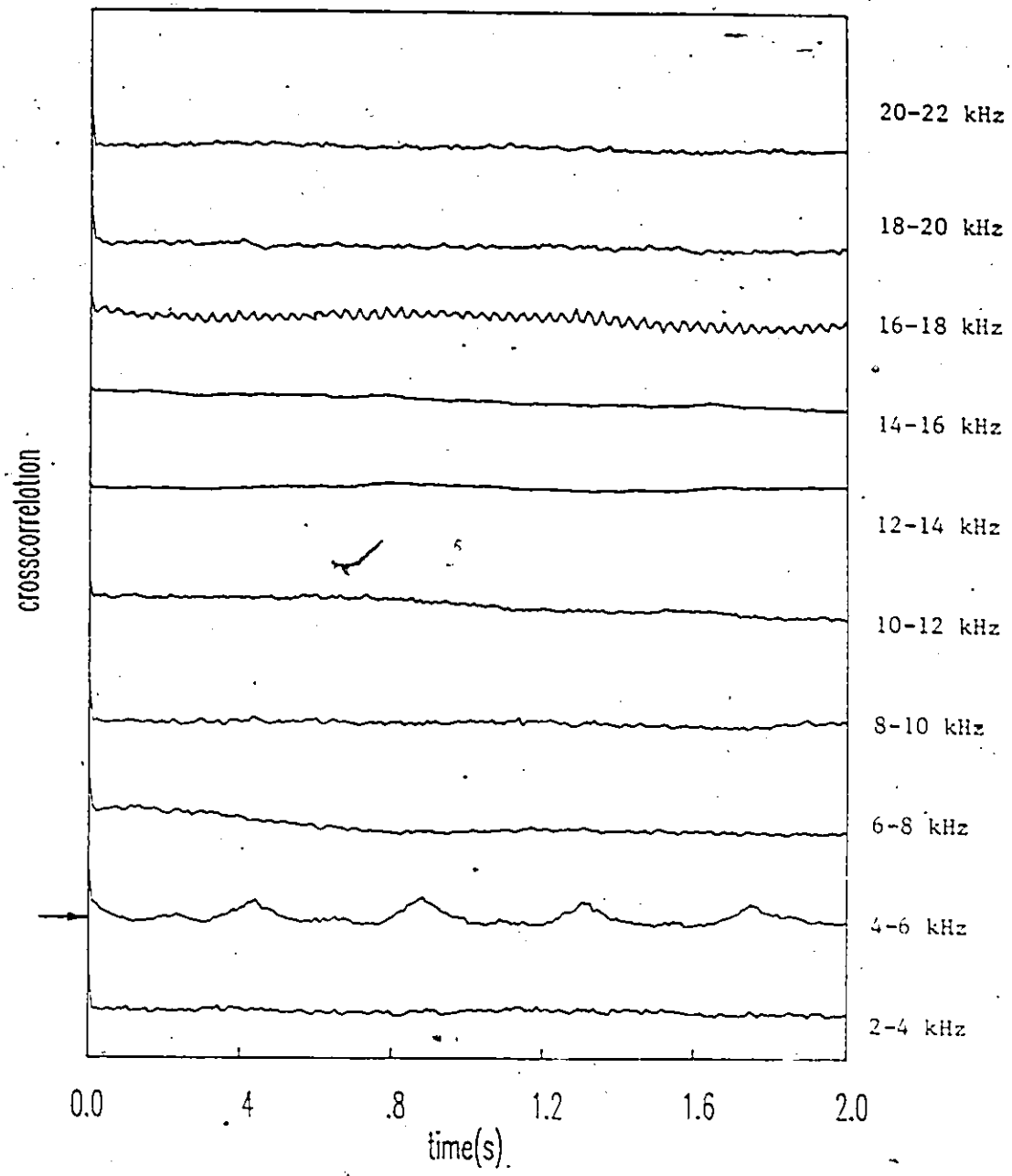

Fig. 5.12 The crosscorrelation curves for 10 different portions of orbit 861 at the 7th minute.

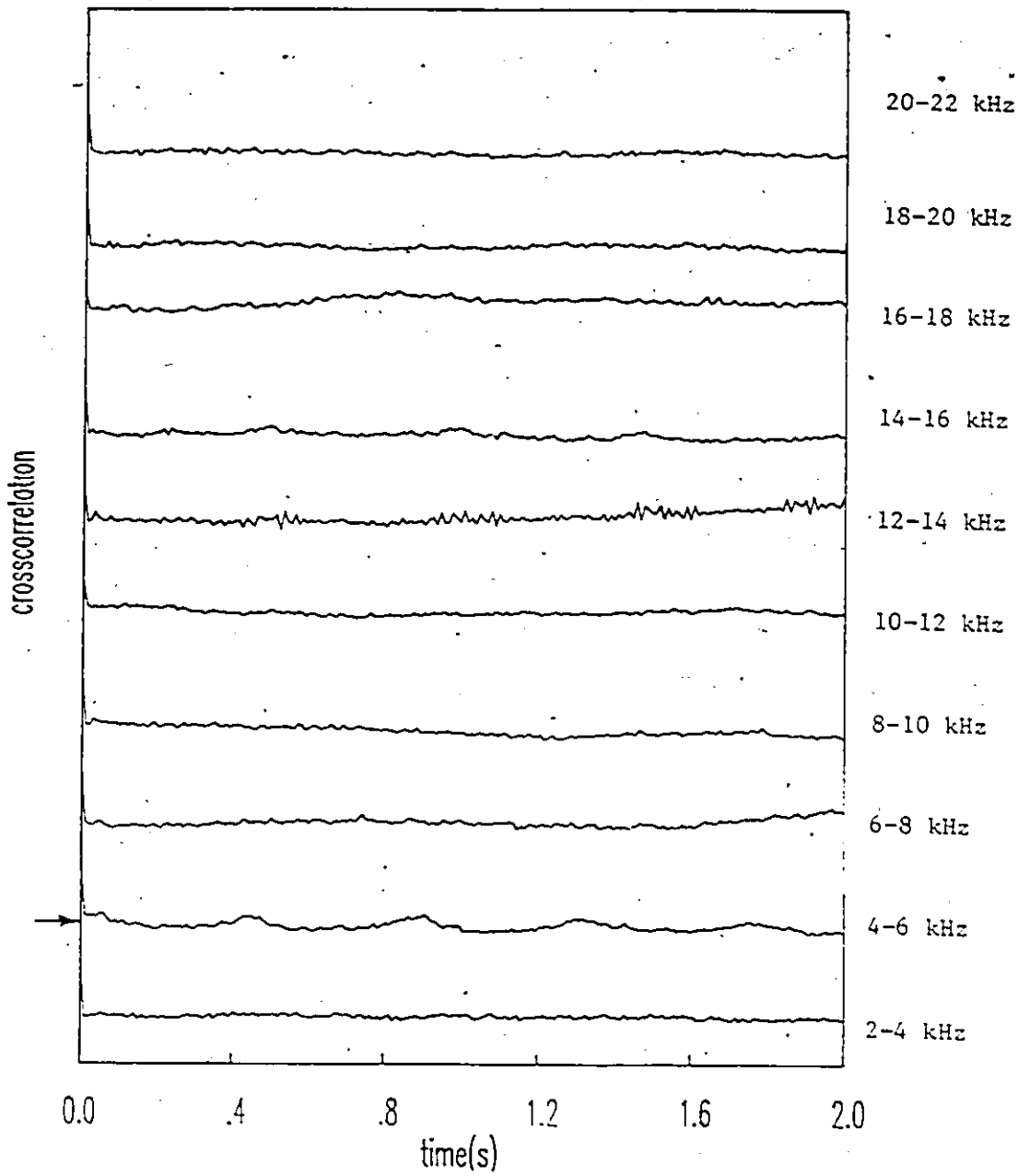

Fig. 5.13 The crosscorrelation curves for 10 different portions of orbit 861 at the 8th minute.

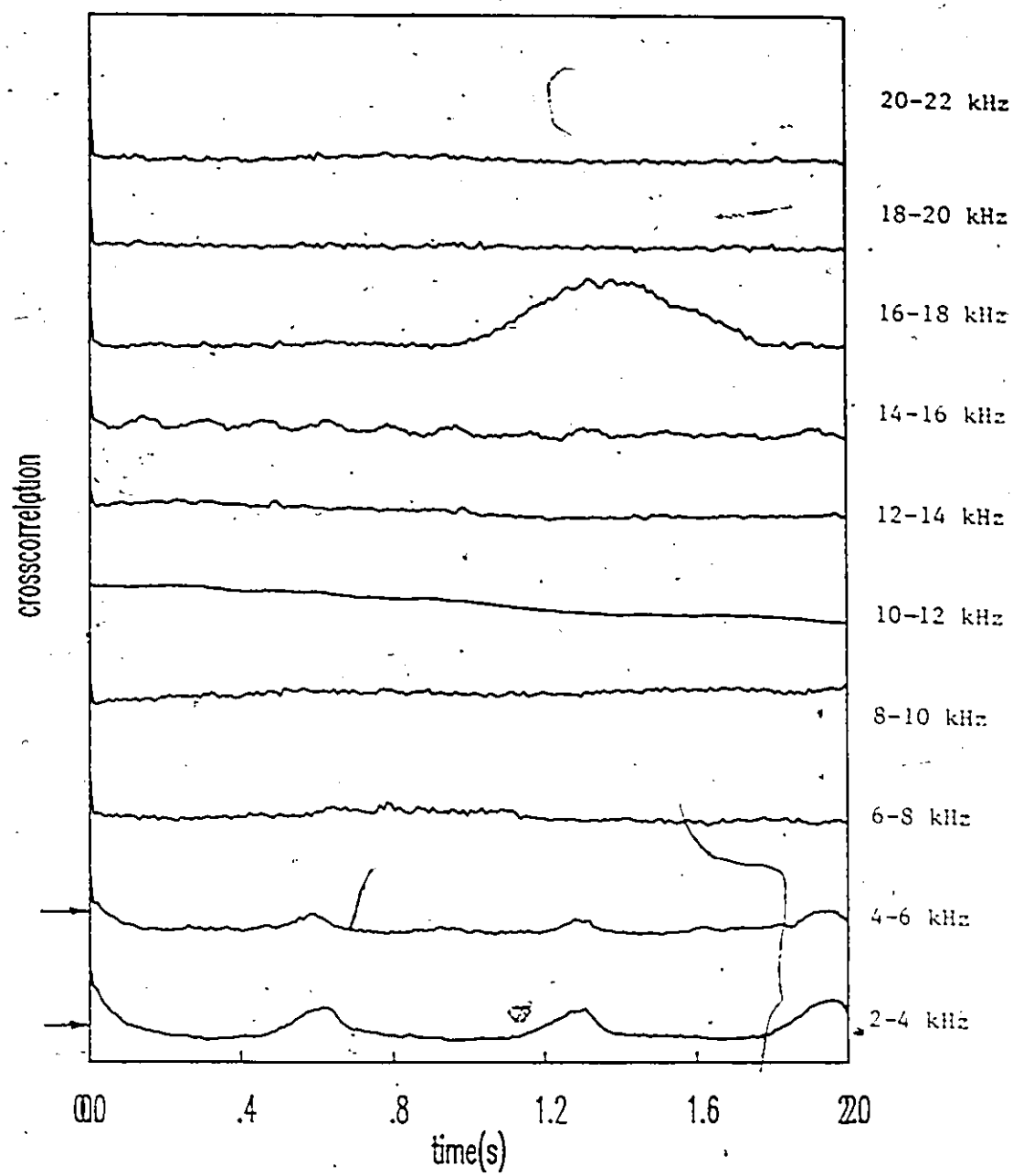

Fig. 5.14 The crosscorrelation curves for 10 different portions of orbit 861 at the 9th minute.

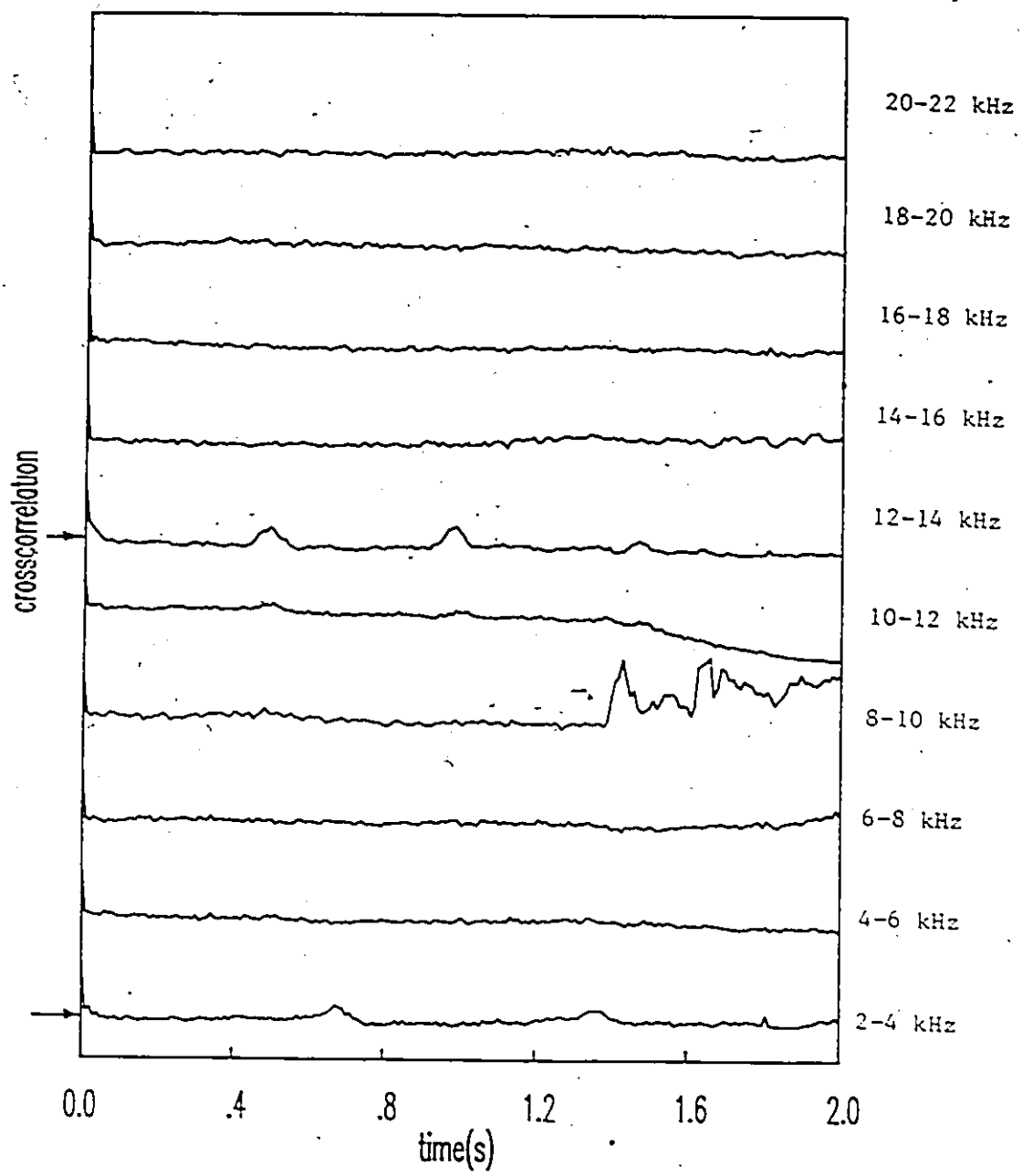

Fig. 5.15 The crosscorrelation curves for 10 different portions of orbit 861 at the 10th minute.

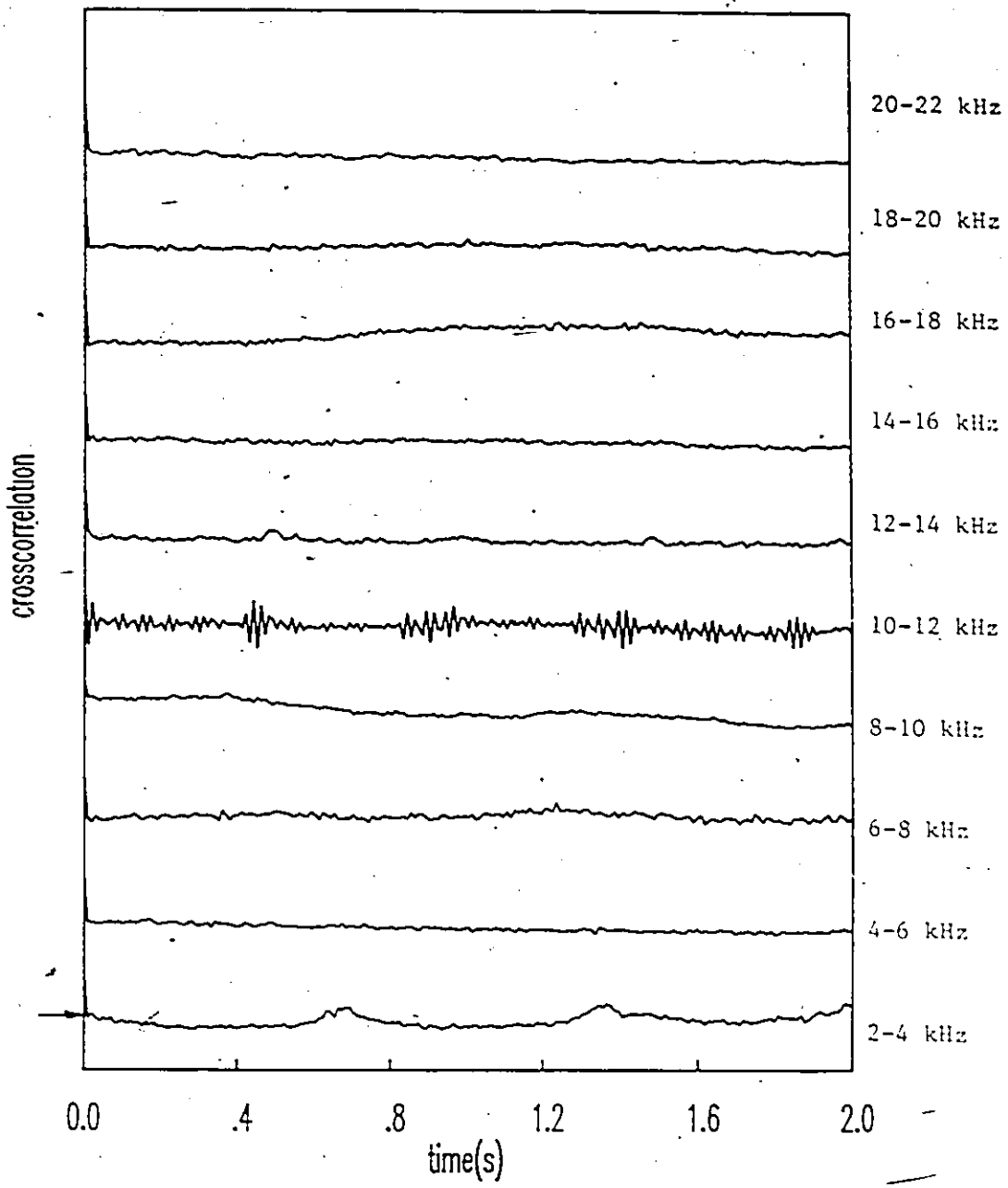

Fig. 5.16 The crosscorrelation curves for 10 different portions of orbit 861 at the 11th minute.

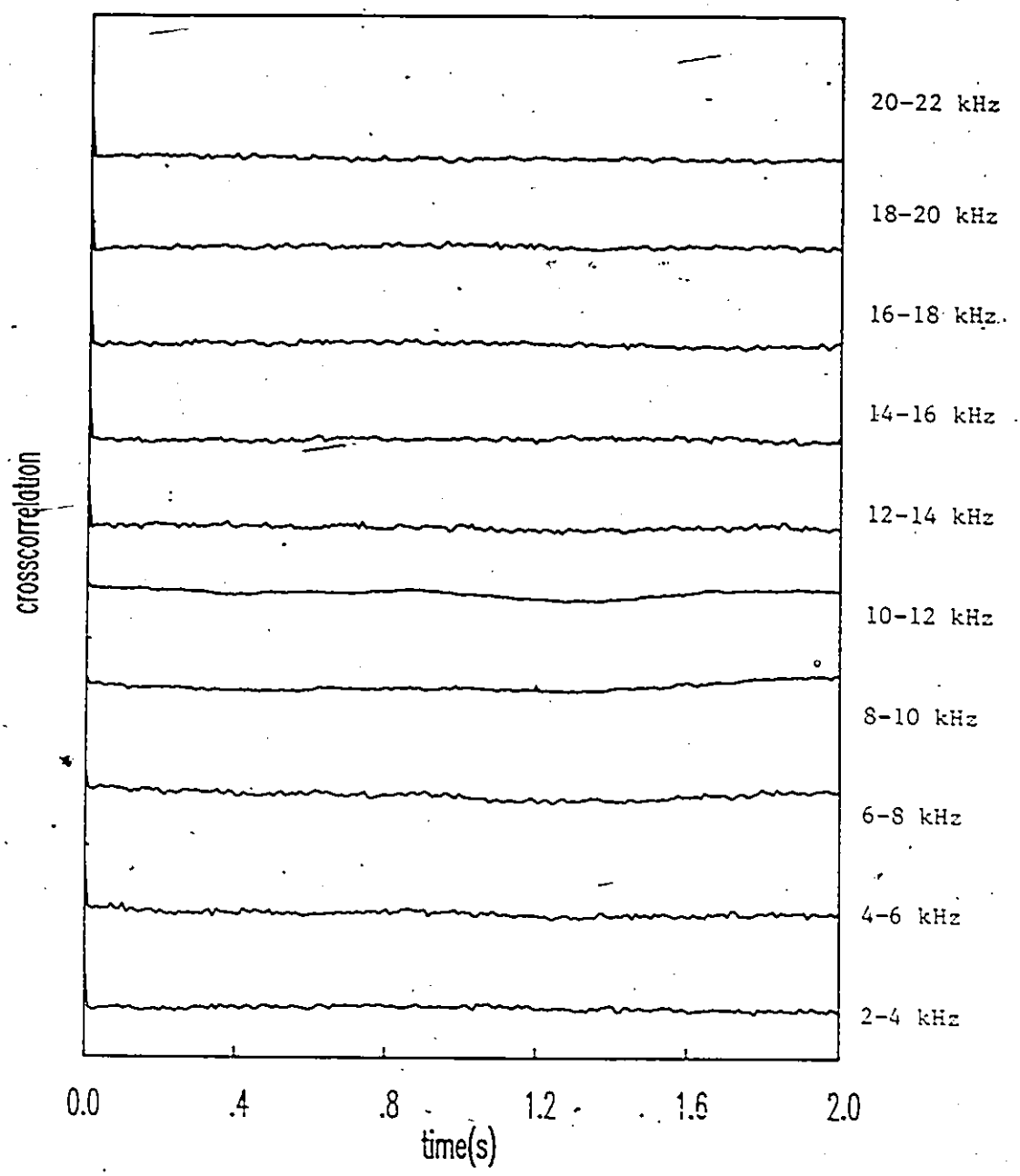

Fig. 5.17 The crosscorrelation curves for 10 different portions of orbit 861 at the 12th minute.

We start the microscopic analysis of the above detected ELT signal by focusing the attention on the range 5-10 kHz at the start of the 4th minute of the available data. During this portion we calculate 5 successive spectra, each being the average of 10 4k-FFT. This is shown in Fig. 5.18. The average of 2 s of data using 50 4K-FFT for the passband 5-10 kHz is shown in Fig. 5.19 from which we notice a signal similar to that manufactured by Narco where the arrow indicates the carrier frequency. For the passband 5-8 kHz, the cross-correlation curve is obtained and shown in Fig. 5.20a along with its corresponding FFT depicted in Fig. 5.20b. The sweep period of this signal is estimated to be $\hat{T}_s = 0.45$ s. The above signal is tracked at 4.5, 5, 5.5 and 6 minutes, as seen from the corresponding cross-correlation plots in Fig. 5.21 through Fig. 5.24. The estimated sweep period in each case is the same and equal 0.45 s implying the detection of the same signal. Due to the satellite motion the signal is Doppler shifted as seen in Fig. 5.25. This figure show five spectra at 4, 4.5, 5, 5.5 and 6 minutes, respectively. Each is the average of 50 4K-FFT (2 s) at the passband 5-8 kHz. A similar plot calculated at the passband 10-15 kHz is depicted in Fig. 5.26 indicating the existence of no ELT signals as previously cocluded from the macroscopic scan.

Figure 5.10 shows the possibility of the existence of an ELT signal in passband 8-10 kHz at the 5th minute. The detailed crosscorrelation curve for this passband is given in Fig. 5.27 which has a pattern similar to an ELT signals. On examining the crosscorrelation curves at 4 and 6 minutes, this signal could not be tracked. Therefore this signal might be due to a source other than an ELT signal or might be an ELT signal that is blocked due to an obstacle such as a mountain peak. This is also concluded from the average spectra depicted in Fig. 5.25, where it exists at the 5th minute only.

There may be another ELT signal present at the 10th min in the frequency band from 12-14 kHz as seen in Fig. 5.15. This signal disappears after the brief transmission. Therefore, we conclude that, in the satellite orbit 861, only three possible ELT signals may

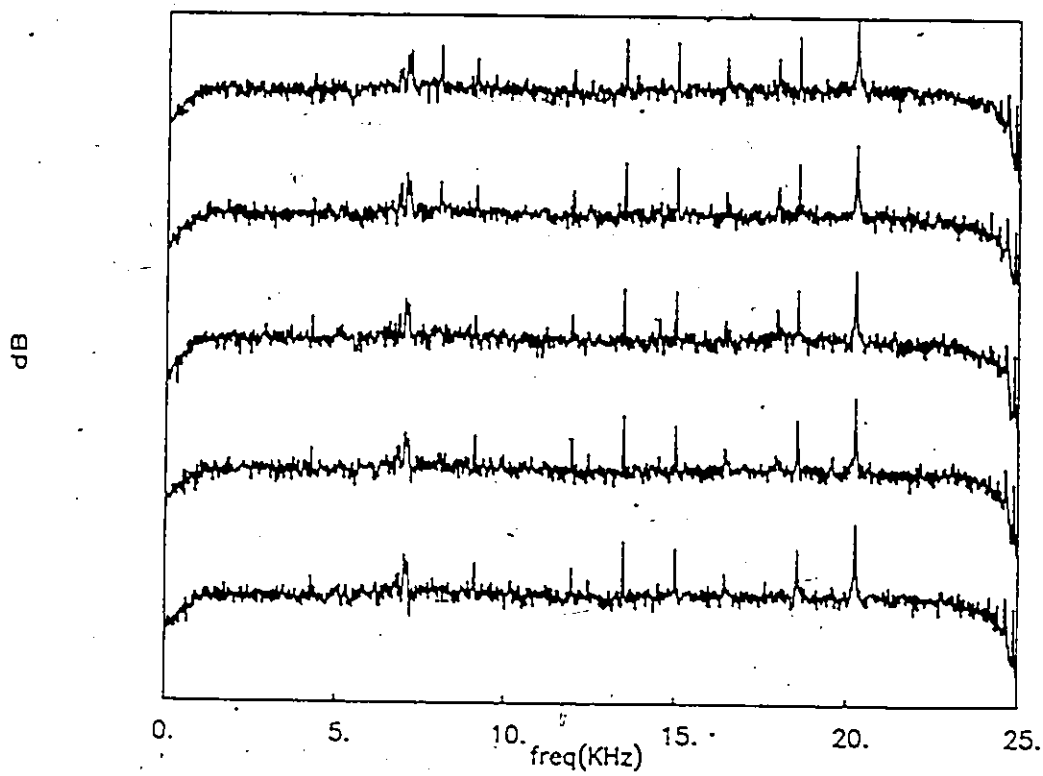

Fig. 5.18 A plot of five consecutive spectra at the 4th minute of satellite pass orbit 861. Each spectrum comprises the average of 10 4k-periodograms.

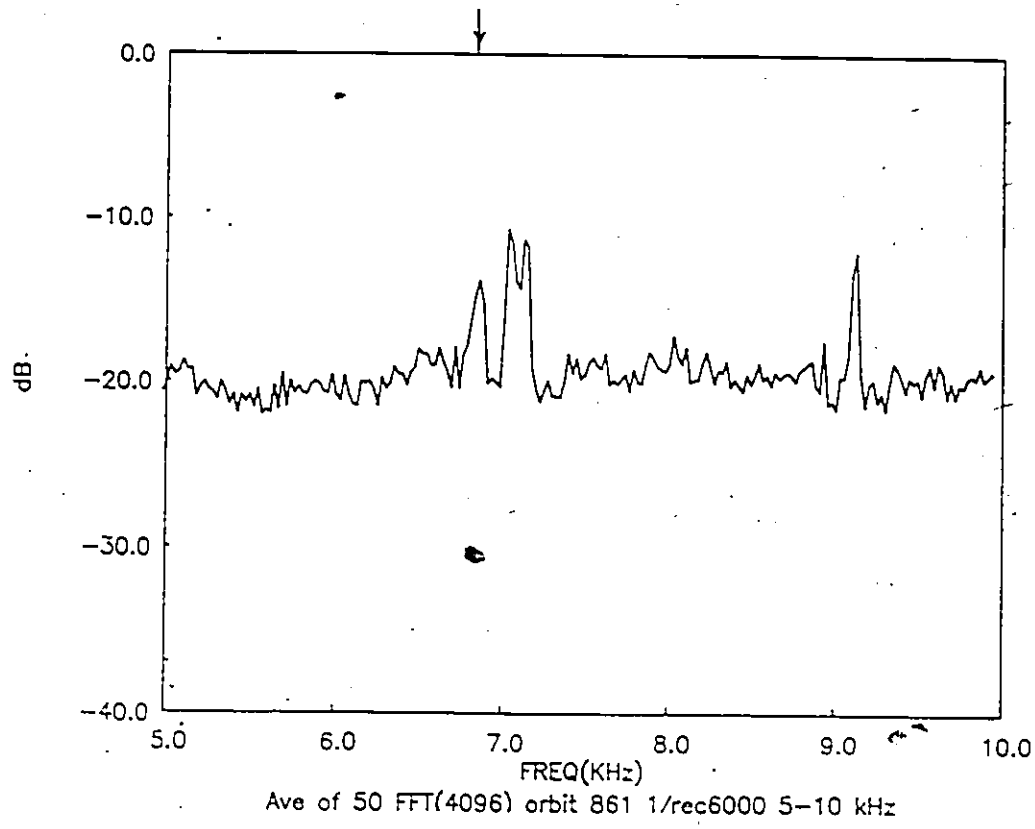

Fig. 5.19 An average of 50 4096-FFT for satellite pass orbit 861 at the 4th minute.

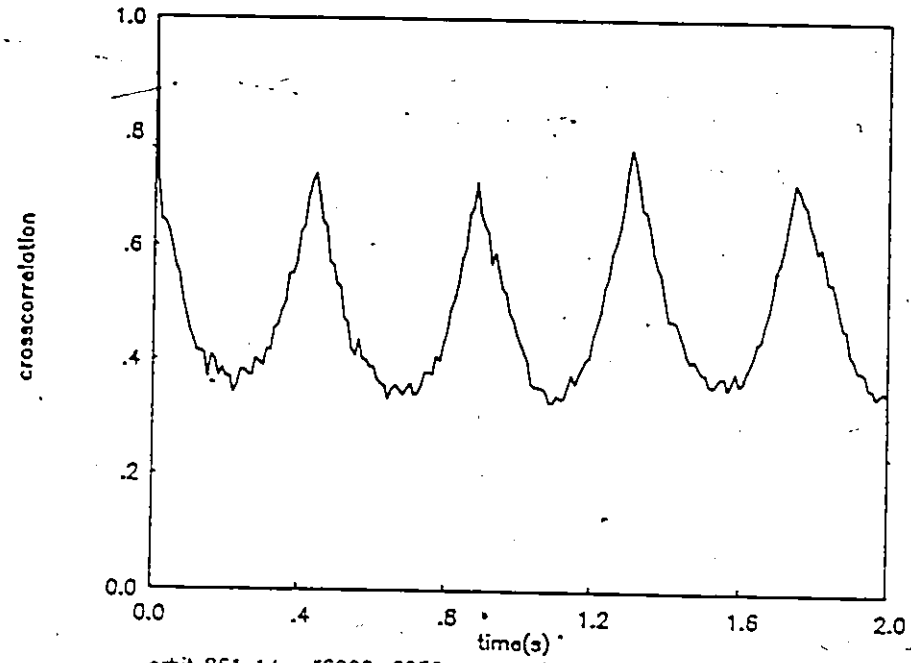

(a)

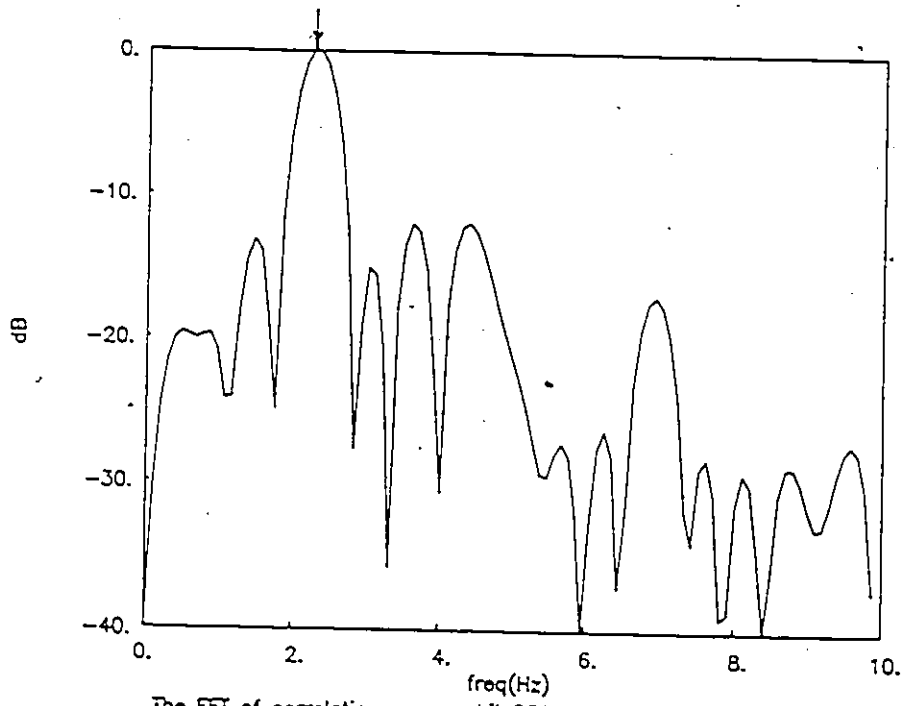

(b)

Fig. 5.20 (a) The crosscorrelation curve for orbit 861 at the 4th minute for frequency band 5-7 kHz.
(b) The FFT of the crosscorrelation curve.

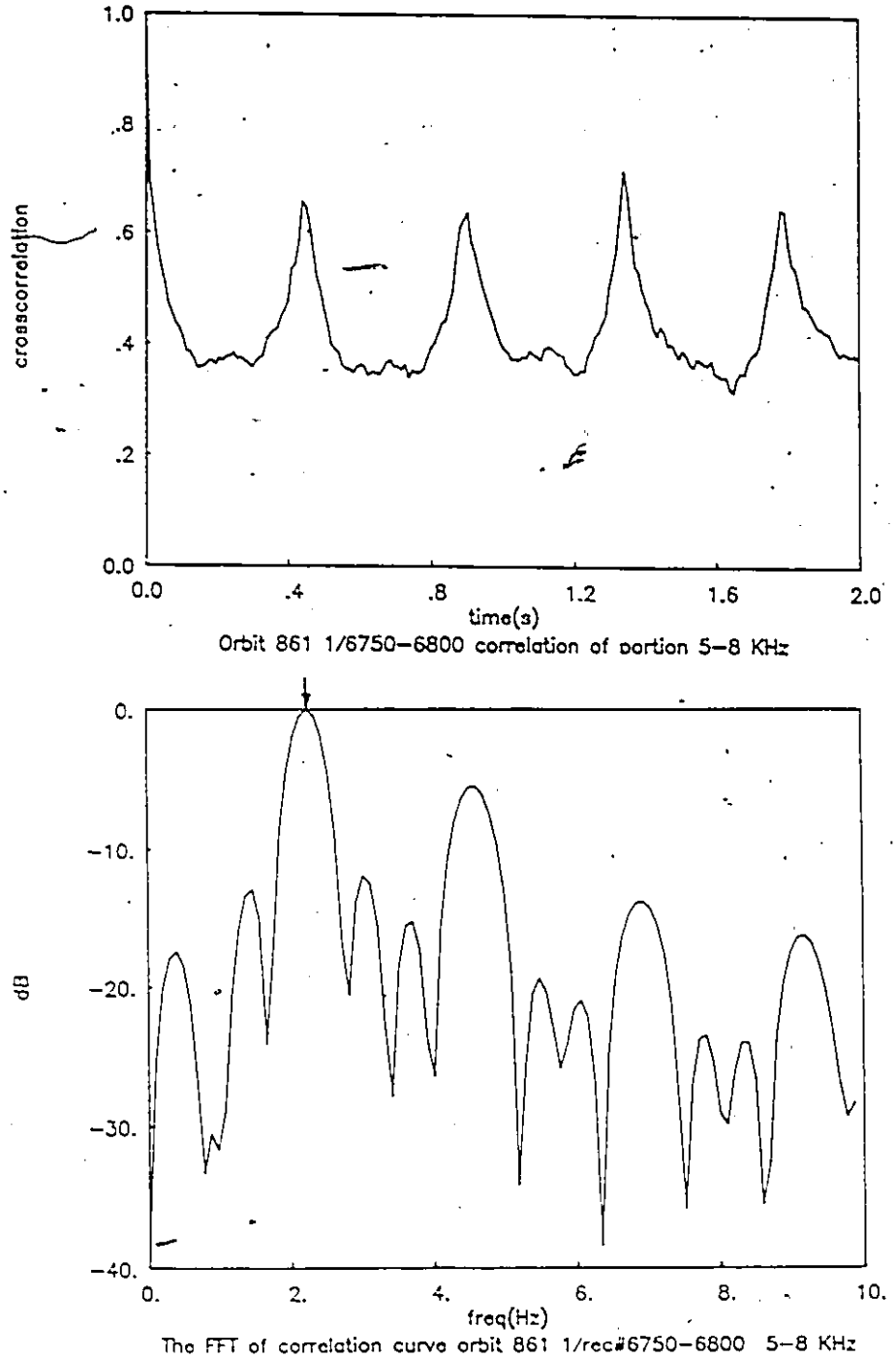

Fig. 5.21 (a) The crosscorrelation curve for orbit 861 at the 4.5th minute for frequency band 5-7 kHz.
(b) The FFT of the crosscorrelation curve.

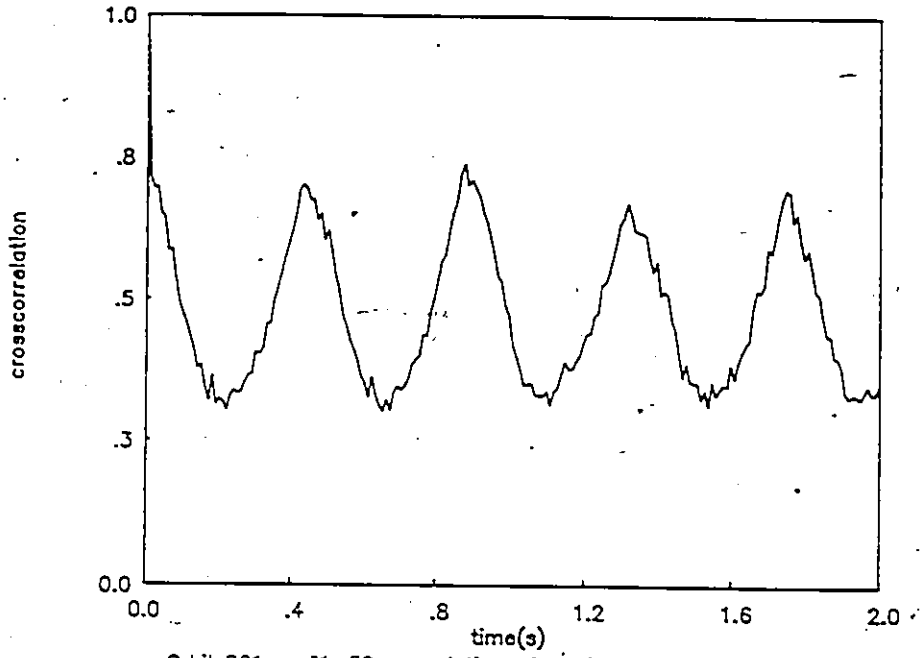

Orbit 861 rec#1–50 correlation of portion between 5KHz– 7KHz

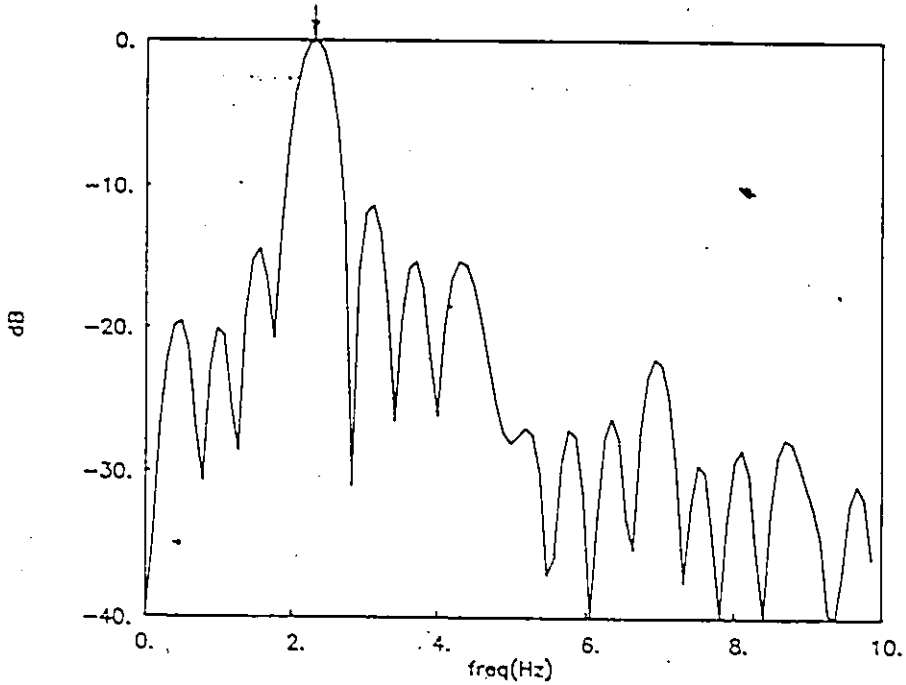

The FFT of correlation curve orbit 861 2/rec#1–50 5–7 KHz

Fig. 5.22 (a) The crosscorrelation curve for orbit 861 at the 5th minute for frequency band 5-7 kHz.
(b) The FFT of the crosscorrelation curve.

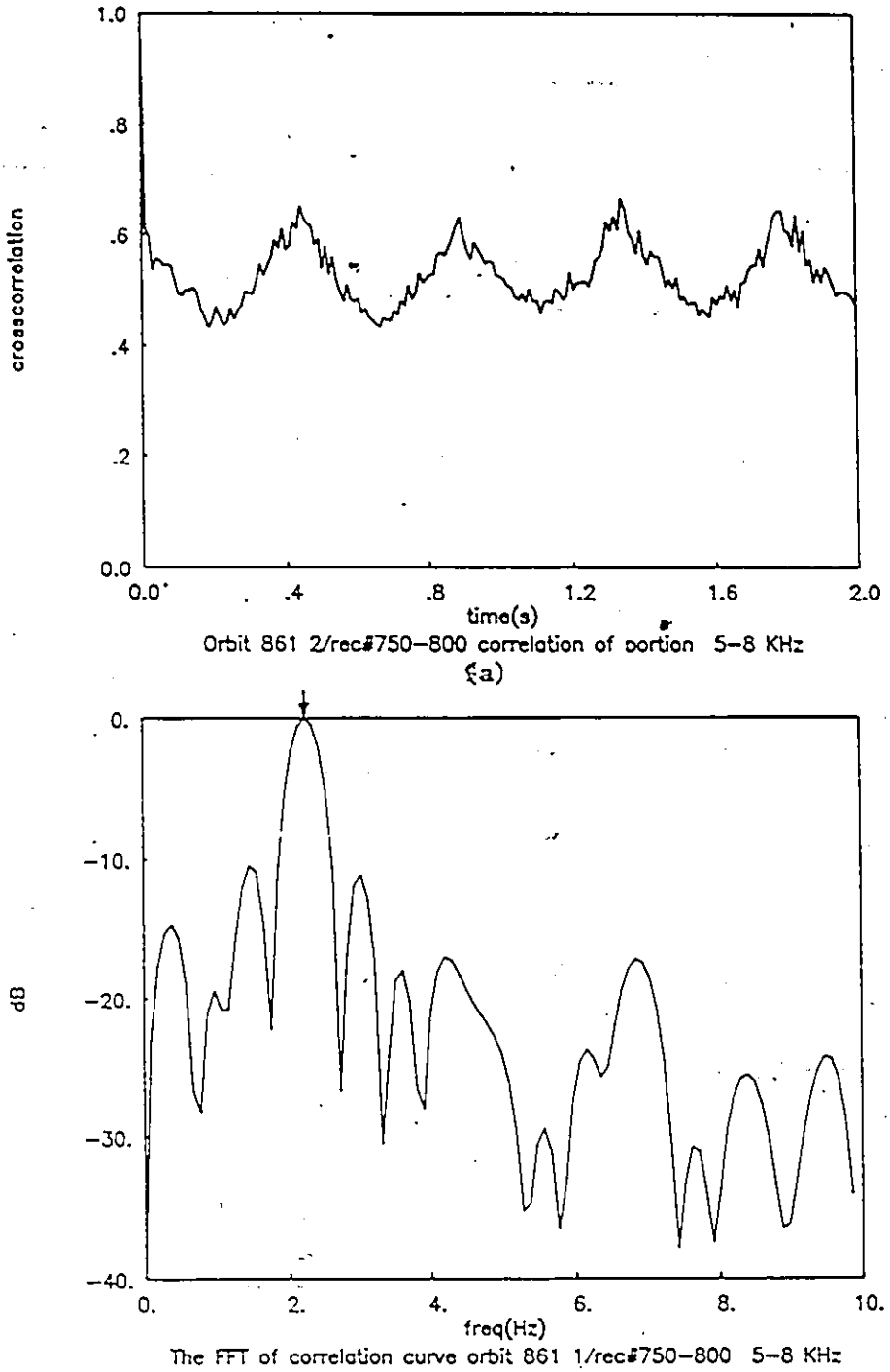

Fig. 5.23 (a) The crosscorrelation curve for orbit 861 at the 5.5th minute for frequency band 5-7 kHz.
(b) The FFT of the crosscorrelation curve.

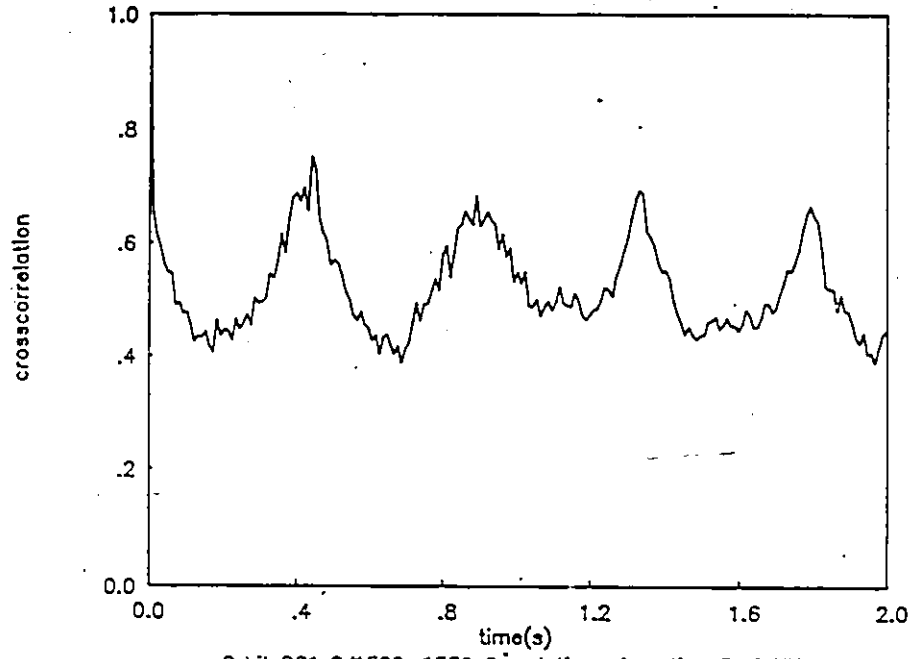

Orbit 861 2/1500–1550 Correlation of portion 5–6 KHz

(a)

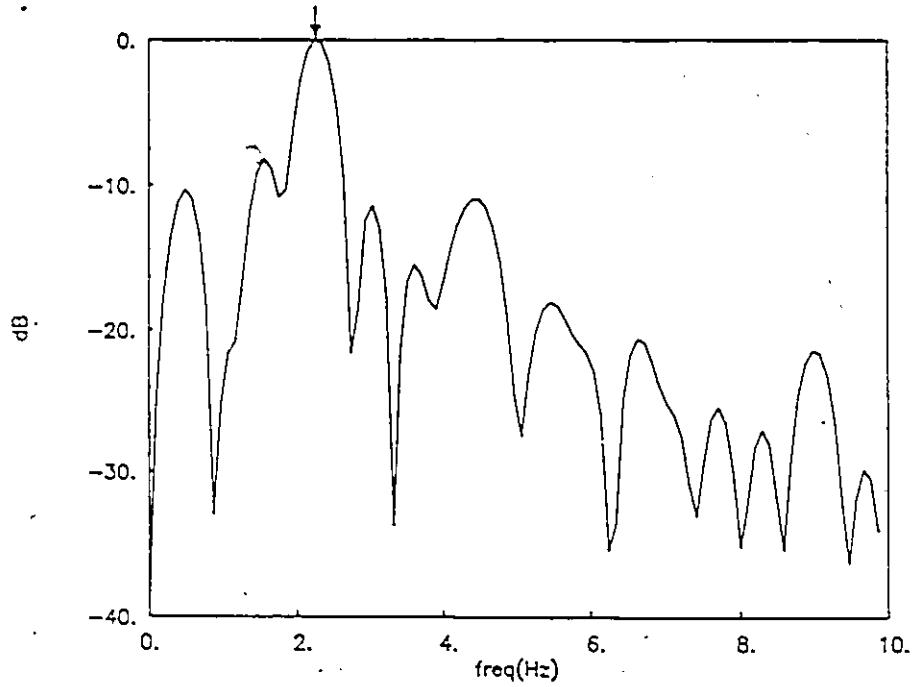

The FFT of correlation curve orbit 861 2/rec#1500–1550 5–6 KHz

(b)

Fig. 5.24 (a) The crosscorrelation curve for orbit 861 at the 6th minute for frequency band 5-7 kHz.
(b) The FFT of the crosscorrelation curve.

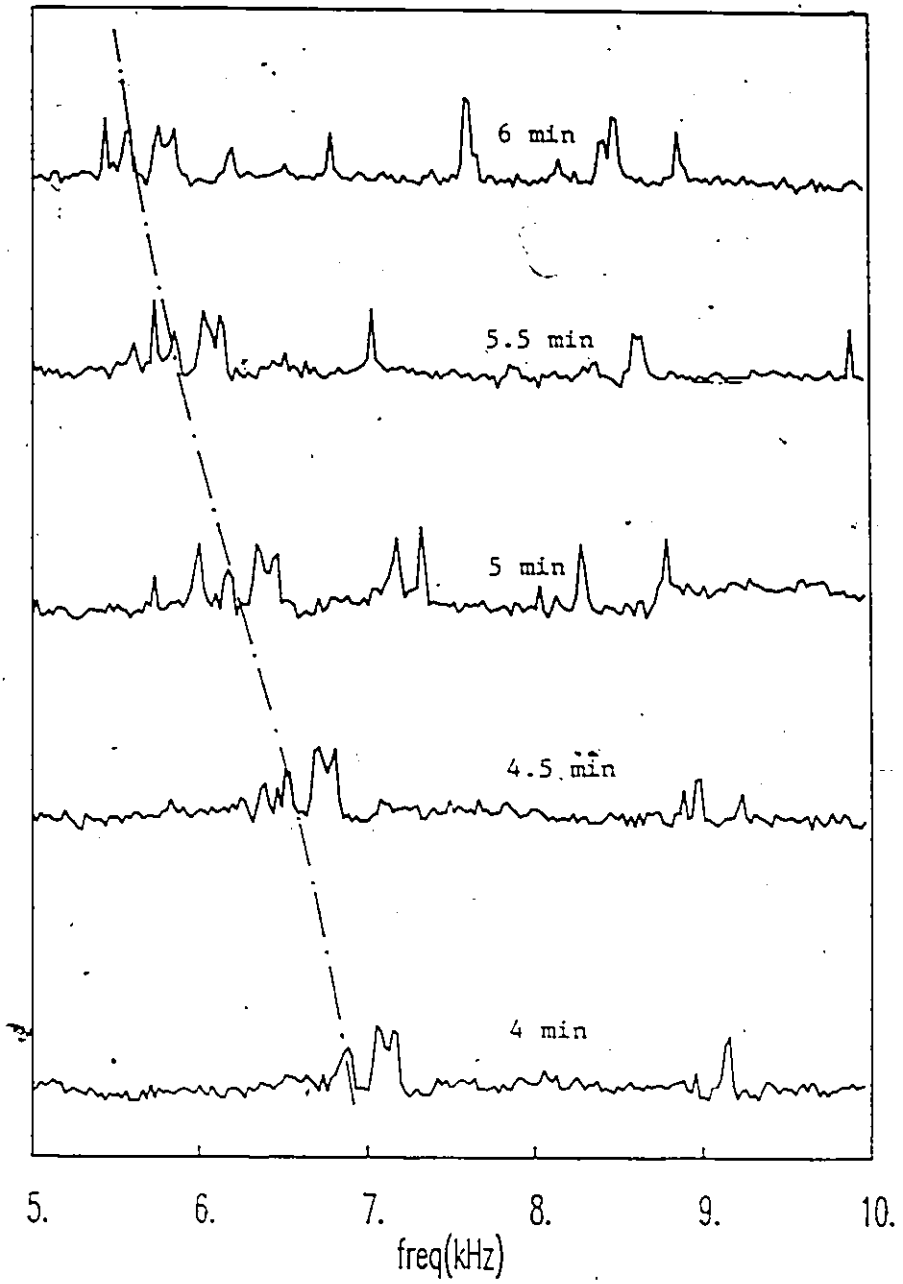

Fig. 5.25 Five average spectra at 4, 4.5, 5, 5.5 and 6 minute orbit 861. Each an average of 50 4096-FFT. Frequency band 5-10 kHz.

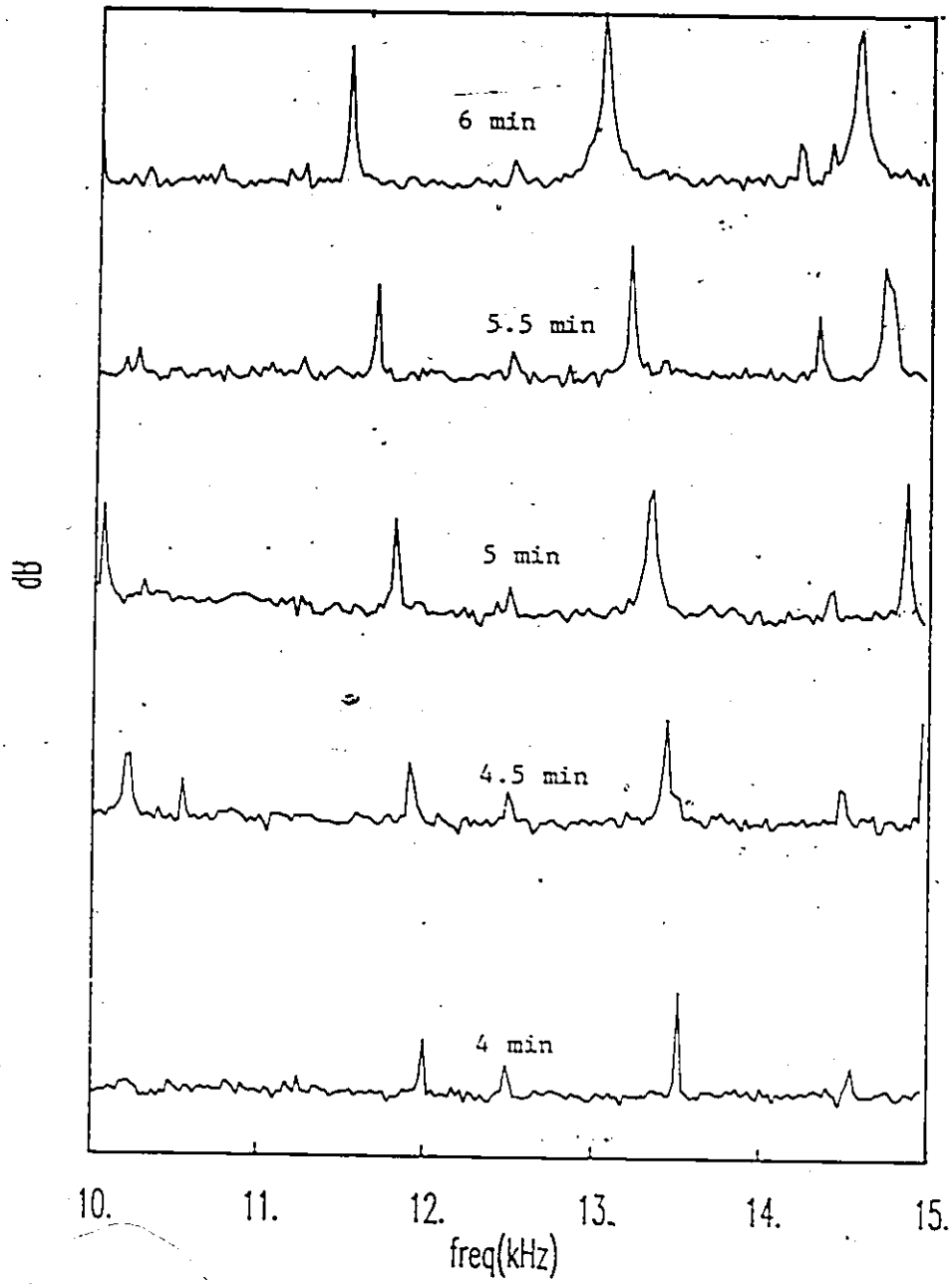

Fig. 5.26 Five average spectra at 4, 4.5, 5, 5.5 and 6 minute orbit 861. Each an average of 50 4096-FFT. Frequency band 10-15 kHz

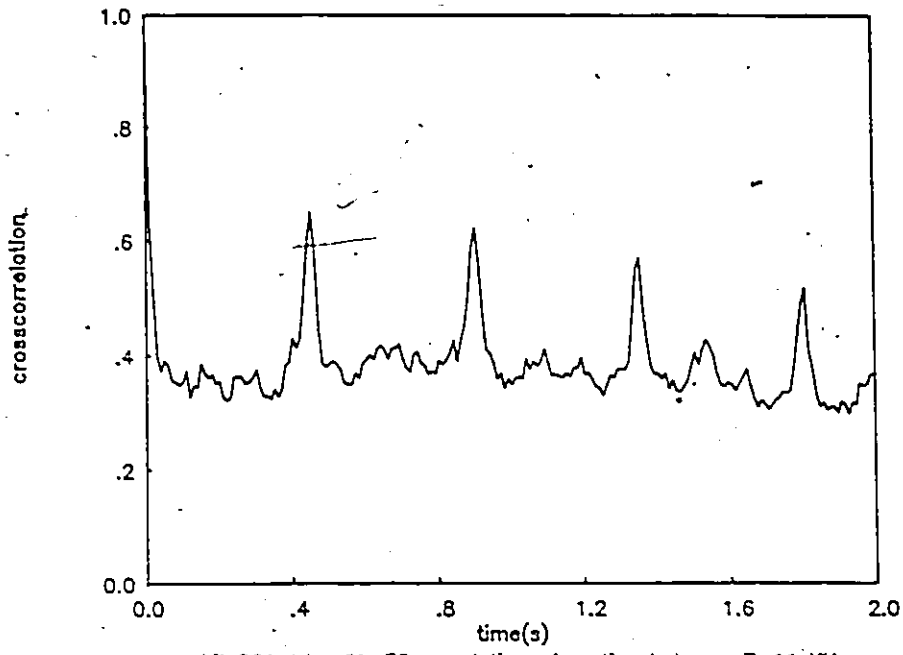

(a)

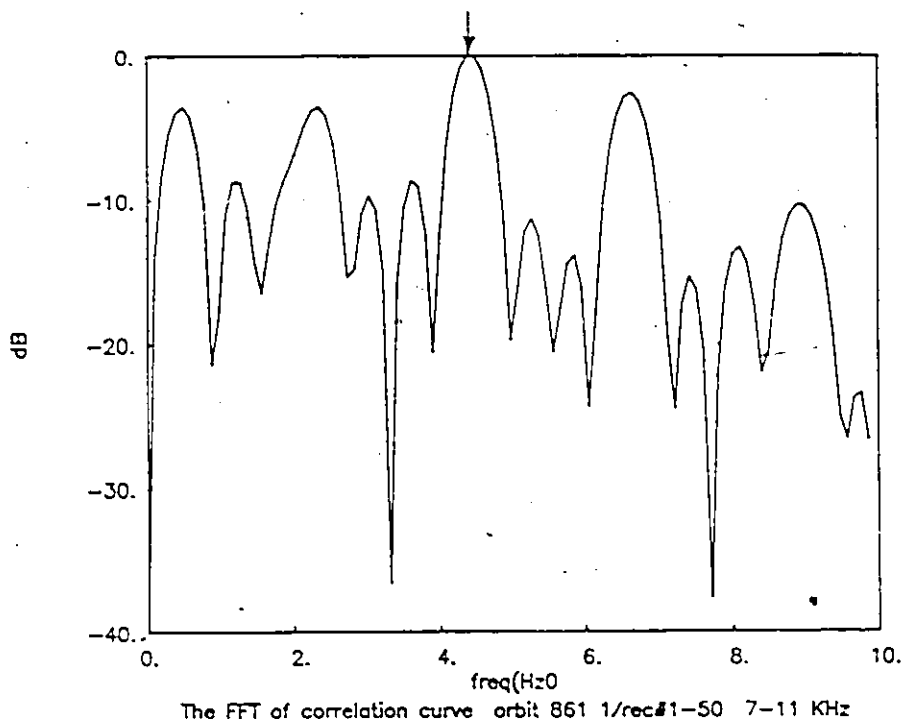

(b)

Fig. 5.27 (a) The crosscorrelation curve for orbit 861 at the 5th minute for frequency band 8-10 kHz.

(b) The FFT of the crosscorrelation curve.

exist and those correspond to the areas of concentrated dots, two in region E and one in region F of Fig. 5.7. The rest of the curves are due to interfering sources which may be discarded. This, in turn, provides us with very useful information about the pass, consequently leading to a significant reduction of interfering sources.

5.4 Analysis of Satellite Pass Orbit 860

The dot-chart of orbit 860 is obtained using the same procedure followed in the section 5.2. The dot-chart of orbit 860 is given in Fig. 5.28. The pass contains about 7 signals. We first investigate the existence of any ELT signal using two different times during the pass; namely at the beginning of the 5th and 10th minutes.

Five successive spectra, each comprising the average of 10 4K-FFT at the 5th min are given in Fig. 5.29. The average spectrum of these 5 plots for the passbands 5-10 kHz and 10-15 kHz are given in Fig. 5.30 showing no ELT signals. To test that conclusion, the cross-correlation curves for frequency bands 11-14 kHz and 15-18 kHz are obtained and plotted in Fig. 5.31. The resulting curves are flat as in the case of interference signals.

Figure 5.32 show 5 successive spectra for the signal received at the 10th min. The average spectrum of the 5 plots in the frequency bands 5-10 kHz and 10-15 kHz are depicted in Fig. 5.33. The crosscorrelation technique is applied to two regions, the first between 8-10 kHz and the second from 12-14 kHz. The corresponding curves are depicted in Fig. 5.35. We note that the crosscorrelation curves are flat, indicating the existence of no ELT signals in this pass.

From the above analysis, it is clear that the crosscorrelation technique provides the means for consolidating the number of ELT detections per day which was one of our aims. For the two satellite passes analysed, with a combined total of about 23 signals, only one ELT signal persisted for a significant duration in the pass. Two other signals which appeared for

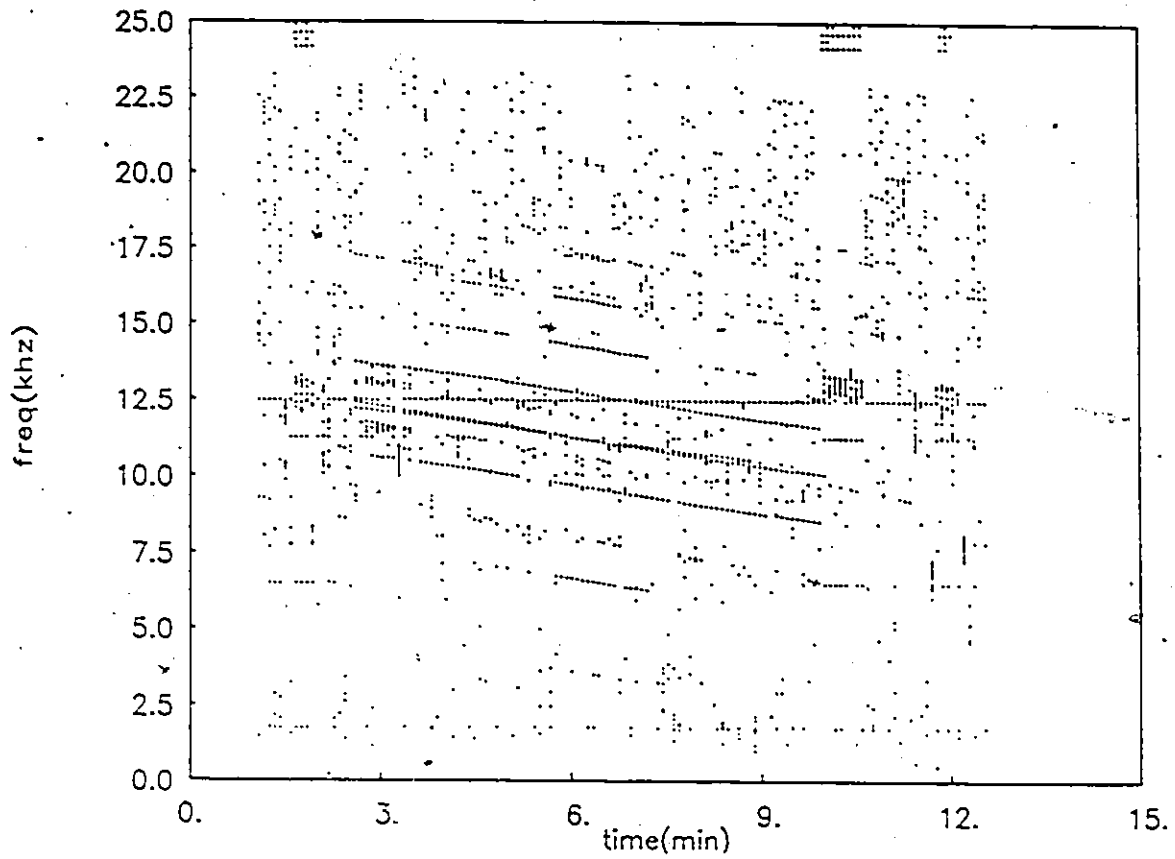

Fig. 5.28 Dot-chart of satellite pass orbit 860 using adaptive threshold with 20 peaks.

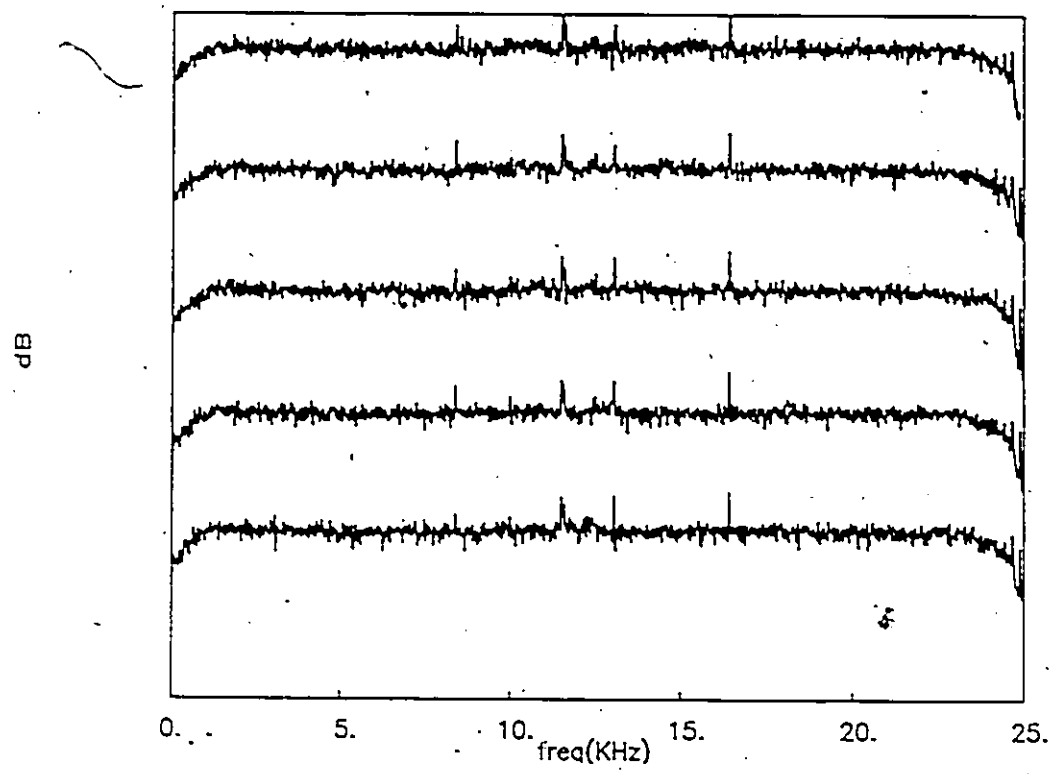

Fig. 5.29 A plot of five consecutive spectra at the 5th minute of satellite pass orbit 860. Each spectrum comprises the average of 10 4k-periodograms.

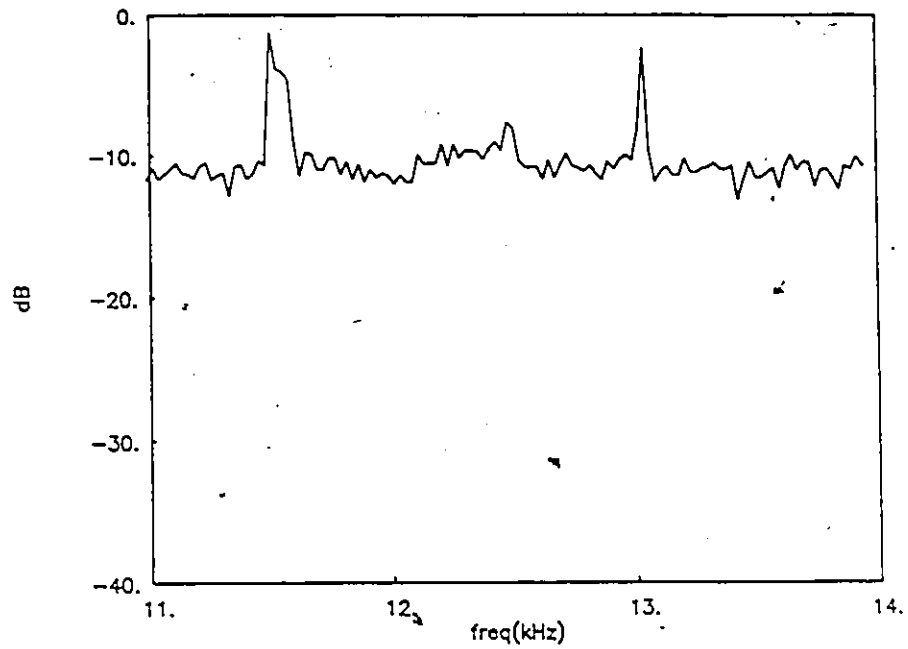

(a)

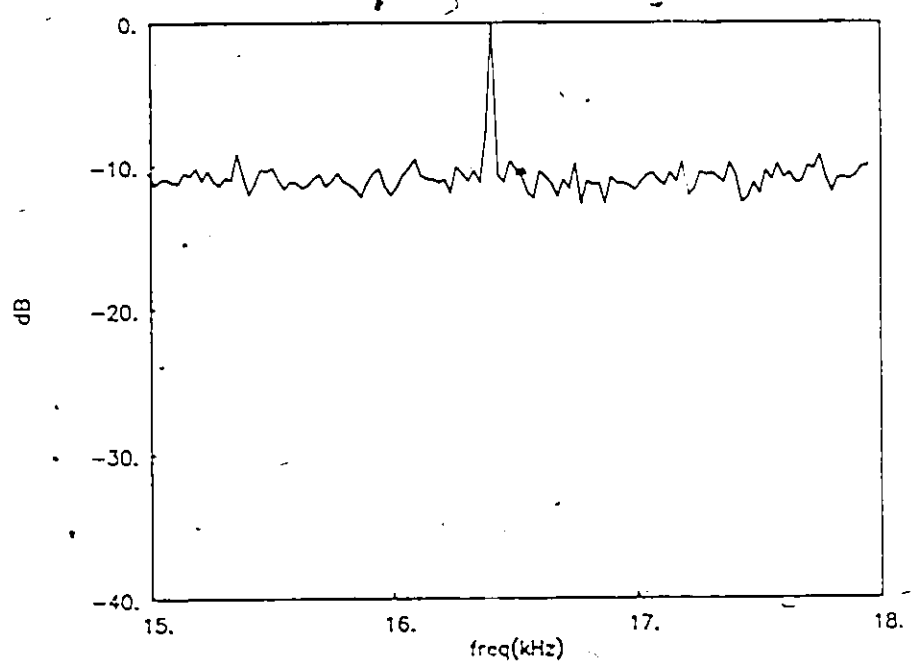

(b)

Fig. 5.30 The average of 50 4k-FFT for satellite pass orbit 860 at the 5th minute.
(a) Passband 11-14 kHz.
(b) Passband 15-18 kHz.

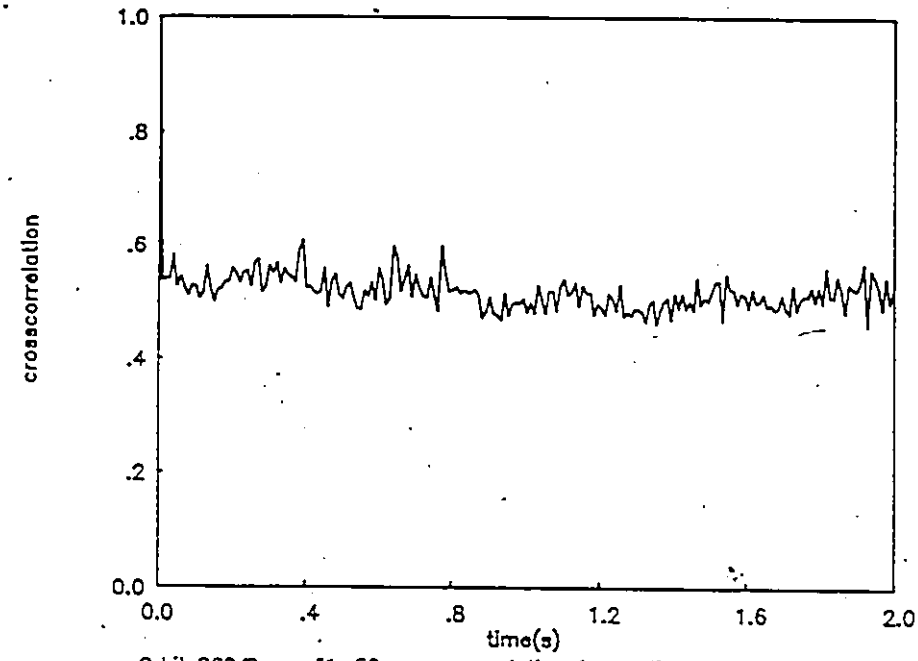

Orbit 860/2 rec#1–50 crosscorrelation for portion between 11–14 KHZ

(a)

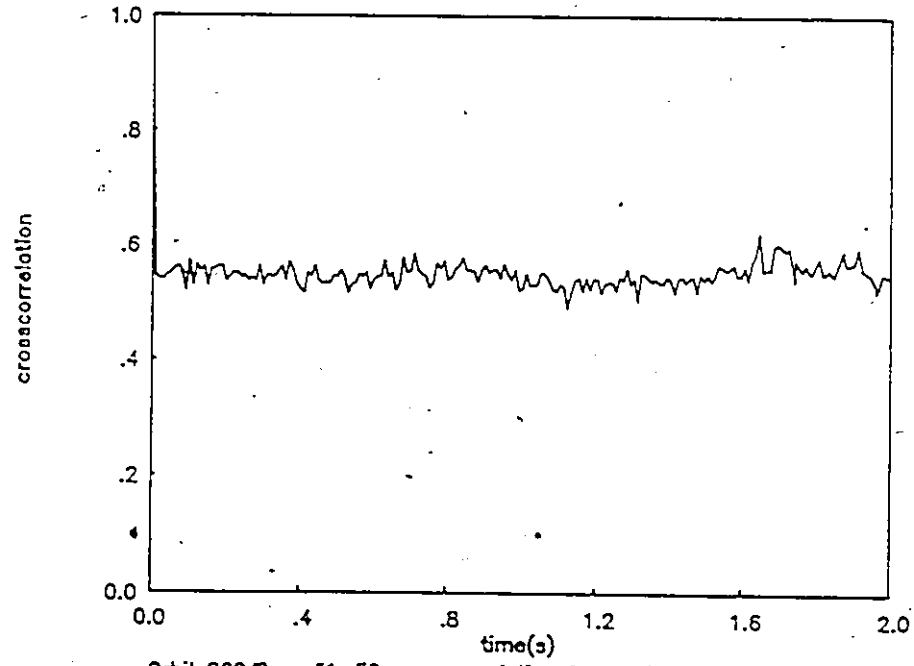

Orbit 860/2 rec#1–50 crosscorrelation for portion betwen 15–18 KHz

(b)

Fig. 5.31 The crosscorrelation curve for orbit 860 at the 5th minute for two frequency bands
(a) 11-14 kHz.
(b) 15-18 kHz.

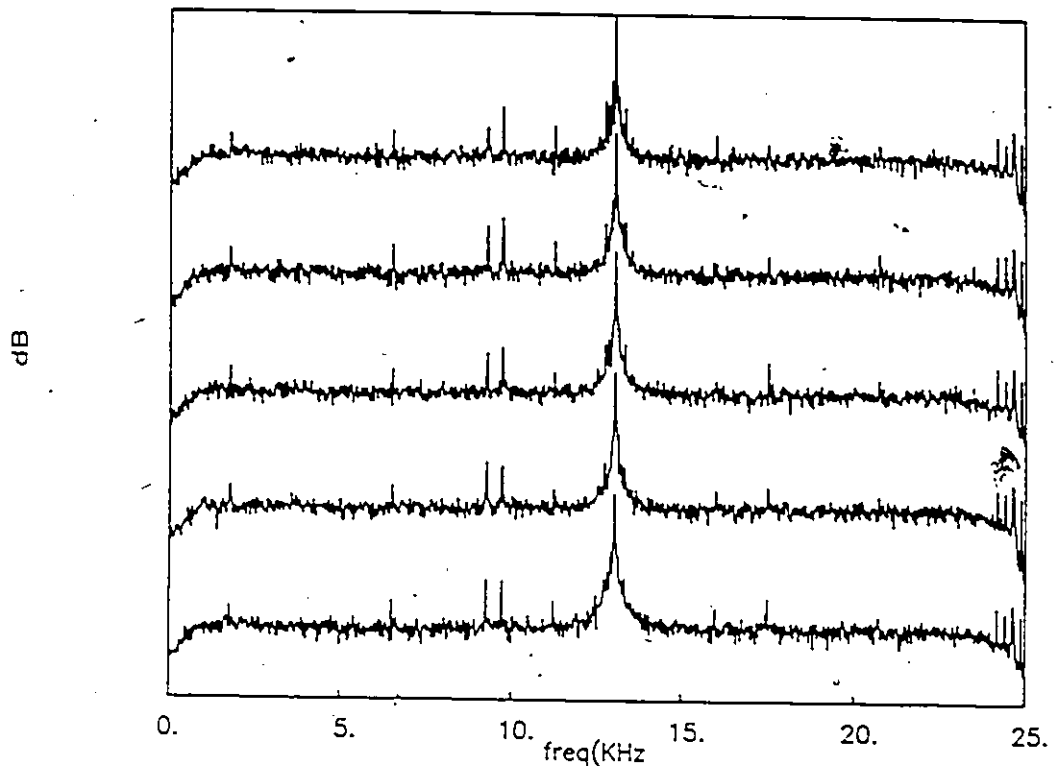

Fig. 5.32 A plot of five consecutive spectra at the 10th minute of satellite pass orbit 860. Each spectrum comprises the average of 10 4k-periodograms.

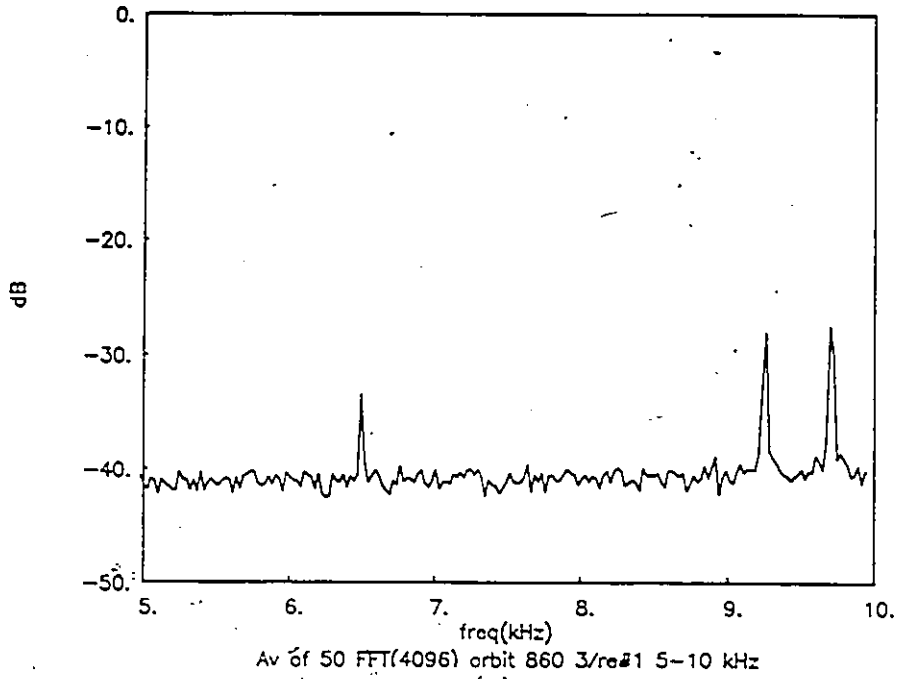

(a)

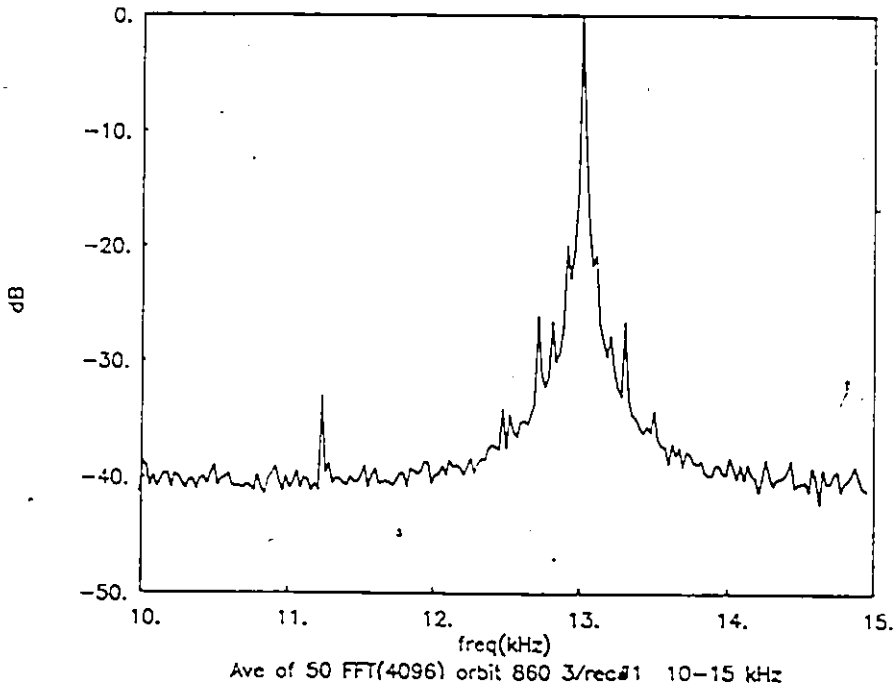

(b)

Fig. 5.33 The average of 50 4k-FFT for satellite pass orbit 860 at the 10th minute.
(a) Passband 5-10 kHz.
(b) Passband 10-15 kHz.

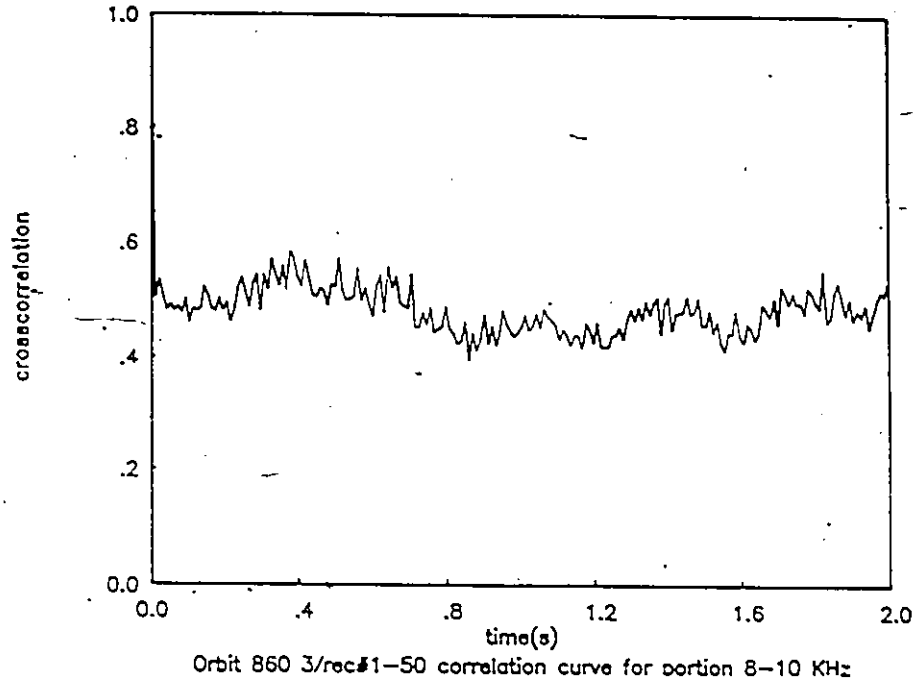

(a)

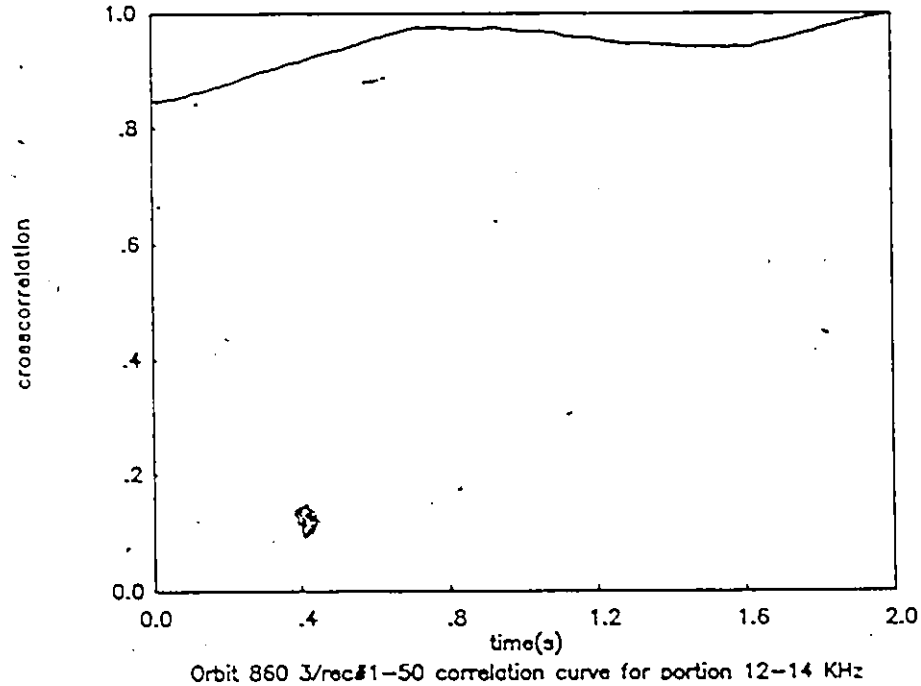

(b)

Fig. 5.34 The crosscorrelation curve for orbit 860 at the 10th minute for two frequency bands
(a) . 5-10 kHz.
(b) 10-15 kHz

short periods were identified as possible ELT signals and the remaining signals were all identified as interference. Thus, the resulting data set for the pass can be reduced by approximately 87%.

5.5 Summary

As a means of identification, the crosscorrelation method proposed in the previous chapters, is applied to real satellite pass signals. The available data are received from orbits 860 and 861 of the COSPAS satellite. The dot-chart of each pass is obtained. A preliminary scan over the 861 pass indicates the detection of three ELT signals among approximatly 16 received signals. The remaining signals are due to interference. Analysing the 860 orbit data results in the conclusions that no ELT signals are present among the 7 received.

CHAPTER 6

CONCLUSIONS AND RECOMMENDATIONS FOR FUTURE RESEARCH

6.1 Conclusions

In the SARSAT system envirnoment it is possible to receive many (up to 20) simultaneous emergency beacon signals combined with voice signals and interference of various types, all signals simultaneously occuping essentially the same frequency-time (dot-chart) space.

Typical ELT units use very simple circuits with poor carrier oscillator stability. Moreover, the specifications allow a wide range of modulation features. Therefore, there is a large number of different ELT signals that can be obtained.

Certain problems can arise in the processing of SARSAT signals and these can be summarized as follows:

(a) In certain cases the S-shaped curves are not complete and it is difficult to determine the inflection point.

(b) The S-shaped curves from two or more ELT signals may cross causing ambiguity in tracking the segments.

(c) Interfering signals may be received and relayed by satellite, to produce S-shaped curves. With no other information, these may be confused with ELT signals.

Specifically, it is concluded that:

1. An identification procedure to distinguish between the different ELT signals can significantly reduce the accumulated data set in the multiple satellite/multiple pass environment.
2. An identification procedure can separate ELT signals from different forms of background interference and significantly reduce the accumulated data set.
3. A set of parameters which uniquely describe the different types of ELT signal can be chosen. These are:
   (a) The widths (W1 and W2) of ELT averaged spectrum sidebands
   (b) The ratio of the averaged spectrum sideband plateaus B1 and B2 with respect to the carrier amplitude level.
   (c) The sweep period T_s.
4. The width W1 and W2 and the sideband plateaus B1 and B2 parameters are estimated using the average spectrum and the integrated average spectrum methods. These methods are tested using testbed ELT signals.
5. The sweep period can be estimated using two different techniques. The first is the sawtooth method which is applicable for high signal-to noise ratio, and the second is the crosscorrelation technique which can be used in any environment. These methods are tested using:
   (a) Computer simulated ELT signals for different values of CNDR ratios. The spectrum is calculated using 1 k-FFT segments. The results indicate the superiority of the crosscorrelation method at low values of CNDR (30 dB-Hz). Also the methods are tested for different sweep periods, and seen to be effective in estimating T_s.

(b) Testbed ELT signals, where the crosscorrelation method is seen effective to estimate the sweep period even for the signal of random phase characteristics.

6. Three different sources of interference, namely: continuous wave (CW); amplitude modulated (AM) signal; and, phase-shift keying (PSK) signals are selected. The crosscorrelation technique can be used to distinguish between ELT signals and interference.

7. The proposed technique is also applied to the case of ELT signals and co-channel interference where the inteference overlaps with the existing ELT signals. The method is seen effective in detecting the ELT signals down to SIR = -5 dB.

8. The non-linear effect of automatic gain control (AGC) at the receiver is seen to cause some difficulty in detecting the weak ELT signals in the presence of strong interference. In this case the ELT signal may be masked by the interference. The proposed method is capable of combatting this effect down to SIR = -15 dB.

9. Finally, the identification techniques are applied to real data from two satellite passes. In the first pass, there are approximately 16 signals present. Using the crosscorrelation method, the number of ELT signals identified then is just three. For the second pass, a total of approximately 7 signals are noted, but none of these are ELT signals. Thus the number of detections have been reduced considerably.

6.2 Recommendations

It is recommended that:

1. The proposed identification methods be tested using additional satellite pass data.

2. A study be performed to develop a locking receiver to automate the tracking of the signal using the identification parameters.

3. An investigation of the performance of the identification parameters as a function of time be carried out.
4. An investigation of the effect of the Doppler shift on the identification parameters be performed.
5. An investigation of the performance of the proposed methods using high resolution spectrum estimation techniques, e.g. the Maximum Entropy (ME) [6] and the autoregressive moving average (ARMA) [21] methods be performed.
6. The field of pattern recognition be investigated for ELT signal identification.

REFERENCES

1. C. Mundo, L. Tami and G. Larson, "Program Plan for Search and Rescue Electronics Alerting and Locating System", Transportation Systems Center, Cambridge, Massachusetts, Report No. DOT-TSC-OST-73-42, February 1974.

2. H.L. Werstiuk and A. E. Winter, "The Search and Rescue (SARSAT) System", North Atlantic Treaty Organization Adevisory Group for Aerospace Research and Development, AGARD Conference Proceedings, No. 238, Operational Modelling of the Aerospace Propagation Environment (in two volumes), Papers presented at the meeting of the Electromagnetic Wave Propagation Panel held in Ottawa, Canada, 24-28 April, 1978, H. Soicher, ed., vol. 1, p. 9-9 to 9-20.

3. A.E. Winter, J.D. Lambert, J.L. Pearce and H.L. Werstiuk, "Satellite-Aided Search and Rescue", IEEE Confrence, Montreal, Canada, 20-22 October, 1976.

4. T. Chung, "Digital Bandpass Processors for SARSAT Signals Using the MEM and FFT", M.Eng. Thesis, McMaster University, August 1982.

5. Department of Communications-Communications Research Centre, Performance Specifications and Requirements - Advanced Development Doppler Processor Internal Report Ref. No. SAR02.01.

6. T. Chung and C.R. Carter (1986), "Basic Concepts in the Processing of SARSAT Signals", submitted to IEEE Transactions on Aerospace and Electronic Systems.

7. C.R. Carter,"Data Recording of ELT Signals for Spectral Analysis", CRL Report No. CRL-110, McMaster University, November 1982.

8. "COSPAS/SARSAT Implementation plan (csip), Joint Canada, France, U.S. and U.S.S.R. Demonstration Project, 22 May, 1980. Co-authors: Communications Research Centre (CRC), Department of Communications, Ottawa, Ontario, Canada. K2H8S2, et al.

9. A.V. Oppenheim and R.W. Schafer, "Digital Signal Processing", Prentice-Hall, Englewood Cliffs, NJ, 1975.

10. A. Antonio,"Digital Filters Analysis and Design", McGraw-Hill, 1979.

11. M.I. Dessouky and C.R. Carter, "A Baseband Processor for SARSAT Signals", Accepted for publication in The Canadian Electrical Engineering Journal.

12. C.R. Carter and T. Chung, "Interference in the 121.5/243 MHz SARSAT Frequency Bands", IEEE Transactions on Aerospace and Electronic Systems AES-21 (November 1985) 804-817.

13. E.N. Skomal, "Man-made Radio Noise", Van Nostrand Reinholt Publ. Co. (1978), New York.

14. W.R. Vincent, "Examples of Signal and Noise in the Radio-Frequency Spectrum", IEEE Trans. on Electromagnetic Compatibility, vol. EMC-19, no. 3, August 1977, pp. 241-253.

15. J.H. Herman, "The Radio Noise Environment in Near Space: A Review", IEEE International Symposium on Electromagnetic Compatibility, (Atlanta, GA, June 20-22, 1978), pp. 339-346.

16. R.M. Smith, "The Extent and Nature of Television Reception Difficulties Associated with CB Radio Transmission", IEEE Trans. on Consumer Electronics, vol. CE-24, no.1, Feb. 1978, pp. 6-15.

17. R.M. Beeman, "Citizens Band Expansion and the Consumer Environment", IEEE Trans. on Consumer Electronics, vol. CE-24, no.1, Feb. 1978, pp. 16-23.

18. W.L. Hand, "Personal Use Radio (CB) and its Effects on TV Reception", IEEE Trans. on Consumer Electronics, Feb. 1977, pp. 78-91.

19. A. Premji, "Processing of ELT Signals for Search and Rescue Satellite Aided Tracking (SARSAT) Using MEM and FFT", M.Eng. Thesis, McMaster University, March 1982.

20. S.Haykin, "Communication Systems", 2nd Ed. John Wiley & Sons, 1983.

21. M.S. El-Hennawey, "A Parametric Approach for Spectrum Analysis and Carrier Frequency Estimations of Search and Rescue Satellite Aided Tracking (SARSAT) Signals", Ph.D. Thesis, McMaster University, September 1985.